

# **Stochastic Methods for the Fermion Determinant in Lattice Quantum Chromodynamics**

DISSERTATION

zur Erlangung des akademischen Grades

Dr. Rer. Nat.  
im Fach Physik

eingereicht an der  
Bergischen Universität Wuppertal  
Fachbereich C

von

**Herrn Dipl.-Phys. Jacob Friedrich Finkenrath**

Rektor der Bergischen Universität Wuppertal:  
Prof. Dr. Lambert Tobias Koch

Dekan des Fachbereichs C:  
Prof. Dr. Wolfgang Wagner

Gutachter:

1. Prof. Dr. Francesco Knechtli
2. Prof. Dr. Ulrich Wolff

**eingereicht am:** 22.12.2014

**Tag der mündlichen Prüfung:** 17.02.2015

---

## Abstract

In this thesis, algorithms in lattice quantum chromodynamics will be presented by developing and using stochastic methods for fermion determinant ratios. For that an integral representation will be proved which can be used also for non hermitian matrices. The stochastic estimation or the Monte Carlo integration of this integral representation introduces stochastic fluctuations which are controlled by using Domain Decomposition of the Dirac operator and introducing interpolation techniques.

Determinant ratios of the lattice fermion operator, here the Wilson Dirac operator, are needed for corrections of the Boltzmann weight. These corrections have interesting applications e.g. in the mass by using mass reweighting. It will be shown that mass reweighting can be used e.g. to improve extrapolation in the light quark mass towards the chiral or physical point or to introduce an isospin breaking by splitting up the mass of the light quark. Furthermore the extraction of the light quark masses will be shown by using dynamical 2 flavor CLS ensembles.

Stochastic estimation of determinant ratios can be used in Monte Carlo algorithms, e.g. in the Partial Stochastic Multi Step algorithm which can sample two mass-degenerate quarks. The idea is to propose a new configuration weighted by the pure gauge weight and including afterwards the fermion weight by using Metropolis accept-reject steps. It will be shown by using an adequate interpolation with relative gauge fixing and a hierarchical filter structure that it is possible to simulate moderate lattices up to  $(2.1 \text{ fm})^4$ . Furthermore the iteration of the pure gauge update can be increased which can decouple long autocorrelation times from the weighting with the fermions.

Moreover a novel Hybrid Monte Carlo algorithm based on Domain Decomposition and combined with mass reweighting will be presented. By using Domain Decomposition it is possible to split up the mass term in the Schur complement and the block operators. By introducing a higher mass in the Schur complement an effective cut-off parameter is introduced and sampling of smaller quark masses is possible. By using mass reweighting the weight can be corrected towards 1+1 ensembles.

In summary it will be shown how stochastic estimation of fermion determinant ratios can be used to improve lattice results in an efficient way with limited numerical effort.

## Abstract

In dieser Arbeit werden Algorithmen, die die stochastische Schätzung von Determinanten-Verhältnissen verwenden, im Bereich der Gittereichtheorie beschrieben und eingeführt. Dafür wurde für die Schätzung eine Integraldarstellung einer komplexen Matrix bewiesen und verwendet. Die Schätzung kann dabei durch Methoden, wie die Gebietszerlegung des Dirac Operators oder Interpolationstechniken verbessert und kontrolliert werden.

Im Boltzmannfaktor der Gittereichtheorie müssen genau dann Determinanten-Verhältnisse betrachtet werden, wenn die Wirkung der Fermionen geändert wird, hier die Wilson-Dirac Wirkung. Dies ist der Fall bei Massenkorrekturen der Quarks, auch als "Mass Reweighting" bekannt. Hier wird Mass Reweighting benutzt, um die Extrapolation in der Masse der leichten Quarks zum chiralen oder physikalischen Punkt zu verbessern und um die Brechung der Isospin-Symmetrie in den leichten Quarks herbeizuführen. Des Weiteren werden die Massen der leichten Quarks auf CLS Ensembles für einen finiten Gitterabstand bestimmt.

Die stochastische Schätzung kann auch in Monte Carlo Algorithmen benutzt werden, wie dem Partial Stochastic Multi Step Algorithmus, der Ensembles gewichtet mit zwei Quarks der gleichen Masse. Es wird gezeigt, dass es mit einer adäquaten Interpolationstechnik mit relativer Eichfixierung und einer hierarchischen Filterstruktur möglich ist, moderat große Gitter bis zu einer Größe von  $(2.1 \text{ fm})^4$  zu simulieren. Die Idee des Algorithmus ist, die neue Konfiguration durch ein reines Eich-Update vorzuschlagen und im Nachhinein unter Einbeziehung des Fermionengewichts durch Metropolis Akzeptanzschritte zu berichtigen. Dies hat den Vorteil, dass die Iteration des Eichupdates unabhängig von der Fermionengewichtung erhöht werden kann, so dass die Autokorrelationszeit dabei reduziert wird.

Des Weiteren wird ein neuer Hybrid Monte Carlo Algorithmus kombiniert mit Mass Reweighting vorgestellt. Bei Benutzung von Gebietszerlegung ist es möglich, den Massenparameter im Schur-Komplement und in den Block Operatoren aufzuspalten. Eine größere Masse im Schur Komplement fungiert dabei als effektiver Cut-Off Parameter, wodurch kleinere Quark Massen simuliert werden können. Durch Benutzung von Mass Reweighting kann das Boltzmann Gewicht eines Ensembles zu einem 1+1 Ensemble verändert werden.

Zusammenfassend wird in dieser Arbeit gezeigt, wie stochastische Schätzungen von Determinanten-Verhältnissen dazu genutzt werden können, Resultate vom Gitter zu verbessern bei gleichzeitig geringerem rechnerischen Aufwand.

Die Dissertation kann wie folgt zitiert werden:

urn:nbn:de:hbz:468-20150316-150522-7

[<http://nbn-resolving.de/urn/resolver.pl?urn=urn%3Anbn%3Ade%3Ahbz%3A468-20150316-150522-7>]

# Contents

<b>1. Introduction</b>	<b>1</b>
<b>2. Theory</b>	<b>5</b>
2.1. Strong Interaction . . . . .	5
2.1.1. Chiral Symmetry . . . . .	7
2.2. Feynman's Path Integral . . . . .	8
2.2.1. Path Integral with Fermions . . . . .	10
2.3. Gluons on the Lattice . . . . .	11
2.4. Wilson Fermions . . . . .	12
2.5. Monte Carlo Methods . . . . .	17
2.5.1. Hybrid Monte Carlo Algorithm . . . . .	19
<b>3. Numerical Computation of Determinants</b>	<b>23</b>
3.1. Definition of the Pseudofermion Integral . . . . .	23
3.2. Stochastic Estimation . . . . .	24
3.3. Fluctuations . . . . .	25
3.4. Fluctuations of Ratio Matrices controlled by Interpolation . . . . .	27
<b>4. Techniques for Lattice QCD</b>	<b>29</b>
4.1. Domain Decomposition . . . . .	29
4.1.1. Schur Complement . . . . .	29
4.1.2. DD in LQCD . . . . .	30
4.2. Correlations . . . . .	34
4.3. Observables . . . . .	36
4.3.1. Correlation Functions on the Lattice . . . . .	36
4.3.2. Gluonic Observable $t_0$ . . . . .	41
4.3.3. Topological Charge . . . . .	42
<b>5. Mass Reweighting</b>	<b>45</b>
5.1. Reweighting Factor . . . . .	46
5.1.1. Fluctuations . . . . .	47
5.1.2. Statistical Errors of Reweighting . . . . .	47
5.2. Mass Reweighting . . . . .	48

5.3.	Stochastic Fluctuations . . . . .	52
5.3.1.	Mass Interpolation . . . . .	52
5.3.2.	Domain Decomposition . . . . .	55
5.3.3.	Twisted-mass Detour . . . . .	57
5.3.4.	Scaling of Stochastic Fluctuations . . . . .	60
5.4.	Ensemble Fluctuations . . . . .	62
5.4.1.	Scaling of Ensemble Fluctuations . . . . .	63
5.4.2.	Errors . . . . .	68
5.4.3.	Bias . . . . .	69
5.4.4.	Beta-Shift . . . . .	69
5.5.	Applications . . . . .	71
5.5.1.	Critical Mass . . . . .	72
5.5.2.	Scale setting with $t_0$ . . . . .	73
5.6.	Tuning of bare Mass Parameters . . . . .	73
5.6.1.	Tuning of $\kappa_u, \kappa_d$ and $\kappa_s$ . . . . .	73
5.6.2.	Strange Quark Reweighting . . . . .	74
5.6.3.	Isospin Reweighting . . . . .	76
5.6.4.	Electromagnetic Reweighting . . . . .	80
5.7.	Conclusion . . . . .	81
5.7.1.	Summary . . . . .	81
5.7.2.	Prospects . . . . .	82
<b>6.</b>	<b>Partial Stochastic Multi Step Algorithm</b>	<b>83</b>
6.1.	Fluctuation and Acceptance . . . . .	83
6.2.	Stochastic Fluctuations . . . . .	85
6.2.1.	Gauge Field Interpolation . . . . .	85
6.2.2.	Relative Gauge Fixing . . . . .	87
6.2.3.	Domain Decomposition . . . . .	89
6.2.4.	Numerical Results . . . . .	90
6.3.	Ensemble Fluctuations . . . . .	92
6.3.1.	Hierarchical Steps . . . . .	92
6.3.2.	Correlations . . . . .	94
6.4.	Numerical Tests . . . . .	96
6.4.1.	Master Theorem . . . . .	97
6.4.2.	Acceptance Rate . . . . .	99
6.4.3.	Autocorrelation . . . . .	103
6.4.4.	Conclusion . . . . .	108
6.5.	Partially smeared HYP-runs . . . . .	109
6.5.1.	Runs . . . . .	111
6.5.2.	Results . . . . .	112
6.6.	Prospects . . . . .	113
6.6.1.	UV - Improvements . . . . .	114

6.6.2. IR - Improvements . . . . .	115
6.6.3. Conclusion . . . . .	115
<b>7. Mass-Split Domain Decomposition HMC Algorithm</b>	<b>117</b>
7.1. Properties of the Algorithm . . . . .	118
7.1.1. Motivation . . . . .	118
7.1.2. MDD-HMC Simulations . . . . .	119
7.1.3. Shift of the Blocks . . . . .	120
7.2. Properties of the Reweighting . . . . .	122
7.3. Costs . . . . .	123
7.4. Conclusion . . . . .	125
<b>8. Conclusion</b>	<b>127</b>
<b>Appendix</b>	<b>133</b>
A. Proof of the Integral Representation . . . . .	134
A.1. Integral . . . . .	134
A.2. Proof: Gauß Elimination without Gauß Elimination . . . . .	137
B. Fluctuations . . . . .	140
B.1. Fluctuations of a complex Estimate . . . . .	140
B.2. Fluctuations by using Stochastic Estimation . . . . .	141
B.3. Expansion . . . . .	142
B.4. Comparing with $n$ th Root . . . . .	143
C. Recursive Domain Decomposition . . . . .	145
D. Error . . . . .	147
D.1. Error and Bias . . . . .	147
D.2. Error and Bias in the Case of Reweighting . . . . .	149
D.3. Expansion . . . . .	150
E. Detailed Balance . . . . .	152
E.1. Accept-reject Steps with exact Weight . . . . .	152
E.2. Accept-reject Steps with partial stochastic Weight . . . . .	153
E.3. Accept-reject Steps with Gauge field Interpolation . . . . .	155
E.4. Remarks . . . . .	156
F. Plain Wilson Ensembles at $\beta = 5.5$ . . . . .	157





# 1. Introduction

The content of my thesis are developments to handle the fermion determinant in the framework of Lattice Quantum Chromodynamics (LQCD). To increase the precision of physical quantities by using LQCD further improvements and developments of numerical techniques are necessary. In this thesis methods are presented to improve the stochastic estimation of determinant ratios and to provide an alternative sampling of the fermion determinant than is done by the Hybrid Monte Carlo (HMC) algorithm. These novel and improved methods will be illustrated in chapter five (reweighting in the quark mass), chapter six (a Monte Carlo algorithm with stochastic accept-reject steps) and chapter seven (a modification of the HMC algorithm by including mass reweighting). In previous chapters, chapter two, three and four, the framework will be clarified and necessary numerical methods to improve techniques and to measure observables will be introduced.

In **chapter two** the framework of LQCD, introduced 1974 by Wilson [1], will be shortly discussed. LQCD is a regularized theory which is able to predict physics described by Quantum Chromodynamics (QCD) in the low energy regime of the Standard Model in particle physics [2]. The chapter will start with a short introduction of the physics of QCD. This will be followed by the illustration of the theoretical environment which is needed in order to map QCD to the lattice. The content will be the presentation of the path integral, the lattice Lagrangian with the pure gauge action [1] and the Wilson Dirac operator [3]. At the end of this chapter the method Monte Carlo simulation will be discussed. Monte Carlo algorithms are used to sample the lattice path integral which enables LQCD to predict physics.

In the **third chapter** the main relation of this thesis will be introduced, an integral representation of a determinant. In LQCD the fermion part of the Boltzmann weight is given by a product over the determinants of the Dirac operators describing the quark flavors. The fermion degrees of freedom can be rewritten by an integral representation, originally introduced 1980 by Weingarten, Petcher [4] and Fucito et. al. [5] for positive definite hermitian matrices. Since then this integral representation is widely used to handle the fermion weight in Monte Carlo simulations or in different weighting methods. However it is restricted to positive definite hermitian matrices which makes a direct treating of non-hermitian ratios of lattice Dirac operators impossible. In this work an integral representation is used and firstly proved which can handle also non-hermitian matrices  $A$  with the condition that  $A + A^\dagger$  is positive definite. The integral can be estimated stochas-

tically in cases where the direct computation is not possible. The understanding of the introduced fluctuations, by the estimation and by the determinant itself, is the key issue in order to develop numerical techniques. An analytic expression for the variance of the stochastic estimation of the hermitian integral representation is given in [6] which implies that the variance is not defined if an eigenvalue of the hermitian matrix is smaller or equal to 0.5. Moreover the variance gets small if the eigenvalues tend to one. However the fluctuations depend on the specific cases and in the case of non-hermitian matrices an understanding via the eigenvalues is not straightforward. Here, the fluctuations will be approximated by traces of matrices. This helps to understand their behavior as a function of a suitable parameter, to improve the effectiveness and to introduce methods which can keep them under control.

In the **fourth chapter** several methods will be presented for improving stochastic techniques and for measuring physical observables. The improvement methods are Domain Decomposition (DD) [7] and a parametrization of correlations. These methods can be used to tame the fluctuations introduced by the fermion determinants. The second part of this chapter will introduce observables which are used to extract physical predictions and information from the lattice. In detail these observables are the mass of the pseudoscalar particles, which corresponds to the pion and the kaon, the PCAC mass, which can be used to calculate the physical quark masses, (see e.g. [8]) gluonic observables like  $t_0$  [9], which can be used to fix the scale, and the topological charge, an observable used to analyze the performance of the different algorithms.

In the **fifth chapter** mass reweighting will be presented [10]. Reweighting was original introduced 1988 by Ferrenberg and Swendsen [11] and applied to the quark mass of two mass-degenerate fermions 2008 by Hasenfratz, Hoffmann and Schaefer [12]. The idea is to reuse an ensemble to compute observables corresponding to an ensemble at a different parameter set. This is applicable and cheaper for small corrections than a new generation of an ensemble. Since 2008 the method mass reweighting was used for several applications like in [13] [14] [15] but a detailed analysis of the behavior of mass reweighting, like the scaling of the fluctuations or a consistent error analysis, was not done. Here, by introducing the integral representation of a non-hermitian matrix the fluctuations (stochastic and ensemble) will be analyzed and used to estimate their scaling behavior with the volume and the quark mass. This is important in order to predict the numerical effort of the method. Moreover an approximation for the introduced error will be derived. Applications of mass reweighting will be presented, e.g. it can be used to tune the quark masses for different cases. Here, it is shown an extrapolation in the pion mass towards the chiral or the physical point is improved or it is also possible by using only one ensemble. The extrapolation will be used to determine the critical mass parameter. Furthermore mass reweighting can be used for tuning the strange quark mass or the isospin splitting in the up- and down quarks. By

---

matching to the physical kaon  $K^* - K^0$  mass splitting the up- and down-quark masses will be extracted and isospin sea quark effects will be estimated. In summary it will be shown that mass reweighting is an efficient method also on large lattices with light quark masses close to the physical point with moderate costs compared to an additional generation of ensembles.

The **sixth chapter** will describe the Partial Stochastic Multi Step (PSMS) algorithm [16] which uses Metropolis accept-rejects steps for the weighting of the fermion action. The PSMS algorithm is motivated by a study in the Schwinger model [17]. In general similar algorithmic concepts are used for fermion actions where force computations are not feasible like hypercubic (HYP)-link smeared staggered fermion actions [18] [6] [19] or for fix point actions like in [20]. Compared to the Hybrid Monte Carlo (HMC) algorithm the PSMS algorithm has the advantage that it does not need force computations. Force computations can be complicated or even impossible if HYP-smearing is used [21]. Although solution exists to simulate smeared fermion actions with the HMC like stout [22], nHYP [23], HEX [24] [25] smeared links or a differentiable approximation to  $SU(3)$  for smeared links [26], one motivation to establish the PSMS algorithm is as an alternative to the HMC algorithm which can handle also complicated fermion actions. Moreover Monte Carlo algorithms get inefficient if the autocorrelation times increase. This happens in LQCD for decreasing lattice spacing  $a$ . In [27] is found that the low modes of the autocorrelation times scale at least with  $a^{-5}$  on periodic lattices. The reason is that the topological charge gets stuck [9]. A possible solution is to use open boundary condition where it was found that the autocorrelation times scale with  $a^{-2}$  [28]. Here in the case of the PSMS algorithm, the idea is to decouple the fermion weight during the proposal from the update of the gauge links with the purpose of changing the topological charge by iterating the gauge updates. Afterwards the fermion weight is taken into account by a hierarchy of Metropolis accept-reject steps [29]. The acceptance rates suffer from fluctuations which are introduced by the proposal and by the estimation technique. Methods which can handle these fluctuations will be introduced in the first part of this chapter. These are interpolation techniques combined with relative gauge fixing and DD to control the stochastic fluctuations and a hierarchical filter system [30] with parametrization of the correlations to control the ensemble fluctuations. Numerical results of the algorithm will be shown which are a scaling analysis of the acceptance and of the autocorrelation time of the topological charge in the lattice spacing  $a$ . Furthermore a comparison is done with standard Hybrid Monte Carlo algorithms, like DD-HMC [31] and the openQCD-HMC [32] on lattices with moderate sizes. The chapter will be closed by a presentation of simulations with a partially smeared fermion action which would not be possible with the HMC algorithm. Smearing has several interesting features, e.g. it improves the chiral properties of lattice fermions [33] and it can tame the fluctuations of the small eigenvalues of the Wilson Dirac operator [25].

In the **seventh chapter** the Mass Split Domain Decomposition HMC algorithm (MDD-HMC) will be introduced, a novel Monte Carlo algorithm based on the DD-HMC algorithm [31] and mass reweighting. The MDD-HMC uses advantages of mass reweighting in order to suppress disadvantages of the HMC. By using DD the idea is to split up the mass term in the Schur complement and the blocks. A higher mass term of the Schur complement can be used as an effective cut-off parameter which stabilizes the HMC-trajectory. By using mass reweighting the ensemble can be reweighted towards a 1+1 ensemble. Several runs are performed and properties like the effectiveness of the higher mass parameter of the Schur complement or the scaling in the lattice volume of the introduced fluctuations will be presented. The chapter will be closed by a comparison to standard techniques, e.g. the DD-HMC algorithm.

In the **conclusion** the major results and techniques will be summarized.

## 2. Theory

### 2.1. Strong Interaction

One part of the Standard Model of elementary particle physics is Quantum Chromodynamics (QCD) [2]. It couples quarks [34] [35] to gluons by demanding a local gauge symmetry of the Lagrangian density. The symmetry group is the non-abelian special unitary group  $SU(3)$  and correspondingly there are three different charges for quarks, called colors. Hadrons are “colorless” particles made up of valence quarks and anti-quarks confined by colored glue bosons, the gluons. The six flavors of the quarks differ only in the mass term in QCD. By introducing other interactions this changes. For example by considering Quantum Electrodynamics (QED) the quarks have an electric charge,  $+2/3$  for the up-, charm- and top-quark and  $-1/3$  for the down-, strange- and bottom-quark (see tab. 2.1).

The Lagrangian density of QCD with  $n_f$  flavors of anticommuting Dirac fields  $\psi_j$  with different masses  $m_j$ , which corresponds to the different quark fields, and  $N^2 - 1$  types of vector bosons or gluons  $A^b$  with one coupling constant  $g$  is given by

$$\mathcal{L} = \sum_{j=1}^{n_f} \bar{\psi}_j (i\gamma^\mu D_\mu - m_j) \psi_j - \frac{1}{4} F_{\mu\nu}^b F_{\mu\nu}^b \quad (2.1)$$

where the covariant derivative is given by  $D_\mu = \partial_\mu - igA_\mu^b t^b$  and the field tensor  $F_{\mu\nu}$  is defined by  $[D_\mu, D_\nu] = F_{\mu\nu} = -igF_{\mu\nu}^b t^b$ . Note repeated indices are summed. The  $N \times N$  hermitian matrices  $t^b$  are the generators of  $SU(N)$  and fulfill the commutation relations

$$[t^b, t^c] = if^{bcd} t^d \quad (2.2)$$

where the structure constants  $f^{bcd}$  are totally antisymmetric and  $\text{tr}(t^a t^b) = \frac{1}{2} \delta^{ab}$ . The  $\gamma$ -matrices fulfill the Dirac algebra  $\{\gamma^\mu, \gamma^\nu\} = 2\gamma^{\mu\nu} \times \mathbb{1}$  with the metric of the Minkowski space  $\gamma^{\mu\nu} = \text{diag}\{+1, -1, -1, -1\}$  (see e.g. modern textbooks like [37]).

QCD can describe the complex hierarchy and relations among hadrons with a small amount of parameters, but the validation of all phenomena and the calculation of many physical quantities is still a major research subject, i.e. methods to solve the underlying theory analytically are not known. The physics of the strong interaction has two significant properties, asymptotic freedom and confinement.

## 2. Theory

---

name	label	charge	mass [36]
up	u	2/3	2.3(7) MeV
down	d	-1/3	4.8(7) MeV
charm	c	2/3	1.28(3) GeV
strange	s	-1/3	95(5) MeV
top	t	2/3	160(5) GeV
bottom	b	-1/3	4.18(3) GeV

Table 2.1.: The table shows some properties of the six different quark flavors. The quarks are fermions and the spins are given by  $S = 1/2$ . The charge is the electrical charge and the mass is given in the  $\overline{\text{MS}}$  renormalization scheme at the scale  $\mu = 2 \text{ GeV}$  for u, d and s and at  $\mu = \overline{m}$  for c, b and t.

The former property was observed in experimental collision experiments which could be described by a perturbative approach. The validation by theory [38] [39] was made by showing perturbatively that the coupling strength for a non abelian  $\text{SU}(N)$  gauge theory with  $n_f$  quarks which fulfills  $11N > 2n_f$  becomes weaker and weaker for larger energies or smaller distances. This follows from the renormalization group equation for the coupling and the beta function at one loop order

$$\mu \frac{\partial g}{\partial \mu} = \beta(g) = -\frac{g^3}{16\pi^2} \left[ \frac{11}{3}N - \frac{2}{3}n_f \right] + \mathcal{O}(g^5). \quad (2.3)$$

For the running of the coupling constant  $g(\mu)$  follows at large  $\mu$

$$\frac{g^2(\mu)}{4\pi} = \frac{4\pi}{11/3N - 2/3n_f} \left[ \ln(\mu^2 / \Lambda_{\text{QCD}}^2) \right]^{-1} + \dots \quad (2.4)$$

with the momentum scale  $\mu$  and the renormalization group invariant scale  $\Lambda_{\text{QCD}}$ . The  $\mu$  dependence of the renormalized mass is given by the renormalization group equation for the mass and the tau function

$$\tau(g) = \frac{\mu}{\overline{m}_i} \frac{\partial \overline{m}_i}{\partial \mu} = -g^2 \frac{6(N^2 - 1)}{2N(4\pi)^2} + \mathcal{O}(g^4). \quad (2.5)$$

The masses depend on the momentum scale  $\mu$  and the renormalization scheme (see tab. 2.1).  $\Lambda_{\text{QCD}}$  depends on the specific renormalization scheme, here the modified minimal-subtraction scheme ( $\overline{\text{MS}}$ -scheme) is used.

In the low energy regime of QCD, that is for energies  $< 2 \text{ GeV}$ , the coupling becomes strong and perturbation theory breaks down. The quarks are confined in colorless hadrons and can not be observed in isolation. Wilson [1] introduced

a discretization of fermions and gauge fields on an Euclidean lattice called Lattice Quantum Chromodynamic (LQCD) which can be simulated on computers to observe confinement [40]. Using developments in computers and numerical methods LQCD makes the computation of properties of QCD at low energies possible, e.g. calculation of hadron masses [41]. Today's target of theoretical elementary particle physics is to increase the precision of predictions for a further validation of the Standard Model or to find physics beyond the Standard Model.

### 2.1.1. Chiral Symmetry

An effective way to understand the phenomena of the mass hierarchy of hadrons in the low energy regime of QCD is chiral symmetry. Due to the Noether theorem [42] symmetries of the Lagrangian density are directly connected to conserved currents and are an essential tool to understand the underlying physics. The QCD Lagrangian is invariant under rotations in the massless limit of the up- and down-quark. By defining a flavor doublet

$$\psi = (u, d) \quad \text{and} \quad \bar{\psi} = (\bar{u}, \bar{d}) \quad (2.6)$$

with  $u$  and  $d$  anticommuting fermion fields and by projecting to the fermion fields with

$$\psi_L = (P_L u, P_L d) \quad \text{and} \quad \psi_R = (P_R u, P_R d) \quad (2.7)$$

with the chiral projectors  $P_L = 1/2(1 - \gamma_5)$  and  $P_R = 1/2(1 + \gamma_5)$  it follows  $\psi = \psi_L + \psi_R$ . In the fermion part of the Lagrangian density for the lightest quarks the left handed part  $\psi_L$  decouple exactly from the right handed part for  $m = 0$  such that the Lagrangian density is given by

$$L_{ud} = \bar{\psi}_L i \gamma^\mu D_\mu \psi_L + \bar{\psi}_R i \gamma^\mu D_\mu \psi_R. \quad (2.8)$$

The singlet axial transformation is given by

$$\psi(x) \rightarrow e^{i\alpha\gamma_5 I} \psi(x) \quad \text{and} \quad \bar{\psi}(x) \rightarrow \bar{\psi}(x) e^{i\alpha\gamma_5 I} \quad (2.9)$$

with  $\alpha \in \mathbb{R}$ ,  $\gamma_5 \equiv i\gamma_0\gamma_1\gamma_2\gamma_3$  and  $I$  the unit matrix in the flavor space, here  $2 \times 2$ . It is a symmetry of  $L_{ud}$  in eq. (2.8). Due to quantum effects the singlet axial symmetry  $U(1)_A$  is explicitly broken, e.g. by the non-invariance of the fermion measure [43] [44] [45] (see also [46]), and the Lagrangian density is invariant under symmetry transformation of the group

$$SU(2)_L \times SU(2)_R \times U(1)_V. \quad (2.10)$$

## 2. Theory

---

where the left handed fermion fields  $\psi_L$  and the right handed fermion fields  $\psi_R$  are separately invariant under  $SU(2)_L$  and  $SU(2)_R$  respectively. The transformation can be expressed by

$$\psi' = e^{i\alpha I} e^{i\beta^b \sigma_b} e^{i\epsilon^c \sigma_c \gamma_5} \psi \quad \text{and} \quad \bar{\psi}' = \bar{\psi} e^{i\epsilon^c \sigma_c \gamma_5} e^{-i\beta^b \sigma_b} e^{-i\alpha I} \quad (2.11)$$

with  $e^{i\alpha} \in U(1)_V$  the singlet vector rotation,  $e^{i\beta^b \sigma_b} \in SU(2)_V$  the vector rotation and  $e^{i\epsilon^c \sigma_c \gamma_5}$  the chiral or axial vector rotation with  $e^{i\epsilon^c \sigma_c} \in SU(2)$ . For the coefficients follows  $\alpha, \beta^b, \epsilon^c \in \mathbb{R}$  and  $\sigma_b, \sigma_c$  are the generators of  $SU(2)$ , the Pauli matrices, and  $I$  the unit matrix. Note that the rotations act on the flavor space of the light quarks, explicitly on the doublet defined in eq. (2.6).

However the symmetries of the QCD Lagrangian density of the light quarks are explicitly broken by the mass terms down to  $U(1)_{up} \times U(1)_{down}$ , which is connected to the conservation of the baryon number. In the limit of mass-degenerate light quarks this symmetry is extended to the isospin vector symmetry which is given by  $SU(2) \times U(1)_V$ . Compared to the typical mass scale of QCD-baryons the symmetry group is a good approximation and can describe well several phenomena which are measured in experiments, e.g. the isospin symmetry in the pions.

For vanishing quark masses chiral symmetry of the Lagrangian density is restored. Due to the small masses of the light quarks chiral symmetry would also be a good approximation to the physics of QCD. However the restored chiral symmetry can not explain the large gap between the lightest mesons, the pions, and the lightest baryons, the proton and neutron (see tab. 2.2). The explanation is that in the confined phase of QCD chiral symmetry is broken spontaneously. This leads to massless mesons in the zero quark mass limit [47], the Goldstone particles [48] [49]. In QCD these mesons are the three pseudoscalar particles also known as pions. Using these properties, the remaining symmetries and the massless pions, it is possible to construct an effective theory, chiral perturbation theory, by using the non-linear sigma model and reintroducing quark masses as perturbation terms. This enables a connection of QCD observables with non-physical finite quark masses to physical or even to massless quarks by using a controlled extrapolation.

## 2.2. Feynman's Path Integral

Feynman's path integral is a mathematical tool for applications of quantum field theory [52] [53]. The Feynman's path integral expresses the quantum mechanical probability amplitude  $\langle x_b | e^{iHt} | x_a \rangle$  for a particle under the Hamiltonian  $H$  to move from  $x_a$  to  $x_b$  in the time interval  $t$  into a multidimensional integral. Feynman's



Name	content	$J^P$	exper. mass [36]	effective QCD mass [50]
Pion $\pi^-$	$d\bar{u}$	$0^-$	139.5702(4) MeV	134.8(3) MeV
Pion $\pi^0$	$u\bar{u} + d\bar{d}$	$0^-$	134.9766(6) MeV	134.6(3) MeV
Kaon $K^-$	$s\bar{u}$	$0^-$	493.677(16) MeV	491.2(5) MeV
Kaon $K^0$	$s\bar{d} + d\bar{s}$	$0^-$	497.617(24) MeV	497.2(4) MeV
...				
Proton $p$	$uud$	$\frac{1}{2}^+$	938.27204(4) MeV	–
Neutron $n$	$udd$	$\frac{1}{2}^+$	939.56538(2) MeV	–
...				

Table 2.2.: The table shows some properties of some light hadrons. In detail these are the mesons, the pions and the kaons and the lightest baryons, the proton and the neutron. The second column illustrates the flavors of the valence quarks which build up the hadrons while they are confined by the gluons. The presented mesons are pseudoscalar particles with spin 1 and parity  $-1$ . The lightest baryons obey the Fermi statistics and are spin  $1/2$  particles with parity  $+1$ . The experimental mass is taken from [36]. Electromagnetic effects are removed in the effective QCD mass [50]. The effective QCD mass for the baryons is not shown here, however the difference can be found for example in [51].

path integral is given by

$$\langle x | e^{iHt} | y \rangle = \int e^{iS(x)} \mathcal{D}x \quad (2.12)$$

where the action  $S = \int \mathcal{L}(x) d^4x$  depends on the Lagrange density  $\mathcal{L}(x)$  and the normalized measure  $\mathcal{D}x$ . The normalized measure integrates over every possible path in the three dimensional space which fulfills  $x(0) = x_a$  and  $x(t) = x_b$ . Note the exponential in the integral is complex and highly oscillating which makes applications of stochastical methods unfeasible in practice. By rotating the real time  $t$  by  $e^{-i\pi/2}$  the Minkowski space transforms into the Euclidean space, where the time  $t$  behaves like a fourth spatial dimension. By applying this so-called Wick-rotation (see for an overview [54]) the path integral transforms into

$$\langle x | e^{-Hx_0} | y \rangle = \int e^{-S_E(x)} \mathcal{D}x \quad (2.13)$$

## 2. Theory

---

with the Euclidean action  $S_E$ . Now the path integral is given as a partition function of a four dimensional statistical system with a positive weight factor  $e^{-S_E}$ , the so-called Boltzmann factor. Note the Wick-rotation enables application of stochastic methods to a Lagrangian density. Although several physical quantities are difficult to recover back into the Minkowski world from now on the Euclidean formulation of the quantum field theory will be used and the index  $E$  will be dropped. For many applications the integral weight becomes positive under a Wick rotation which enables Monte Carlo methods also in the case of LQCD.

### 2.2.1. Path Integral with Fermions

The expectation value for a physical quantity  $O$  in the Euclidean path integral representation of QCD is given by

$$\langle O \rangle = \frac{1}{Z} \int O e^{-S(A,\psi,\bar{\psi})} \mathcal{D}A \mathcal{D}\psi \mathcal{D}\bar{\psi} \quad (2.14)$$

where  $Z$  is the partition function defined such that the vacuum expectation value  $\langle 1 \rangle = 1$ . The Euclidean QCD action is given by  $S = \int \mathcal{L} d^4x$  with the Lagrangian density

$$\mathcal{L} = \sum_{j=1}^{n_f} \bar{\psi}_j (\gamma^\mu D_\mu + m_j) \psi_j + \frac{1}{4} F_{\mu\nu}^b F_{\mu\nu}^b \quad (2.15)$$

and the integration over every possible field configuration. The fermion variables are anticommuting Grassmann variables. A function of Grassmann  $n$ -variables can be presented exactly by a Taylor-serie with

$$f(\psi) = a + \sum_i b_i \psi_i + \sum_{i<j} c_{ij} \psi_i \psi_j + \dots + z \psi_1 \dots \psi_n. \quad (2.16)$$

with constants  $a, b_i, c_{ij}, \dots, z \in \mathbb{C}$ . By using the anticommuting properties the derivatives of Grassmann variables are given by

$$\frac{\partial}{\partial \psi_j} \psi_i = \delta_{ij}, \quad \frac{\partial}{\partial \psi_j} \quad \text{and} \quad \frac{\partial}{\partial \psi_k} \psi_i \psi_j = \delta_{ik} \psi_j - \delta_{jk} \psi_i. \quad (2.17)$$

The integration rules for Grassmann variables are quite similar to the derivative rules and are given by

$$\int \psi_i d\psi_j = \delta_{ij}, \quad \int a d\psi_j = 0 \quad \text{and} \quad \int \psi_i \psi_j d\psi_k = -\delta_{ik} \psi_j + \delta_{jk} \psi_i. \quad (2.18)$$

Note an important property of eq. (2.14) is that the fermion field  $\bar{\psi}_i$  is independent of  $\psi_i$ . Using the integration rules eq. (2.18) the fermion degrees of freedom can be integrated out, also known as the Matthews-Salam formula [55] and the partition function reduces to

$$Z = \int e^{-S_g} \cdot \left[ \prod_{j=1}^{n_f} \det D(A, m_j) \right] DA \quad (2.19)$$

where  $D(A, m_j)$  is the Dirac operator and  $S_g = F_{\mu\nu}^b F_{\mu\nu}^b / 4$  the pure gauge action. These expressions are formal and a finite and computable expression can be given on the lattice.

## 2.3. Gluons on the Lattice

The discretization of the continuous world introduces an Ultraviolet(UV) cut-off. The limitation to a box introduces an Infrared(IR) cut-off for appropriate boundary conditions. These steps regularize the path integral and the lattice is given by

$$\Lambda = \left\{ x \mid x_0 = 0, \dots, T - a, \quad x_k = 0, \dots, L - a \right\} \quad (2.20)$$

with  $x_0$  the time coordinate,  $x_k$  with  $k = 1, 2, 3$  the spatial coordinates. The main parameters of the isotropic lattice are the lattice spacing  $a$ , the number of lattice points in the Euclidean time direction  $T$  and the Euclidean spatial directions  $L$ . Continuum physics is recovered by performing the limit  $a \rightarrow 0$  by keeping the physical volume  $V_{phys} = T \times L^3$ .

The discretization of the Lagrangian density eq. (2.15) has to recover the physical Lagrangian density in the continuum limit. The lattice breaks the spatial continuum symmetries down to lattice symmetries. In general a good lattice action preserves a maximal amount of symmetries and simultaneously moderate numerical efforts in the computation. For the Lagrangian density of LQCD local gauge symmetry is demanded. Here the Yang Mills action [56]

$$S_{YM} = \frac{1}{4} \int F_{\mu\nu}^b F_{\mu\nu}^b d^4x \quad (2.21)$$

will be discretized. For that a gauge link is defined between the nearest neighbour lattice points  $x$  and  $x + \hat{\mu}$  in  $\mu$ -direction by

$$U_\mu(x) \in SU(3) \quad (2.22)$$

## 2. Theory

---

which transforms under the local lattice gauge transformation with

$$U_\mu(x) \longrightarrow g(x)U_\mu(x)g(x + \hat{\mu})^\dagger \quad (2.23)$$

with arbitrary  $SU(3)$ -matrices  $g(x)$  at all lattice points. Now, traces of closed loops on the lattice are invariant under this local gauge symmetry, e.g. the Wilson plaquette [1]

$$P_{\mu\nu}(x) = U_\mu(x)U_\nu(x + \hat{\mu})U_\mu^\dagger(x + \hat{\nu})U_\nu^\dagger(x) \quad (2.24)$$

where  $U^\dagger = \bar{U}^T$  is the complex conjugate transpose matrix  $U$ . Wilson constructed, by using the trace of the sum over every plaquette, the Wilson gauge action

$$S_g = \frac{\beta}{3} \sum_x \sum_{\substack{\mu, \nu \\ \mu < \nu}} \text{Re} [\text{Tr}(I - P_{\mu\nu}(x))] \quad (2.25)$$

with  $x \in \Lambda$ ,  $\mu, \nu \in \{0, 1, 2, 3\} \forall x$  and a  $3 \times 3$  unit matrix  $I$ . By performing the continuum limit using the relation

$$U_\mu(x) = \exp\{igaA_\mu^b(x + \frac{a}{2}\hat{\mu})t^b\} \quad (2.26)$$

and the Baker-Campbell-Hausdorff-formula  $e^A e^B = e^{A+B+[A,B]}$  with the commutator  $[A, B] = AB - BA$  the Wilson pure gauge action recovers the Yang-Mills action [56]

$$S_g = -\frac{\beta}{12} \sum_x a^4 \text{Tr} F_{\mu\nu} F_{\mu\nu} + \mathcal{O}(a^6) \longrightarrow S_{YM} = \frac{1}{4} \int F_{\mu\nu}^b F_{\mu\nu}^b d^4x \quad (2.27)$$

where  $\beta = \frac{6}{g^2}$  and  $F_{\mu\nu} = -igF_{\mu\nu}^b t^b$ . Furthermore the continuum scaling behavior can be improved by adding higher loop terms, e.g. six link terms, to the lattice pure gauge action (e.g. see [57] [58]).

### 2.4. Wilson Fermions

The discretization of the forward covariant derivative is given by

$$D_\mu \rightarrow \frac{1}{a} (U_\mu(x) \delta_{x, y-\hat{\mu}} - \delta_{x, y}) = (D_\mu)_{x, y} \quad (2.28)$$

with  $\delta_{x,y}\psi(y) := \psi(x)$  (see e.g. in textbooks like [54] [59] [46]). The backward covariant derivative is defined by

$$D_\mu^* \rightarrow \frac{1}{a}(-U_\mu^\dagger(x - \hat{\mu})\delta_{x,y+\hat{\mu}} + \delta_{x,y}) = (D_\mu^*)_{x,y}. \quad (2.29)$$

However, the discretization in the case of the fermion action is not straightforward due to the doubling problem. In the naive discretization, the so called naive fermion operator is given by

$$D_{naive}(m)_{x,y} = m\delta_{x,y} + \frac{1}{2a} \sum_\mu \gamma_\mu \left( U_\mu(x)\delta_{x,y-\hat{\mu}} - U_\mu^\dagger(x - \hat{\mu})\delta_{x,y+\hat{\mu}} \right) \quad (2.30)$$

where  $a$  is the lattice spacing,  $m$  is the bare mass parameter and  $\gamma_\mu$  are the  $\gamma$ -matrices of the Euclidean space which fulfill the relation  $\{\gamma_\mu, \gamma_\nu\} = \delta_{\mu\nu} \times I$ . The  $\gamma$ -matrices act on the spinor space with 4 degrees of freedom, the links  $U(x)$  act on the color space with 3 degrees of freedom and the Dirac operator can be represented as a  $12V \times 12V$  matrix with  $V = \frac{T}{a} \times \left(\frac{L}{a}\right)^3$ . The naive fermion operator is normal, which means it fulfills the relation  $A^\dagger A = A A^\dagger$ . For massless quarks, the naive fermion operator is anti-hermitian and invariant under the chiral or axial transformations with  $\{D_{naive}, \gamma_5\} = 0$ .

In the free case the Fourier transformed naive Dirac operator is given by ( $U \equiv 1$ )

$$\tilde{D}(p) = m + \frac{i}{a} \sum_{\mu=1}^4 \gamma_\mu \sin(p_\mu a) \quad (2.31)$$

with corresponding momenta  $p_\mu \in \{-\frac{\pi}{a}, \frac{\pi}{a}\}$ . The naive Dirac operator has 16 poles. This follows by inverting eq. (2.31), which corresponds to the free propagator  $\tilde{S}(p)$  (see e.g. [46])

$$\frac{1}{a}\tilde{D}^{-1}(p) = \frac{1}{a}\tilde{S}(p) = \frac{-i\gamma_\mu \sin(p_\mu a) + ma}{\sum_\mu \sin^2(p_\mu a) + m^2 a^2}. \quad (2.32)$$

These 16 mass-degenerate fermions remain in the continuum and the continuous Dirac operator is not recovered.

Nielsen and Ninomiya [60] express this doubling problem in a theorem which is given here as a simple form for the free Dirac operator following [45]. By using the free Dirac operator  $\tilde{D}(p)$  in momentum space the theorem states that the following properties can not coexist:

- (a)  $\tilde{D}(p)$  is an analytic and periodic function in the momenta  $p_\mu$  with periodicity  $2\pi/a$ ,

## 2. Theory

---

(b) the continuum limit for  $\tilde{D}(p)$  is given by  $\tilde{D}(p) = i\gamma_\mu p_\mu + \mathcal{O}(ap^2)$ ,

(c)  $\tilde{D}(p)$  is invertible for all non-zero momenta and

(d)  $D\gamma_5 = -\gamma_5 D$ .

The condition (a) states that  $D$  is a local operator, the conditions (b) and (c) ensure that  $D$  has the correct continuum limit and condition (d) is the continuous chiral symmetry of the Dirac operator. A consequence is that an action which fulfills (b) violates at least one of the requirements (a), (c) or (d).

Wilson's approach is to shift 15 of these fermions towards the UV-cut-off while performing the continuum limit. The idea is to add an irrelevant  $\mathcal{O}(a^5)$  operator to the naive fermion action, the so called Wilson term

$$\begin{aligned}\Delta_W(r)_{xy} &= \frac{ar}{2} (D_\mu^* D^\mu)_{xy} \\ &= -\frac{4r}{a} \delta_{x,y} + \frac{r}{2a} \sum_\mu (U_\mu(x) \delta_{x,y-\hat{\mu}} + U_\mu^\dagger(x-\hat{\mu}) \delta_{x,y+\hat{\mu}}).\end{aligned}\quad (2.33)$$

Now the propagator in the free case becomes

$$\frac{1}{a} \tilde{S}(p) = \frac{-i\gamma_\mu \sin(p_\mu a) + ma - r \sum_\mu (\cos(p_\mu a) - 1)}{\sum_\mu \sin^2(p_\mu a) + [ma - r \sum_\mu \cos(p_\mu a) - 1]^2}.\quad (2.34)$$

This gives a mass term proportional to  $r/a$  to the non-physical fermions which decouple in the continuum limit due to the divergence. The Wilson Dirac operator [3]

$$D(m, r) = D_{naive}(m) - \Delta_W(r)\quad (2.35)$$

does not fulfill the condition (d) and breaks chiral symmetry explicitly. The parameter  $r$  is conventionally set to unity. For a finite coupling the physical fermion gets an additional mass shift which is perturbatively known [61] and is given to the first order in the coupling constant by

$$am_c = -0.43413 \cdot \frac{6}{\beta} + \mathcal{O}\left(\frac{1}{\beta^2}\right).\quad (2.36)$$

The critical mass  $m_c$  can be defined by requiring that the partially conserved axial current (PCAC) mass vanishes. At zero quark masses chiral symmetry is restored in the continuum limit [62]. However the smallest eigenvalue of  $\sqrt{D^\dagger D}$  is unbounded and fluctuates with  $\sigma \sim \sqrt{V}^{-1}$  [8]. The eigenvalues of  $\sqrt{D^\dagger D}$  are directly connected to the singular values of the Wilson Dirac operator. This limits the Monte Carlo simulation where the inversion of  $D$  is required and physical

quark masses can be achieved only for large lattice volumes.

The Wilson term breaks the anti-hermiticity of the naive operator and the Wilson Dirac operator is non-normal, even for zero PCAC quark mass. However due to the  $\gamma_5$ -hermiticity, which is given by  $D = \gamma_5 D^\dagger \gamma_5$ , the determinant remains real and the eigenvalues come in complex conjugate pairs or are real. It is possible to improve the continuum extrapolation by adding an additional irrelevant  $\mathcal{O}(a^5)$  term, the so called clover-term [63]

$$D_{sw} = a \cdot \sigma_{\mu\nu} \hat{F}_{\mu\nu} \delta_{x,y} \quad (2.37)$$

with the matrices  $\sigma_{\mu\nu} = -i/2[\gamma_\mu, \gamma_\nu]$  which act on the spinor space and the matrices  $\hat{F}_{\mu\nu} = i/8(Q_{\mu\nu}(x) - Q_{\mu\nu}^\dagger(x))$  with the clover plaquette term

$$Q_{\mu\nu} = P_{\mu,\nu}(x) + P_{-\nu,\mu}(x) + P_{-\mu,-\nu}(x) + P_{\nu,-\mu}(x) \quad (2.38)$$

which act on the color space. The clover plaquette terms are given exactly with  $P_{\mu,\nu}(x) = P_{\mu\nu}(x)$  (eq. (2.24)) and

$$\begin{aligned} P_{-\nu,\mu}(x) &= U_\nu^\dagger(x - \hat{\nu}) U_\mu(x - \hat{\nu}) U_\nu(x - \hat{\nu} + \hat{\mu}) U_\mu^\dagger(x + \hat{\mu}), \\ P_{-\mu,\nu}(x) &= U_\mu^\dagger(x - \hat{\mu}) U_\nu^\dagger(x - \hat{\mu} - \hat{\nu}) U_\mu(x - \hat{\mu} - \hat{\nu}) U_\nu(x - \hat{\nu}) \quad \text{and} \\ P_{\nu,-\mu}(x) &= U_\nu(x) U_\mu^\dagger(x + \hat{\nu} - \hat{\mu}) U_\nu^\dagger(x - \hat{\mu}) U_\mu(x - \hat{\mu}). \end{aligned}$$

The  $\mathcal{O}(a)$ -improved Wilson Dirac operator is then given by

$$D_w(m, c_{sw}) = D_{naive}(m) - \Delta_W(1) + c_{sw} D_{sw} = \left(\frac{4}{a} + m\right) \delta_{xy} + \frac{1}{2a} \mathcal{K}(U, c_{sw}) \quad (2.39)$$

with a properly chosen parameter  $c_{sw}$  [64]. Note the clover term acts also on the critical mass term and the coefficient of eq. (2.36) changes to  $-0.27008$  for  $c_{sw} = 1.0$  (see [61] for a precise derivation). By defining the hopping parameter

$$\kappa = \frac{1}{2(4 + am)} \quad (2.40)$$

and rescaling the fermion fields by

$$a^{3/2} \sqrt{am + 4} \psi(x) \rightarrow \psi(x) \quad \text{and} \quad a^{3/2} \sqrt{am + 4} \bar{\psi}(x) \rightarrow \bar{\psi}(x) \quad (2.41)$$

the Wilson Dirac operator in the matrix representation has the form

$$D(m) = I + \kappa \mathcal{K}(U). \quad (2.42)$$

where the  $c_{sw}$ -term dependence is implicit and  $I$  is the unit matrix in  $\mathbb{C}^{12V \times 12V}$ .

## 2. Theory

---

In general many fermion discretizations exist which have pros and cons. An interesting approach is the Neuberger overlap operator [65] which fulfills a modified lattice version of the chiral symmetry, the Ginsberg-Wilson relation [66]. However operators which fulfill (approximately) this symmetry need a larger numerical effort compared to Wilson type fermions and are in principle difficult to simulate (e.g. have difficulties with ergodicity [67]). Here, Wilson fermions are used, a common lattice version due to the fact that a relatively low effort is needed in computations compared to other fermion discretizations on the lattice.

### Remarks

- **Boundaries:** It is common to close the lattice periodically up to a phase, which is called *periodic boundary conditions*. In general in this thesis *anti-periodic boundary conditions* are used. For *anti-periodic boundary conditions* the quark fields are multiplied with  $e^{i\pi}$  at the temporal boundary, while at the spatial boundaries the quark fields remain periodic. For an algorithm comparison *open boundary conditions* are used in this work. In this case the gauge links are set to zero in time direction at the boundaries, while the gauge links at the spatial boundaries remain periodic. For *Dirichlet boundary conditions* the gauge links in the boundaries are set to zero for all directions. For the free case follows that the fermion modes have a lowest momentum with  $p_\mu = \pi/L$ . This is different in the case of periodic boundary condition where  $p_\mu = 0$  is possible.
- **Finite volume effects:** Measurements on the lattice are influenced by the finite size and discretization. Both effects have to be taken into account if physical quantities are determined by LQCD. The finite volume effects can be understood on a periodic lattice by the self-interaction of particles. In the case of pions this increases the mass  $m_\pi$ . In general these finite size effects are small for lattices which fulfill  $Lm_\pi \geq 4$ . This makes lattice simulations expensive for decreasing lattice spacing and small pion masses. Note that finite size effects can be also effectively corrected by using chiral perturbation theory (see e.g. [68] [69]).
- **Discretization:** The finite discretization effects can be suppressed by improving the lattice action and operators. This can be done by removing the  $\mathcal{O}(a)$ -effects by adding additional irrelevant operators, like the clover term in the case of the Wilson Dirac operator or in the case of the axial vector current  $A_\mu$  (see subsec. 4.3.1). In general simulations are done for several lattice spacings in order to guarantee a proper continuum extrapolation.



## 2.5. Monte Carlo Methods

Using a proper lattice action, expectation values of observables can be evaluated on the discretized space by calculating the appropriate path integral depending on a bare parameter set  $a = \{\beta, m_1, m_2, \dots\}$

$$\langle O \rangle_a = \frac{1}{Z_a} \int O_a(U) e^{-S_a(U)} DU \quad (2.43)$$

where, for LQCD, the integration measure is given as a product over every link variable by  $DU = \prod_{x,\mu} dH(U_\mu(x))$  with the Haar measure  $dH$  of the group  $SU(3)$  (see e.g. [46]). The fermionic degrees of freedom are integrated out using the Matthews-Salam formula (compare subsec. 2.2.1) and the lattice action  $S_a(U)$  is given by

$$S_a(U) = S_g(\beta) - \sum_{j=1}^{n_f} \ln(\det D(U, m_j)). \quad (2.44)$$

A common method used to evaluate high dimensional integrals like eq. (2.43) is Monte Carlo integration. In the case of the path integral, the idea is to generate an ensemble, which is a set of representative field configurations, weighted by the Boltzmann weight  $P_a(U) = e^{-S_a(U)} / Z_a$ . The ensemble average is given by

$$\bar{O}_a = \frac{1}{N_{cnfg}} \sum_{j=1}^{N_{cnfg}} O(U_j) \quad (2.45)$$

and for eq. (2.43), it follows that

$$\langle O \rangle_a = \bar{O}_a + \mathcal{O}\left(\sqrt{N_{cnfg}^{-1}}\right). \quad (2.46)$$

This is only true if the generated configuration belongs to the equilibrium distribution which is reached for a sufficient long Markov Chain generated by a Monte Carlo algorithm.

A well-defined Monte Carlo algorithm has to fulfill several conditions in order that convergence to the equilibrium distribution is satisfied ( see e.g. [70] [71] [72] [73] [74] [75]). The general idea is to use *importance sampling* to sample the integral eq. (2.43). This is done by weighting the configurations with the Boltzmann weight  $P_a(U) = e^{-S_a(U)} / Z_a$ . A Markov Chain is defined by using the previous configuration  $U$  to propose a new configuration  $U'$  which is obtained with the transition probability  $T(U \rightarrow U')$ . The transition probability is a stochastic process and has

## 2. Theory

---

to fulfill the requirements

$$T(U \rightarrow U') \geq 0 \quad \text{and} \quad \int T(U \rightarrow U_j) DU_j = 1. \quad (2.47)$$

Additionally the probability distribution  $P_a(U)$  for the configuration has to fulfill

$$P_a(U) > 0 \quad \text{and} \quad \int P_a(U_j) DU_j = 1, \quad (2.48)$$

since the Boltzmann weight has to be real and positive. This can be achieved in LQCD by working in Euclidean space (see sec. 2.2). Systems which do not fulfill these requirements suffer under the so-called sign-problem.

It is possible to show that if the Markov chain can reach, for a finite Monte Carlo time, every possible configuration (*ergodicity*) and  $T(U \rightarrow U) > 0$  and fulfill the stability condition

$$P_a(U') = \int P_a(U_i) T(U_i \rightarrow U') DU_i \quad (2.49)$$

that the Monte Carlo algorithm converges to the equilibrium probability distribution and eq. (2.46) is true. In practice a sufficient condition is used to satisfy the stability condition eq. (2.49). The sufficient condition is given by

$$P_a(U) T(U \rightarrow U') = P_a(U') T(U' \rightarrow U) \quad \forall U, U'. \quad (2.50)$$

In general this condition, called *detailed balance*, is used to prove the correctness of the Monte Carlo algorithms in lattice QCD.

There exist several approaches for a transition probability and in LQCD combinations of several transition probabilities are used to generate a properly weighted ensemble, like in the case of the Hybrid Monte Carlo or the Partial Stochastic Multi Step algorithm.

The most common definitions are

- **Metropolis algorithm:** The transition probability of the Metropolis algorithm [29] is given by

$$T(U \rightarrow U') = \min \left\{ 1, \frac{P_a(U')}{P_a(U)} \right\} P(U \rightarrow U') + (1 - A) \delta_{U,U'} \quad (2.51)$$

where  $P(U \rightarrow U')$  is the probability of the proposal  $U \rightarrow U'$  and  $A = \int P(U \rightarrow U'') \min\{1, P(U)/P(U'')\} DU''$ . The probability of the proposal has to be symmetric,  $P(U \rightarrow U') = P(U' \rightarrow U)$ . The Metropolis algorithm was originally introduced 1953 by Metropolis et al. [29] and the Metropolis accept-reject step is used to correct the proposal  $U'$  towards the weight  $P_a(U')$ . In practice, a random number  $r$  selected from the interval  $[0, 1)$  is

used to accept or reject the configuration  $U$ . The new configuration will be accepted if  $r < \min\{1, P_a(U')/P_a(U)\}$ . Otherwise the configuration will be rejected and a new configuration has to be proposed based on  $U$ .

- **Heat bath algorithm:** A transition probability is straightforwardly given by

$$T(U \rightarrow U') = P_a(U'). \quad (2.52)$$

However a proposal of a properly distributed configuration  $U'$  under the distribution function  $P_a(U')$  is limited to simple distribution functions, e.g. if  $P(x) = \exp\{-x^2\}/\sqrt{\pi}$ , it is possible to propose randomly an exponential distributed  $x$ . This is independent sampling. This can not be realized in practice because the configuration space is huge. In the case of a pure gauge action, an efficient algorithm exists [76] [77] for updating one link at a time, which is called a heat bath. It is a combination of a independent sampled trial distribution and a correction step to get the proper weight.

The expectation value eq. (2.46) can be evaluated by using an ensemble average over the sampled configurations. This ensemble is finite and it is necessary to estimate the error of the approximation. Following eq. (2.46) the error of a Monte Carlo sampled ensemble is reduced proportional to the square root of the number of configurations  $\sqrt{1/N_{cnfg}}$ . In appendix D, a detailed discussion of the errors is presented based on [78]. In general, the error of an observable  $O$  is given by  $\delta O = \sqrt{2\tau_{int}\sigma^2(O)/N_{cnfg}}$  with the integrated autocorrelation time  $\tau_{int} \geq 0.5$  which takes into account that the configurations are correlated with each other. The variance  $\sigma^2(O)$  is defined by

$$\sigma^2(O) = \langle O^2 \rangle - \langle O \rangle^2. \quad (2.53)$$

In LQCD, the autocorrelation times increase with decreasing lattice spacing  $a$  and are a property of the specific Monte Carlo algorithm. This can spoil simulations, i.e. for very fine lattices in the case of the Hybrid Monte Carlo algorithm [27].

### 2.5.1. Hybrid Monte Carlo Algorithm

The Hybrid Monte Carlo (HMC) algorithm [79] [80] can sample configurations weighted with a lattice fermion action. A direct weighting with the fermion determinant is not feasible. The computational cost would increase with the third power of the size of the matrix  $\mathcal{O}(n^3)$ . The general idea is to use an integral identity to rewrite the determinant of a non-singular matrix  $D$  [4] [5] as

$$\det [D^\dagger(U, m)D(U, m)] = \int e^{-\eta^\dagger [D(U, m)D^\dagger(U, m)]^{-1} \eta} \mathcal{D}[\eta], \quad (2.54)$$

## 2. Theory

---

where  $\eta^\dagger (DD^\dagger)^{-1} \eta > 0$  for all  $\eta \in \mathbb{C}^{12V} \setminus 0$  with a normalized integral measure  $D[\eta] = \prod_{j=1}^{12V} dx_j dy_j / \pi$ . Now the so-called pseudofermion fields  $\eta$  can be treated as new field variables, and the lattice action is given by

$$S_a(U, \eta) = S_g(\beta) + \eta^\dagger \left[ D(U, m_j) D^\dagger(U, m_j) \right]^{-1} \eta. \quad (2.55)$$

Note that in a Monte Carlo algorithm, the integral eq. (2.54) has to be positive and real. In general, lattice QCD simulations are performed in the isospin symmetric case by setting the lightest quarks to the same value  $m_{ud}$ . For Wilson Dirac fermions the positive definiteness of the operator which enters the integrand, eq. (2.54), can be imposed in the light quark sector by using the  $\gamma_5$  hermiticity and with  $\det \gamma_5 = 1$  follows

$$\det D^2(U, m_{ud}) = \det \left[ D^\dagger(U, m_{ud}) D(U, m_{ud}) \right]. \quad (2.56)$$

The idea of the HMC algorithm is to use the Hybrid Molecular Dynamics techniques to update the configuration by an integration of the corresponding Hamiltonian in the microcanonical ensemble (see e.g. [81]). This can be performed by numerical integration schemes which have to be time reversible and area preserving in order to satisfy the condition of detailed balance. In the case of LQCD the molecular dynamics requires fields which belong to  $\mathfrak{su}(3)$  [82] and can be defined by

$$\pi_\mu(x) = \pi_\mu^a(x) t^a \quad \pi^a(x) \in \mathbb{R} \quad (2.57)$$

with the generators  $t^a$  of  $SU(3)$ . In general these variables can be added to the LQCD action by the integral identity

$$\int \mathcal{O}(U) e^{-S(U)} DU = \int \mathcal{O}(U) e^{-H(U, \pi)} DU D\pi \quad (2.58)$$

with the Hamiltonian

$$H(U, \pi) = \frac{1}{2}(\pi, \pi) + S(U) \quad (\pi, \pi) = \sum_{x, \mu} \pi_\mu^a(x) \pi_\mu^a(x), \quad (2.59)$$

an observable  $\mathcal{O}(U)$  which depends on the gauge field  $U$  and a normalized integral measure  $D\pi$ . Note by adding so called auxiliary variables or conjugate momenta  $\pi$  to the action, the results remain unchanged. Now, the system can be integrated via Hamilton's equations [82] which change in the  $\mathfrak{su}(3)$ -case to

$$\dot{U}_\mu(x) = \pi_\mu(x) U_\mu(x) \quad \text{and} \quad \dot{\pi}_\mu(x) = -F_\mu(x) \quad (2.60)$$

with the force term

$$F_\mu^a(x) = \left. \frac{\partial S(e^\omega U)}{\partial \omega_\mu^a(x)} \right|_{\omega=0}. \quad (2.61)$$

The integration is called Hybrid Molecular Dynamics. For a more mathematical formal introduction see [83]. The time differential in the Hamilton equation eq. (2.60) is done with respect to a fictitious time, the ‘‘Molecular dynamic time’’. An integration unit of  $\tau = 1$  is called Molecular Dynamic Unit (MDU). By integrating the equations in this time the variables  $U_\mu(x)$  and  $\pi_\mu(x)$  perform trajectories in field space.

For a two flavor mass-degenerate fermion action, the simple Hybrid Monte Carlo algorithm is given by

1. **Generating of conjugated momenta:** The momenta are generated by a heat bath via the gaussian distribution  $P(x) = 1/\sqrt{2\pi} \exp\{-x^2/2\}$ .
2. **Generating of pseudofermion fields:** The pseudofermion field can be generated by a heat bath at the beginning of the trajectory. The pseudofermion field  $\eta \in \mathbb{C}^{12V}$  has to be distributed by

$$P(\eta) = 1/\pi^{12V} 1/\det[D^\dagger(U, m)D(U, m)] \exp\{-\eta^\dagger [D(U)D^\dagger(U)]^{-1} \eta\}. \quad (2.62)$$

The approach is to generate a complex field  $\chi = x + i \cdot y \in \mathbb{C}^{12V}$  with  $P(x_j) = 1/\sqrt{\pi} \exp\{-x_j^2\}$  and  $P(y_j) = 1/\sqrt{\pi} \exp\{-y_j^2\}$ . By substituting  $\eta = D(U, m) \cdot \chi$  it follows that the pseudofermion field is distributed via  $P(\eta)$  eq. (2.62).

3. **Integration of Hamiltons equations:** The Hamilton equations eq. (2.60) are integrated via a numerical integration scheme. Detailed balance requires that the integrator is time reversible and area preserving. In general the integration scheme can be constructed by the operations (see e.g. [81])

$$\mathcal{J}_0(\epsilon) : \pi, U \rightarrow \pi - \epsilon F, U \quad \text{and} \quad \mathcal{J}_U(\epsilon) : \pi, U \rightarrow \pi, e^{\epsilon\pi} U. \quad (2.63)$$

Now, the integration from  $t = 0$  to  $t = \tau$  can be given by the leap frog scheme with

$$\mathfrak{J}(\epsilon, N) = \left( \mathcal{J}_0\left(\frac{\epsilon}{2}\right) \mathcal{J}_U(\epsilon) \mathcal{J}_0\left(\frac{\epsilon}{2}\right) \right)^N \quad (2.64)$$

with  $\epsilon = \tau/N$ . The discretization errors increase as  $\delta H \propto N\epsilon^3 = \epsilon^2\tau$  by using a leap frog integration scheme. Note the pseudofermion field is kept constant during the integration. The integration is time reversible if the momenta at the endpoint are changed to  $\pi(t = \tau) \rightarrow -\pi(t = \tau)$ .

4. **Metropolis accept–reject step:** The usage of a numerical integration scheme introduces discretization errors and the energy conservation is violated. For a proper sampling the weight of the new configuration has to be corrected. The correction is done by a Metropolis accept–reject step with the acceptance probability

$$P_{acc}(U(t=0) \rightarrow U(t=\tau)) = \min \left\{ 1, e^{-\delta H} \right\} \quad (2.65)$$

with the difference of the Hamiltonians

$$\delta H = H(U(t=\tau), \pi(t=\tau), \eta) - H(U(t=0), \pi(t=0), \eta). \quad (2.66)$$

The procedure 1. – 4. is iterated. The cost of the HMC is given by the integration and the Metropolis accept–reject step. During the integration the force has to be evaluated. This requires two inversions per integration step for the introduced fermion action. In general the inversion of the Wilson Dirac operator scales with the lattice size  $V$  see e.g. [84]. The fluctuations of  $\delta H$  determine the acceptance rate. In general the integration step size has to be decreased by  $\sqrt[4]{V}$  to keep the acceptance rate constant (see e.g. [54]). Moreover in Monte Carlo simulations, the autocorrelation time increases the cost. In case of the HMC the autocorrelation time scales with  $a^{-5}$  in the lattice spacing on a lattice without boundary conditions [27, 85].

To summarize the cost for generating a new decorrelated configuration by the HMC algorithm on a lattice with anti–periodic boundary condition is proportional to

$$cost_{HMC}(U \rightarrow U') \propto V_{phys}^{5/4} a^{-10} \quad (2.67)$$

with the physical volume  $V_{phys} = Va^4$  [27] by neglecting the quark mass dependence. Since 1987 several improvements of the HMC are introduced which enable the HMC algorithm to become a method to simulate dynamical fermions at physical quark masses. One improvement is given by the Hasenbusch mass preconditioning [86]. The idea is to introduce additional pseudofermion fields in the Hybrid Molecular Dynamics. This can be done by splitting up the fermion weight like

$$\det D(U, m_1) = \det M(U, m_1, m_2) \cdot \det D(U, m_2) \quad (2.68)$$

with the ratio matrix  $M = D^{-1}(U, m_2)D(U, m_1)$ . By choosing  $m_1 < m_2$  the absolute values of the forces decrease which makes it possible to simulate smaller quark masses. A similar idea is given by Domain Decomposition [31], which will be discussed in detail in sec. 4.1. Note that in principle the cost of the algorithm increases by lowering the quark mass, i.e. the solver costs increase and the integration step size has to be decreased because the force increases.

### 3. Numerical Computation of Determinants

The fermionic part of the Boltzmann factor

$$P(U) = \frac{1}{Z} \exp\{-\beta S_g(U)\} \cdot \prod_{i=1}^{n_f} \det D(U, m_i, \dots) \quad (3.1)$$

of LQCD is given by a product of determinants of the lattice Dirac operator as a function of the bare mass parameters  $m_i$  of all flavors. The determinants make the Boltzmann weight non-local in the gauge field and dominates the computational costs of today's lattice calculations.

In this chapter a technique to deal with determinants as a weight factor will be introduced. The three main methods of this thesis are based on this technique. The pseudofermion integral, which rewrites the determinant into an integral is reintroduced and modified. The idea is to use stochastic estimation to evaluate this integral which introduces stochastic fluctuations. The stochastic fluctuations can be understood by rewriting the determinant into a trace power series by using a perturbative series of the specific matrix. The chapter will be closed by an introduction of an interpolation technique to improve and control the stochastic estimation.

#### 3.1. Definition of the Pseudofermion Integral

Since the early days of LQCD it was clear that a direct calculation of the determinants in numerical computations is quite difficult. The cost to calculate a determinant increases to the third power with the size of the matrix. This is practical only on small lattices up to around  $6^4$ .

The idea is to rewrite the determinant as a complex integral [5] [4]. Here a more general identity is introduced which holds also for non-normal complex matrices  $A \in \mathbb{C}^{n \times n}$ , see app. A

$$\frac{1}{\det A} = \int e^{-\eta^\dagger A \eta} D[\eta] \quad \text{if } \operatorname{Re}(\eta^\dagger A \eta) > 0 \quad \forall \eta \in \mathbb{C}^n \setminus 0 \quad (3.2)$$

### 3. Numerical Computation of Determinants

---

with a complex pseudofermion field  $\eta \in \mathbb{C}^n$  and a normalized integral measure by  $D[\eta] = \prod_{j=1}^n dx_j dy_j / \pi$  with  $\eta_j = x_j + iy_j$ . This integral representation of the determinant of a non-hermitian matrix has some advantages to the standard approach (see e.g. [4] [5]), for example it can deal with complex determinants. The condition  $\text{Re}(\eta^\dagger A \eta) > 0$  of eq. (3.2) is equivalent to  $\lambda(A + A^\dagger) > 0$ , with  $\lambda(B) = \{\lambda_i | B\psi_i = \lambda_i \psi_i, \lambda_i \in \mathbb{C}, \psi \in \mathbb{C}^n\}$  the eigenvalue spectrum of the matrix  $B \in \mathbb{C}^{n \times n}$ .

### 3.2. Stochastic Estimation

In order to evaluate a high dimensional integral like in eq. (3.2), a common method used in numerical mathematics is Monte Carlo integration. By selecting  $N_\eta$  random complex valued fields  $\eta$  distributed via the normalized distribution function  $\propto e^{-\eta^\dagger \eta}$ , an unbiased stochastic estimation of the integral eq. (3.2) is given by

$$\int \exp\{-\eta^\dagger A \eta\} D[\eta] = \frac{1}{N_\eta} \sum_{i=1}^{N_\eta} \left[ \frac{\exp\{-\eta_i^\dagger A \eta_i\}}{\exp\{-\eta_i^\dagger \eta_i\}} \right] + \mathcal{O}\left(\frac{1}{\sqrt{N_\eta}}\right). \quad (3.3)$$

The error of a Monte Carlo integration behaves like  $\sigma_{st} / \sqrt{N_\eta}$  with  $\sigma_{st}^2$  the variance of the stochastic estimation which is labeled as stochastic fluctuations.

In general the variance of the stochastic estimation is given by

$$\sigma_{st}^2 = \left\langle e^{-\eta^\dagger (A + A^\dagger - 2I) \eta} \right\rangle_\eta - \left\langle e^{-\eta^\dagger (A - I) \eta} \right\rangle_\eta \left\langle e^{-\eta^\dagger (A^\dagger - I) \eta} \right\rangle_\eta \quad (3.4)$$

where  $\langle f \rangle_\eta = \int e^{-\eta^\dagger \eta} f(\eta) D[\eta]$  is the average over the field  $\eta$  distributed by  $\exp(-\eta^\dagger \eta)$ . Note this quantity is the sum of the variance of the real part and the imaginary part of the stochastic estimation (see app. B). From eq. (3.2) it follows

$$\left\langle e^{-\eta^\dagger (A + A^\dagger - 2I) \eta} \right\rangle_\eta = \int e^{-\eta^\dagger (A + A^\dagger - I) \eta} D[\eta] = \frac{1}{\det(A + A^\dagger - I)} \quad (3.5)$$

if and only if the condition

$$\lambda(A + A^\dagger) > 1 \quad (3.6)$$

is fulfilled. With the second term of eq. (3.4) the variance reduces to

$$\sigma_{st}^2 = \frac{1}{\det(A + A^\dagger - I)} - \frac{1}{\det(A^\dagger A)}. \quad (3.7)$$

If the matrix  $A$  is hermitian it is obvious that an eigenvalue  $\lambda = 1$  of  $A$  does not



contribute to the variance. In general methods, which act such on a spectrum of a matrix that the eigenvalues get closer to one, decrease the variance.

#### Remarks

- **Variance of stochastic estimation:** The variance of the stochastic estimation is an appropriate tool to control the correctness and to enhance the effectiveness of the method. The necessary condition for the existence of the variance  $\lambda(A + A^\dagger) > 1$  is a sufficient condition for the existence of the identity eq. (3.2) and is easy to detect in practice.
- **Usage of the pseudofermion integral:** There are two different contexts in which the so called “pseudofermion” integral eq. (3.2) appears. Firstly by redefining the Boltzmann weight  $P(U) \rightarrow P(U, \eta)$  and introducing the complex field  $\eta$  as new degrees of freedom and secondly by a direct stochastic estimation. The former case is used in the algorithm framework, i.e for the Hybrid Monte Carlo algorithm (see subsec. 2.5.1). For this case the complex field  $\eta$  is called “pseudofermion field” [4] [5] and it is only possible to draw one field to represent eq. (3.2) in order to satisfying detailed balance (see e.g. app. E). This is different in the latter case, which is used in mass reweighting. Here it is possible to draw  $N_\eta$  complex fields  $\eta$  to estimate eq. (3.2).

### 3.3. Fluctuations

Monte Carlo integration of the path integral generates a representative ensemble of field configurations which introduces ensemble fluctuations due to the finite sample size (see sec. 2.5). By using a stochastic estimator to evaluate an observable additional stochastic fluctuations are introduced on top of these ensemble fluctuations. In principle these stochastic fluctuations can always be reduced by increasing the numerical effort.

Here the behavior of the fluctuations for the estimation of the integral eq. (3.3) is derived by using an expansion in a parameter  $\epsilon$ . The matrix  $A$  is rewritten as  $A = 1 + \epsilon H + \mathcal{O}(\epsilon^2)$  (see app. B for a general discussion and [6] for the hermitian case). By drawing  $N_\eta$  pseudofermion fields the fluctuations of the determinant

### 3. Numerical Computation of Determinants

---

are given by

$$\begin{aligned} \sigma^2 &= \left\langle \left\langle \frac{1}{N_\eta^2} \sum_{j,k=1}^{N_\eta} e^{-\eta_j^\dagger (A-I)\eta_j - \eta_k^\dagger (A^\dagger - I)\eta_k} \right\rangle_\eta \right\rangle \\ &\quad - \left\langle \left\langle \frac{1}{N_\eta} \sum_{j=1}^{N_\eta} e^{-\eta_j^\dagger (A-I)\eta_j} \right\rangle_\eta \right\rangle \left\langle \left\langle \frac{1}{N_\eta} \sum_{k=1}^{N_\eta} e^{-\eta_k^\dagger (A^\dagger - I)\eta_k} \right\rangle_\eta \right\rangle, \end{aligned} \quad (3.8)$$

where  $\langle \rangle$  is the ensemble average over the gauge fields  $U$  and

$$\langle f \rangle_\eta = \int (f(\eta_1, \dots, \eta_{N_\eta}) \prod_{j=1}^{N_\eta} e^{-\eta_j^\dagger \eta_j} \mathcal{D}[\eta_j]). \quad (3.9)$$

The integration over  $\eta_j$ 's gives (see app. B)

$$\begin{aligned} \sigma^2 &= \frac{1}{N_\eta} \left( \left\langle \frac{1}{\det(A + A^\dagger - I)} \right\rangle - \left\langle \frac{1}{\det AA^\dagger} \right\rangle \right) \\ &\quad + \left\langle \frac{1}{\det AA^\dagger} \right\rangle - \left\langle \frac{1}{\det A} \right\rangle \left\langle \frac{1}{\det A^\dagger} \right\rangle. \end{aligned} \quad (3.10)$$

The stochastic fluctuations decouple exactly from the ensemble fluctuations and are given by

$$\sigma_{st}^2 = \frac{1}{N_\eta} \left( \left\langle \frac{1}{\det(A + A^\dagger - I)} \right\rangle - \left\langle \frac{1}{\det AA^\dagger} \right\rangle \right). \quad (3.11)$$

The ensemble fluctuations are

$$\sigma_{ens}^2 = \left\langle \frac{1}{\det AA^\dagger} \right\rangle - \left\langle \frac{1}{\det A} \right\rangle \left\langle \frac{1}{\det A^\dagger} \right\rangle \quad (3.12)$$

and  $\sigma^2 = \sigma_{st}^2 + \sigma_{ens}^2$ . Using  $\det A = \exp\{\text{Tr} \ln A\}$  and expanding in  $\epsilon$  (see app. B) the stochastic fluctuations reduce to

$$\sigma_{st}^2(N_\eta) = \frac{\epsilon^2}{N_\eta} \left\langle \text{Tr} (H^\dagger H) \right\rangle + \mathcal{O}(\epsilon^3). \quad (3.13)$$

For the ensemble fluctuations it follows that

$$\sigma_{ens}^2 = \epsilon^2 \text{var} (\text{Tr} (H)) + \mathcal{O}(\epsilon^3) \quad (3.14)$$

by assuming  $H = \gamma_5 H^\dagger \gamma_5$  and using trace properties. If  $H$  is not  $\gamma_5$ -hermitian the ensemble fluctuations eq. (3.14) are given by the covariance of  $\text{Tr}H$  and  $\text{Tr}H^\dagger$  (see app. B). By increasing  $N_\eta$  it is possible to control the precision of the stochastic estimation and the fluctuations are dominated by the ensemble fluctuations for sufficiently large  $N_\eta$ . However this is only true if the variance eq. (3.6) is defined. Note increasing  $N_\eta$  has no effect on the eigenvalues of the matrix  $A$ . If the stochastic variance is not defined or a larger number of  $N_\eta > 1$  is not allowed (e.g. due to detailed balance in the PSMS algorithm see app. E) another method has to be introduced to control the stochastic fluctuations.

### 3.4. Fluctuations of Ratio Matrices controlled by Interpolation

The stochastic estimation of a determinant is constrained to matrices  $A$  which fulfill  $\lambda(A + A^\dagger) > 1$ . In practice, a small variance is needed implying that the eigenvalues have to cluster around one. It is possible to show that this is the case for ratio matrices  $A = B'/B$  if the matrices are not singular as it is shown below. This is always the case if the matrix is hermitian and positive definite. By using the  $n$ th root [87] the determinant can be split up into a product

$$\det A = \prod_{j=1}^n \det A^{1/n}. \quad (3.15)$$

By writing  $A = 1 + \epsilon H$  the  $n$ th root of  $A$  is given by

$$A^{1/n} = (1 + \epsilon H)^{1/n} = 1 + \frac{1}{n}\epsilon H + \left(\frac{1}{n^2} - \frac{1}{n}\right)\epsilon^2 H^2 + \mathcal{O}(\epsilon^3). \quad (3.16)$$

If for sufficiently large  $n$  the spectral norm of  $\|\frac{\epsilon}{n}H\|$  fulfills  $\|\frac{\epsilon}{n}H\| < 1$ , the eigenvalues of  $A^{1/n}$  cluster around one. For large enough  $n$  it can be inferred that the condition for the integral representation eq. (3.2) is fulfilled. However, the same principle also works for applications without root matrix functions. The idea is to factorize the matrix ratio further. Let

$$A = \frac{B'}{B} = 1 + \epsilon H \quad (3.17)$$

with  $B' = B + (B' - B)$  and  $\epsilon H = (B' - B)/B$ . The ratio can be factorized by introducing intermediate matrices like  $B'' = (B + B')/2$  which is the simplest choice. It follows that

$$A = \frac{B''}{B} \frac{B'}{B''} \quad (3.18)$$

### 3. Numerical Computation of Determinants

---

with

$$\frac{B''}{B} = 1 + \frac{1}{2} \frac{B' - B}{B} \quad (3.19)$$

and similarly

$$\frac{B'}{B''} = 1 + \frac{1}{2} \frac{B' - B}{B''}. \quad (3.20)$$

Now by redefining  $E = (B' - B)$  and introducing  $N$  intermediate matrices

$$B_i = \frac{(N-i)}{N} B + \frac{i}{N} B' = B + i \frac{E}{N} \quad \text{with } i = 0, 1, \dots, N-1, N, \quad (3.21)$$

$B_0 = B$  and  $B_N = B'$ , the ratio can be factorized further with

$$\frac{B_{i+1}}{B_i} = 1 + \frac{1}{N} \frac{E}{B_i}. \quad (3.22)$$

If and only if the intermediate matrices are non-singular the spectral norm fulfills  $\|\frac{E}{N} H_i\| < 1 \forall i$  with  $H_i = 1/B_{i-1}$  for sufficiently large  $N$ . Note, if  $A$  is a non-normal matrix the spectral norm is given by  $\|A\| = \max \sqrt{\lambda(AA^\dagger)}$  which corresponds to the maximal singular value of  $A$ . The interpolation method acts on the eigenspace of the ratio matrix  $A$  and can control the stochastic estimation by using sufficient many interpolation steps  $N$ .

Up to first order increasing the number of interpolation steps  $N$  has the same effect on the variance as increasing  $N_\eta$ . By estimating each ratio independently

$$\frac{1}{\det A} = \prod_{j=1}^N \frac{1}{\det A_j} = \frac{1}{N_\eta} \prod_{j=1}^N \sum_{i=1}^{N_\eta} \exp \left\{ -\eta_{i,j}^\dagger (A_j - I) \eta_{i,j} \right\} + \mathcal{O} \left( \frac{1}{\sqrt{NN_\eta}} \right) \quad (3.23)$$

with  $A_i = B_i^{-1} B_{i-1}$  the stochastic estimation is unbiased. The stochastic fluctuations take the form by an expansion in  $1/N$

$$\sigma_{st}^2(N, N_\eta) \leq \frac{1}{NN_\eta} \max_i \left[ \text{Tr} \left( E^\dagger H_i^\dagger E H_i \right) \right] + \mathcal{O} \left( \frac{1}{N^2 N_\eta} \right). \quad (3.24)$$

At second order the interpolation differs from increasing  $N_\eta$ , which can be also observed via the eigenvalues in the hermitian case (see app. B.4). The interpolation technique is comparable to drawing more pseudofermion fields for one specific ratio if higher order corrections in eq. (3.24) are negligible. In general the interpolation techniques depend on the ratio and a detailed analysis is necessary to introduce additional improvements for the particular case.

## 4. Techniques for Lattice QCD

In the first part of this chapter methods to improve the stochastic estimation of a determinant and to suppress fluctuations will be described. The first method is Domain Decomposition of the lattice. It can be used to factorize the determinant of the Dirac operator into a part which couples mainly to the IR-modes and a part which couples to the UV-modes. Domain Decomposition is essential for the three main methods, the mass reweighting method, the PSMS-algorithm and the MDD-HMC algorithm. The second method can suppress the ensemble fluctuations by using correlations between different parts of the lattice actions. These correlations can be used to cancel parts of the fluctuations by introducing and tuning additional parameters.

In the second part of this chapter techniques to measure observables will be introduced, which are used to analyze the performance of the algorithm and to derive physical quantities. These are measurements of the PCAC (partial conservation of axial current) mass and the lightest pseudoscalar mass. Furthermore the Wilson flow will be introduced which can be used to measure the gluonic observable  $t_0$ . This observable can fix the scale. The chapter will end with the definition of the topological charge on the lattice. The topological charge couples to slow modes of the autocorrelation time in Monte Carlo simulations and can be used to analyze the scaling behavior of algorithms.

### 4.1. Domain Decomposition

Domain Decomposition (DD) methods are known from several mathematical and physical frameworks. The idea [7] is to decompose a problem into decoupled local components and into a component which couples the local components by incorporating the boundary parts. In principle this speeds up the calculations and through the localization it is ideal for parallelization.

#### 4.1.1. Schur Complement

Let  $A$  be a square matrix, then it is straightforward to impose a substructure on  $A$  by (see e.g. [88])

$$A = \begin{bmatrix} A_{11} & A_{12} \\ A_{21} & A_{22} \end{bmatrix}. \quad (4.1)$$

#### 4. Techniques for Lattice QCD

---

with square matrix elements  $A_{ij}$ . By demanding that  $A_{11}$  and  $A_{22}$  are invertible the Schur complement is defined by

$$\tilde{S} = 1 - A_{22}^{-1} A_{21} A_{11}^{-1} A_{12}. \quad (4.2)$$

The Schur complement is invertible if the inverse matrix  $A^{-1}$  exists. The inverse is given by

$$\tilde{S}^{-1} = \cancel{A}_{22} \cancel{A}_{22} = 1 - \cancel{A}_{21} \cancel{A}_{12} \quad (4.3)$$

with the inverse matrix

$$A^{-1} = \begin{bmatrix} \cancel{A}_{11} & \cancel{A}_{12} \\ \cancel{A}_{21} & \cancel{A}_{22} \end{bmatrix} \quad (4.4)$$

by using the same substructure as for the matrix  $A$ . The proof for eq. (4.3) follows by using  $\cancel{A}_{21} \cancel{A}_{11} + \cancel{A}_{22} \cancel{A}_{21} = 0$  and  $\cancel{A}_{21} \cancel{A}_{12} + \cancel{A}_{22} \cancel{A}_{22} = I$ . The crucial observation is that the determinant of the matrix factorizes exactly into

$$\det A = \det A_{11} \det A_{22} \cdot \det \tilde{S}. \quad (4.5)$$

However it is not obvious how the eigenvalues of the matrix  $A$  are connected to the Schur complement. A direct relation is only possible for a matrix with unit matrices  $A_{11}$  and  $A_{22}$ . It follows that the eigenvalues of the Schur complement  $\tilde{S}$  are given by

$$\lambda_{\tilde{S}} = \lambda_A (2 - \lambda_A) \quad (4.6)$$

with  $\lambda_A$  an eigenvalue of the matrix

$$A = \begin{bmatrix} 1 & A_{12} \\ A_{21} & 1 \end{bmatrix}. \quad (4.7)$$

The eigenvalue relation follows from  $A\psi = \lambda\psi$  and inserting  $\psi_1 + A_{12}\psi_2 = \lambda\psi_1$  into  $A_{21}\psi_1 + \psi_2 = \lambda\psi_2$  by eliminating  $\psi_1$ . If  $A$  is a positive definite hermitian matrix it follows by rescaling the eigenvalues to the interval  $(\mu, 1]$  with  $0 < \mu \ll 1$  that the eigenvalues of  $\tilde{S}$  belong to the interval  $(\mu(2 - \mu), 1]$ . It follows for  $\mu \ll 1$  that the condition number of the Schur complement is decreased by roughly  $1/2$ .

#### 4.1.2. DD in LQCD

In LQCD it is possible to decompose directly the lattice into sub-domains [89] [90] [31]. The dimension of these sub-domains depends on the problem, e.g. for the usage in Monte-Carlo algorithm it is useful that links which will be updated decouple from neighboring sub-domains, the so called active links. Here, 4 dimensional domains will be used by dividing the lattice into non-overlapping blocks (see fig. 4.1). For the following discussion a Dirac operator with nearest neighbor

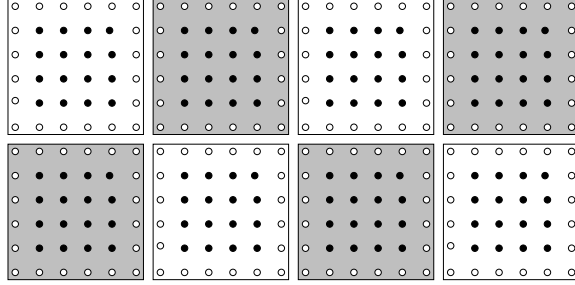


Figure 4.1.: The picture, taken from [31], shows a decomposition of a 2-dimensional lattice in non-overlapping black and white blocks.

coupling will be used, like the  $\mathcal{O}(a)$ -improved Wilson Dirac operator (see sec. 2.4).

By decomposing the lattice into similar blocks the blocks can be ordered into two groups, i.e. the blocks can be chessboard colored (see fig. 4.1). Blocks which belong to the same group do not have a shared boundary part and have only boundaries with blocks which belong to the other group. Now it is possible to label the lattice sites such that the sites which belong to the first black block come first, then the second black block and so on. After the last black block comes the first white block so that the Dirac operator can be written as

$$D = \begin{bmatrix} D_{bb} & D_{bw} \\ D_{wb} & D_{ww} \end{bmatrix}. \quad (4.8)$$

The operator  $D_{bb}$  and  $D_{ww}$  contains the block operators, which are Dirac operator  $D_b$  of the size of the blocks with Dirichlet boundaries while the operators  $D_{bw}$  and  $D_{wb}$  contain the coupling terms between the white and black blocks. The operator  $D_{bb}$  and  $D_{ww}$  are block diagonal if the Dirac operator contains only nearest neighbor coupling and have the same square size. Using eq. (4.5) the determinant factorizes into

$$\det D = \det \hat{D} \cdot \prod_k \det D_k \quad (4.9)$$

with the (projected) Schur complement

$$\hat{D} = 1 - P_{bw} D_{ww}^{-1} D_{wb} D_{bb}^{-1} D_{bw}. \quad (4.10)$$

The origin of the projector  $P_{bw}$  is due to the spin structure of the Dirac operator which imposes projectors in the spin space of the coupling terms between lattice points by  $1 \pm \gamma_\mu$ . The projector  $P_{bw}$  satisfies the properties  $D_{bw} P_{bw} = D_{bw}$  and

is restricted to the space of  $D_{bw}$  with  $\text{rank}(P_{bw}) = \text{rank}(D_{bw})$ . By using these properties it follows the relation

$$\det \tilde{D} = \det(1 - D_{ww}^{-1} D_{wb} D_{bb}^{-1} D_{bw} P_{bw}) \quad (4.11)$$

$$= \det(1 - P_{bw} D_{ww}^{-1} D_{wb} D_{bb}^{-1} D_{bw} P_{bw}) = \det \hat{D}, \quad (4.12)$$

by using Sylvester's determinant theorem [91] with

$$\det(1 + AB) = \det(1 + BA). \quad (4.13)$$

Now it is possible to project directly on the space of  $P_{bw}$  which reduces the dimension of the corresponding Schur complement. By using an elementary 4 dimensional geometry, the dimension of the projector is given by

$$\dim P_{bw} = 6 \prod_{\mu=0}^3 \frac{L_{\mu}}{l_{\mu}} \left( \sum_{\mu=0}^3 \frac{l_0 l_1 l_2 l_3}{l_{\mu}} - 4 \cdot \sum_{\mu=0}^3 (l_{\mu} - 1) \right) \quad (4.14)$$

where  $l_{\mu}$  is the block length and  $L_{\mu}$  the lattice length in direction  $\mu$ . If the volume  $V = T \times L^3$  is increased while keeping the ratio  $L_{\mu}/l_{\mu}$  fixed it follows that the dimension of  $P_{bw}$  only scales with  $V^{3/4}$ .

The factorization of the determinant into determinants of the blocks and the determinant of the Schur complement leads to the separation of UV- and IR-fluctuations. In the free theory modes of the blocks are bounded from below by  $a\pi/L$  due to the Dirichlet boundaries. The IR-modes are captured by the Schur complement. In LQCD domain decomposition can effectively decouple the UV- and the IR-modes. This makes DD efficient for many applications in LQCD like in the case of solvers [90], [84] or [92].

#### Remarks

- **Even-odd Wilson Dirac operator:** A special case is the so-called even-odd preconditioned Wilson Dirac operator. It is given by reordering the label of the lattice sites such that first comes every even point with  $(x_0 + x_1 + x_2 + x_3) \bmod 2 = 0$ . This is equivalent to decomposing the lattice in blocks of length  $l = 1$ . It follows that the Schur complement in this case is equal to the even-odd preconditioned Wilson Dirac operator. For the unimproved Wilson Dirac operator the eigenvalue relation eq. (4.6) is true and the condition number of the Schur complement is roughly a factor 2 smaller than for the non-decomposed operator.
- **Determinant factorization in practice:** In order to calculate the determinant by using eq. (4.9), it is efficient to use different techniques for different



sizes of matrices. For large matrices, a stochastic estimation is favored if the stochastic fluctuations can be controlled efficiently. For sparse matrices up to a size of  $12 \cdot 6^4$ , an exact calculation of the determinant via LU-decomposition has a relative moderate numerical effort and is possible. An appropriated algorithm is implemented and available in the Software package *UMFPACK* [93–95]. For example the LU-decomposition of the Wilson-Dirac operator of size  $12 \cdot 6^4$  takes roughly about 1 min on a single CPU (an AMD Opteron Processor 6172 with 2100 MHz). Note in this case there is no effect by using the even-odd preconditioned Wilson-Dirac matrix. The reason is that the LU-decomposition of the package profits from the sparse structure of the operator.

- **Recursive DD:** For some application larger blocks are favored, e.g. to have enough links which are decoupled from the neighboring blocks. It is possible to iterate the factorization further by using recursive DD and factorize the determinant of a block by

$$\det D_k = \det \hat{D}_k \cdot \prod_{k'} \det D_{k'} \quad (4.15)$$

with a Schur complement  $\hat{D}_k$  which obeys Dirichlet boundaries. Recursive DD is, in this work, implemented in the framework of the DD-HMC algorithm [96] (see for further information see app. C).

- **Active links:** To benefit from DD in an algorithmic framework it is useful to restrict the update only to the active links inside the blocks which do not couple to neighboring blocks. The active links will be defined by

$$l_{act} = (l - 2d) \quad (4.16)$$

with  $l$  the block length and  $d$  the minimal distance to the boundary of a point where an active link starts or ends. For the pure gauge action or the Wilson Dirac operator it follows that  $d \geq 0$ . For  $d = 0$ , links have at least one endpoint which is not in the boundaries of the block (see left fig. 4.2).

For an improved gauge action, such as the Lüscher–Weisz action [58] or for using smeared fermion actions, it is necessary to restrict the active links to the core of the blocks, e.g. by using an improved gauge action with a rectangular term which is given by

$$P_{\mu\nu}^{rec} = U_\mu(x)U_\nu(x + \hat{\mu})U_\nu(x + \hat{\mu} + \hat{\nu})U_\mu^\dagger(x + 2\hat{\nu})U_\nu^\dagger(x + \hat{\nu})U_\nu^\dagger(x) \quad (4.17)$$

the parameter  $d$  has to fulfill  $d \geq 1$  (see right fig. 4.2). Moreover for some applications it is useful to have  $d \geq 1$ , e.g. this is used in the PSMS algorithm

to achieve a better acceptance rate for larger blocks with  $l \geq 6$ .

The number of active links in a cube block is given by

$$N_{act.links}(l_{act}) = 4 \cdot (l_{act} - 2)^3 (l_{act} - 1). \quad (4.18)$$

For a block length of  $l = 8$  with  $l_{act} = 8$  the total amount of active links is given by  $R_{act} = 36.9\%$ . This reduces to  $R_{act} = 7.8\%$  for  $l_{act} = 6$ . In order to update all links the lattice has to be shifted. Note this has to be done in a way that detailed balance and ergodicity is preserved, e.g. by a randomized shift (see app. C of [31]).

- **DD-HMC:** Domain Decomposition can be used to improve the HMC algorithm (see subsec. 2.5.1). The idea [31] is to use the exact factorization of the determinant of the Dirac operator eq. (4.9). It is possible to introduce for each part an independent pseudofermion field. This factorizes the force terms and the blocks and the Schur complement can be treated independently in the HMC trajectory. By only updating the active links inside the blocks the blocks capture the fluctuations of UV-modes and the Schur complement the fluctuations of IR-modes. This tames the fluctuations in the force terms of the Schur complement [89]. Furthermore the first step of the algorithm has to be changed. Before the generation of the conjugate momenta is done the lattice has to be shifted so that all links of the lattice are updated iteratively. Due to the factorization of the force terms the Domain Decomposition-HMC (DD-HMC) algorithm can simulate smaller quark mass than the usual HMC algorithm.

## 4.2. Correlations

In a statistical framework it is important to control the variance of the finite data-sample, the ensemble fluctuations. A technique to minimize the total variance is given by using correlations with other quantities.

In LQCD, parts of the action are correlated, e.g. due to symmetries of the Dirac operator the UV-modes are correlated with the IR-modes. A quite obvious origin of correlations between parts of the lattice action is the dependence on the same gauge links. Due to this the UV-modes of the Dirac operator are strongly correlated with the plaquette action. This is easy to see by an expansion of the determinant in powers of the hopping parameter  $\kappa$ . The so called hopping parameter expansion is given by (see e.g. [54])

$$\det D(U) = \exp \{ \text{tr} [\log(1 + \kappa \mathcal{K}(U))] \} = \exp \left( - \sum_{j=1}^{\infty} \frac{\kappa^j}{j} \text{tr} [\mathcal{K}(U)^j] \right). \quad (4.19)$$

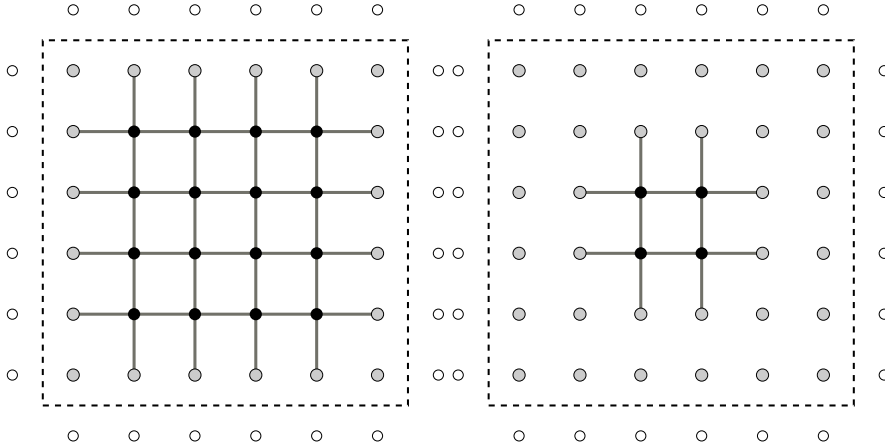


Figure 4.2.: The left figure, taken from [89], illustrates the active links in a two-dimensional block with length  $l = 6$  and  $d = 0$ . The right figure shows the active links for  $l = 6$  and  $d = 1$ .

For the unimproved Wilson Dirac operator the first term which depends on the gauge links is given by

$$\text{tr} [\mathcal{K}(\mathcal{U})^4] = -12 \sum_{x, \mu < \nu} \text{Re} (\text{tr} [P_{\mu\nu}]) \quad (4.20)$$

with  $P_{\mu\nu}$  the plaquette (see eq. (2.24)). It is possible to rewrite the determinant as a sum over a series of Wilson loops, closed loops of links. This was used to sample configurations with approximated lattice actions [97].

In this work the correlations are used to reduce the ensemble fluctuations, which enhance the acceptance in a Metropolis accept-reject step or for controlling the statistical error. In order to minimize the variance  $\sigma^2(A)$  (see eq. (2.53)) let us take a look to a combined variance by adding a quantity  $B$  which is parametrized by  $b$

$$\sigma^2(A + b \cdot B) = \sigma^2(A) + b^2 \sigma^2(B) + 2b \cdot \text{cov}(A, B) \quad (4.21)$$

with  $\text{cov}(A, B) = \langle A \cdot B \rangle - \langle A \rangle \langle B \rangle$  the covariance of the quantities  $A$  and  $B$ . By setting the parameter  $b$  to

$$b = -\frac{\text{cov}(A, B)}{\sigma^2(B)} \quad (4.22)$$

the overall variance is minimized. In the framework of the PSMS algorithm it is possible to introduce such parameters explicitly. An example is the correla-

tion between the determinant of the Wilson Dirac operator and the plaquette. It is straightforward to introduce a beta-shift, a shift in the pure gauge coupling  $\beta$ , which can be determined by the covariance of both terms. If the observable is a more complicated function of the parameter the determination of the shift eq. (4.22) does not hold anymore and the determination has to be done by an approximation. In this work the usage of correlations between different parts of the lattice action are an essential tool to improve methods and their scaling behavior.

### 4.3. Observables

In this section some observables will be defined which are used to analyze the different introduced numerical methods. These are the PCAC and pseudoscalar (PS) masses (subsec. 4.3.1), the Wilson flow observable  $t_0$  (subsec. 4.3.2) and the topological charge  $Q$  (subsec. 4.3.3).

#### 4.3.1. Correlation Functions on the Lattice

In this subsection the calculation of correlation functions on the lattice will be described by following [8] and [98]. Note that the techniques which will be described here are also used in the work [99]. Correlation functions are suitable to extract masses from lattice data. For example, masses of hadrons can be measured by calculating the propagation of the particle from a creation time  $t = 0$  to an annihilation time  $t = t_1$ . The correlation function for the pseudoscalar meson is described by the two-point function

$$f_{PP}^a(x_0) = -a^3 \sum_{\vec{x}} \langle P^a(x) P^{a\dagger}(0) \rangle \quad (4.23)$$

with  $x = (x_0, \vec{x})$  and  $x_0 = t_1 - 0$  the time difference. The pseudoscalar density is given by

$$P^a(x) = \bar{\psi}(x) t^a \gamma_5 \psi(x) = \sum_{c,f,f',\alpha,\alpha'} \bar{\psi}^{c,\alpha,f}(x) (t^a)^{f,f'} (\gamma_5)^{\alpha,\alpha'} \psi^{c,\alpha',f'}(x) \quad (4.24)$$

with a generator of the unitary subgroup  $t^a$  (compare subsec. 2.1.1) which acts on the flavor space  $f, f'$  and  $\gamma_5$  which acts on the spin space  $\alpha, \alpha'$ . The summation contracts the color, spin and the flavor indices. The index  $a$  will be dropped from now on and  $t^a$  is set to  $\sigma^1 = [0, 1; 1, 0]$  with  $a = 1$  for different flavors  $f = r$  and  $f' = s$  with  $r \neq s$  and  $t^a = I$  for one flavor  $r = s$ . The indices  $r$  and  $s$  are flavor indices, e.g. if  $r$  corresponds to the up-quark and  $s$  to the down quark the pseudoscalar meson corresponds to the charged pion (compare tab. 2.2). The

pseudoscalar density is now given by  $P^{rs} = \overline{\psi}_r \gamma_5 \psi_s$ . The two-point function can be rewritten in the representation of Feynman's path integral and is given with eq. (2.14) on the lattice by averaging over the time slice at  $t = 0$  using translation invariance

$$\begin{aligned}
 f_{PP}^{rs}(x_0) &= \frac{1}{Z} \sum_{\vec{x}, \vec{y}} \int P^{rs}(x_0, \vec{x}) P^{rs\dagger}(0, \vec{y}) e^{-S(U, \psi, \overline{\psi})} \mathcal{D}\psi \mathcal{D}\overline{\psi} \mathcal{D}U \\
 &= \frac{1}{Z} \int \text{Tr} \left[ D(m_r)_{x_0, 0}^{-1} \gamma_5 D(m_s)_{0, x_0}^{-1} \gamma_5 \right] \left[ e^{-S_g(U)} \cdot \prod_{j=1}^{n_f} \det D(U, m_j) \right] \mathcal{D}U \\
 &= \frac{1}{Z} \int \text{Tr} \left[ D(m_r)_{x_0, 0}^{-1} \gamma_5 D(m_s)_{0, x_0}^{-1} \gamma_5 \right] P(U, m_1, \dots) \mathcal{D}U \quad (4.25)
 \end{aligned}$$

with the lattice Boltzmann factor  $P(U, m_1, \dots)$  and  $D_{x_0, 0}^{-1}$  the matrix element of time slice  $x_0$  to time slice 0. The trace sums over the three dimensional space  $\vec{x}$  and over the spin and color indices. The generalization to different two-point functions is straightforward, e.g. the two-point function of the time component of the axial vector current is given by

$$f_{AP}^{rs}(x_0) = -a^3 \sum_{\vec{x}} \langle A_0^{rs}(x) P^{sr}(0) \rangle \quad (4.26)$$

with the axial vector density  $A_0^{rs} = \overline{\psi}_r \gamma_0 \gamma_5 \psi_s$  (see e.g. [8] [98]).

The evaluation of the two-point function eq. (4.25) requires the explicit knowledge of the matrix elements of the inverse matrix of the Dirac operator  $D(m_r)$  and  $D^\dagger(m_s)$  of the parts which connect the time slices  $x_0$  and 0. An explicit calculation scales with  $V^3$  and the numerical effort is impractical for larger lattices. An efficient method is to introduce a stochastic method to estimate the trace [100]. This can be done by using  $U(1)$ -random-noise which is given by  $u = e^{ir}$  where  $r$  is randomly chosen from the interval  $[0, 2\pi)$ . The  $U(1)$  noise fulfills the condition

$$\langle u_i^\dagger u_j \rangle_u = \delta_{ij} \quad \text{with } i = (x, c, \alpha) \quad \text{and } j = (y, c', \alpha') \quad (4.27)$$

with  $\langle \rangle_u$  the average over the noise numbers  $u = (u_1, u_2, \dots, u_n)$  with  $u_i \in U(1)$ . Using the condition eq. (4.27), it is straightforward to show

$$\text{Tr} A = \langle u^\dagger A u \rangle_u \quad (4.28)$$

with a complex square matrix  $A \in \mathbb{C}^{n \times n}$ . Now the  $U(1)$  noise source can be defined on a time slice with  $\eta_t^{c, \alpha}(y) = \delta_{t, y_0} u^{c, \alpha}(\vec{y})$  with the dimension  $n = 12L^3$  and can be used to estimate the trace in eq. (4.25). The two-point functions from

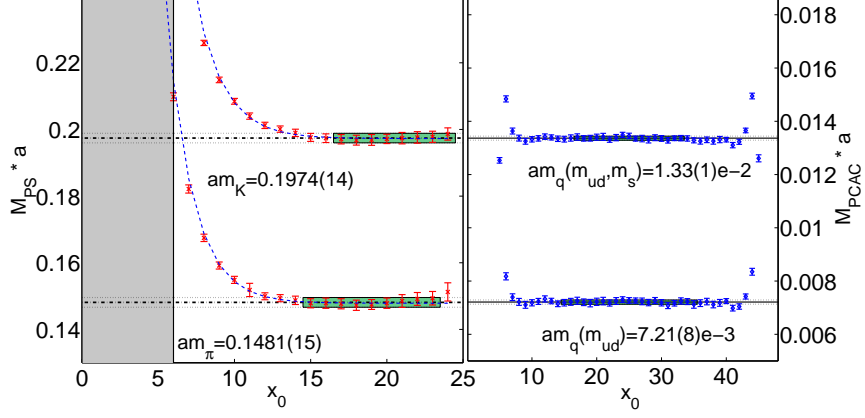


Figure 4.3.: The figure shows the plateaus of the mass states plotted versus the time difference  $x_0$ . The pseudoscalar two point and the axial two point functions are measured on the D5 ensemble (two flavor  $\mathcal{O}(a)$ -improved Wilson fermions with  $a = 0.066$  fm (see tab. 5.1)). The left figure shows the effective masses of PS correlators which correspond to the pion (lower plateau) and the kaon (upper plateau) mass. The right figure shows the ratio of correlators eq. (4.32).

$x_0 + t_i$  to  $t_i$  is estimated by using  $N_s$  random sources by

$$a^3 f_{PP}^{rs}(x_0) = \left\langle \frac{1}{N_s} \sum_{i=1}^{N_s} \eta_{t_i}^\dagger Q_{t_i, x_0+t_i}^{-1}(m_r) Q_{x_0+t_i, t_i}^{-1}(m_s) \eta_{t_i} \right\rangle \quad (4.29)$$

and

$$a^3 f_{AP}^{rs}(x_0) = \left\langle \frac{1}{N_s} \sum_{i=1}^{N_s} \eta_{t_i}^\dagger Q_{t_i, x_0+t_i}^{-1}(m_r) \gamma_0 Q_{x_0+t_i, t_i}^{-1}(m_s) \eta_{t_i} \right\rangle \quad (4.30)$$

where  $Q_{t_i, x_0+t_i}^{-1}(m) = [D(m)\gamma_5]_{t_i, x_0+t_i}^{-1}$  is the matrix element of the inverse Operator  $D\gamma_5$  at time slice  $t_i$  and  $x_0 + t_i$ . Note here is  $D(m)$  given by the Wilson Dirac operator eq. (2.42). In this work the number of  $U(1)$ -random sources is given by  $N_s = 10$  on randomly chosen time slices. This reduces the computational effort by keeping at the same time the stochastic fluctuations under control. For small quark masses this number is increased to  $N_s = 30$  to have a better noise to signal ratio (on the G8 ensemble compare tab. 5.1).

### PCAC mass

Due to the explicit breaking of the chiral symmetry of the Wilson term the bare mass  $m$  gets an additional mass shift. This additional mass shift can be determined by using the partial conservation of axial current (PCAC) relation. The PCAC relation is given by a Ward identity (see e.g. [54]). By using the derivation given in [101] the PCAC relation on the lattice is given by

$$\langle \partial_\mu A_\mu^{rs}(x) O_{ext} \rangle = 2m_{PCAC} \langle P^{rs}(x) O_{ext} \rangle + \mathcal{O}(a) \quad (4.31)$$

for an operator  $O_{ext}$  which is located with a finite distance from  $x$ . The critical mass can now be defined non perturbatively by  $m_{PCAC} = 0$  (compare eq. (2.36)). By using the PCAC relation eq. (4.31) and as an external source the pseudoscalar density  $P^{rs}$  the average quark mass can be directly defined (see e.g. [8] [98])

$$m_{PCAC}^{rs}(x_0) = \frac{(\partial_0 + \partial_0^*) f_{AP}^{rs}(x_0) + 2 \cdot c_A a \partial_0^* \partial_0 f_{PP}^{rs}(x_0)}{4 f_{PP}^{rs}(x_0)} \quad (4.32)$$

by using the correlation functions eq. (4.23) and eq. (4.26). The Ward identity is an exact relation. However, for short distances to the external source the identity is forged. These cut-off effects are suppressed for larger time distances  $x_0$  and the PCAC mass can be calculated by an average over these larger time distances. The additional term with the improvement coefficient  $c_A$  is introduced for  $\mathcal{O}(a)$ -improved Wilson fermions to cancel cut-off effects which scale with the lattice spacing  $a$  (see eq. (4.31)). The improvement parameter is given by the non-perturbative interpolation formula [102]

$$c_A = -0.00756 \cdot 6/\beta \frac{(1 - 0.4485 \cdot 6/\beta)}{(1 - 0.8098 \cdot 6/\beta)}. \quad (4.33)$$

### Pseudoscalar mass

The extraction of the PCAC mass is straightforward (see fig. 4.3 and eq. (4.32)). This is different in the case of the pseudoscalar mass. Here, a non-linear equation has to be solved and excited modes have to be suppressed. The extraction of the pseudoscalar mass is technical and will be discussed in this subsection.

The pseudoscalar correlator  $f_{PP}(x_0)$  can be written in energy eigenstates by inserting the eigenbasis in eq. (4.23) (see e.g. [8] or [98]) and is given on an anti-periodic lattice by

$$f_{PP}(x_0) = - \sum_{i=0}^{\infty} \sum_{j=0}^{\infty} c_{ij} h(x_0, E_i, E_j) \quad (4.34)$$

with

$$h(x_0, E, E') = 2 \exp\{-(E + E')T/2\} \cdot \cosh\{(E - E')(x_0 - T/2)\} \quad (4.35)$$

where  $E_i$  with  $0 = E_0 < E_i < E_{i+1}$  are the energy states and  $c_{ij} \geq 0$  are the spectral weights. Because of the vacuum property  $\langle 0|P|0\rangle = 0$  it follows  $c_{00} = 0$ . Note from now on the flavor indices  $r, s$  are dropped.

Now the approach is that the correlator  $f_{PP}$  is for large time distances dominated by the first eigenstate. This first eigenstate corresponds to the pseudoscalar mass  $E_1 = M_{PS}$ . In order to calculate  $M_{PS}$  an effective mass  $M_{eff}$  is defined by solving the equation

$$\frac{h(x_0 - a, 0, M_{eff}(x_0))}{h(x_0, 0, M_{eff}(x_0))} = \frac{f_{PP}(x_0 - a)}{f_{PP}(x_0)}. \quad (4.36)$$

For  $x_0, T \rightarrow \infty$  the effective mass  $M_{eff}(x_0)$  converges to the pseudoscalar mass  $M_{PS}$ . Because of the large  $T$  extent of the ensembles the effective mass  $M_{eff}(x_0)$  approaches a plateau for large  $x_0$ . By determining the plateau  $x_0 \in [t_0; T/2 - k]$  the mass  $M_{PS}$  is extracted by averaging  $M_{eff}(x_0)$  over  $x_0 \in [t_0; T/2 - k]$ .

#### Technical details to extract the plateau average of $M_{PS}$

The plateau is estimated by using the behavior of the  $f_{PP}$  correlator eq. (4.34) and taking for time slices  $t \gtrsim 5$  the first two eigenstates  $E_1$  and  $E_2$  into account. The pseudoscalar correlator is fitted with

$$y(x_0) = -c_1 \cosh\{E_1(x_0 - T/2)\} - c_2 \cosh\{E_2(x_0 - T/2)\} \quad (4.37)$$

with 4 fit constants  $c_1, c_2, E_1, E_2$ . Now  $M'_{eff}(x_0)$  is estimated by solving eq. (4.36) where the real data is replaced by  $f'_{PP}(x_0) = y(x_0)$ . The starting point of the plateau is defined such that for the smallest  $x_0$  the condition  $|E_1 - M'_{eff}(x_0)| \leq 0.25 \cdot \delta M_{eff}(x_0)$  holds with  $\delta M_{eff}(x_0)$  the statistical error of  $M_{eff}(x_0)$ . The plateau is stopped as soon as the condition  $2\delta M_{eff}(t_0) < \delta M_{eff}(T/2 - k)$  or the condition  $|M'_{eff}(T/2 - k) - M_{eff}(T/2 - k)| \geq 2.5\delta M_{eff}(T/2 - k)$  is fulfilled. The pseudoscalar mass value is now given by the plateau average value (see fig. 4.3).

#### Remarks

- **PCAC mass:** The PCAC mass is measured by using an average over the plateau  $x_0 \in [t_0 - 2; T - t_0 + 2]$  (see fig. 4.3) with  $t_0$  the starting point of the plateau derived for the pseudoscalar mass. The direct measured PCAC mass is a non-renormalized quantity and can be renormalized by the coefficient



$Z_A(\beta)/Z_P(\beta, \mu)$ . Here,  $Z_A$  and  $Z_P$  quoted in app. E of [98] is used to match the value with the physical quark mass. Note the renormalization coefficient  $Z_P(\beta, \mu)$  depends also on the momentum scale of the renormalization group (compare eq. (2.4)) while  $Z_A(\beta)$  only on the gauge coupling  $\beta$ .

- **Quenched strange quark:** Note by adding a quenched strange quark to a dynamical two flavor ensemble the corresponding pseudoscalar meson built up by a strange quark and a light quark corresponds to the kaon. By using eq. (4.29) the kaon masses can be extracted by using a proper tuned quenched strange quark (see e.g. [98]). In a quenched approximation the Boltzmann weight of the corresponding quark is set to a constant. This means that the corresponding sea quark mass is set to infinity while the valence quark is tuned to the right physical value.
- **Pseudoscalar decay constant:** The pseudoscalar decay constant can be calculated by

$$f_{PS} = 2\sqrt{2}\frac{m_{PCAC}}{M_{PS}^2}G_{PS} \quad (4.38)$$

with the quark mass  $m_{PCAC}$ , the pseudoscalar mass  $M_{PS}$  and the vacuum-to-meson matrix element  $G_{PS}$ . The pseudoscalar correlation function (see eq. (4.25)) can be written by

$$f_{PP}(x_0) = -\frac{G_{PS}^2}{M_{PS}}e^{-M_{PS}x_0} + \dots \quad (4.39)$$

and the vacuum-to-meson matrix element can be calculated by an average over the plateau of

$$G_{eff}(x_0) = \left[ -M_{eff}(x_0) \frac{f_{PP}(x_0)}{h(x_0, 0, M_{eff}(x_0))} \right]^{1/2}. \quad (4.40)$$

For this a similar technique is used like in the case of the pseudoscalar mass  $M_{PS}$ . Note the pseudoscalar decay constant has to be renormalized by multiplying with  $Z_A$  (see e.g. [98]).

### 4.3.2. Gluonic Observable $t_0$

Recently, the Wilson flow has become an interesting tool for several applications in LQCD, like the relative scale setting, proposed in [9, 103]. The Wilson flow smooths the gauge links for positive flow time by moving in the field space (see [104]). It is given by a partial differential equation which can be solved by using numerical integration schemes forward and backward in the flow time  $t'$ .

The gluonic observable  $t_0$  is defined by the Wilson flow time if the discretized gauge action density  $E$  fulfills the following condition

$$t'^2 \langle E(t') \rangle \Big|_{t'=t_0} = 0.3. \quad (4.41)$$

The discretization of the gauge action density  $E$  is arbitrary as long as the action density converges to the continuum one. In general the symmetric discretized Yang Mills action density  $E$ , see eq. (2.27), shows smaller  $\mathcal{O}(a^2)$  cut-off-effects and has a better continuum scaling than the Wilson plaquette action density (see e.g. [9]). The observable can be used combined with mass reweighting to set relative the scale which is done in subsec. 5.5.2 and sec. 6.5.

### 4.3.3. Topological Charge

In the continuum the topological charge of a gauge field is defined by

$$Q_{con} = \frac{1}{16\pi^2} \int \text{Tr} (F_{\mu\nu}(x) \tilde{F}_{\mu\nu}(x)) dx^4 \quad (4.42)$$

with  $F_{\mu\nu}$  the field strength tensor and the dual tensor  $\tilde{F}_{\mu\nu}(x) = \epsilon_{\mu\nu\sigma\rho} F_{\sigma\rho}(x)$ . The topological charge is an integer number and is linked via the Atiyah-Singer theorem to the index of the Dirac operator [105]

$$Q_{con} = n_+ - n_- \quad (4.43)$$

where  $n_{+/-}$  are the number of the zero modes with positive (negative) chirality. On the lattice the topological charge can be defined by (see e.g. [106])

$$Q = \frac{1}{16\pi^2} \sum_x \text{Tr} [\epsilon_{\mu\nu\sigma\rho} F_{\mu\nu}(x) F_{\sigma\rho}(x)]. \quad (4.44)$$

Due to ultraviolet fluctuation of the gauge links in general  $Q$  is not an integer number on the lattice. However by smearing out such fluctuations it is possible to measure  $Q$  on the lattice such that a proper continuum limit can be performed. This smearing method can be hypercubic (HYP)-smearing [21], like it was used in [107] or by using the Wilson flow for positive flow times. In general in this work the former method is used, which has roughly the same behavior as the latter method.

The topological charge can be used for several observations. It has a large overlap with the slow modes in a Monte Carlo algorithm and is an indicator for critical slowing down of the used algorithm. This is important for decreasing lattice spacing due to the increase of the autocorrelation time of roughly  $a^{-5}$  by using

up-to-date algorithms with periodic boundary conditions [27]. Another indicator for a proper sampling is the ensemble average

$$\langle Q \rangle = 0. \quad (4.45)$$

A physical interesting observable is the topological susceptibility defined by

$$\chi_t = \lim_{V \rightarrow \infty} \frac{\langle Q^2 \rangle}{V}. \quad (4.46)$$

In this work the topological charge is used to study the autocorrelation times for different kinds of algorithms, see e.g. subsec. 6.4.3.



## 5. Mass Reweighting

The most general way to evaluate the path integral is to weight configurations with the desired Boltzmann weight by using a Monte Carlo algorithm. This can be quite expensive, e.g. for mass-degenerate dynamical fermions, or even more expensive, e.g. for one flavor simulations, or even impossible, e.g. for non-zero chemical potential if determinants of non-hermitian matrices enter the game. For many applications it is convenient to use a different weight factor for the sampling of the configurations. Afterwards the discrepancy can be corrected by the so called reweighting factor, which is the ratio of the target over the simulated weight. This introduces new statistical fluctuations which limit the reweighting range, the so called overlap problem.

Reweighting has many applications in LQCD. For example it can be used to incorporate effects like isospin breaking by splitting up the up- and down-quark mass and to introducing electromagnetic interactions [15] or to introduce a finite chemical potential [108]. Other applications are correction of approximated actions, e.g. reweighting twisted mass fermions towards un-twisted mass fermions [109] or the correction of the polynomial square root approximation in the case of the strange quark (e.g. [32]).

This chapter will start with an overview of reweighting in the case where determinants enter the reweighting factor and followed by a discussion of how the overlap problem manifests itself as fluctuations. This will be followed by a detailed discussion about mass reweighting [12]. Mass reweighting is a special and interesting case of reweighting which shifts the mass of the sea quarks. The mass parameter enters the fermion determinant which is treated by using stochastic estimation. Stochastic estimation of the determinant introduces stochastic fluctuations (see sec. 5.3). Additionally reweighting introduces ensemble fluctuations (see sec. 5.4). By using the mass shift it is possible to analyze the mass dependence of observables. This has many interesting applications (see sec. 5.5), e.g. to deduce the critical mass or to perform the chiral limit for observables. Other applications are corrections of the strange quark mass or a split-up of the up- and down-quark mass (see sec. 5.6).

## 5.1. Reweighting Factor

The unnormalized Boltzmann factor  $V(U)$  for the gauge configurations  $U$  corresponding to a gauge coupling  $\beta$  and the masses  $m_i$  for  $n_f$  different fermions is defined by

$$V_a(U) = \exp\{-\beta S_g(U)\} \cdot \prod_{i=1}^{n_f} \det D(U, m_i, \dots) \quad (5.1)$$

at a specific parameter set  $a = \{\beta, m_1, m_2, \dots\}$ . Additional possible parameters of the fermion action are for example the twisted mass parameter  $i\mu_i$ , the chemical potential  $\mu_i$  or the electrical charge  $eQ_i$  if QED effects are included. If an ensemble  $\{U^{(a)}\}$  is generated with the appropriate weight

$$P_a(U) = \frac{V_a(U)}{Z_a} \quad (5.2)$$

with the partition function  $Z_a$ , it is possible to calculate an observable  $O$  at a different parameter set  $b = \{\beta', m'_1, m'_2, \dots\}$  [11]

$$\langle O(b) \rangle_b = \frac{\langle O(b)W \rangle_a}{\langle W \rangle_a} \quad (5.3)$$

by introducing the reweighting factor

$$W(U, a, b) = \frac{V_b(U)}{V_a(U)} = \frac{\exp\{-\beta' S_g(U)\} \cdot \prod_{i=1}^{n_f} \det D(U, m'_i, \dots)}{\exp\{-\beta S_g(U)\} \cdot \prod_{i=1}^{n_f} \det D(U, m_i, \dots)}. \quad (5.4)$$

Now the Boltzmann weight of the parameter set  $b$  is given by

$$P_b(U) = \frac{P_a(U)W(U, a, b)}{\int P_a(U)W(U, a, b)DU} = \frac{V_b(U)}{Z_b}. \quad (5.5)$$

In general it is convenient to express the fermion part of the reweighting factor as

$$W = \frac{\prod_{i=1}^{n_f} \det D(U, m'_i, \dots)}{\prod_{i=1}^{n_f} \det D(U, m_i, \dots)} = \frac{1}{\prod_{i=1}^{n_f} \det D(U, m'_i, \dots)^{-1} D(U, m_i, \dots)} = \frac{1}{\det M_{a,b}}. \quad (5.6)$$

The Dirac operator is a sparse matrix where the size scales with the lattice volume. Here the stochastic estimation technique of determinants, discussed in chap. 3, will be used for the evaluation. To conclude the technique of reweighting in combination with stochastic estimation of the determinant ratios can be applied in the whole parameter space but it is limited due to the introduced fluctuations.

### 5.1.1. Fluctuations

The fermion part of the reweighting factor is given by

$$W = \frac{1}{\det M_{a,b}}. \quad (5.7)$$

Note that at the level of the determinant the ordering of the matrices is arbitrary. This is also true for inserting  $\gamma_5$ -matrices. The origin of the stochastic fluctuations is the stochastic noise of the estimation of the determinant. Let us write the ratio matrix as  $M = I + \epsilon H + \mathcal{O}(\epsilon^2)$  and follow the discussion of app. B. The stochastic fluctuations are given up to the second order in  $\epsilon$  by

$$\sigma_{st}^2(N_\eta) = \frac{\epsilon^2}{N_\eta} \left\langle \text{Tr} \left( HH^\dagger \right) \right\rangle + \mathcal{O}(\epsilon^3). \quad (5.8)$$

by using the estimation of app. B and eq. (3.13). The origin of the ensemble fluctuations is the increase of the statistical noise, originally introduced by the Monte Carlo integration of the path integral, due to the reweighting factor. An approximation is given by eq. (3.14)

$$\sigma_{ens}^2 = \epsilon^2 \text{cov} \left\{ \text{Tr} (H), \text{Tr} \left( H^\dagger \right) \right\} + \mathcal{O}(\epsilon^3). \quad (5.9)$$

The understanding of the dependence on physical or lattice parameters of the terms  $\text{Tr}(HH^\dagger)$  and  $\text{cov}(\text{Tr}H, \text{Tr}H^\dagger)$  is the key for the usage of a specific reweighting method. Obviously the nature of the stochastic fluctuations is different in comparison to the ensemble fluctuations. This difference can be a source of a non-proper usage of the evaluation technique, i.e. it makes the stochastic estimation inefficient. The crucial point is if the magnitude of stochastic fluctuations is not of the same order as the ensemble fluctuations reweighting techniques get expensive and inefficient. For example if the first order in  $\epsilon^2$  cancels in the ensemble fluctuations eq. (5.9) in many cases a proper combination and ordering of the ratio matrix  $M$  can be done to cancel the first order term  $\mathcal{O}(\epsilon^2)$  in the stochastic fluctuations eq. (5.8), i.e. determinants of matrices are commutative but the matrices which enter the ratio matrix  $M$  do not commute in general (see for example isospin reweighting in sec. 5.2).

### 5.1.2. Statistical Errors of Reweighting

By using reweighting the statistical error of observables increases (see app. D for a general discussion of the error terms). The increase of the statistical error depends primarily on the correlation of the observable with the reweighting factor. Here

## 5. Mass Reweighting

---

the error is shown by an expansion of the reweighting factor in the parameter  $\epsilon$  similar like in the last subsection for the ratio matrix  $M$  with  $W(U) = 1 - \epsilon H + \mathcal{O}(\epsilon^2)$ . Now, terms which scale with the order  $\epsilon^3$  or even higher are neglected and the error can be cast in the form (see eq. (D.31) and previous discussion for further informations)

$$\delta_O^2 \sim \frac{1}{N} \left( \frac{1}{N \langle W \rangle^2} \sum_{i,j} [(O_i - \langle O \rangle) W_i (O_j - \langle O \rangle) W_j] - \frac{2 \text{cov}(O, W)}{\langle W \rangle^2} C_{O,W} \right). \quad (5.10)$$

where the observable  $O_i$  and the reweighting factor  $W_i$  depend on the configuration  $i$  of the ensemble. The term  $C_{O,W}$  is given by  $C_{O,W} = 1/N \sum_{i,j} [(O_i - \langle O \rangle)(W_j - \langle W \rangle)]$  which is equal to the covariance  $\text{cov}(O, W)$  if the autocorrelation time is neglected.

The fluctuations of reweighting are directly connected to the ‘‘overlap problem’’. The overlap problem is given due to the finite ensemble size by using reweighting for the Monte Carlo sampled ensemble. Obviously reweighting fails for cases where reweighting crosses a phase transition. For a continuously connected configuration space the overlap problem enters the ensemble average as fluctuations and increases the statistical error. Using interpolation techniques it is possible to observe this continuous increase and the overlap problem is tamed. However reweighting introduces additional bias which has to be analyzed if the ensemble size is too small (see eq. (D.18)). To conclude, for reweighting to work a proper ensemble size is necessary to reduce the bias.

### 5.2. Mass Reweighting

The most general mass reweighting factor is given in the two flavor case by shifting  $\{m_1, m_2\} \rightarrow \{m'_1, m'_2\}$  with

$$W(\{m'_1, m'_2\}, \{m_1, m_2\}) = \frac{\det D_{m'_1} \det D_{m'_2}}{\det D_{m_1} \det D_{m_2}} = \frac{1}{\det M} \quad (5.11)$$

with the ratio matrix  $M = D_{m'_1}^{-1} D_{m_1} D_{m'_2}^{-1} D_{m_2}$  and setting the mass parameter of the Wilson Dirac operator (see sec. 2.4) as  $D(m) = D_m$ . By using  $\Delta m = m_1 - m'_1$  and  $\Delta m_2 = m_2 - m'_2 = -\gamma \Delta m$  the ratio matrix is given by

$$M_{2f}^{-1} = I - \Delta m \left( \frac{1}{D_{m_1}} - \frac{\gamma}{D_{m_2}} \right) - \frac{\Delta m^2 \gamma}{D_{m_1} D_{m_2}} \quad (5.12)$$



and for the expansion parameter defined through  $M = I + \epsilon H + \mathcal{O}(\epsilon^2)$  follows  $\epsilon = \Delta m$ . By using the two flavor mass reweighting factor several mass reweighting cases can be defined. In general the strange quark reweighting factor is given by setting  $0 < \gamma < 1$ . Here the quark masses are  $m_1 \neq m_2$  and the factor eq. (5.12) can be rewritten to

$$M_{2f}^{-1} = I - \Delta m \frac{(\gamma - 1)D_{m_+} + (\gamma + 1)m_- + \gamma \Delta m}{D_{m_+}^2 - m_-^2} \quad (5.13)$$

with  $m_{\pm} = 0.5(m_2 \pm m_1)$ . A special case is given for the so called isospin reweighting defined by  $\gamma = 1$  and  $m_1 = m_{ud} = m_2$ , i.e. to include an isospin splitting in the up- and down-quark mass. In this case the expansion parameter is given by  $\epsilon = \Delta m^2$  and the isospin reweighting factor is given by

$$M_{Iso}^{-1} = I - \Delta m^2 \frac{1}{D_{m_{ud}}^2}. \quad (5.14)$$

Note if the ratio matrix is set to  $M = D_{m'_1}^{\dagger-1} D_{m_{ud}}^{\dagger} D_{m'_2}^{-1} D_{m_{ud}}$  the first order in  $\epsilon$  do not vanish in the stochastic fluctuations and mass reweighting gets ineffective (compare subsec. 5.1.1).

Another case is the one flavor mass reweighting factor (obtained by setting  $m_2 = m'_2$  in eq. (5.11)) given by  $\gamma = 0$  in eq. (5.12)

$$W_{1f}(\{m'_1\}, \{m_1\}) = \frac{\det D_{m'_1}}{\det D_{m_1}} = \frac{1}{\det M_{1fl}} \quad (5.15)$$

with the ratio matrix

$$M_{1f}^{-1} = D_{m_1}^{-1} D_{m'_1} = I - \Delta m \frac{1}{D_{m_1}}. \quad (5.16)$$

The expansion parameter in the one flavor case is given by  $\epsilon = \Delta m = m_1 - m'_1$ . The one flavor reweighting can be extended to the two-flavor mass-degenerate reweighting factor by  $W_{2fl,de} = W_{1fl}^{\dagger} W_{1fl}$ . In this case the ratio matrix can be defined by  $M_{2f,de} = M_{1f}^{\dagger} M_{1f}$  which can be evaluated without an additional inversion in contrary to the case with  $\gamma = -1$  and  $m_1 = m_2$ .

The mass reweighting factor is given by a determinant of a ratio matrix. The size of the ratio matrix increases with the lattice size and an exact calculation of the determinant is not feasible for volumes larger than  $V > 6^4$  of the Dirac operator. Therefore the determinant evaluation will be done by using stochastic estimation, introduced in chap. 3 with several improvements like interpolation techniques

## 5. Mass Reweighting

---

Table 5.1.: The table lists the analyzed CLS ensembles used for mass reweighting [98]. The used action is a two flavor mass-degenerate  $\mathcal{O}(a)$ -improved Wilson Dirac fermion action with a Wilson plaquette action. The parameter of the clover term is tuned by using [64]. The lattice spacing is fixed by using the kaon decay constant  $F_K$  [98]. Further details of the G8 ensemble can also be found in [113]. The ensembles are generated by using a Hasenbusch mass-preconditioned HMC for the ensembles D5, G8 and O7 while for the other ensembles the DD-HMC is used. Note the D5 ensemble is specially generated for the analysis of mass reweighting.

ID	$V$	$\beta$	$c_{SW}$	$a$ [fm]	$\kappa$	$M_\pi$ [MeV]
A5	$64 \times 32^3$	5.2	2.01715	0.0755(11)	0.135940	330
E4	$64 \times 32^3$	5.3	1.90952	0.0658(10)	0.136100	580
D5	$48 \times 24^3$				0.136250	440
E5	$64 \times 32^3$				0.136250	440
F7	$96 \times 48^3$				0.136380	270
G8	$128 \times 64^3$				0.136417	192
O7	$128 \times 64^3$	5.5	1.75150	0.0486(6)	0.136710	270

and DD. In detail the cases one flavor reweighting and isospin reweighting will be discussed in the next subsection.

The implementations which were done for this work is based on the package DD-HMC [96] and recently on the package open-QCD [110]. The reweighting package based on the open-QCD-package is publicly available [111]. The analysis of reweighting is done by using several two flavor mass-degenerate  $\mathcal{O}(a)$ -improved Wilson Dirac fermion ensembles of the CLS consortium [98]. The specific parameters are shown in table 5.1. In general isospin reweighting is applied to all ensembles with the maximal mass shift quoted in tab. 5.2. Note this means that the down quark mass too is symmetrically increased while the up-quark mass is decreased. For the analysis presented in [112] one flavor mass reweighting is applied for a large mass shift. For this analysis only the up-quark mass is lowered. Specific details of the statistics are shown in table 5.3.

Table 5.2.: The table shows parameters of the applied mass reweighting method to the CLS ensembles listed in tab. 5.1. The reweighting techniques are given by isospin reweighting by using an even-odd Schur complement (even-odd Iso.-Rew.) or by using the full operator without DD (Iso.-Rew. (w. full op.)). The one flavor reweighting method is applied to the CLS ensemble E5 and the ensemble D5. For the E5 ensemble DD is used with  $8^4$  blocks and for the D5 ensemble with  $6^4$  blocks. The quark masses  $\overline{m}$  are determined by using the PCAC mass and properly chosen renormalization constants (see [98]) in the  $\overline{\text{MS}}$ -scheme. The corresponding bare mass parameter for the largest shift in the case of the up-quark mass is given by  $\kappa_u'$ . The mass shift  $\Delta\overline{m}$  [MeV] is given by  $\Delta\overline{m} = \overline{m}_{ud} - \overline{m}_u'$ .

ID	Reweighting technique	$\kappa_u'$	$\overline{m}_u'$ [MeV]	$\Delta\overline{m}$ [MeV]
A5	even-odd Iso.-Rew.	0.1359620	14.91(42)	4.43(60)
E4	even-odd Iso.-Rew.	0.1361300	53.6(11)	7.1(17)
D5	DD-one flavor Rew.	0.1363500	16.12(66)	16.24(97)
	Iso.-Rew. (w. full op.)	0.1362750	29.41(66)	5.9(10)
E5	DD one flavor Rew.	0.1363500	--	--
	even-odd Iso.-Rew.	0.1362750	29.47(63)	6.01(96)
F7	Iso.-Rew. (w. full op.)	0.1364000	9.67(22)	5.01(38)
G8	even-odd Iso.-Rew.	0.1364363	2.80(56)	5.86(56)
O7	even-odd Iso.-Rew.	0.1367260	10.45(24)	5.63(40)

### 5.3. Stochastic Fluctuations

Stochastic estimation of the mass reweighting factor introduces stochastic fluctuations. The stochastic fluctuations eq. (5.8) for the two flavor reweighting factor are given by

$$\sigma_{st,2f}^2 = \Delta m^2 \text{Tr} \left( \left( \frac{1}{D_{m_1}} - \frac{\gamma}{D_{m_2}} \right)^\dagger \left( \frac{1}{D_{m_1}} - \frac{\gamma}{D_{m_2}} \right) \right) + \mathcal{O}(\Delta m^3). \quad (5.17)$$

Note the first order vanishes in the case of isospin-reweighting with  $m_1 = m_{ud} = m_2$  and  $\gamma = 1$ . It follows

$$\sigma_{st,Iso}^2 = \Delta m^4 \text{Tr} \left( \frac{1}{[D_{m_{ud}}^\dagger D_{m_{ud}}]^2} \right) \quad (5.18)$$

For the stochastic fluctuations eq. (5.8) of the one flavor reweighting factor follows

$$\sigma_{st,1f}^2 = \Delta m^2 \text{Tr} \left( (D_m D_m^\dagger)^{-1} \right) + \mathcal{O}(\Delta m^3). \quad (5.19)$$

The square of the error is given by the fluctuations divided by the number  $N_\eta$  of drawn pseudofermion fields  $\eta$  and for the reweighting factor follows

$$W = \frac{1}{N_\eta} \sum_{j=1}^{N_\eta} e^{-\eta_j^\dagger M \eta_j} + \mathcal{O} \left( \frac{1}{\sqrt{N_\eta}} \right) \quad (5.20)$$

with the ratio matrix  $M$  (see for the isospin reweighting case eq. (5.12) and for the one flavor case eq. (5.16)). Note eq. (5.20) is only correct if  $\lambda(M + M^\dagger) > 1$ . Further improvements can be used to increase the efficiency of the estimation and the correctness of eq. (5.20). These are shown in the next subsections. The section will be closed by a discussion of the scaling of the stochastic fluctuations with the lattice volume  $V$ , the quark mass  $\overline{m}$  and the lattice spacing  $a$ .

#### 5.3.1. Mass Interpolation

Mass interpolation, based on the interpolation technique introduced in subsec. 3.4, factorizes the determinant ratio in several ratios by introducing determinants of operators depending on intermediate masses. This reduces the mass shift  $\Delta m \rightarrow \Delta m/N$  and the eigenvalues of the ratio matrix are shifted closer to one (for a detailed discussion see subsec. 3.4). This can be used to ensure that the condition  $\lambda(M + M^\dagger) > 1$  is fulfilled for ratio matrices. By setting  $N_\eta = 1$  and introducing

$N$  intermediate mass terms the reweighting factor gets the form

$$W = \prod_{i=0}^{N-1} W_i, \quad W_i = \left\langle \exp \left\{ -\eta_i^\dagger (M_i - I) \eta_i \right\} \right\rangle_{\eta_i} \quad (5.21)$$

with  $M_i$  depending on  $m_i$  the  $i$ th mass parameter and  $m_{i-1}$  the  $(i-1)$ th mass parameter for the one flavor case given by

$$M_{1f,i}^{-1} = D_{m_i}^{-1} D_{m_{i+1}} = I - \frac{\Delta m}{N} \frac{1}{D_{m_i}} \quad (5.22)$$

and additionally on  $\gamma$  for the 2 flavor case. The parametrization of the interpolation is arbitrary and the optimal choice depends on the different mass reweighting cases and the environment, e.g. the stochastic fluctuations for reweighting towards small quark masses can depend on the smallest eigenvalue of  $D_m$ . For large enough quark masses a linear interpolation with intermediate masses

$$m_i = m_1' \frac{i}{N} + m_1 \frac{N-i}{N} \quad \text{with } i = 0, \dots, N \quad (5.23)$$

is sufficient for the one flavor reweighting case. By following app. B.4 or subsec. 3.4 the stochastic fluctuations reduce to

$$\sigma_{st}^2(N, N_\eta) \leq \frac{1}{NN_\eta} \max_i \left[ \frac{\Delta m^2}{\text{Tr}[D_{m_i} D_{m_i}^\dagger]} \right] + \mathcal{O} \left( \frac{\Delta m^3}{N^2 N_\eta} \right). \quad (5.24)$$

Increasing the mass interpolation steps is more effective to reduce the stochastic fluctuations than to increase the number of estimations for one ratio  $N_\eta$ . However increasing  $N$  compared to  $N_\eta$  makes no difference if the first order in  $\Delta m^2$  dominates. In [112] it was found on the D5 ensemble that for a mass shift of  $\Delta m = \bar{m}/2$  an amount of  $N = 8$  mass interpolation steps are large enough so that the  $\mathcal{O}(\Delta m^3)$  do not contribute to the error.

The situation for the two flavor case is different. If  $\gamma > 0$  the mass distance between both quarks increases and this dominates also the stochastic fluctuations if linear interpolation is used. By demanding that the stochastic fluctuations are constant during the interpolation the interpolation technique has to be corrected. This can be done by using a reordering of the reweighting factors or by modifying the linear interpolation.

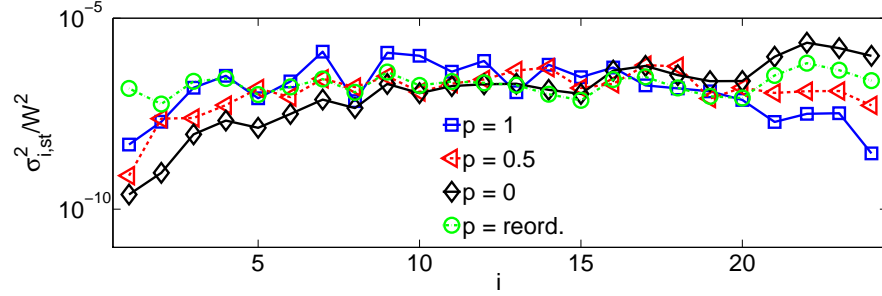


Figure 5.1.: Comparison of different mass interpolations by plotting the stochastic fluctuations  $\sigma_{i, \text{st}}^2 / W^2$  of each interpolation step against the interpolation steps  $i$  on a configuration of the D5 ensemble by using isospin reweighting.

### Reordering

Reordering is motivated by the dependence of the stochastic fluctuations on the total mass distance  $m_-$ . By setting  $\gamma = 1$  the ratio matrix eq. (5.14) is given by

$$M_{2f}^{-1} = I - \Delta m \frac{2m_- + \Delta m}{D_{m_+}^2 - m_-^2}. \quad (5.25)$$

with  $m_{\pm} = 0.5(m_2 \pm m_1)$ . By introducing a mass interpolation the mass difference  $m_-$  increases step by step for  $m_- > 0$  and thereby the stochastic fluctuations. The idea is to fix the total mass difference by reordering the combinations of reweighting factors. This means that the first mass step of  $m_1$  is combined with the  $N$ th of  $m_2$ , the second mass step of  $m_1$  is combined with second last step of  $m_2$  and so on. Numerically it is found for moderate quark masses that by using reordering the stochastic fluctuations are roughly constant during the interpolation (see fig. 5.1 (green, circle)). However reordering is only useful if the target masses of the two-flavor mass reweighting are known. Notice also if the one flavor reweighting factors are known, a recombination of these factors to intermediated masses would lead to large stochastic fluctuations. The reason is the different scaling of the stochastic fluctuations for one flavor and two flavor reweighting.

### Polynomial Interpolation

Another method is to modify the sizes of the steps during the interpolation (see documentation of [111]). Note the ratio of the stochastic fluctuations over the ensemble fluctuations is not constant during an interpolation, it decreases because

the number of inversions increases. The interpolation is generalized by demanding that for  $N \rightarrow \infty$  the step size  $\delta m_i = m_i - m_{i-1} \rightarrow 0$ . This condition is fulfilled for

$$m_i = m + S_i^p \frac{m' - m}{S_N^p} \quad \text{with} \quad S_i^p = \sum_{k=1}^i k^p \quad (5.26)$$

and the mass shift in the  $i$ th step is given by  $m_i - m_{i-1} = i^p(m' - m)/S_N^p$ . For  $p = 0$  the linear interpolation is recovered. Numerically it is found that in the case of isospin reweighting  $p \in [0.25, 0.5]$  minimizes the stochastic fluctuations. By choosing an appropriated  $p$  a similar magnitude of the order of the stochastic fluctuations compared to the reordered case is found. This is shown in figure 5.1. Using  $p \in [0.25, 0.5]$  and isospin reweighting the relative stochastic error is roughly given by  $\sigma_{st}/\sqrt{N_{int}}|W| \sim 9 \cdot 10^{-4}$  with  $N_{int} = NN_\eta$  for  $N = 24$  and  $N_\eta = 6$  on one configuration of the D5 ensemble (compare tab. 5.2). The relative error is comparable with the reordering (circle, green, dash-dot) but is improved compared to the ordinary case with  $p = 0$  with  $\sigma_{st}/\sqrt{N_{int}}|W| \sim 12 \cdot 10^{-4}$ .

### 5.3.2. Domain Decomposition

By using DD (see section 4.1) the determinant exactly factorizes into determinants of the Schur complement and the block operators eq. (4.10) with  $\det D = \det \hat{D} \cdot \prod_k \det D_k$ . For small enough block length  $LU$ -decomposition is used to calculate the block determinants. Then the reweighting factor for  $N_\eta = 1$  is given by

$$W = \frac{1}{\prod_k \det M_k} \prod_{i=0}^{N-1} \hat{W}_i, \quad W_i = \left\langle \exp \left\{ -\eta_i^\dagger (\hat{M}_i - I) \eta_i \right\} \right\rangle_{e^{-\eta_i^\dagger \eta_i}} \quad (5.27)$$

where  $\det M_k = \det D_{k,m'_1}^{-1} \det D_{k,m'_2}^{-1} \det D_{k,m_1} \det D_{k,m_2}$ . The determinants can be calculated exactly for blocks with  $\tilde{l} \leq 6$ . For larger block recursive DD is used such that the block length is given by  $l \leq 6$ . A stochastic estimation can also be used for the Dirichlet Schur complements with mass interpolation. In general the Schur complement can be rewritten as  $\hat{D}_{m+\Delta m} = \hat{D}_m + \Delta m X_m + \mathcal{O}(\Delta m^2)$  where

$$X_m = P_{wb} D_{ww}^{-1} \left( \hat{D}_m - I - D_{wb} D_{bb}^{-2} D_{bw} \right) \quad (5.28)$$

and the operators depend on  $m$ . Now the ratio matrix  $\hat{M}_i$  for the one flavor case is given by

$$\hat{M}_{i,1f}^{-1} = I - \Delta m \hat{D}_{m_i}^{-1} X_{m_i} + \mathcal{O}(\Delta m^2) \quad (5.29)$$

## 5. Mass Reweighting

---

and for the stochastic fluctuations follows

$$\sigma_{1f}^2(N_\eta, N) \approx \frac{\Delta m^2}{N_\eta N} \text{Tr} \left( X_m X_m^\dagger (\hat{D}_m \hat{D}_m^\dagger)^{-1} \right) + \mathcal{O} \left( \frac{\Delta m^3}{N^2 N_\eta} \right). \quad (5.30)$$

However because  $X$  does not commute with  $X^\dagger$  the ordering of the matrices is important in the two flavor case. By ordering

$$\hat{M}_{i,2f}^{-1} = I - \Delta m (\hat{D}_{m_1}^{-1} X_{m_1} - \gamma \hat{D}_{m_2}^{-1} X_{m_2}) + \mathcal{O}(\Delta m^2) \quad (5.31)$$

the stochastic fluctuations of the two flavor case are given by

$$\begin{aligned} \sigma_{2fl}^2(N_\eta, N) &\approx \frac{\Delta m^2}{N_\eta N} \text{Tr} \left( (\hat{D}_{m_1}^{-1} X_{m_1} - \gamma \hat{D}_{m_2}^{-1} X_{m_2})^\dagger (\hat{D}_{m_1}^{-1} X_{m_1} - \gamma \hat{D}_{m_2}^{-1} X_{m_2}) \right) \\ &+ \mathcal{O} \left( \frac{\Delta m^3}{N_\eta N^2} \right). \end{aligned} \quad (5.32)$$

Note that in this case the fluctuations of the isospin reweighting scale with  $\Delta m^4$ .

The dimension of the operator which captures the IR modes is reduced by using DD. This reduction depends on the block size and can scale with  $V^{3/4}$  by choosing a block length which scales with  $L/2$  (see subsec. 4.1.2). Numerically it was found that the stochastic fluctuations of the Schur complement do not scale linear with the dimension and depend on the used reweighting technique. This analysis is done on the CLS ensembles D5 and E5 (compare tab. 5.2). For one flavor mass reweighting DD helps and can reduce the stochastic fluctuations by at least a factor 2 [112]. However the effect depends marginally on the block size. An explanation is that the number of the IR-modes dominates the fluctuations which increase with the volume  $V$ . This behavior persists also if the volume of the blocks is increased. To conclude it is sufficient to use the even-odd Schur complement with block length  $l = 1$  in the case of one flavor reweighting.

The effect of DD in the two flavor reweighting case with  $\gamma \approx 1$  differs. A different magnitude of the stochastic fluctuations is not found by using DD or the non decomposed full operator. This behavior does not change by using different interpolation strategies. Also in this case an explanation is given by the IR-modes. If already the stochastic fluctuations for the full operator are dominated by the IR-modes this behavior persists for the Schur complement and no improvement can be expected.



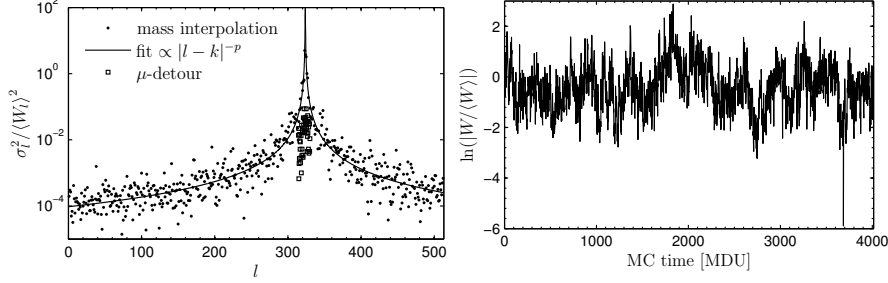


Figure 5.2.: The left figure shows the variance during a linear mass interpolation for a mass shift of  $\Delta m = \bar{m}/2$  of the D5 ensemble (dot). During this mass interpolation a real eigenvalue crosses the zero and the variance diverges roughly with a power of  $p = -1.8$  (fit,line). To satisfy a right estimation a  $\mu$ -interpolation is performed (square). After the  $\mu$ -detour the estimation is negative which can be understood by a sign flip of one eigenvalue. The right figure shows the history of the logarithm of the reweighting factor  $|W/\langle W \rangle|$  of the D5 ensemble in the case of one flavor reweighting towards a quark mass of  $m_{ud} = 16.12(66)$  MeV (compare tab. 5.2). For the configuration with the zero crossing a  $\mu$ -detour is used.

### 5.3.3. Twisted-mass Detour

In practice HMC-like algorithms get unstable for small quark masses and a possible method to perform an unquenched analysis of observables for small quark masses is to use mass reweighting. By shifting the mass towards smaller values the smallest real eigenvalue of the Wilson Dirac operator tends to zero and it is possible that it crosses the zero and changes the sign. In such cases stochastic estimation with mass interpolation fails because the integral representation eq. (3.2) is undefined at least for the ratio where the sign flip happens. Such illness can be detected by a dramatic increasing of the variance (see fig. 5.2). By introducing a twisted mass term  $i\gamma_5\mu$  and performing a  $\mu$ -detour, it is possible to estimate the reweighting factor if a real eigenvalue changes the sign. The twisted mass operator  $D_m(\mu) = D_m + i\gamma_5\mu$  breaks  $\gamma_5$ -hermiticity of the Wilson Dirac operator and shifts the real eigenvalue into the complex plane [114]. The effect is a cut-off for the spectrum which acts on the hermitian operator  $D_m(\mu)D_m^\dagger(\mu) = D_mD_m^\dagger + \mu^2$  like a shift with  $\mu^2$ .

A  $\mu$ -detour is arbitrary. A requirement is that the variance is small and defined. Following eq. (3.6) this is true if the smallest eigenvalue fulfills  $1/2\lambda(M^\dagger + M) > 1/2$ . By assuming a similar condition for the largest eigenvalue with  $1/2\lambda(M^\dagger + M) < 2$  a rough condition in the one flavor case is given for the step sizes  $\Delta m$  and  $\Delta\mu$  for a crossing real eigenvalue. Note the stochastic variance is defined for the

## 5. Mass Reweighting

---

second condition, but if the largest eigenvalue increases rapidly the variance does the same. Let us write

$$M_i = I + \frac{\Delta m_i + i\gamma_5 \Delta \mu_i}{D + m_i + i\gamma_5 \mu_i}. \quad (5.33)$$

By using the spectral norm of the matrix and the approximation to the smallest singular value of the denominator with  $\|(D + m_i + i\gamma_5 \mu_i)^{-1}\| = (\epsilon^2 \chi_0^2 + \mu^2)^{-1/2}$  it follows

$$1 + \frac{\Delta m_i + \Delta \mu_i}{\sqrt{\epsilon^2 \chi_0^2 + \mu^2}} < 2. \quad (5.34)$$

$\chi_0 = v_i^\dagger \gamma_5 v_i$  is the chirality of the normalized eigenvector to the smallest eigenvalue of  $D + m_i$  and  $\epsilon^2 = (m - m_0)^2$  with  $m_0$  the mass parameter where the eigenvalue is zero (see app. B and C of [16]). Now it is straightforward to derive conditions for the step-size in  $\Delta m$  with  $\Delta \mu = 0$

$$\mu > \Delta m \quad (5.35)$$

and for  $\Delta \mu$  with  $\Delta m = 0$

$$\Delta \mu < \sqrt{\mu^2 + \chi_0^2 \epsilon^2}. \quad (5.36)$$

To conclude the distance to the zero eigenvalue has to be larger in the  $\mu$ -direction than in the step size  $\Delta m$ . Additional if the smallest eigenvalue is almost zero several steps have to be done in  $\Delta \mu$  to exit the  $\mu$ -plane.

In general by keeping  $\Delta m^2 + \Delta \mu^2$  constant also the stochastic fluctuations are constant. This is used in practice for the  $\mu$ -detour (for more details see app. B and C of [16]).

### Practice

In the numerical studies shown in fig. 5.2 it is demanded that the relative stochastic error of the reweighting factors should have the same order for all configurations. By assuming this a  $\mu$ -detour has to be performed only for configurations where a real eigenvalue flips the sign. This is done for the reweighting of the configurations shown in fig. 5.2. Here a mass interpolation with  $N = 512$  steps is performed and the variance increases for values around  $i = 314, \dots, 330$ . To avoid an ill-defined method a circular  $\mu$ -detour with a maximal value of  $a\mu = 0.00003$  and 48 steps is performed. Due to the breaking of the  $\gamma_5$  hermiticity the reweighting factor is complex during the  $\mu$ -detour. Due to that the sign flip happens continuously during the detour depending on the maximal  $\mu$  and the shape of the trajectory.

In order to guarantee the interchangeability of the integral over the gaugelinks and the pseudofermion fields to estimate the reweighting factor a rectangular  $\mu$ -

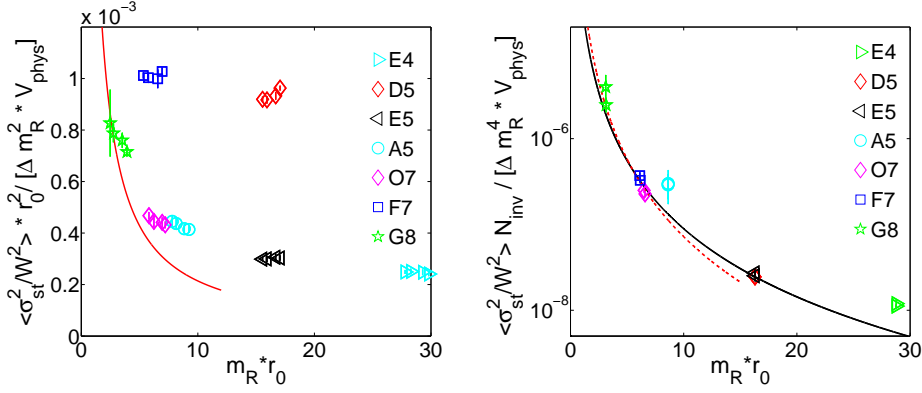


Figure 5.3.: The figures show the scaling of the relative stochastic fluctuations in the renormalized mass  $\bar{m}$  in units of  $r_0$ . The stochastic fluctuations are normalized by the physical volume  $V_{phys} = Va^4$ . The left figure shows the fluctuations in the case of one flavor reweighting. The right figure shows the fluctuations in the case of two flavor reweighting.

detour has to be used for every configuration<sup>1</sup>. This can be done by performing a  $\mu$ -detour with the corners  $\{(m_1, 0), (m_1, \mu), (m'_1, \mu), (m'_1, 0)\}$ . This introduces additional cost due to the additional noise for every configuration. However by a combination of the reweighting steps of the start and the end of the rectangular trajectory it is possible to reduce the stochastic errors in proportional to  $\mu^2 \Delta m^2$ . The second approach is available in the package [111].

### Remarks

In general the expectation is that the fluctuations would increase dramatically if too many configurations have a zero crossing eigenvalue or have very small eigenvalues in the smallest mass. Due to that the  $\mu$ -detour is only practical for special cases. This can be seen in the right figure 5.2 where the configuration with a zero crossing eigenvalue has a small reweighting factor. Note the very small reweighting factor  $\mathcal{O}(10^{-16})$  of the right figure 5.2 corresponds to an exceptional configuration [115] [33]. For the smallest mass this leads to a pole in the pseudoscalar correlator which is regularized by the reweighting factor.

### 5.3.4. Scaling of Stochastic Fluctuations

In this subsection the scaling of the stochastic fluctuations will be discussed based on numerical results and dependences of the traces  $\text{Tr}(D^\dagger D)^{-1}$  eq. (5.19) and  $\text{Tr}(D^\dagger D)^{-2}$  eq. (5.18). By using DD it is possible to connect these behaviors to the IR- and UV-modes.

Chiral perturbation theory gives some insights into the quark mass dependence of the traces eq. (5.19) and eq. (5.17) of the stochastic fluctuations. It follows from the lowest order in the chiral expansion [116]

$$\left\langle \text{Tr} \left( (D_m D_m^\dagger)^{-p} \right) \right\rangle \cong \frac{\overline{m} \Sigma V_{phys} \Gamma(p-0.5)}{\overline{m}^{2p} \sqrt{\pi} \Gamma(p)} \quad (5.37)$$

with the physical volume  $V_{phys} = Va^4$ , the chiral condensate  $\Sigma$  and the renormalized quark mass  $\overline{m}$ .

For the one flavor case  $p = 1$  is set to one and for the isospin reweighting case with  $\gamma = 1$  the parameter  $p$  is set to two with  $p = 2$ . Numerically the data are fitted with

$$\sigma_{st,p,rel}^2 = \left\langle \frac{\sigma_{st,p}^2}{W_{p,fl}^2} \right\rangle = \frac{k_{st}^{(pf)} V_{phys} \Delta \overline{m}^{2p}}{NN_\eta r_0^{4-2p+q} \overline{m}^q} \quad (5.38)$$

where  $k_{st}^{(pf)}$  is a dimensionless quantity which depends on the used operators,  $V_{phys}$  is the physical volume,  $\Delta \overline{m}$  is the mass-shift in the renormalized mass, the scale  $r_0$  [117] is used to form dimensionless quantities and the number of inversions of the Dirac operator is given by  $p \cdot NN_\eta$ . The scaling is shown by the numerical results in fig. 5.3 by using the results of the isospin reweighting shown in tab. 5.2. Note that two points are shown which correspond to the half mass shift  $\Delta m/2$  and to the full mass shift  $\Delta m$ . The relative stochastic fluctuations  $\sigma_{st,p,rel}^2$  are used for the analysis of the scaling. For the one flavor reweighting case the direct estimation of  $\langle \sigma_{st,1f}^2 \rangle$  has large errors. In the case of isospin reweighting for the relative stochastic fluctuations numerically follows  $\langle \sigma_{st,Iso}^2 / W_{Iso}^2 \rangle \approx \langle \sigma_{st,Iso}^2 \rangle$ .

The quark mass dependence of the full operator is extremely weak for the one flavor reweighting case in the analyzed mass range (see left fig. 5.3 where D5 (red, diamond), F7 (blue, square)). This slightly changes for the even-odd preconditioned operator (E4 (cyan, star), E5 (black, triangle), A5 (cyan, triangle), O7 (magenta, circle) and G8 (green, star)). Here, the fit is done (red line) in left fig. 5.3 with the expectation of the quark mass dependence from chiral perturbation theory  $1/m_q$  applied to the data of the G8, O7 and A5 ensemble. The fit shows that for larger quark masses the mass dependence gets weaker and does not follow the expectation of the chiral perturbation theory.

<sup>1</sup>Thanks to M. Lüscher and S. Schaefer for pointing this out.

The behavior of the full operator is complementary to the observation that the stochastic fluctuations depend also strongly on the UV-modes. However the expectation for decreasing quark mass is that the IR-mode dependence will increase. If this is the case the expected quark mass behavior will dominate also for the fluctuations of the full operator.

For the case of isospin reweighting with  $p = 2$  the behavior is roughly given by  $q \sim 3$  (see right fig. 5.3). The global fit to the quark mass behavior (black line) is performed for all ensembles and is given by  $m^q$  with  $q = 2.63(5)$ . For the different fit (red, dotted line) the quark mass behavior is fixed to  $1/m^q$  with  $q = 3$  which is the expectation of chiral perturbation theory by only including the G8, F7, O7, and A5 ensembles. This shows that for smaller quark masses the data behaves like it is expected from chiral perturbation theory. Note there is no improvement in the isospin reweighting case by using the Schur complement (compare tab. 5.2). The IR-modes dominate already the full operator.

### Practice

Like in [10] some practical issues of mass reweighting will be summarized in this subsection.

- By using  $N_\eta \geq 6$  the variance of the estimation can be monitored to detect eigenvalues which approaching the zero or even crosses. Another hint can be obtained by monitoring the total value of the estimation, which decreases drastically if an eigenvalue tends to zero. Here, the stochastic fluctuations are estimated for each mass interpolation step and afterwards propagated such that  $\sigma_{st,rel}^2 = \sum_{i=1}^N \sigma^2(W_i) / (1/N_\eta \sum_j W_{i,j})$ .
- The number of inversions is given by  $p' \cdot NN_\eta$ , where  $p' = 1$  for the one flavor case and  $p' = 2$  for the two flavor reweighting case. Note if two flavor reweighting is used also the reweighting factor for the one flavor cases can be easily computed without any further inversion. Furthermore the one flavor reweighting factor can easily be extended to the two flavor mass-degenerate case also without an additional inversion. The trick is to estimate  $1/\det M^\dagger M$  instead of  $1/\det M$  by calculating the scalar product  $\chi^\dagger \chi$  instead of  $\eta^\dagger \chi$  with  $\chi = M\eta$  in the stochastic estimation procedure.
- If the reweighting factor is real an improved estimator is the real part of the reweighting factor. This improves the estimation during the mass interpolation, although the effect is very small. Furthermore this trick it necessary to demand that a real weight is real also by using reweighting.
- If the reweighting factor is not dominated by the small eigenvalues DD improves the estimation. This is only the case for one flavor mass reweighting

and QED-reweighting (see sec. 5.6.4). Due to the fact that the case of one flavor reweighting can be achieved by using two flavor reweighting with  $0 < \gamma \leq 1$  it is wise to use also DD in this case. In general it is sufficient to use the even-odd Schur complement. For larger block sizes the computational cost increases by only a negligibly small improvement of the stochastic estimation.

- For the isospin reweighting case a mass interpolation with  $p \in [0.25, 0.5]$  minimizes the stochastic fluctuations. Note for the analysis in this thesis the conservative interpolation is used with  $p = 0$ .
- For the used mass shifts, listed in tab. 5.2, zero crossing eigenvalues are not found for most of the ensembles except the mass shift of the one flavor reweighting case for the D5 ensemble. However one configuration of the G8 ensemble has a small eigenvalue which is close to zero for the largest mass shift in the up-quark mass. In this case more interpolation steps are done close to this point which keep the stochastic fluctuations under control. Note this enters only the largest mass shift in G8.

## 5.4. Ensemble Fluctuations

In this section the ensemble fluctuations in the case of mass reweighting will be discussed. From eq. (5.9) it follows that the fluctuations are given for the two flavor mass reweighting case by

$$\sigma_{ens,2f}^2 = \Delta m^2 \text{var} \left\{ \text{Tr} \left( \frac{1}{D_{m_1}} - \frac{\gamma}{D_{m_2}} \right) \right\} + \mathcal{O}(\Delta m^3) \quad (5.39)$$

by using the  $\gamma_5$ -hermiticity of the Wilson Dirac operator and the trace properties  $\text{Tr}(D^\dagger) = \text{Tr}(\gamma_5 D \gamma_5) = \text{Tr}(D)$ . The fluctuations for the isospin reweighting follow with  $\gamma = 1$

$$\sigma_{ens,Iso}^2 = \Delta m^4 \text{var} \left\{ \text{Tr} \frac{1}{D^2} \right\} + \mathcal{O}(\Delta m^6) \quad (5.40)$$

In the case of one flavor reweighting the ensemble fluctuations eq. (3.14) reduce to

$$\sigma_{ens,1f}^2 = \Delta m^2 \text{var} \left\{ \text{Tr} \frac{1}{D} \right\} + \mathcal{O}(\Delta m^3). \quad (5.41)$$

In the following subsections the behavior of the ensemble fluctuations will be discussed. The ensemble fluctuations do not depend on the estimation method, i.e. the fluctuations can not be reduced by using improvement methods like DD.

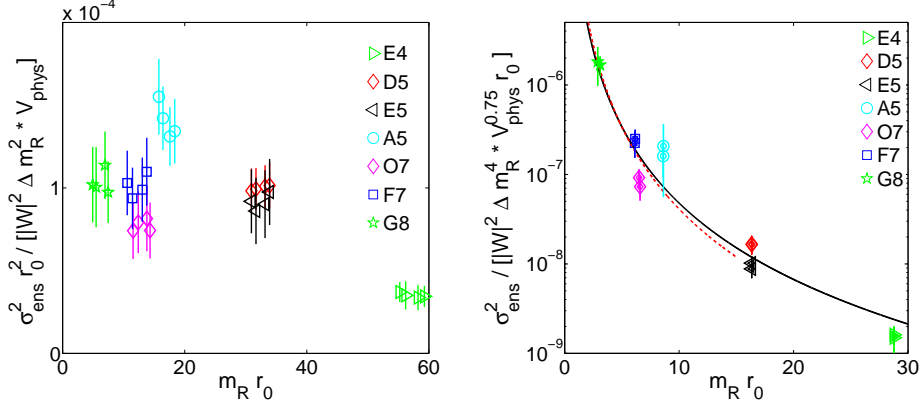


Figure 5.4.: The figures show the scaling of the ensemble fluctuations in the quark mass  $\bar{m}$  in units of  $r_0$ . The left figure shows the fluctuations in the case of one flavor reweighting normalized by the physical volume. The right figure shows the fluctuations in the case of isospin reweighting. The global fit (black line) is done for all ensembles, the red dashed line for G8, F7, O7 and A5.

However DD can be used to study the dependency of fluctuations on the IR-modes (Schur complement) and on the “UV”-modes.

Furthermore the increase of the statistical error in measurement of the observables will be discussed. Moreover mass reweighting introduces bias which becomes important for large fluctuations. In general the ensemble fluctuations can be tamed by using correlation with parts of the lattice action, for example with the plaquette action.

### 5.4.1. Scaling of Ensemble Fluctuations

A similar formula to eq. (5.38) is used to fit the numerical data of the ensemble fluctuations (see fig. 5.4)

$$\frac{\sigma_{en,p}^2}{\langle W_{p,fl} \rangle^2} = k_{en}^{(p)} \frac{V_{phys}^r \Delta \bar{m}^{2p}}{r_0^{4r-2p+q'} \bar{m}^{q'}} \quad (5.42)$$

with the dimensionless parameter  $k_{en}^{(p)}$  which depends on the mass reweighting case and  $r_0 = 0.503$  fm [117] given in the chiral limit. The value of  $p$  is 1 for one-flavor and 2 for isospin reweighting. The analysis is done by using isospin reweighting for the CLS ensembles (see tab. 5.2). In figure 5.4 the quark mass behavior of the fluctuations is shown. Similarly to the stochastic fluctuations the

ensemble fluctuations in the one flavor case depend only slightly on the quark mass. Furthermore a linear volume dependence is observed and for the one flavor reweighting case follows  $q' = 0$  and  $r = 1$ .

For the isospin reweighting case a milder volume dependence is found with  $r \approx 0.25 \dots 0.75$ . The large range of the parameter  $r$  is due to the interplay with the quark mass behavior. For a volume dependence of  $r = 0.25$  follows  $q' \approx 4$  while for  $r = 0.75$  a mass dependence of  $q' \approx 3$  follows (compare fig. 5.4). It is difficult to deduce the absolute scaling dependence from the numerical results. Furthermore there are some contrary hints:

- **Scaling by fixed volume behavior:** The ensembles D5 and E5 can be used to study the scaling in the volume without a dependence of the quark masses. The ratio of the ensemble fluctuations in the case of isospin reweighting gives  $\sigma^2(E5)/\sigma^2(D5) = 1.66$  for a change in the volume of  $\sim 3.16$ . Another hint of a weak volume behavior is the  $\chi^2$  of the mass fits by neglecting the E4 ensemble. The minimum is given for  $r = 0.15$  with  $\chi^2 = 15.7$ . By neglecting also the D5 ensemble the minimum of  $\chi^2$  is reached for negative  $r$ . For  $r = 0.01$  the  $\chi^2$  is given by  $\chi^2 = 14.5$ .
- **Scaling by fixing the quark mass behavior:** The expectation of the quark mass behavior from chiral perturbation theory for the term  $\text{Tr}(DD^\dagger)^{-2}$  is given by  $m^{-3}$  (see eq. (5.37)). In the case of isospin reweighting the ensemble fluctuations are based on the terms  $[\text{Tr}(D^{-2})]^2$ . By assuming a similar scaling in the quark mass with  $m^{-3}$  like in the stochastic fluctuations the data suggests a volume scaling of  $r = 0.75$ . This behavior is shown in the right figure of fig. 5.4 where the volume is fixed to  $r = 0.75$ . In general by setting  $q' = 3$  and varying the volume behavior the best  $\chi^2$  is given by  $r \sim 0.61$  if all ensemble values except E4 are included. By only including E5, F7 and G8 the parameter is given by  $r \sim 0.82$ . Furthermore the analysis of the volume scaling of the MDD-HMC algorithm suggests a scaling with  $r \approx 0.75$  (see chap. 7).

In the whole another pair of volumes at the same mass is needed to determine the scaling more precisely.

### Volume scaling

The behavior of the ensemble fluctuations can be understood by using DD. DD allows to separate the fluctuations of the Schur complement and the blocks, which can be interpreted as IR-dominated and UV-dominated. If the IR- and the UV-modes can be separated the fluctuations split up into

$$\sigma^2 \sim V\Delta m^{2p} [\text{var}(\lambda_{IR}) + \text{var}(\lambda_{UV}) + 2\text{cov}(\lambda_{UV}, \lambda_{IR})] \quad (5.43)$$



by assuming that the number of IR- and UV-modes scales with the volume  $V$ . By using this approximation the volume behavior of the different reweighting cases can be described.

For one flavor reweighting (see tab. 5.2) the fluctuations of the Schur complement  $\sigma_{\hat{S}}^2$  scale roughly with  $\sqrt{V}$  in contrast to a linear volume dependence of the fluctuations of the blocks  $\sigma_{\prod_k D_k}^2 = N_{blk} \sigma_{D_k}^2$  with  $N_{blk} \propto V$  the number of the blocks [112]. Furthermore the fluctuations of the full operator scale linear with the volume. However for the used lattice sizes the magnitude of the block fluctuations is around 20% of the Schur complement for block sizes  $l \geq 4$ . Due to that the block fluctuations can not explain the linear volume dependence of the full operator. The explanation is the covariance of the blocks with the Schur complement which scales with the volume. The mild volume behavior of the Schur complement in the one flavor case can be understood by the domination of the IR-modes with  $\sigma_{\hat{S}}^2 \sim V \Delta m^2 \text{var}(\lambda_{IR})$ . For the fluctuations of the smallest eigenvalues of  $\sqrt{D^\dagger D}$  is found that it scales with  $1/V$  while the small eigenvalues with  $1/V^2$  [8]. Obviously if the small eigenvalues were completely decoupled from each other it would follow  $\sigma_{\hat{S}}^2 \propto 1$ . This is not the case but the small eigenvalues are correlated between each other and DD can only approximately separate the IR- from the UV-modes.

The numerical analysis of fluctuations in the isospin reweighting case suggests, following the previous argumentation based on eq. (5.43), that it is dominated by the IR-modes in the analyzed mass range. Again this analysis can be done by using DD, here by using the even-odd decomposition. The ensemble fluctuations of the Schur complement have again a mild volume behavior of roughly  $r \sim 0.5$ . However this behavior is also found for the full operator. An explanation is that the UV-fluctuations are sub-dominant. The ratio of fluctuations of the Schur complement over the fluctuations of the blocks is given by  $\sigma_{\hat{S}}^2 / \sigma_{\prod_k D_k}^2 \sim 5 \cdot 10^4$  for the E5 ensemble. This is roughly the square of the ratio of the correlation of the blocks with the Schur complement over the fluctuations of the blocks,  $\text{cov}_{\hat{S}, \prod_k D_k} / \sigma_{\prod_k D_k}^2 \sim 50$ . It follows that the fluctuations are dominated by the small eigenvalues because the covariance with the blocks and the variance of the blocks is negligible and it follows

$$\sigma^2 \sim V \Delta m^4 [\text{var}(\lambda_{IR}) + \text{var}(\lambda_{UV}) + 2 \text{cov}(\lambda_{UV}, \lambda_{IR})] \sim V \Delta m^4 \text{var}(\lambda_{IR}). \quad (5.44)$$

A similar behavior is found also for the ensemble fluctuations in the case of  $\mu$ -reweighting [109]. In general the analysis suggest that DD is sufficient to separate the UV- and the IR-modes of the Dirac operator.

## 5. Mass Reweighting

---

Table 5.3.: The table shows the statistics used for the applications of the reweighting method to the CLS ensembles. The distance between the used configurations are given in MDU (Molecular Dynamic Units) multiplied by the ratio of the active links  $R_{act}$  (compare eq. (4.18)). For D5, 2012 configurations were used to analyze the reweighting in the one flavor reweighting case. For the isospin reweighting 503 configurations were used with a distance of 8 MDU's. The ratios of the fluctuations  $\sigma_{st,rel}^2/\sigma_{ens}^2|_{Iso}$  and  $\sigma_{st,rel}^2/\sigma_{ens}^2|_{1fl}$  are calculated at the maximal shift. The relative stochastic fluctuations are given by  $\sigma_{st,rel}^2 = \langle \sigma_{st}^2/W^2 \rangle$  and depend explicitly on  $N$  and  $N_\eta$ . The ratios of the fluctuations for the one flavor case are given for decreasing the up-quark mass.

ID	$N_{cnfg}$	MDU's/config· $R_{act}$	$N_\eta$	$N$	$\sigma_{st,rel}^2/\sigma_{ens}^2 _{Iso}$	$\sigma_{st,rel}^2/\sigma_{ens}^2 _{1fl}$
A5	202	20 · 1	6	8	0.17(6)	0.060(1)
E4	100	16 · 0.37	6	8	0.26(1)	0.112(3)
D5	2012	2 · 1	6	8	–	0.150(2)
	503	8 · 1	6	8	0.09(28)	–
E5	99	160 · 0.37	6	8	0.21(2)	0.056(2)
F7	350	16 · 0.37	6	8	0.20(3)	0.150(2)
G8	90	8 · 1	12	8	0.12(2)	0.086(9)
O7	98	40 · 1	6	8	0.23(2)	0.093(3)

### Numerical costs

The stochastic estimation introduces additional noise to the ensemble noise. To have a significant signal of the reweighting factor the ensemble noise should dominate over the stochastic noise. The ratios of the fluctuations are given in table 5.3 for the used ensembles for the maximal shift in the case of the isospin reweighting. By demanding that the ratio of  $\sigma_{st,rel}^2/\sigma_{en}^2 \sim 0.1$  with  $\sigma_{st,rel}^2 = \langle \sigma_{st}^2/W^2 \rangle$  it is possible to estimate the cost of mass reweighting.

A possible way is to extract the costs from the fits of  $\sigma_{fl}^2$  and  $\sigma_{ens}^2$  with the fit constants  $k_{st}$  and  $k_{ens}$ . For the one flavor case the ratio is given by

$$\frac{\sigma_{st,rel}^2}{\sigma_{en}^2} NN_\eta = \frac{k_{st}}{k_{en}} \sim 2.5 \dots 7.5 \quad (5.45)$$

(lower bound given by using DD). In general 48 estimations with  $N_\eta = 6$  and  $N = 8$  for each ensemble seem to be sufficient to have a good noise to signal ratio. For the isospin reweighting case the ratio is given by

$$\frac{\sigma_{st,rel}^2}{\sigma_{en}^2} NN_\eta \sim \frac{9V^{1-r}}{(48 \times 28^3)^{1-r}} \frac{a^{4(1-r)}}{[0.066 \text{ fm}]^{4(1-r)}} \frac{[32 \text{ MeV}]^{q'-3}}{\bar{m}^{q'-3}} \quad (5.46)$$

by using  $r \approx 1/4 \dots 3/4$  and  $q' \approx 4 \dots 3$ . Assuming that the solver cost scales proportional to  $V$  the cost of reweighting scales as  $V^{3/2}$  in order to keep  $\sigma_{st}^2/\sigma_{en}^2$  constant.

### Ensemble fluctuations for strange quark reweighting

Similar to the case of the one flavor or the two flavor isospin reweighting eq. (5.38) and eq. (5.42) the scaling in the lattice volume is analyzed for the fluctuations of strange quark reweighting. By setting  $\gamma = 1$  and a quenched strange quark to the mass  $\bar{m}_s = 4\bar{m}_r$  (with  $m_r$  the light quark mass on the D5/E5 ensemble) the ensemble fluctuations are given by

$$\sigma_{en,sq}^2(\gamma = 1) = k_{en}^{(sq)} \frac{V_{phys}^r \Delta \bar{m}^{2p'}}{r_0^{4r-2p'+q'} \bar{m}^{q'}}. \quad (5.47)$$

The scaling in the mass shift  $\Delta m$  follows from eq. (5.17), is observed in the numerical analysis and is given by  $p' = 1$ . The volume scaling is deduced from the ensembles D5 and E5 and is roughly given by the square root of the volume  $r \sim 0.5$ . It is found that the stochastic fluctuations scale with the volume and thus

the expectation for the numerical cost is given by

$$\frac{\sigma_{st,rel}^2}{\sigma_{en}^2} NN_\eta \sim 11 \frac{\sqrt{V}}{\sqrt{48 \times 24^3}} \frac{a^2}{(0.066 \text{ fm})^2} \quad (5.48)$$

where the quark mass behavior is kept constant and not analyzed here. However DD suggests that the ensemble fluctuations are dominated by the IR-modes, i.e. DD has no effect on the stochastic fluctuations as in the case of isospin reweighting.

#### 5.4.2. Errors

Using mass reweighting the statistical error of the observables increases. In this subsection the behavior of the error is discussed by using eq. (5.10) (eq. (D.31)) derived in app. D. The increase of the error can be understood by a decreasing of the effective ensemble size with  $N_{eff} = N \cdot \delta_O^2 / \delta_{OW}^2$  with  $\delta_O$  the error without the reweighting factor. By expanding the reweighting factor in  $\Delta m^p$  the error can be approximated by terms which scale less or proportional to  $\Delta m^{2p}$  with  $p = 1$  for the one flavor and  $p = 2$  for the isospin reweighting case. Numerical analysis shows that the first term of the approximated error eq. (5.10) dominates the error. This can be understood due to the fact that the correlation between  $O_i$  and  $O_j W_j^2$  is larger than the correlation between  $O_i$  and  $W_j$ . In general the approximation eq. (D.32)

$$\delta_{OW}^2 \sim \frac{1}{N^2 \langle W \rangle^2} \sum_{i,j} [(O_i - \langle O \rangle) W_i (O_j - \langle O \rangle) W_j] \quad (5.49)$$

describes the error well for primary fermionic observables like for the correlators  $f_{AP}$  and  $f_{PP}$ . For example on the D5 ensemble in the case of one flavor reweighting the error is very well approximated up to large shifts with  $\Delta \overline{m} < 12$  MeV. For larger shifts the error is overestimated. Here at a shift of  $\Delta \overline{m} = 16$  MeV, the effective ensemble size is reduced by roughly a factor 6 which corresponds to an increase of the error by a factor  $\sqrt{6}$ . Moreover it is found that the effective ensemble size reduces proportional to  $\Delta m^2$ . In the case of isospin reweighting the error is dominated by the observable error and an effect is not observed also in the case of the G8 ensemble.

In the case of gluonic observables the formula eq. (5.49) also gives a rough estimate of the error. Numerically a tendency to larger errors is found in case of one flavor reweighting. The effective ensemble size is reduced roughly by a factor 3.5 on the D5 ensemble for the largest mass shift. Like in the case for fermion observables this effect scales roughly with  $\Delta m^2$ .

### 5.4.3. Bias

Reweighted observables have a bias in contrast to the stochastic estimation of the reweighting factor. The bias is given in eq. (D.18) of the app. D where an approximation is given by eq. (D.30)

$$\langle \bar{F} - F \rangle \sim -\frac{1}{N^2 \langle W \rangle^2} \sum_{ij} [(O_i W_i - \langle OW \rangle)(W_j - \langle W \rangle)] \quad (5.50)$$

where  $O_i$  and  $W_i$  depend on the configuration  $i$ . The formula eq. (5.50) is derived by expanding the reweighting factor and neglecting higher order terms with  $\mathcal{O}(\Delta m^{3p})$ . It is found that for the analyzed observables and mass range the approximation formula eq. (5.50) of the bias works well.

The bias becomes important for small sample sizes, where the  $1/N$  reduction of the bias has an impact compared to the statistical error reduction of  $1/\sqrt{N}$ . Due to the fact that many observables in LQCD are secondary and have a bias a proper sample size has to be chosen such that the statistical error is dominating. The same has to be done in the case of mass reweighting to suppress the bias. However for large reweighting ranges the effective number of configurations is reduced substantially. In this case the bias becomes important and the result is affected. This can be seen for the largest mass shift of the F7 and G8 ensembles in the case of the  $t_0$  reweighting (see right fig. 5.6). On the G8 ensemble in the case of two flavor mass-degenerate reweighting the error has the same size as the bias with  $\sim 10^{-3}$  for the largest mass shift.

### 5.4.4. $\beta$ -Shift

The reweighting factor is correlated with the plaquette and it is possible by an additional shift in the Boltzmann factor to minimize the ensemble fluctuations (see sec. 4.2). Note here the analysis is restricted to the one flavor reweighting case with  $\gamma = 0$ . The best reweighting strategy leads to changing the pure gauge coupling  $\beta \rightarrow \beta'$ . Following eq. (4.22) a  $\beta$ -shift can be introduced via

$$\Delta\beta = -\frac{\text{cov}(S_g, \ln W)}{\text{var}(S_g)}. \quad (5.51)$$

This minimizes the ensemble fluctuations and the Boltzmann factor takes the form  $V_{\beta'} = V_{\beta} W$  with the reweighting factor

$$W = \exp\{-\Delta\beta S_g\} \cdot \frac{\prod_{i=1}^{n_f} \det D(U, m'_i, \dots)}{\prod_{i=1}^{n_f} \det D(U, m_i, \dots)} \quad (5.52)$$

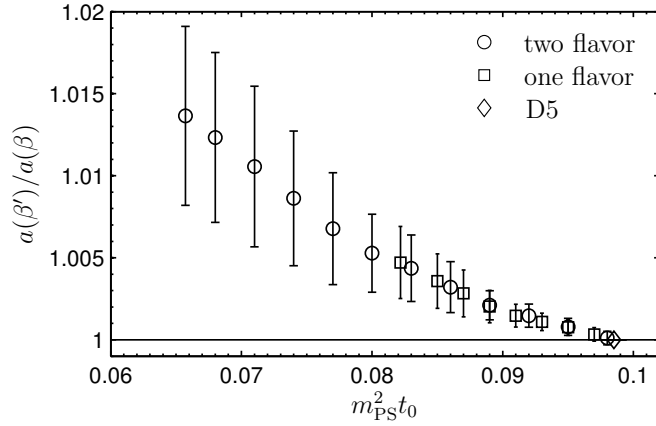


Figure 5.5.: The figure shows the lattice spacing-dependence  $a$  of the  $\beta$ -shift. The lattice space variation during a minimization of the ensemble fluctuations is plotted versus the pseudoscalar mass scaled by  $t_0$  for the one flavor (square) and the two flavor mass-degenerate reweighting case (circle) measured on the D5 ensemble.

with  $\Delta\beta = \beta' - \beta$ . The  $\beta$ -shift  $\Delta\beta$  grows linear proportional to the number of the flavors  $n_f$ , the mass shift  $\Delta m$  and it has the opposite sign of  $\Delta m$ . This property can be understood by the hopping parameter expansion (see sec. 4.2). Numerically for a mass-shift of  $\Delta\bar{m} = \bar{m}/2$  on the D5 ensemble a  $\beta$ -shift of  $\Delta\beta/n_f \simeq 3 \times 10^{-4}$  is found. This gives a reduction of the ensemble fluctuations by a factor  $\sim 0.4$ .

Using the pure gauge coupling  $\beta$  to fix the lattice spacing  $a$  the  $\beta$ -shift shifts also the lattice spacing. In order to estimate the order of the shift the gluonic observable  $t_0$  is measured and compared with its mass behavior to the pure mass reweighting case. The change is shown in fig. 5.5 where the ratio of  $a(\beta')/a(\beta) = \sqrt{t_0(\beta)/t_0(\beta')}$  is plotted versus the non-singlet pseudoscalar mass  $m_{\text{PS}}^2 t_0$  in units of  $t_0$  for the one flavor and the two flavor mass-degenerate case. The total change of the lattice spacing for  $\Delta\bar{m} = \bar{m}/2$  is roughly around 1% – 2% and lies in the accuracy of the lattice spacing  $a$  [98]. Note for non-perturbatively  $\mathcal{O}(a)$ -improved lattice operators a shift in  $\beta$  shifts also the improvement parameters, e.g. the  $c_{\text{SW}}$  parameter. However in the presented case the  $\beta$ -shift is quite small and the shift in the improvement parameter  $c_{\text{SW}}$  is negligible because the error-bounds are larger. In general the  $\beta$ -shift by reweighting towards smaller quark masses increases the lattice spacing which in turn diminishes the physical mass shift.

Also other lattice parts which are correlated with the reweighting factor can be used to reduce the fluctuations, e.g. by introducing a HYP-smearred plaquette [12].

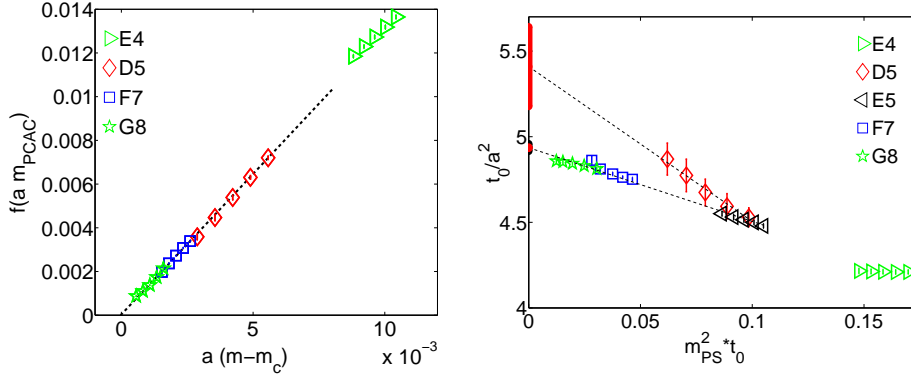


Figure 5.6.: The figures show the application of the two flavor mass-degenerate reweighting to the observables  $m_{PCAC}$  and  $t_0$  for the CLS ensembles with  $\beta = 5.3$ . The left figure shows the extrapolation of the  $m_{PCAC}$  corrected by the first order in lattice perturbation theory with the function given in eq. 5.53 towards the critical mass. The right figure shows the extrapolation of  $t_0$  towards the chiral limit. By using the data of the E5, F7 and G8. The extrapolation corresponds to the chiral limit of [118]. The extrapolation by using only data of the D5 ensemble deviates from the expectation due to large finite volume effects in the pion mass.

Another concept is to use mass shifts of other quarks to reduce the fluctuations. This is nothing else than to use two flavor mass reweighting with a properly tuned  $\gamma$  (see for example subsec. 5.6.2 and subsec. 5.6.3).

## 5.5. Applications

The knowledge of the mass behavior of observables is one of the key points in LQCD to derive physical observables. It is used to connect the observables to the chiral limit, where the quark masses vanish, and to the physical point, where the pion mass corresponds to the physical mass. By using an effective theory the so called chiral perturbation theory, it is possible to perform controlled fits by using data of the observables depending on different quark masses. By using two flavor mass-degenerate reweighting it is possible to measure these observables for different mass values by using only one ensemble. In this section the potential and the limit of mass reweighting is shown.

## 5. Mass Reweighting

Table 5.4.: The table shows the critical  $\kappa$  and chiral  $t_0/a^2$  determined by using two flavor mass-degenerate reweighting compared to the results of [98] for the critical hopping mass parameter  $\kappa$  and to the results of [118] for the chiral values of  $t_0/a^2$ . Note the error is underestimated, e.g. systematic uncertainties are coming from linear extrapolation of  $t_0(m_{PS})$  and  $\tau_{exp}$  is not used in the error estimation.

$\beta$	$\kappa_{crit}$ [98]	$\kappa_{crit}$ using 2 fl	$t_0/a^2$ [118]	$t_0/a^2$ using 2 fl
5.2	0.1360546(128)	0.1360694(131)	3.451(18)	3.518( 17)
5.3	0.1364572(47)	0.1364582( 5)	4.937(22)	4.936( 4)
5.5	0.1367749(13)	0.1367759( 39)	9.544(48)	9.416(129)

### 5.5.1. Critical Mass

If the lattice discretization of the fermion operator breaks exact chiral symmetry the critical mass parameter, the bare mass parameter at which the quark masses vanish gets an additional mass shift which depends on the lattice spacing  $a$ . An extrapolation towards zero quark masses has to be performed to deduce the critical mass parameter. The PCAC mass can be connected to the bare quark mass  $m_q = m - m_c$  following app. E of [98] via

$$m_{PCAC}^{rs}(1 + \tilde{b}_r a m_{PCAC}^{rs}) = Zr_m m_q. \quad (5.53)$$

with a renormalization constant  $Zr_m$ . The improvement coefficient  $\tilde{b}_r$  is given to one loop in perturbation theory by  $\tilde{b}_r = \frac{1}{2} + 0.0500\frac{6}{\beta}$  [119, 120]. The extrapolation can be done by using two flavor mass-degenerate reweighting. The deduction of the critical mass parameter is shown in the left figure 5.6 by using eq. (5.53). The results are shown in table 5.4 and compared to the results of [98]. Note the error could be in principle underestimated, i.e.  $\tau_{int}$  is estimated by  $UWerr.m$  [78] and a more conservative analysis with a proper chosen  $\tau_{exp}$  [27] is only done by using the F7 ensemble. The extrapolation gives for the F7 ensemble a critical hopping mass parameter of  $\kappa_{crit} = 0.1364581(106)$  compared to an error  $37 \cdot 10^{-7}$  if  $\tau_{exp}$  is set to zero. Note that for the ensembles with the gauge coupling  $\beta = 5.2$  and  $\beta = 5.5$  only one ensemble is used to determine the critical mass parameter. In general the results show that it is possible to deduce the critical mass parameter by using only one ensemble. Moreover mass reweighting can improve the extrapolation result. Although two flavor mass-degenerate reweighting introduces large fluctuations the data show that it is applicable for lattice volumes up to  $128 \times 64^3$  with moderate mass shifts of  $\Delta\bar{m} \approx \bar{m}/3$ .



### 5.5.2. Scale setting with $t_0$

The mass behavior of gluonic observables like  $t_0$  (see subsec.4.3.2) can be derived by using two flavor mass–degenerate reweighting. In general  $t_0$  can be used to fix the lattice spacing  $a$  to a physical dimension relative to another ensemble in the chiral limit [118].

The results are shown in table 5.4 and in the right fig. 5.6. The chiral extrapolation is done by assuming a linear dependence of  $t_0/a^2$  in the quantity  $m_{PS}^2 t_0$ . The results are compared to the extrapolation done in [118]. For the  $\beta = 5.2$  and  $\beta = 5.5$  only one ensemble is used while in the case of  $\beta = 5.3$  the ensembles E5, F7 and G8 are used to determine the chiral value. The error analysis is done by using *UWerr.m* [78] while by a more conservative assumption the error increases in the case of the  $\beta = 5.3$  lattices with a proper  $\tau_{exp}/MDU's \sim 200$  (see [98], [27]) by roughly by a factor 2 to 0.007. This shows that two flavor mass–degenerate reweighting can enhance the extrapolation properties and thus increases the precision of the deduced results (see tab. 5.4). Only the values of the E4 ensemble and A5 show deviations from the expected behavior (see fig. 5.6 and tab. 5.4). An explanation could be a larger quark mass. Note that the pseudoscalar mass of the D5 ensemble has large finite size effects which explain the different scaling behavior.

Furthermore the extrapolation is quite robust, i.e. by neglecting the largest shifts in both mass directions of the F7 and G8 ensembles due to the expectation of bias the chiral value changes only slightly to 4.935(4).

## 5.6. Tuning of bare Mass Parameters

### 5.6.1. Tuning of $\kappa_u, \kappa_d$ and $\kappa_s$

Dimensionless ratios of physical quantities can be used to fix the bare mass parameters. This is discussed in [98] for the bare mass parameters of the strange quark  $\kappa_s$  and of the two mass–degenerate light quarks  $\kappa_{ud}$  by using the ratios

$$R'_1 = \frac{m_K^2}{f_K^2} \quad \text{and} \quad R'_3 = \frac{m_\pi^2}{f_K^2}. \quad (5.54)$$

$R'_1$  can be used to tune  $\kappa_s$  such that  $R'_1 \equiv R'_{1,phys}$ . Now, a mass extrapolation can be performed towards the physical point by using chiral perturbation theory ( $\chi$ pt) in  $R'_3$  such that  $R'_3 \equiv R'_{3,phys}$  with  $R'_{1,phys} = 494.2^2/155^2$  and  $R'_{3,phys} = 134.8^2/155^2$  [50].

Here, a splitting of the up- and down quark is introduced. The ratios have to be modified and the mass–degenerate pseudoscalar particles  $K$  and  $\pi$  split up into  $K^0, K^\pm$  and  $\pi^0, \pi^\pm$ . A third tuning condition  $R'_2$  is added and by demanding that

## 5. Mass Reweighting

---

the conditions eq. (5.54) change only at next to leading order in chiral perturbation theory the new conditions are given by

$$R_1 = 2 \frac{m_{K^0}^2 + m_{K^\pm}^2}{(f_{K^0} + f_{K^\pm})^2}, \quad R_2 = 4 \frac{m_{K^0}^2 - m_{K^\pm}^2}{(f_{K^0} + f_{K^\pm})^2}$$

and

$$R_3 = 4 \frac{m_{\pi^\pm}^2}{(f_{K^0} + f_{K^\pm})^2}. \quad (5.55)$$

The decay constants can be approximated by  $0.5(f_{K^0} + f_{K^\pm}) \approx 155$  MeV. In leading order  $\chi$ pt the ratios are given by [121]

$$R_1 = \frac{B}{F^2} \left( \frac{m_u + m_d}{2} + m_s \right), \quad R_2 = \frac{B}{F^2} (m_d - m_u) (1 - C(m_u + m_d))$$

and

$$R_3 = \frac{B}{F^2} (m_u + m_d) \quad (5.56)$$

with the constants  $B$ ,  $C$  and  $F$ . By using the electric neutral corrected pseudoscalar masses  $m_{\pi^\pm,phys} = 134.8$  MeV,  $m_{K^\pm,phys} = 491.2$  MeV and  $m_{K^0,phys} = 497.2$  MeV [50] the dimensionless tuning conditions are straightforward to derive. However these numbers are derived by using Dashens theorem [122] to subtract the quantum electrodynamics (QED) effects.

The approach is to fix first  $m_s$  such that  $R_1 \equiv R_{1,phys}$  and  $\Delta m_{ud} = m_d - m_u$  such that  $R_2 \equiv R_{2,phys}$  and then to perform the extrapolation in  $R_3$  to  $R_{3,phys}$  in order to fix  $2m_{ud} = m_d + m_u$ . Two flavor mass reweighting is appropriated to fix the sea quark contributions for every of these three different conditions. This is more feasible for  $R_1$  and  $R_2$  by a combined approach with an optimal  $\gamma$ , see for optimal tuning of  $R_1$  next subsec. 5.6.2 and for  $R_2$  subsec. 5.6.3. For the case  $R_3$  if  $R_2$  is not tuned two-flavor mass-degenerate reweighting can be used which is only feasible for relatively small shifts in the quark mass (see previous sec. 5.5).

### 5.6.2. Strange Quark Reweighting

#### Tuning of $\gamma$

Two flavor reweighting is appropriated to correct the strange quark mass. The idea is to minimize the fluctuations by using the correlation with the reweighting factors of the light quarks and to reduce these fluctuations further by deriving an optimal  $\gamma$ . Using a similar approach as in sec. 4.2 the two flavor reweighting factor can be rewritten from eq. 5.12 as

$$M^{-1} = I - \Delta m \frac{(\gamma - 1)D_{m_+} + (\gamma + 1)m_- + \gamma \Delta m}{D_{m_+}^2 - m_-^2} \quad (5.57)$$

with  $m_{\pm} = 0.5(m_2 \pm m_1)$ . The determinant is expanded

$$W_{2fl} = \exp(w), \quad w = -\Delta m[(\gamma - 1)\text{Tr } b + (\gamma + 1)\text{Tr } c] + \mathcal{O}(\Delta m^2) \quad (5.58)$$

with  $b = D_{m_+}/(D_{m_+}^2 - m_-^2)$  and  $c = m_-/(D_{m_+}^2 - m_-^2)$ . By minimizing the variance of the exponent with respect to  $\gamma$  it follows

$$\gamma^* \approx \frac{\text{var}(\text{Tr } b) - \text{var}(\text{Tr } c)}{\text{var}(\text{Tr } b + \text{Tr } c)}. \quad (5.59)$$

By assuming that  $m_-$  is small it follows  $\text{var}(\text{Tr } b) \sim \text{var}(\text{Tr } D_{m_+}^{-1}) \sim k_{1f}V$  and  $\text{var}(\text{Tr } c) \sim m_-^2 \text{var}(\text{Tr } D_{m_+}^{-2}) \sim m_-^2 k_{\pm} \sqrt{V}$  (see subsec. 5.6.3) and by neglecting the covariance  $\text{cov}(\text{Tr } b, \text{Tr } c)$  eq. (5.59) takes the form

$$\gamma^* \sim 1 - 2m_-^2 \frac{k_{\pm}}{k_{1f}\sqrt{V}} + \mathcal{O}(\Delta m, m_-^3). \quad (5.60)$$

It follows for the D5 ensemble  $\gamma^* \approx 0.86$  by inserting  $m_- = 50$  MeV and the value  $k_{\pm}/k_{1f}$ , which is derived in subsec. 5.4.1 for  $m_+ \approx \bar{m}/3$  for the D5 ensemble. Note the volume dependence of  $\gamma$  is proportional to  $\Delta\gamma^* \approx -1/\sqrt{V}$ . By a direct minimization of the fluctuations the coefficient  $\gamma^*$  is given by  $\gamma^* = 0.82(1)$  for the D5 ensemble.

### Practice

A sufficient condition to minimize the ensemble fluctuations by varying the bare mass parameters is given by

$$\text{const} = \frac{m_u + m_d}{2\gamma} + m_s \quad (5.61)$$

in the first approximation by an optimal tuning of  $\gamma > 0$ . Now the strange quark mass  $m_s$  can be varied such that tuning condition  $R_1$  is fulfilled with  $R_1(m'_s) \equiv R_{1,phys}$ . Note that this is a strategy for 2+1 simulations. Here  $\kappa_s$  is taken from [98]. By using two flavor mass reweighting the idea is to reweight the light quark separately by first  $(m_d, m_s) \rightarrow (m_s + \delta m/2, m_d - \gamma\delta m/2)$  with  $\delta m = m'_s - m_s$  and second  $(m_u, m_s + \delta m/2) \rightarrow (m'_s, m_u - \gamma\delta m/2)$ . This process can be optimized by alternating the reweighting steps in the light quarks. Furthermore an improved interpolation can be introduced by using the reordering approach or the polynomial approach (see subsec. 5.3.1). Note for the former case the endpoint has to be known.

In principle if the strange quark mass is set to a lighter mass in the simulation a

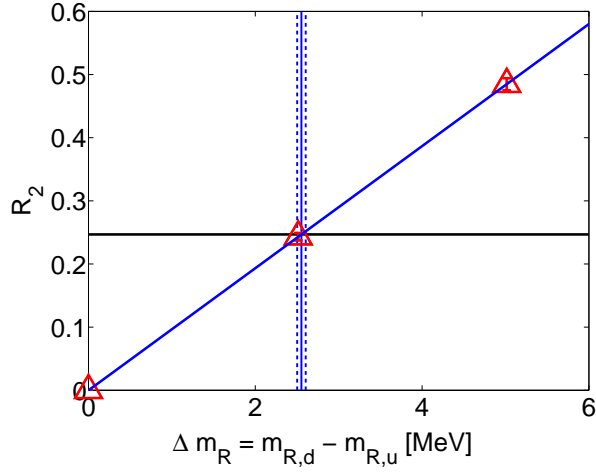


Figure 5.7.: The figure shows the tuning of  $\Delta m_{ud} = m_d - m_u$  by using  $R_2$  for the F7 ensemble.  $R_2$  is plotted versus the renormalized quark mass difference  $\Delta \bar{m}_{ud} = \bar{m}_d - \bar{m}_u$  in the  $\overline{\text{MS}}$ -scheme with  $\bar{m} = m_R$ .

tuning of  $R_1$  would lower the light quark masses. This is an interesting approach due to the fact that simulation gets unstable and expensive if the light quark masses are lowered.

### 5.6.3. Isospin Reweighting

To avoid partially quenched chiral perturbation theory in measurements of broken isospin effects mass reweighting can be used to incorporate these sea quark effects. However for large quark masses the sea quark effects are suppressed compared to the valence quark effects and the correction effect is quite small. This can change if the physical point is approached which can be observed in partially quenched chiral perturbation theory. Partially quenched chiral perturbation theory has an IR divergence term and breaks down if the mass of a partially quenched quark becomes too small (see e.g. [123] and the quoted condition on page 50  $|m_{sea}^2 - m_{val}^2| < \min(m_{sea}^2, m_{val}^2)$ ).

Table 5.5.: Isospin tuning of  $\kappa_u$  and  $\kappa_d$ .

ID	$\kappa_u$	$\kappa_d$	$\overline{m}_{ud}$	$\Delta\overline{m}_{ud}$
A5	0.1359501(1)	0.1359298(1)	17.2(3)	2.57(11)
E4	0.1361152(1)	0.1360848(1)	57.2(4)	2.92( 4)
D5	0.1362633(1)	0.1362367(1)	32.4(4)	2.60( 6)
E5	0.1362632(1)	0.1362368(1)	32.5(3)	2.73( 7)
F7	0.1363908(1)	0.1363692(1)	12.3(1)	2.55( 6)
G8	0.1364174(1)	0.1364166(1)	6.2(1)	2.62(14)
O7	0.1367182(2)	0.1367018(2)	13.2(1)	2.55(13)

### Tuning of $R_2$

The idea is to use isospin mass reweighting to tune the second condition  $R_2$  by introducing a mass shift in the light quarks. By fulfilling the condition

$$const = m_u + m_d \quad (5.62)$$

which follows from eq. (5.61) the tuning for the ensemble F7 is shown in fig. 5.7. The tuned bare quark mass parameters  $\kappa_u$  and  $\kappa_d$  are shown in table 5.5. Numerically it is found that the tuning procedure  $R_2$  has a tiny shift to the condition  $R_1$  which is negligible due to larger statistical error.

For unphysical quark masses the sea quark effects are dominated by the sum of the light quarks and the ensemble fluctuations are given by  $\sigma_{ens,Iso}^2 \approx 0.4 \cdot 10^{-3}$  for the F7 ensemble at the physical isospin broken point. For smaller quark masses the fluctuations become larger and can be significant at the physical point. By using eq. (5.42) the fluctuations are roughly given by  $\sigma_{ens,Iso}^2|_{m_{phys}} \approx 0.03$  at a lattice volume of  $128 \times 64^3$ .

### Quark masses

The light quark masses can be extracted by using the tuning conditions  $R_2$  and extrapolating in  $R_3$ . By measuring the PCAC mass eq. (4.32) the light quark mass difference  $\Delta m_{ud} = m_d - m_u$  and the average mass  $m_{ud} = 0.5(m_u + m_d)$  is deduced in the  $\overline{\text{MS}}$ -scheme for finite lattice spacings  $a$ . The chiral extrapolation towards the physical point is done by using the first order in chiral perturbation theory for the

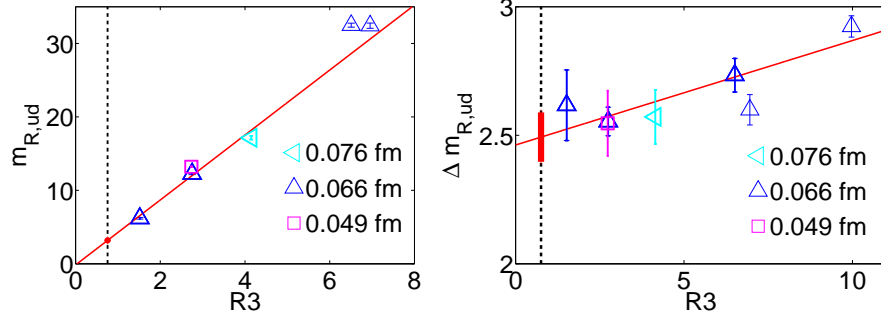


Figure 5.8.: The figure shows the light quark masses extrapolation in the quantity  $R_3$ . The left figure shows the renormalized light average quark mass  $\overline{m}_{ud}$  for all analyzed ensembles except E4. The extrapolation (red line) towards the physical point (black dotted line) is done by using the ensembles F7 and G8. The right figure shows the renormalized light quark mass difference  $\Delta\overline{m}_{ud}$  by showing the values of every analyzed configuration. The extrapolation (red line) towards the physical point (black dotted line) is done by using the ensembles E5, F7 and G8.

difference (see eq. (5.56))

$$\Delta m_{ud}(R_3) = \Delta m_{ud}|_{chiral} + b \cdot R_3 + \mathcal{O}(\Delta m_{ud} R_3) \quad (5.63)$$

and for the average

$$m_{ud}(R_3) = c \cdot R_3 + \mathcal{O}(\Delta m_{ud}^2, R_3^2) \quad (5.64)$$

with constants  $b$  and  $c$ . The result is shown in figure 5.8. The average quark mass for  $\beta = 5.3$  is given by  $\overline{m}_{ud} = 3.19(11)$  MeV where the extrapolation is done by using F7 and G8. By using the ensembles E5, F7 and G8 the mass difference at the physical point is given by  $\Delta\overline{m}_{ud} = 2.49(10)$  MeV. For a continuum's limit the lattice spacing dependence  $a$  has to be deduced for which additional ensembles at  $\beta = 5.5$  and  $\beta = 5.2$  are necessary. However the condition  $\Delta m_{ud}$  shows a small dependency on  $R_3$ . A tendency to larger quark masses for finer lattice spacing is found in the case of the average quark mass (see fig. 5.8) which agree with the expectation of the literature for 2 flavor ensembles (see [50]).

### Isospin effects

In general isospin breaking effects originating from the sea quarks are small and scale with the mass split  $\Delta m_{ud}^2$ . Note the corrections are given directly by the

isospin mass reweighting factor. In general the statistical error has to be small so that the effects can be deduced.

In the pseudoscalar mass isospin breaking effects of sea quarks shift the mass with

$$M' = M + \Delta M. \quad (5.65)$$

The mass shift can be extracted from the correlators. The correlator is given by eq. (4.34) and by neglecting the higher energy levels than  $E_0$  it follows

$$\begin{aligned} f_{PP}(x_0) &= a_{01} \cosh(M'(x_0 - T/2)) + \dots \\ &= a_{01} \cosh(My_0) (\cosh(\Delta My_0) + \tanh(My_0) \sinh(\Delta My_0)) + \dots \\ &= h(x_0, 0, M(x_0)) f(\Delta M(x_0), A(x_0, M(x_0))) \end{aligned} \quad (5.66)$$

with  $y_0 = (x_0 - T/2)$  and the function

$$f(m, A) = \frac{1}{2} ((1 + A)e^m + (1 - A)e^{-m}) \quad (5.67)$$

with the coefficient

$$A(x_0, M(x_0)) = \tanh(M(x_0)(x_0 - T/2)). \quad (5.68)$$

The isospin effects enter the correlator with the covariance between the unshifted case and the isospin reweighting factor with

$$\begin{aligned} \langle f_{PP}^b(x_0) \rangle_b &= \langle f_{PP}^b(x_0) \rangle_a \left( 1 + \frac{\text{cov}(f_{PP}^b(x_0), W(a, b))}{\langle W(a, b) \rangle_a \langle f_{PP}^b(x_0) \rangle_a} \right) \\ &= \langle f_{PP}^b(x_0) \rangle_a \cdot \delta f_{PP, W}^b(x_0) \end{aligned} \quad (5.69)$$

with the parameter sets  $b = \{\beta, m_u, m_d, \dots\}$  determined by fixing  $R_2 \equiv R_{2, phy}$  in the light quarks  $m_u \neq m_d$  and  $a = \{\beta, m_{ud}, m_{ud}, \dots\}$  with mass-degenerate light quarks  $m_u = m_{ud} = m_d$ .

Now it is possible to define an effective mass shift  $\Delta M_{eff}(x_0)$  similar to eq. (4.36) by comparing eq. (5.66) and eq. (5.69)

$$\frac{f(\Delta M_{eff}(x_0 - a), A(M_{eff}(x_0)x_0 - a))}{f(\Delta M_{eff}x_0, A(M_{eff}(x_0), x_0))} = \frac{\delta f_{PP, W}^b(x_0 - a)}{\delta f_{PP, W}^b(x_0)} \quad (5.70)$$

with  $M_{eff}(x_0)$  deduced from the equation eq. (4.36) without isospin sea quark effects by using the propagator  $\langle f_{PP}^b(x_0) \rangle_a$ . In general the effective mass shift is quite noisy and a start and an end point of the plateau is difficult to deduce (see left fig. 5.9). Here, the start and end point which are used for the effective mass

## 5. Mass Reweighting

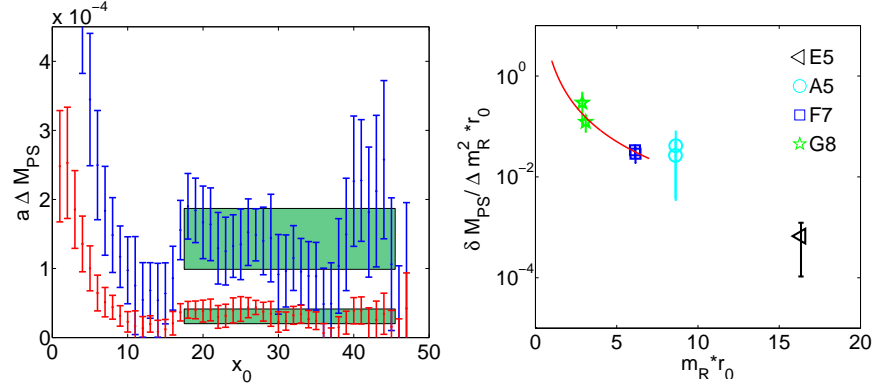


Figure 5.9.: The figures show the sea quark effects to the pion mass. The left figures shows the effective plateaus of  $a\Delta M_{PS}$  measured on the F7 ensemble at  $\Delta m/2$  (red) and  $\Delta m$  (blue). The right figure shows the mass shift in MeV normalized by the mass shift scaled with  $r_0$  of the ensembles E5, A5, F7 and G8. The fit is done by using the normalized mass shifts of F7 and G8.

are applied. The signal to noise ratio in the case of the kaon mass is too large that a deviation from zero could be found for all analyzed ensembles. In the case of the pion this is different. Also if the error is quite large a significant signal for the mass shift could be calculated on A5, F7 and G8. This is shown in figure (5.9). Note that for the O7 a negative value of  $\Delta M$  is found with large errors in contrast to the positive values of the other ensembles. However a scaling analysis is done for the F7 and G8 ensemble which is given by

$$r_0 \Delta M = k \frac{\delta m^2 r_0^2}{(m_q r_0)^{q'}} \quad (5.71)$$

with  $k = 2.0(18)$  and  $q' = 2.29(57)$ . Note by extrapolating towards the physical point the mass shift is given by  $\Delta M_{phys} \cong 0.50$  MeV. To deduce the isospin in the continuum ensembles of smaller quark masses on finer lattices have to be analyzed.

### 5.6.4. Electromagnetic Reweighting

One possibility to include electromagnetic effects into the weight factor is to generate a quenched QED ensemble and to incorporate unquenching effects by the reweighting factor. Following [124] a  $U(1)$ -action can be used to generate a QED-ensemble of  $U(1)$ -links. The QED-effects are coupled to a QCD-ensemble by mod-



ifying the  $SU(3)$  link  $U_\mu(x)$  by

$$U_\mu(x) \longrightarrow U_{\mu,Q} = \exp\{-ieQA_\mu(x)\} \cdot U_\mu(x). \quad (5.72)$$

with  $eQ$  the physical electrical charge of the involved quark and  $A_\mu(x) \in [0, 2\pi)$ . The  $SU(3)$  links are changed to elements of the  $U(3)$  group.

By using a combination of QED-reweighting for a quark with positive charge and for a quark with a negative charge the ratio matrix gets the form

$$M^{-1} = \frac{D + m' + ieQ \cdot \mathcal{U}}{D + m'} \frac{D + m - ieQ \cdot \mathcal{U}}{D + m} + \mathcal{O}(eQ^2) \quad (5.73)$$

by expanding the  $U(1)$  link with  $e^{-ieQA_\mu(x)} = 1 - ieQA_\mu(x) + \mathcal{O}(eQ^2 A_\mu(x)^2)$ . The matrix  $\mathcal{U}$  contains every element of the Dirac operator which depends on  $eQ$  and is multiplied by  $A_\mu(x)$ . In general this is the next-neighbor coupling terms and the clover term. Note the matrix  $\mathcal{U}$  does not commute with  $D$  and a correct ordering is given with  $M^{-1} = D_{m'}(Q)D_{m'}^{-1}(0)D_m(-Q)D_m^{-1}(0)$ . This enables stochastic estimation to be an efficient method and can be used for small correction (compare subsec. 5.1.1). Here, an estimation of the expectation of the fluctuations in the case of QED reweighting is given. The  $U(1)$ -links are generated randomly and coupled by the coupling constant  $e$  to the gauge links

$$U_{\mu,Q}(x) = e^{-ieQr_\mu(x)}U_\mu(x) \quad (5.74)$$

with  $Q$  the charge of the quark and  $r \in [0, 2\pi)$ . By using the D5 ensemble with  $Q_1 = -Q_2$  and  $e \sim 0.014$  the stochastic fluctuations are improved by using DD also for the two flavor reweighting. This suggests that the fluctuations scale linear with the volume. Compared to the mass reweighting case the electric charge acts on the eigenspace of the Dirac operator. Due to that the ratio is given by  $k_{st}/k_{en} \sim 184$  by using the even-odd Schur complement for the D5 ensemble. The cost increases by a factor 20 compared to the isospin reweighting and if the ensemble fluctuations scale linear with the volume the cost of QED-reweighting is of the order  $\mathcal{O}(V)$ .

## 5.7. Conclusion

### 5.7.1. Summary

The introduced reweighting technique can be used to fix the bare mass parameters  $\kappa_s, \kappa_d$  and  $\kappa_u$ . The results are:

- Two flavor mass-degenerate reweighting: Using two flavor mass-degenerate

reweighting it is possible to perform the mass extrapolation towards the physical and chiral point if  $R_2$  is not tuned. The numerical effort scales with  $\mathcal{O}(V)$  and  $\sim 48$  inversions are adequate to suppress the stochastic fluctuations. However two flavor degenerate mass reweighting introduces large ensemble fluctuations which limit the reweighting range for larger volumes. However in sec. 5.5.1 and sec. 5.5.2 was shown that it is possible to deduce the critical mass value and to perform a chiral extrapolation in observables like  $t_0$  by only using one ensemble. Furthermore reweighting can be used to reduce the statistical error of the extrapolation.

- $R_2$  : Using isospin mass reweighting it is possible to introduce isospin splitting in the down and up quark. The numerical effort scales roughly with  $\mathcal{O}(V^{3/2})$  and for an ensemble with bare parameters which correspond to the F7 ensemble  $\sim 96$  inversions are adequate to suppress the stochastic fluctuations. The sea quark effects by using isospin reweighting are quite tiny and they become only sizable for very small quark masses. By using  $R_2$  it is possible to introduce a mass shift in the light quark. The extrapolation towards the physical mass gives  $\Delta\bar{m}_{ud} = 2.49(10)$  MeV for the mass split and  $\bar{m}_{ud} = 3.19(11)$  MeV for the average quark mass deduced on the CLS-ensembles with a gauge coupling of  $\beta = 5.3$ .
- $R_1$  : Using two flavor mass reweighting it is possible to correct the strange quark mass in a sufficient way by introducing moderate ensemble fluctuations by a proper tuning of  $\gamma$ . In particular towards the physical point strange quark reweighting becomes interesting due to the fact that it can lower the light quark masses.

The presented techniques are available in a public version *mrw* [111] which is based on this work and which can be used in the *openQCD* package [110].

### 5.7.2. Prospects

The introduced combined reweighting technique can be used to reweight 2+1 QCD ensembles towards a 1+1+1 QCD+QED ensemble by introducing moderate increasing ensemble fluctuations. The estimate, done here, shows that QED-reweighting is an order of magnitude more expensive than mass reweighting, which is also found in [15]. Moreover other improvement effects like properly generated QED configurations and relative gauge fixing can shrink the cost further. 1+1+1 QCD+QED ensembles are necessary to understand isospin breaking effects which are accessible by using the introduced reweighting techniques by using QCD ensembles.

## 6. Partial Stochastic Multi Step Algorithm

The Partial Stochastic Multi Step algorithm (PSMS) [16], [125] is a Monte Carlo algorithm to sample gauge configurations with the Boltzmann weight of lattice QCD with two mass-degenerate Wilson type fermions. The motivation is to introduce an alternative to the HMC algorithm, i.e. to avoid force computation.

The idea is to split up the Boltzmann weight by proposing a new gauge configuration weighted by the pure gauge weight followed by cost ordered Metropolis accept-reject steps to correct the weight according to the Boltzmann weight of the system.

There are two major points to take into account to establish such an algorithm. The first point is the effectiveness. The acceptance rate of the Metropolis accept-reject steps suffers from fluctuations caused by the correction of the weight. These fluctuations split up into stochastic (see sec. 6.2) and ensemble fluctuations (see sec. 6.3). The second point is the correctness of the algorithm. Due to techniques to estimate the correction terms in the Metropolis accept-reject steps and to control the fluctuations it is not obvious that *detailed balance* is fulfilled, but can be shown (see app. E).

The chapter will end with an analysis of scaling features in the lattice spacing  $a$  and the volume  $V$  and some prospects of this kind of algorithms will be illustrated, e.g. with the PSMS it is possible to simulate partial HYP-smearred actions (see sec. 6.5).

### 6.1. Fluctuation and Acceptance

The idea is to decouple the pure gauge weighting from the fermion weighting by splitting up the mass-degenerate two-flavor Boltzmann factor

$$V_a(U) = \exp\{-\beta S_g(U)\} \cdot \det D^2(U, m) = V_{pg}(U, \beta) \cdot V_{2fl}(U, m). \quad (6.1)$$

with  $D^2(U, m)$  the Wilson Dirac operator eq. (2.42) and  $S_g(U)$  the Wilson plaquette action eq. (2.25). The simplest algorithm is a two-step algorithm, where the first step is done by a pure gauge update weighted by the pure gauge weight  $V_{pg}(U, \beta) = \exp\{-\beta S_g(U)\}$  followed by an accept-reject step with the fermion

## 6. Partial Stochastic Multi Step Algorithm

---

weight  $V_{2fl}(U, m) = \det D^2(U, m)$ . The mass of the mass-degenerate light quarks in the argument will be dropped from now on. For the pure gauge a combination of heat bath and overrelaxation steps is used (see sec. 2.5, [126], [127], [128]) which updates the configuration  $U$  to  $U'$ . The accept-reject step is done by a Metropolis accept-reject step [29] which corrects the weight to the mass-degenerate two-flavor Boltzmann factor by

$$P_{acc}(U \rightarrow U') = \min \left\{ 1, \frac{V_{pg}(U)V_a(U')}{V_{pg}(U')V_a(U)} \right\} = \min \left\{ 1, \frac{V_{2fl}(U')}{V_{2fl}(U)} \right\} \quad (6.2)$$

where the ratio of the fermion weight  $V_{2fl}$  enters the Metropolis accept-reject step as  $\frac{V_{2fl}(U')}{V_{2fl}(U)} = \exp\{-\Delta(U, U')\}$ . The crucial point is the acceptance rate of the Metropolis acceptance steps. Assuming a Gaussian distribution of  $\Delta(U, U')$  it follows [17] [97] for the acceptance rate

$$\langle P_{acc} \rangle_{U, U'} = \text{erfc} \left\{ \sqrt{\frac{\sigma^2}{8}} \right\} \quad (6.3)$$

with the variance  $\sigma^2(\Delta(U, U'))$ . The action ratio which enters the Metropolis accept-reject step can be rewritten in terms of a ratio matrix

$$\frac{V_{2fl}(U')}{V_{2fl}(U)} = \frac{\det D^2(U')}{\det D^2(U)} = \frac{1}{\det M^\dagger(U, U')M(U, U')} \quad (6.4)$$

with the ratio matrix  $M = D(U')^{-1}D(U)$  and  $\det D = \det D^\dagger$  which follows directly from the property  $D = \gamma_5 D^\dagger \gamma_5$ . The ratio matrix can be rewritten by

$$M = \frac{1 + \kappa\mathcal{K}(U)}{1 + \kappa\mathcal{K}(U')} = 1 + \kappa \frac{\mathcal{K}(U) - \mathcal{K}(U')}{1 + \kappa\mathcal{K}(U')} = 1 + \kappa\Delta K + \mathcal{O}(\kappa^2) \quad (6.5)$$

by using the Wilson Dirac operator  $D(U) = 1 + \kappa\mathcal{K}(U)$  eq. (2.42), the hopping parameter  $\kappa$  and  $\Delta K = [\mathcal{K}(U) - \mathcal{K}(U')]$ . The matrix size increases with the lattice size and to handle this the stochastic estimation method introduced in chap. 3 is used for the calculation of the determinant ratio eq. (6.4). One inversion is required to estimate the determinant of the hermitian ratio matrix  $M^\dagger M$ . Note that in an algorithm framework detailed balance requires that only one random field  $\eta$  can be drawn for each ratio (see app. E). Now it follows that an estimation of eq. (6.4) is given by

$$w(U, U', \eta) = \exp\{-\chi(U, U', \eta)^\dagger \chi(U, U', \eta) + \eta^\dagger \eta\} \quad (6.6)$$

with  $\chi(U, U', \eta) = D(U')^{-1}D(U)\eta$  and  $\eta \in \mathbb{C}^{12V}$  with the lattice volume  $V = T \times L^3$ . In the average over  $\eta$  follows  $\frac{V_{2fl}(U')}{V_{2fl}(U)} = \langle w(U, U', \eta) \rangle_\eta$ . By introducing stochastic estimation the fluctuations are given by (see sec. 3.3)

$$\sigma^2 = \sigma_{st}^2 + \sigma_{ens}^2 = \kappa^2 \left\{ \left\langle \text{Tr} \left( \Delta K + \Delta K^\dagger \right)^2 \right\rangle + \text{var} \left\{ \text{Tr} \left( \Delta K + \Delta K^\dagger \right) \right\} \right\} + \mathcal{O}(\kappa^3) \quad (6.7)$$

This shows that the two-step algorithm is not feasible due to the volume scaling of the fluctuations. The acceptance rate scales with  $\exp\{-V\}$  which is less than a percent for volumes larger than  $\sim (0.2 \text{ fm})^4$  on a pure gauge ensemble with gauge parameter  $\beta = 6.0$ . However by understanding and minimizing the fluctuations it is possible to establish a **P**atial **S**tochastic **M**ulti **S**tep (**PSMS**) algorithm which has a good acceptance rate up to  $(2.1 \text{ fm})^4$ . The key issues are techniques to minimize the stochastic and ensemble fluctuations.

## 6.2. Stochastic Fluctuations

The stochastic fluctuations are given by eq. (3.13)

$$\sigma_{st}^2 = \kappa^2 \left\langle \text{Tr} \left( \Delta K + \Delta K^\dagger \right)^2 \right\rangle + \mathcal{O}(\kappa^3). \quad (6.8)$$

In general to minimize the variance  $\sigma_{st}^2$  techniques have to be used which reduce the difference  $\Delta K = \mathcal{K}(U) - \mathcal{K}(U')$ . Note that the properties of  $\Delta K$  show the general difference of the stochastic fluctuations to the mass reweighting case chap. 5. In the mass reweighting case the parameter  $\Delta m$  can be used to control the fluctuations. Here, the matrix difference  $\Delta K$  has to be used. Furthermore the difference is not diagonal and the new configuration changes the eigenspace of the Dirac operator. The consequence is that techniques to control  $\Delta K$  are not straightforward. However the next subsections will describe an approach that can also handle the stochastic fluctuations by interpolation techniques.

### 6.2.1. Gauge Field Interpolation

An approach to keep the stochastic fluctuations under control is to use an interpolation method to perform the transition

$$\mathcal{K}(U) \longrightarrow \mathcal{K}(U'). \quad (6.9)$$

## 6. Partial Stochastic Multi Step Algorithm

---

The simplest way is a linear trajectory in the gauge field by introducing intermediate gauge fields by

$$U_{\mu,j}(x) = \frac{N-j}{N}U_{\mu}^g(x) + \frac{j}{N}U_{\mu}^{\prime g^{-1}}(x), \quad j = 0, 1, \dots, N \quad (6.10)$$

with  $U_{\mu}^g(x) = g(x)U_{\mu}(x)g^{\dagger}(x + \mu)$  with  $g(x) \in SU(3)$ . In general it is possible to choose a local gauge transformation such that the distance  $\Delta K$  is minimized (see sec. 6.2.2). By introducing intermediate gauge fields it is possible to factorize the determinant of the ratio matrix  $\det M^{\dagger}M$  by

$$\det M^{\dagger}M = \prod_{j=0}^{N-1} \det M_j^{\dagger}M_j \quad (6.11)$$

with the intermediate ratio matrix  $M_j = D(U_{j+1})^{-1}D(U_j)$ .

This factorization holds also for stochastic estimation. The only restriction is that detailed balance only holds if and only if the trajectory of the introduced intermediate gauge fields are invariant under an exchange of  $U$  by  $U'$  (see app. E). This is the case if the number of interpolation steps  $N$  is fixed. Furthermore each ratio has to be estimated independently. This requires one new inversion of the operator  $D(U_{j+1})$  for each step and the number of inversions of the Dirac operator increases with  $N$ .

Factorizing the determinant with  $N$  gauge field interpolation steps and using the unimproved Wilson Dirac operator with  $c_{5W} = 0$  the variance eq. (6.8) is reduced up to the second order in  $\kappa$  to

$$\sigma_{st,N}^2 = \frac{\kappa^2}{N} \left\langle \text{Tr} \left( \Delta K + \Delta K^{\dagger} \right)^2 \right\rangle + \mathcal{O} \left( \frac{\kappa^3}{N^2} \right) \quad (6.12)$$

with  $\Delta K_j = K(U_j) - K(U_{j+1}) = \Delta K/N$ . The error  $\mathcal{O}(\kappa^3/N^2)$  is dominated by the expansion of  $1/D(U_j)$  in  $\kappa$ . The numerical data shows that the higher order terms in the expansion like  $1/D(U_j)$  can dominate the fluctuations and a precise numerical analysis is necessary to establish a working interpolation. However the approximation eq. (6.12) shows the scaling in the parameter and for  $N \rightarrow \infty$  the stochastic estimation becomes exact. Another important issue is that the gauge field interpolation acts on the eigenspace of the ratio matrix. Using a perturbation approach shown in app. B for the eigenvalues it follows

$$\lambda_i = 1 + \frac{1}{N}\lambda_i^{(1)} + \mathcal{O} \left( \frac{1}{N^2} \right) \quad (6.13)$$

and for large  $N$  the eigenvalues  $\lambda_i$  tend to one. This is important because only if

every eigenvalue of the hermitian ratio matrix is larger than 0.5 the variance of the stochastic estimation is defined. Note that for hermitian matrices  $A = M^\dagger M$  the condition  $\lambda(A + A^\dagger) > 1$  (eq. (3.6)), which implies that the variance is defined, requires that  $\lambda(M^\dagger M) > 0.5$ . If this is not the case it is not possible to assure *ergodicity* and thus the convergence of the Markov Chain to the equilibrium probability distribution.

### 6.2.2. Relative Gauge Fixing

A technique which reduces the difference of  $\Delta K$  is to fix the gauge degrees of freedom which are related to a local gauge transformation  $g(x)$ . The idea is to use relative gauge fixing before doing the interpolation eq. (6.10) by fixing the gauge of the configuration  $U$  relative to the new gauge field  $U'$ . In general LQCD actions are invariant under a local gauge transformation  $U(x, \mu) \rightarrow g(x)U(x, \mu)g(x + \hat{\mu})^{-1}$  with  $g(x) \in SU(3)$ , e.g. the local gauge transformation enters the fermion part of the action as

$$\det D(U) = \det GD(U)G^\dagger = \det D(U^g) \quad (6.14)$$

with  $G_{x,y} = g(x)\delta_{x,y}$  where  $x$  and  $y$  label the sites and  $G$  is diagonal in the spin-space. A scalar product in the color-space can be defined by

$$(U, U') = \frac{1}{12V} \sum_x \sum_{\mu=0}^3 \text{Re Tr} \left\{ I - U_\mu^\dagger(x)U'_\mu(x) \right\}. \quad (6.15)$$

with a sum over all lattice points  $x$  and a  $3 \times 3$  unit matrix  $I$ . Now it is possible to minimize the distance  $\Delta K$  by minimizing the scalar product eq. (6.15)

$$R(U^{g_1}, U'^{g_2}) = \frac{1}{12V} \min_{g_1, g_2} \sum_x \sum_{\mu=0}^3 \text{Re Tr} \left\{ I - g_1(x + \hat{\mu})U_\mu(x)^\dagger g_1(x)^{-1} g_2(x)U'_\mu(x)g_2(x + \hat{\mu})^{-1} \right\} \quad (6.16)$$

by introducing gauge transformations  $g_1$  for  $U$  and  $g_2$  for  $U'$ . Note because of the trace the condition is invariant under the transformation  $g_1 \rightarrow g_1 h$  and  $g_2 \rightarrow g_2 h$  by another gauge transformation  $h(x)$ . These degrees of freedom are fixed<sup>1</sup> by setting

$$g_1 = g_2^{-1} = g. \quad (6.17)$$

The minimization condition eq. (6.17) changes to  $R(U^g, U'^{g^{-1}})$  by introducing only one gauge transformation  $g$  for  $U$  and  $U'$ . Now, the relative gauge fixing enters

<sup>1</sup>Thanks to U. Wolff for suggesting this.

the ratio matrix with

$$M = D(U'^{g^{-1}})^{-1}D(U^g) = G^{-1}D(U')^{-1}G^2D(U)G. \quad (6.18)$$

Detailed balance is fulfilled if the minimization by using eq. (6.15) leads to the same  $g$  and  $M$  transforms into  $M^{-1}$  by interchanging the gauge field  $U$  and  $U'$ . The first property is ensured because the minimization condition is invariant by interchanging  $U$  with  $U'$ . By using the trace and the real term properties it follows directly  $R(U^g, U'^{g^{-1}}) = R(U'^{g^{-1}}, U^g)$ . The second property follows by using eq. (6.18) and interchanging  $U$  with  $U'$

$$M \longrightarrow M' = G^{-1}D(U)^{-1}G^2D(U')G = M^{-1}. \quad (6.19)$$

### Minimizing

A numerical algorithm to find a suitable gauge transformation  $g$  which minimizes the condition eq. (6.17) is given by a steepest descent method introduced in [129] [130]. The original condition, the Landau gauge condition

$$L(U^g) = \frac{1}{12V} \min_g \sum_x \sum_{\mu=0}^3 \text{Re Tr}\{I - g(x + \hat{\mu})U_\mu(x)^\dagger g(x)^{-1}I\}. \quad (6.20)$$

was used to fix the gauge of  $U$  [130]. The relative gaugefix condition is a generalization of the Landau gauge condition with  $L((U'^{g^{-1}})^\dagger U^g) = R(U'^{g^{-1}}, U^g)$ . It is straightforward to generalize the steepest descent method of the Landau case to the relative gauge fixing case. The idea is to find a gauge transformation  $g$  by an iteration through the lattice sites  $x$ . The condition for each  $g(x)$  is

$$\min_{g(x)} \text{Re Tr} \left( I - (g(x)^\dagger)^2 \Delta(x) \right) \quad (6.21)$$

with

$$\Delta(x) = W_f(x) + W_b(x) \quad (6.22)$$

where

$$W_f(x) = \sum_{\mu} U'_\mu(x) g(x + \hat{\mu})^2 U_\mu^\dagger(x) \quad (6.23)$$

and

$$W_b(x) = \sum_{\mu} U_\mu^\dagger(x - \hat{\mu}) g(x - \hat{\mu})^2 U_\mu(x - \hat{\mu}). \quad (6.24)$$



The gauge transformation field is given iteratively for each point by the steepest descent equation (see [130] or e.g. [75]) given by

$$\mathcal{U}(t+1) = e^{if_a t^a} \cdot \mathcal{U}(t) \quad (6.25)$$

with the force term

$$f_a(\mathcal{U}(t+1)) = \alpha \left. \frac{\partial L(e^\omega \mathcal{U})}{\partial \omega_\mu^a(x)} \right|_{\omega=0}, \quad (6.26)$$

$t^a$  the generators of SU(3) and a minimization parameter  $\alpha$ . Note that the force term is formally given by  $\partial L(e^\omega \mathcal{U}) / \partial \mathcal{U}(x)$  with  $\mathcal{U} = (U'g^{-1})^\dagger U g$  (see e.g. [81] [54] for the definition of the derivative). This leads to

$$g(x) = \exp \left\{ -\frac{\alpha}{2} \left[ \Delta(x) - \Delta^\dagger(x) - \frac{1}{3} \text{Tr}(\Delta(x) - \Delta^\dagger(x)) \right] \right\}. \quad (6.27)$$

A local minimum is reached if the quantity

$$\Theta(x) = \text{Tr} \left[ \Delta(x) - \Delta^\dagger(x) - \frac{1}{3} \text{Tr}(\Delta(x) - \Delta^\dagger(x)) \right]^2 \quad (6.28)$$

vanishes.  $\Theta(x)$  can be computed during the iteration in order to control the convergence. In the numerical tests done in this thesis the parameter  $\alpha$  is set to  $\alpha = 1.4$  and is reduced automatically if the minimization condition eq. (6.28) does not converge.

### Practice

It is sufficient to run the iterative minimization until the quantity  $\Theta(x)$  reaches a precision of  $\Theta(x) < 10^{-3}$ . This stabilizes the gauge field interpolation and a fixing to a higher precision does not yield additional improvements.

### 6.2.3. Domain Decomposition

Domain Decomposition (DD) can reduce the stochastic fluctuations eq. (6.8) by a reduction of the dimension of the operator  $D$  by using the exact factorization eq. (4.9)

$$\det D = \det \hat{D} \cdot \prod_k \det D_k. \quad (6.29)$$

Using such factorization the ratio matrix  $M$  is replaced by a ratio matrix consisting of the ratio of the Schur complements and stochastic estimation can be used as in the case of the full operator. Using the projected Schur complement  $\hat{D}$  (eq. (4.10))

the dimension of the operator is given by the rank of the projector  $P_{bw}$  to the boundaries of the even sub-domains eq. (4.14). Following eq. (4.14) the dimension reduction scales with  $V^{3/4}$  by using sub-domains with block length  $l = L/2$ . However the analysis of the stochastic fluctuations in the case of mass reweighting (see subsec. 5.3.2) shows that the fluctuations do not scale linearly with the dimension of  $P_{bw}$ . The magnitude of the stochastic fluctuations are reduced at least by a factor 2 compared to the full operator  $D$ . Note another advantage of DD is that it can also be used to handle the ensemble fluctuations which is described in the next section.

In the DD framework the gauge update will be restricted to the active links (see subsec. 4.1.2). This has some implication for the relative gauge fixing procedure. The iteration can be also restricted to points inside the blocks and thus the gauge fixing is restricted to links inside the blocks. This has several advantages. The gauge fixing is localized, which speeds up the minimization and can be performed easily in parallel without communication. Furthermore active links are still decoupled from the neighboring blocks after the minimization.

Note that the Schur complement is invariant under a gauge transformation which is restricted to the active links inside the blocks and would have no effect on the estimation procedure. However this does not hold for the gauge interpolation. In the next section it will be shown that relative gauge fixing is also necessary when DD is used.

#### 6.2.4. Numerical Results

The trajectory during the interpolation of the gauge field is non physical and only a tool to minimize the stochastic fluctuations. Many possibilities exist to transform  $U$  into  $U'$ . Here, the linear interpolation eq. (6.10) is used but other trajectories are possible, e.g. a trajectory over  $SU(3)$  elements [75]. The effect of the gauge field is non-trivial and advantages of the linear interpolation technique are deduced by numerical tests. The intermediate gauge field with relative gauge fixing is given by eq. (6.10) and the links  $U_{\mu,j}^g(x)$  during the trajectory are complex matrices  $\mathbb{C}^{3 \times 3}$ . The result of the numerical analysis is that a linear interpolation with relative gauge fixing is suitable to control the stochastic estimation.

The interpolation between  $U$  and  $U'$  acts on the eigenspace of the Dirac operator  $D$ . For  $m = 0$  the real part of the spectrum of the free Wilson Dirac operator is distributed in the interval  $[0, 8/a]$ . This interval shrinks for finite gauge couplings to  $[m_c(\beta), 8/a]$  with the critical mass  $m_c(\beta)$  eq. (2.36). Note for  $c_{SW} = 0$  the interval is given  $[m_c(\beta), 8/a - m_c(\beta)]$  which is used in this part of the discussion. In general the mass term in the Wilson Dirac operator  $m = -m_c(\beta) + m_0$  depends on the gauge coupling  $\beta$  and shifts the spectrum to the interval  $[m_0, 8/a - 2m_c + m_0]$ .

However if a linear interpolation is used for the transition  $U$  to  $U'$ , the links do

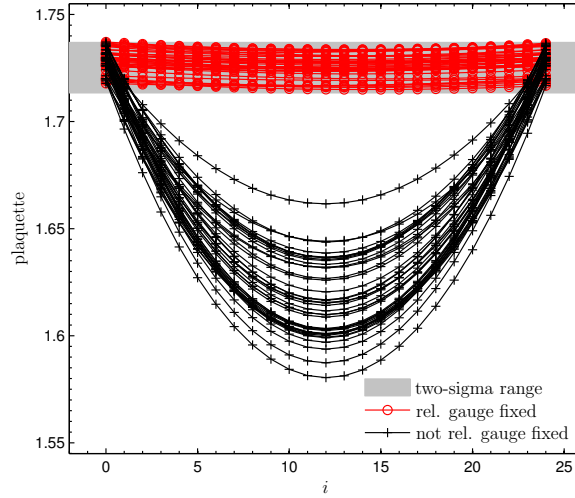


Figure 6.1.: The figure shows the plaquette term of  $U_i$  during the gauge field interpolation by  $N = 24$  steps. The used starting and end configurations are generated by a simulation of a plain Wilson fermions run of a  $8^4$  lattice with the bare parameters  $\beta = 5.6$  and  $\kappa = 0.15825$ . Only the active links in  $4^4$  blocks are changed. The effect of the relative gauge fixing (red, circles) is compared to the unfixed case (black, pluses).

not belong to the special unitary group  $SU(3)$  during the interpolation. Due to that also the critical mass  $m_c(\beta)$  can change during the trajectory. To ensure a stable algorithm it is necessary to analyze the behavior of the eigenvalues of the Dirac operator during the trajectory. This is done by using quenched  $4^4$  configurations for several different lattice spacings.

If the links are not fixed by using relative gauge fixing the eigenvalues behave as if the gauge coupling parameter  $\beta$  is lowered with  $\beta|_{i \neq 0, N} < \beta|_{i=0, N}$  during the trajectory and reaches a minimal value for the middle point of the trajectory. In contrast to that if relative gauge fixing is used the eigenvalues behave as if  $\beta$  is fixed (see fig. 6.1 in case of the plaquette).

If the spectrum of the Dirac operators changes it has also an effect on the ratio matrix. The spectrum spreads out for smaller  $\beta$  and the stochastic fluctuations increase. In contrary the additional mass-shift in the Dirac operator gets smaller for increasing  $\beta$  (this is true in perturbation theory see eq. (2.36). and also non perturbatively for small lattice spacings). Note that if the interpolation technique would increase the  $\beta$  an additional mass-shift during the trajectory would have to be introduced in order to avoid zero and/or negative eigenvalues in the Wil-

son Dirac operator. This is numerically found if the intermediate gaugelinks are normalized such that they belong to  $SL(3, \mathbb{C})$ .

The numerical analysis shows that an additional mass shift is not necessary (see fig. 6.1 in case of the plaquette) and the setup with the Schur complement with relative gauge fixing and an unnormalized linear gauge field interpolation eq. (6.10) is used in practice and is suitable to control the stochastic fluctuations in a stable way.

### 6.3. Ensemble Fluctuations

The ensemble fluctuations of an acceptance step with the Wilson Dirac operator are given by eq. (3.14)

$$\sigma_{ens}^2 = \kappa^2 \text{var} \left\{ \text{Tr} \left( \Delta K + \Delta K^\dagger \right) \right\} + \mathcal{O}(\kappa^3). \quad (6.30)$$

To increase the acceptance rate the fluctuations  $\sigma_{ens}^2$  have to be minimized. Until now the simple two step algorithm has been discussed where the full Dirac operator enters in the second step. From now on the fermion action will be split up so that hierarchical accept–rejects steps can be introduced. This splits up also the fluctuations so that the acceptance rate of each step can be improved. Furthermore it is possible to use correlations between different terms. A hierarchy of these accept–reject steps can be inserted to increase the effectiveness of the algorithm, e.g. by using a cost–ordering.

#### 6.3.1. Hierarchical Steps

The idea is to exactly factorize the Boltzmann factor into a product of weight factors

$$P(U) = P_0(U)P_1(U) \cdots P_n(U). \quad (6.31)$$

Now, additional accept–reject steps can be introduced for the different action parts and the following chain of transition steps fulfills the requirement of detailed bal-

ance

$$\begin{aligned}
& 0) \text{ Propose } U' \text{ according to } T_0(U \rightarrow U') \\
& 1) P_{\text{acc}}^{(1)}(U \rightarrow U') = \min \left\{ 1, \frac{P_1(U')}{P_1(U)} \right\} \\
& 2) P_{\text{acc}}^{(2)}(U \rightarrow U') = \min \left\{ 1, \frac{P_2(U')}{P_2(U)} \right\} \\
& \dots \\
& n) P_{\text{acc}}^{(n)}(U \rightarrow U') = \min \left\{ 1, \frac{P_n(U')}{P_n(U)} \right\}.
\end{aligned} \tag{6.32}$$

The first step is given by a pure gauge proposal with the corresponding transition probability  $T_0(U \rightarrow U')$ . Note that due to detailed balance the transition probability  $T_0(U \rightarrow U')$  has to be symmetrized by  $T_0(U \rightarrow U') = T_0(U' \rightarrow U)$  [30]. The other steps are corrections given by Metropolis accept–reject steps with the probability  $P_{\text{acc}}^{(i)}(U \rightarrow U')$ . Note the acceptance rate of each accept–reject step is given by eq. (6.3). Now the ensemble fluctuations of the Boltzmann factor are factorized and separated in these different accept–reject steps.

The hierarchy of the accept–reject levels can be given by the numerical cost respectively by the parallelization. In practice it is possible to perform local Markov–steps in parallel if the updated action parts do not contribute to each other. The steps of the algorithm **PSMS** (**P**artial **S**tochastic **M**ulti **S**tep – algorithm) are given by the pure gauge proposal, the different filter levels and the global step to correct the weight.

Now, it is possible to iterate the lower levels in order to propose an adequate amount of updated gauge–links for the global accept–reject step. Detailed balance demands that the iteration steps have to be constant in every proposal step. Furthermore the ordering and the factorization is arbitrary and can be optimized for the given set of parameters, e.g. the gauge coupling, the lattice volume or the fermion masses, and the specific action, e.g. Wilson fermions with or without  $\mathcal{O}(a)$ –improvement or with or without smeared gauge links. In this thesis several examples are presented and it will be shown how such an algorithm can be ordered to establish an efficient algorithm for different kinds of actions and parameters.

### Domain Decomposition

DD (see sec. 4.1) is a method which can split up the fermion part of the Boltzmann factor in an exact way. The determinant can be exactly factorized into  $\det D = \det \hat{D} \cdot \prod_k \det D_k$ , which can be recursively iterated by decomposing the blocks and so on. Now, a hierarchy of accept–reject steps ordered by the numerical

cost which implies an ordering in the size of the operators can be introduced. In principle local parts of the action do not need communication to neighboring domains due to the locality, need only moderate numerical effort for the evaluation and thus can be treated in parallel.

The idea is to update only the active links (see subsec. 4.1.2), which are decoupled from each other in the lower accept–reject levels. For example by using the Wilson plaquette action and the Wilson Dirac operator, links which lie in the boundary or connect blocks do not decouple in the lower level of the accept–reject steps and are not updated in the gauge proposal. For larger blocks it can be suitable to update only the core of the block (compare subsec. 4.1.2). In practice this refers to active links in a  $6^4$  core in a  $8^4$  block.

Another advantage is that DD can separate the IR-modes from the UV-modes. The expectation is that the UV-modes introduce large fluctuations which scale with the volume. If only such links inside the blocks are updated which do not have a contribution to the neighboring blocks an accept–reject step can be performed separately for each block. This reduces the fluctuations of the UV-modes which now scale only with the dimension of one block and it increases the acceptance rate.

### 6.3.2. Correlations

By introducing a cost ordered hierarchy of accept–reject steps a hierarchy of filters is established. If the different parts of the action are correlated it is possible to use these correlations to enhance additionally the acceptance rate by introducing a parametrization (see sec. 4.2).

Let us take as an example the 3 step algorithm, with a pure gauge update of the active links in blocks as the first level step, with accept–reject steps of each block determinant separately at the second level and a global step with the Schur complement as the last step. The Boltzmann factor is split up exactly into three parts. These three parts have finite correlations between each other. By choosing parameters for the different actions in different accept–reject steps it is possible to enhance the acceptance rate. Let us write the action of the  $i$ th level step as

$$S_i(U) = \sum_{j=0}^i \beta_i^{(j)} S^{(j)}(U), \quad i = 1, 2, \dots, n \quad (6.33)$$

where the accept–reject steps have a probability

$$q = \min[1, \exp\{-\Delta_i\}] \quad (6.34)$$

with

$$\Delta_i = S_i(U') - S_i(U). \quad (6.35)$$

Demanding a cost-ordered hierarchy means higher level (higher costs) actions do not contribute at lower level (lower costs), e.g. the Schur complement does not enter the low level accept-reject steps. This is achieved for  $\beta_i^{(j)} = 0$  for  $i < j$ . Additionally the introduced parameters have to sum up to the original parameters  $\sum_{i=1}^n \beta_i^{(j)} = \beta^{(j)}$ , e.g. the parameter of the gauge action has to sum up to the target  $\beta$ , the parameter of the block determinant has to sum up to 1 and so on.

The acceptance rates of the different accept-reject steps can be enhanced by minimizing the variance of the differences in each step (see e.g. sec. 4.2). The minimization leads to coupled linear equation systems for the introduced parameters. These linear equations can be exactly solved by starting with the highest order of the accept-reject steps which fixed  $\beta_n^{(i)}$  with  $j = 0, \dots, n-1$  and proceeding afterwards to the lower ones. The exactly solvable system of linear equations is given in the order  $i = n, n-1, \dots, 1$  by

$$2C^{(jj)}\beta_i^{(j)} + \sum_{\substack{k=0 \\ k \neq j}}^i C^{(jk)}\beta_i^{(k)} = -C^{(ji)}\beta_i^{(i)}, \quad j = 0, \dots, i-1 \quad (6.36)$$

where  $C^{jk} = \langle \Delta^{(j)}\Delta^{(k)} \rangle - \langle \Delta^{(j)} \rangle \langle \Delta^{(k)} \rangle$  the covariance of the difference  $\Delta^{(j)} = S^{(j)}(U') - S^{(j)}(U)$ . By using the constraint  $\beta_i^{(i)} = \beta^{(i)} - \sum_{j=i+1}^n \beta_j^{(i)}$  the linear equation system eq. (6.36) can be solved uniquely to determine the parameters  $\beta_i^{(0)}, \dots, \beta_i^{(i-1)}$ .

In practice it is essential to use correlations in order to have a reasonable acceptance rate at each level, e.g. the block acceptance rate for block sizes larger than  $4^4$  with  $a > 0.05$  fm decreases quite fast and is small without a parametrization. The behavior of the parameter of the simple 3-step algorithm depends on the kind of action and on the factorization. In general the expectation is for the pure gauge update a  $\beta$ -shift towards a larger pure gauge coupling  $\beta$ . The block determinants are correlated with the determinant of the Schur complement. Due to that the corresponding parameter in the global accept-reject step is negative, e.g. see tab. 6.4, tab. 6.5 or tab. F.2 in app. F for some representative parameter sets of the PSMS algorithm. For larger blocks it is useful to introduce different kinds of actions, which do not necessarily contribute to the final Boltzmann factor. This is practical if they are correlated with parts of the final Boltzmann weight. For such action terms the corresponding parameters have to sum up to 0. The 1-level HYP-smear plaquette action can be such a different action [21]. In simulations with smeared links in the fermion action it might be necessary to use such a smeared plaquette action in order to improve the acceptance rate in the lower levels. To summarize: a possible low level structure of the PSMS  $n$ -step algorithm is presented in table 6.1. To conclude: the parametrization enhances the acceptance of the gauge proposal

Table 6.1.: Structure of a possible PSMS  $n$ -step algorithm.

i	action which enters the $i$ th level
0	pure gauge action
1	HYP plaquette action
2	block determinant $4^4$ in $8^4$
3	Schur complement $8^4$ with $4^4$ blocks
$\vdots$	$\vdots$
$n - 1$	global Schur complement

which does not know about the fermions and increases the effectiveness of the PSMS algorithm also for larger lattice sizes.

#### Remarks

- **Parameter setting:** The parameters are fixed by first simulating and measuring the accept-reject steps  $i = 1, \dots, n - 1$  by neglecting the global step  $i = n$  and by starting in a pure gauge environment. After fixing the low level parameters the global step is included in order to fix all parameters. After this step the parameters are almost converged to their optimal value.
- **Parameter for a stochastically estimated variable:** In a stochastic estimation procedure the parameter enters as the power of the ratio matrix, i.e. if  $\beta'$  is a proper chosen parameter the estimate is given by

$$w(\eta) = \exp\{-\eta((M^\dagger M)^{\beta'} - I)\eta\} \quad (6.37)$$

with  $-\beta \cdot \log \det M^\dagger M = \log(\langle w(\eta) \rangle_\eta)$ . For an unbiased estimation matrix functions for roots have to be used to estimate this factor. Furthermore these action terms have to be recalculated in every new step. Due to that parts of the action which are stochastically estimated are not parameterized in the PSMS-framework.

## 6.4. Numerical Tests

For a practical usage of the PSMS algorithm it is important to estimate the numerical effort to sample a completely decorrelated new configuration. Let us define



the cost by

$$\text{cost}(U \rightarrow U^{\text{new}}) = c_{gl.step} \cdot P_{acc}^{-1}(U, U') \cdot \tau_{int}(U \rightarrow U^{\text{new}}) \cdot R_{act}. \quad (6.38)$$

The different parts of this formula will be discussed in the next subsections, the scaling of the cost for the global accept–reject steps  $c_{gl.step}$  in the next subsec. 6.4.1, the acceptance rate for the global accept–reject step  $P_{acc}(U, U')$  for a specific action set in subsec. 6.4.2 and the scaling of the autocorrelation time  $\tau_{int}(U \rightarrow U^{\text{new}})$  in subsec. 6.4.3. The ratio of the number of the active links over all links is given  $R_{act} = \frac{N_{act.links}}{N_{links}}$  with  $N_{act.links}$  follows from eq. (4.18). The section will be concluded by a summary of these results in subsec. 6.4.4.

### 6.4.1. Master Theorem

The main cost of the PSMS algorithm is given by the evaluation of the fermion determinant. By using a recursive DD an iterative method is introduced with a recurrence of the form

$$T(n) = a \cdot T\left(\frac{n}{b}\right) + f(n) \quad (6.39)$$

with constants  $a \geq 1$ ,  $b > 1$ , a positive function  $f(n)$  and a function  $T(n)$  which describes the running time of an algorithm depending on the problem size  $n$  (here  $n = V$ ). The recurrence is given by dividing the problem of size  $n$  with corresponding cost function  $T(n)$  into  $a$  problems of size  $n/b$  with running time functions  $T(n/b)$  and an additional problem depending on  $n$ . In the case of DD in the first recurrence step the time function  $T(n)$  corresponds to a problem which contains the Dirac operator, the function  $T(n/b)$  corresponds to the block operators and the function  $f(n)$  corresponds to the Schur complement. A recurrence relation is given by using recursive DD.

From the so called “Master theorem” (see e.g. [131]) follows the cost for the global accept–reject step of the PSMS algorithm. The cost to evaluate the positive function  $f(n)$  is given by  $\mathcal{O}(n^c)$  with a positive constant  $c$ . By dividing the problem of size  $n$  into  $a$  problems of size  $n/b$  it follows

if  $\log_b(a) < c$ ,  $T(n)$  scales in general with  $f(n) = \mathcal{O}(n^c)$ ,

if  $\log_b(a) = c$ ,  $T(n)$  scales with  $\mathcal{O}(n \cdot \ln n)$  and

if  $\log_b(a) > c$ , the running time  $T(n)$  scales with  $n^{\log_b(a)}$ .

The general setup for the PSMS algorithm in this work is given by a division of the lattice in each recursive step into blocks where the block length is divided by 2. For the parameters follows  $b = 16$  and  $a = 16 \cdot n_{it}$  with  $n_{it}$  the number of iteration in the next lower level stage. This implies  $\log_b(a) = 1 + \log_{16}(n_{it})$ . The timing

## 6. Partial Stochastic Multi Step Algorithm

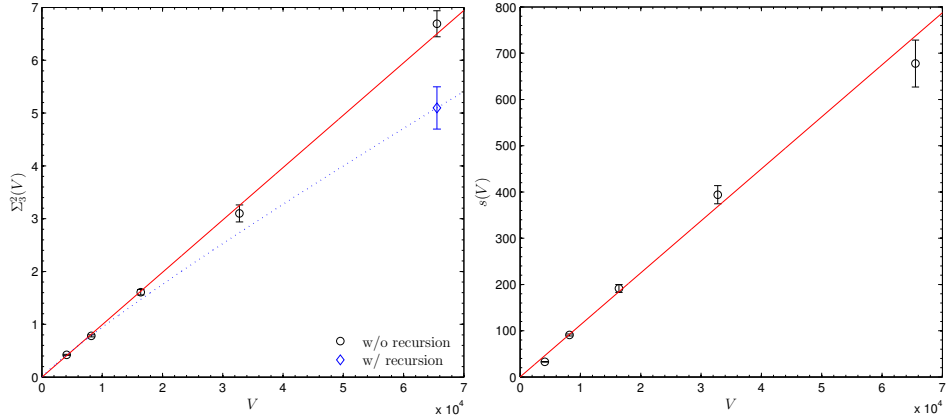


Figure 6.2.: The left figure shows the ensemble fluctuations  $\Sigma_n^2 = \sigma_{ens}^2(\beta_n^{(i)})$  (black, circles) for different volume sizes from  $8^4$  to  $16^4$  from simulations of the A3 parameter set. The simulations are done with the 4-step PSMS algorithm by using active links of the  $4^4$  blocks. A fit is performed which shows the linear volume behavior (red line) in the lattice volume  $V$ . Additionally the blue diamond corresponds to a simulation with a 5-step PSMS algorithm. The right figure shows the volume dependence of the slope  $s(V) = \sigma_{st}^2$  of eq. (6.43). In this case also a linear fit in the volume is performed.

function  $f(n)$  of the global step is dominated by the solver cost  $\mathcal{O}(V)$  which scales with the volume  $V$  and the number of gauge field interpolation steps  $N(V)$ . It follows

$$f(V) \propto N(V) \cdot \mathcal{O}(V). \quad (6.40)$$

By demanding that the ratios of the ensemble and stochastic fluctuations are constant at a constant lattice spacing  $a$  the number of interpolation steps  $N(V) = const$  are also constant (see next subsec. 6.4.2) and it follows  $f(V) = \mathcal{O}(V^c)$  with  $c = 1$ . Using the master theorem the cost of global acceptance step scales with

$$c_{gl.step} = \begin{cases} V \cdot \ln(V) & \text{if } n_{it} = 1 \\ V^{1+\log_{16}(n_{it})} & \text{if } n_{it} > 1. \end{cases} \quad (6.41)$$

Table 6.2.: The table lists the used parameters for the PSMS runs with mass-degenerate plain Wilson fermions. In general plain Wilson fermions are unimproved Wilson fermions with  $c_{SW} = 0.0$ . The pion mass and the lattice spacing of the finer lattices (A3, B4) are taken from [8, 132]. For the coarse lattice (Z4) the values are extrapolated from ensembles with larger masses (see app. F). Note that in this chapter the A ensemble corresponds to a plain Wilson ensemble (the A ensemble in chap. 5 and chap. 7 is  $\mathcal{O}(a)$ -improved, e.g. see tab. 5.1). Note additionally that the Z ensemble has large systematic errors in the pion mass and the lattice spacing (see app. F).

Ensembles	$\beta$	$a$ [fm]	$\kappa$	$M_\pi$ [MeV]
Z4	5.5	0.0900(20)	0.16097	370
A3	5.6	0.0717(14)	0.15825	404
B4	5.8	0.0521( 7)	0.15462	381

### 6.4.2. Acceptance Rate

The acceptance rate is given by  $P_{acc} = \text{erfc} \left\{ \sqrt{\frac{\sigma^2(\Delta)}{8}} \right\}$  eq. (6.3) with the difference  $\Delta$  of the global step

$$\Delta = \sum_{i=0}^{N-1} \eta_i^\dagger M_i^\dagger M_i \eta_i + \sum_{j=0}^{n-1} \beta_n^{(i)} \Delta_i \quad (6.42)$$

where the parameters  $\beta_n^{(i)}$  are given by  $\beta_n^{(i)} = 0$  for all stochastic estimated action parts. The fluctuations of the global action part ( $i = n$ ) split up

$$\sigma_n^2(\Delta) \cong \sigma_{ens}^2 \left( \beta_n^{(i)} \right) + \frac{\sigma_{st}^2}{N} \quad (6.43)$$

for an optimal set of parameters  $\beta_n^{(i)}$  which minimizes  $\sigma_{ens}^2$  (in [16]  $\sigma_{ens}^2(\beta_n^{(i)}) = \Sigma_n^2$  and  $s(V) = \sigma_{st}^2$ ). By performing the limit  $N \rightarrow \infty$  it is possible to extrapolate to the acceptance rate without stochastic noise. The limit corresponds to the acceptance rate by using the exact action.

In order to analyze the scaling behavior of the acceptance rate in the lattice volume  $V$  and the lattice spacing  $a$  three different ensembles with different lattice spacings are used. The scaling in the quark mass will not be analyzed and it is assumed that the pion mass differences of the three ensembles can be neglected. The lattice action is given by two flavor mass-degenerate plain Wilson fermions

( $c_{SW} = 0.0$ ) combined with the Wilson plaquette action. The properties and parameters are listed in tab. 6.2.

The volume behavior of the exact acceptance rate is analyzed by varying the lattice volume from  $8^4$  to  $16^4$  and using the parameters which correspond to the A3 lattice. The setup of the PSMS algorithm for the  $\beta = 5.6$  ensemble is given by a 4-step algorithm (for the used parameters see tab. 1 of [16]). The block volume is set to  $4^4$  by using  $4^4$  active links. 9.8% of all links are updated per global acceptance step. The 1-level HYP-plaquette is used as the first filter step ( $i=1$ ) and the  $4^4$  block determinants as a second filter step ( $n=2$ ). By using this filter structure the global accept-reject step ( $i=3$ ) is performed for different numbers of interpolation steps  $N$ . Respectively for each volume an extrapolation with  $N \rightarrow \infty$  is performed. The fluctuations scale linear with the lattice volume  $V$

$$\sigma^2(\Delta) = V \left( C(a) + \frac{B(a)}{N} \right) \quad (6.44)$$

with  $\sigma_{ens}^2(\beta_n^{(i)}) = C(a) \cdot V$  and  $\sigma_{st}^2 = B(a) \cdot V$  (see fig. 6.2 and compare eq. (6.43)). By knowing the coefficient  $C(a)$  and  $B(a)$  an optimal  $N$  can be found by maximizing  $1 - (1 - P_{acc}(N))^{n_{st}}$  with the condition  $\min(n_{st} \cdot N)$ . This can be done numerically, e.g. by using *MATLAB* functions like *fmincon*. Note that the tuning equation can be generalized and extended to the lower filter steps to minimize the total cost for updating the lattice.

However the linear volume behavior implies that the Schur complement does not capture only the IR-modes. It is found [109] [133] that the small (smallest) modes of the Wilson Dirac operator have a variance proportional to  $1/V^2$  ( $1/V$ ). This behavior should result in a weaker volume scaling of the ensemble fluctuations which are dominated by IR-modes. Here, such behavior is not found on lattices up to a volume of  $32 \times 16^3$ . A possible reason could be that such behavior is only observable for larger block sizes with block length  $l$ , i.e. if the blocks are large enough the blocks could sufficiently capture the UV-modes with energies larger than  $\pi/(a \cdot l)$  and that the Schur complement contains only the modes with  $< \pi/(a \cdot l)$ . For example for the simulations with a lattice spacing of  $a = 0.0521$  fm a block with length  $l = 8$  seems to be too small, i.e. the block captures modes approximately down to 500 MeV.

The exact acceptance rate decreases up to volumes of  $16^3 \times 8$  approximately linear in the volumes and decreases asymptotically proportional to  $\exp\{-V\}$  for larger volumes (see fig. 6.3). This makes the algorithm inefficient. However by introducing a better filter-structure it is possible to additionally reduce the ensemble fluctuations, i.e. by using a recursive filter structure the scaling reduces to  $\sigma_{ens}^2 \propto V^{0.9}$  (w / recursion point in the left picture of fig. 6.3). This can be easily done by using recursive domain decomposition and a 5-step algorithm. For this lattice of size  $16^4$  the recursive decomposition is given by a decomposition into  $8^4$

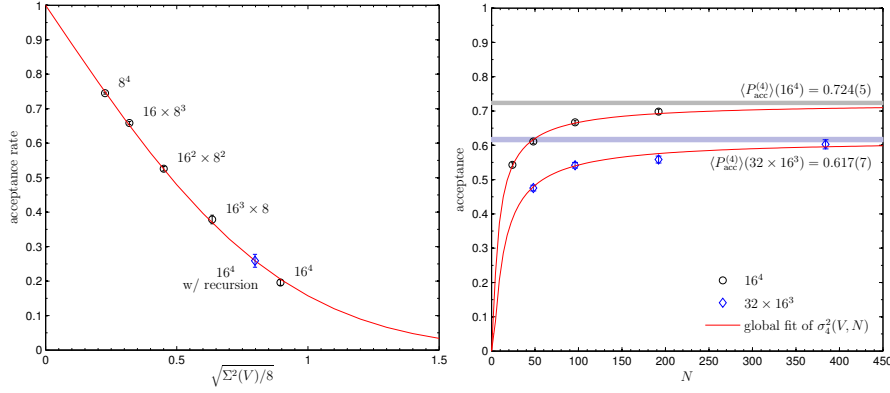


Figure 6.3.: The left figure shows the acceptance rate by varying the lattice volume from  $8^4$  to  $16^4$ . It shows the acceptance rate of the 4-step PSMS algorithm for a pure gauge coupling  $\beta = 5.6$  (black, circles) respectively 5-step PSMS algorithm (blue, diamond). The right figure shows the acceptance in the global step for simulations of plain Wilson fermions which corresponds to the B4 ensemble by using  $6^4$  active links. The fluctuations  $\sigma_n^2(\Delta)$  for  $V = 16^4$  (circles) and  $V = 32 \times 16^3$  (diamonds) can be very well fitted by a function which scales with  $1/N$  by using a global linear fit (red lines). The fit and the data are then mapped to the acceptance by  $P_{acc} = \text{erfc} \left\{ \sqrt{\frac{\sigma^2(\Delta)}{8}} \right\}$  and plotted versus the number of interpolation steps  $N$ .

and a further decomposition into  $4^4$  blocks. However the improvement is small and the acceptance rate tends for larger volume to the  $\exp\{-V\}$  behavior. To increase the acceptance rate further a possibility is to introduce further improvements of the IR-filter structure or to change the lower level update.

The lower level filter can be improved by only updating links which have a certain distance from the block boundary. For example this can be  $6^4$  active links inside of  $8^4$  blocks. This choice increases the global acceptance rate so that for the lattice with a gauge coupling of  $\beta = 5.8$  the  $\exp\{-V\}$ -region starts at lattices with lattice volumes of  $32^4$  with an assumed acceptance rate  $P_{acc} \sim 16\%$ . This is deduced from runs with volumes  $16^4$  and  $32 \times 16^3$  shown in the right figure 6.3. Note that the runs will be discussed in the next subsection 6.4.3 (for the used parameter set see tab. 2 of [16]).

To analyze the scaling behavior in the lattice spacing the coefficient  $B(a)$  and  $C(a)$  are deduced by using a 4-step PSMS algorithm for the B4 and the A3 ensembles and a 5-step algorithm for the Z4 ensemble. For all three different parameter

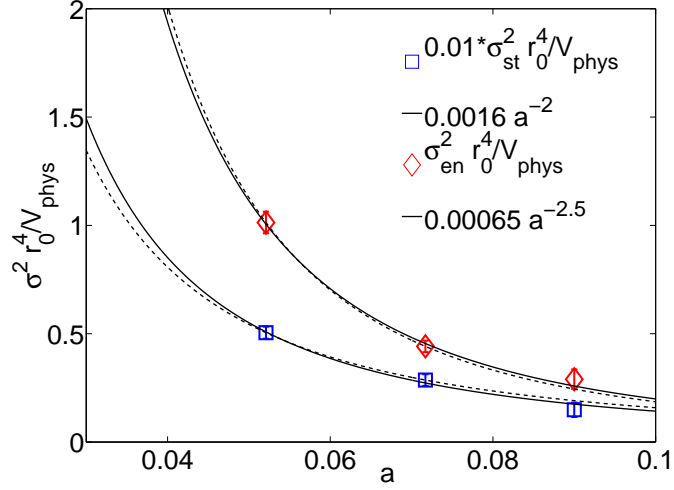


Figure 6.4.: The figure shows the scaling of the fluctuations of the global step of the 4-step PSMS algorithm with the lattice spacing at fixed physical volume. The stochastic fluctuations are rescaled by  $10^{-2}$  and scales roughly with  $a^{-2}$  (blue, square) while the ensemble fluctuations scale with  $a^{-2.5}$  (red, diamond). Two different fits are performed, one for all ensembles (solid line) and one for the ensembles A3 and B4 (dotted line).

sets shown in tab. 6.2  $6^4$  active links and a lattice volume of  $16^4$  are used. The result for the scaling is shown in fig. 6.4.

The coefficients are analyzed by fixed physical volume with  $V_{phys} = V \cdot a^4$  and plotted by  $B(a) = \sigma_{st}^2 V_{phys} a^c / r_0^4$  and  $C(a) = \sigma_{ens}^2 V_{phys} a^d / r_0^4$ . An  $a^{-2}$ -scaling is found for the stochastic fluctuations, with an exponent  $c = -1.95(28)$  by using all three lattice spacings (solid line) and  $c = -1.78(34)$  by only using the finer ones (A3,B4) (dotted line). For the ensemble fluctuations the scaling is given by roughly  $a^{-2.5}$ . The fit gives  $d = -2.48(20)$  for all three ensembles (solid line) and  $d = -2.60(24)$  by using only A3 and B4 (dotted line).

By demanding that the quotient of the fluctuations  $\sigma_{st}^2 / N$  over  $\sigma_{ens}^2$  is constant with  $\sigma_{st}^2 / N \sigma_{ens}^2 = const$  and using  $C(a) = V_{phys} C' / a^{2.5}$  and  $B(a) = V_{phys} B' / a^2$  it follows the scaling of the number of interpolation steps  $N$

$$N(a) = \frac{1}{const} \frac{C'}{B'} a^{d-c} \quad (6.45)$$

with constants  $C'/B' = 244(241)$  and  $d - c \sim 0.5$ . The volume is canceled but

the number of steps depends slightly on the lattice spacing. It follows that for smaller lattice spacings the number of steps decreases. However the acceptance rate decreases for fixed physical volume by decreasing the lattice spacing. Note that the ratio  $C'/B'$  is dimensionful.

### 6.4.3. Autocorrelation

The efficiency of Monte Carlo algorithms in LQCD can suffer from large autocorrelation times, like the HMC or the combination of a heat bath-/ overrelaxation algorithm in the pure gauge case. In [27] it was found that the autocorrelation time increases dramatically for finer lattices by roughly proportional to  $a^{-5}$  in the case of anti-periodic boundaries. For the PSMS algorithm the autocorrelation is analyzed. This is done by measuring and comparing the topological charge (see subsec. 4.3.3) for different setups of the PSMS algorithm, for the DD-HMC algorithm [31] with anti-periodic boundaries and for the openQCD-HMC algorithm [32] with open boundary conditions (see tab. 6.3).

In general by using dynamical fermions in the simulation the  $a^{-5}$ -scaling of the slow modes is coupled to the high computation costs of the fermions, which scale roughly with  $V^{5/4}$  in the case of the HMC algorithm. The idea of the PSMS algorithm is to solve this problem by decoupling the fermion weight from the proposal of the new gauge links. Then it is possible to iterate the pure gauge updates intensively before the accept-reject steps are performed. However by using DD the PSMS algorithm can only update gauge links inside the sub-domains. It is not obvious if the slow modes decouple sufficiently if the sub-domains are too small. By using the fine lattice B4 it was numerically found that a pure gauge update of sub-domains which update  $6^4$ -active links inside  $8^4$  blocks is sufficient to sample the topological charge properly in contrast to  $4^4$  blocks.

The runs of the PSMS algorithm are performed for all three different parameter sets shown in tab. 6.2 with a lattice volume of  $16^4$ . A 4-step algorithm is used by generating 4 replica for the finer lattice spacings (B4, A3) and a 5-step algorithm is used to sample one ensemble for the coarser lattice (Z4). The gauge proposals are performed on  $6^4$ -active links inside of  $8^4$  blocks with  $n_0 = 75$  iterations for all three lattice spacings and additional with  $n_0 = 300$  for the finest lattice with gauge parameter  $\beta = 5.8$  in order to analyze the effect of the pure gauge update.

In the case of the 4-step algorithm the first filter step (i=1) is given by a product over determinants of  $4^4$  blocks inside of the  $8^4$  sub-domain. The second filter step (i=2) is given by the Dirichlet Schur complement of the  $8^4$  blocks with these  $4^4$  blocks. This is done by using stochastic estimation combined with a linear gauge field interpolation. The final step (i=3) is the global acceptance step with the  $16^4$  Schur complement with  $8^4$  blocks. Note that details for the setup of the 5-step PSMS algorithm in the case of the Z4 ensemble can be found in app. F.

Table 6.3.: Topologies and autocorrelation times of the plain Wilson runs are listed in the table. In most of the PSMS runs the number of pure gauge iterations is set to  $n_0 = 75$ . Only for the ensemble (PSMS\*) the number of pure gauge iterations is set to  $n_0 = 300$ . The trajectory length for the simulations with HMC algorithms is set to  $\tau = 2$  for the DD-HMC algorithm and for the openQCD HMC algorithm respectively (oQCD-HMC). For all simulated ensembles the ensemble averages for the topological charge  $\langle Q \rangle$  and the square of the  $\langle Q^2 \rangle$  are shown. The autocorrelation time of the topological charge is measured in units of global acceptance steps. Furthermore the acceptance rate of the global steps is given by  $P_{acc}$  and the number of inversions per step by  $N_{inv}$ . For the openQCD run Hasenbusch preconditioning is used and 18 inversions are done for the smallest mass and 54 inversions for all masses during a HMC trajectory. The number of global acceptance steps is given by  $N_{acc}$ , which corresponds to the number of Metropolis accept-rejects for the global Schur complement in case of the PSMS algorithm and to the number of Metropolis accept-rejects at the end of every trajectory of the HMC algorithm.

Ensembles	$\langle Q \rangle$	$\langle Q^2 \rangle$	$\tau_{int}(Q)$	$P_{acc}$	$N_{inv}$	$N_{acc}$
Z4 (PSMS)	-0.09(42)	1.23(57)	33(16)	0.32	96	511
A3 (PSMS)	0.02(18)	3.37(49)	40(10)	0.53	96	8220
A3 (DD-HMC)	0.64(27)	4.00(86)	21( 7)	0.91	42	2000
B4 (PSMS)	0.01( 9)	0.37(15)	148(50)	0.62	96	13306
B4 (PSMS*)	-0.07( 4)	0.18( 6)	83(22)	0.61	96	16000
B4 (DD-HMC)	0.05( 6)	0.28( 8)	47(13)	0.96	42	16000
B4 (oQCD-HMC)	0.03(14)	0.34(14)	96(43)	0.97	18(54)	3512



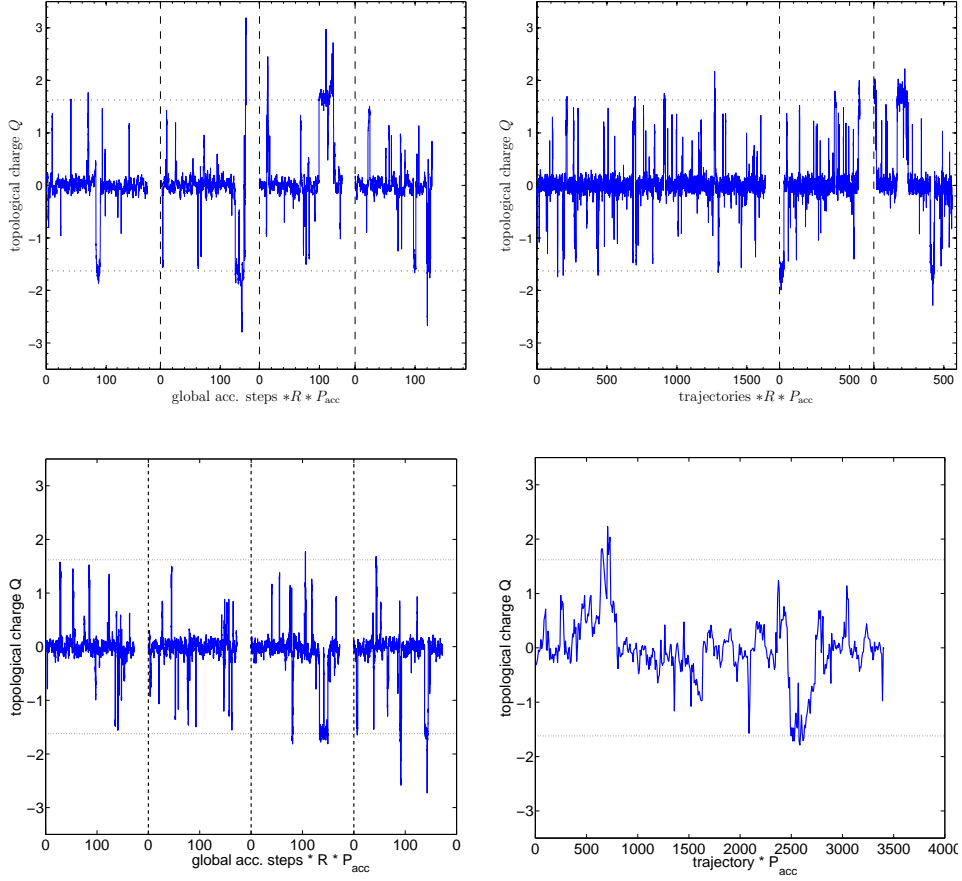


Figure 6.5.: The figure shows histories of the topological charge  $Q$  for four kinds of Monte Carlo algorithms (left-upper fig. [4-step PSMS with  $n_0 = 75$ ], right-upper fig. [DD-HMC], left-lower fig. [4-step PSMS with  $n_0 = 300$ ] and right-lower fig. [OpenQCD]) on a fine lattice with  $V = 16^4$ . The horizontal lines are given by the maximal values of a double Gaussian distribution which is fitted to positive folded values of the PSMS replica runs with  $n_0 = 75$  with  $Q_{(0)} = 0$  and  $Q_{(\pm 1)} \sim \pm 1.6$ .

For the simulation with the DD-HMC algorithm  $8^4$  sub-domain are used with  $8^4$  active links. The lattice volume is set to  $16^4$  and parameters correspond to the A3 and B4 ensembles. For the simulation of the openQCD-HMC run an ensemble which corresponds to the B4 ensemble is simulated. The boundary conditions are open in time direction and the time extent is increased by a factor 2.5 to  $T = 40$ . The algorithm is stabilized by using Hasenbusch mass preconditioning by introducing two additional operators with twisted masses of  $\mu_1 = 0.02$  and  $\mu_2 = 0.3$ .

On most of the generated ensembles the topological charge is measured by using 3-level HYP-smearing. Only for the open boundary run the Wilson flow is used to measure the topological charge at the integration time of  $t_0$  (see sub-sec. 4.3.2).

The results for the B4 lattices with a gauge coupling of  $\beta = 5.8$  are shown in figure 6.5. The topological charge is plotted against the number of a total updates of the lattice which means that the number of global acceptance steps is scaled by the total amount of updated links in one step  $R_{acc}$  together with the acceptance rate  $P_{acc}$ . A long HMC run has been performed (see the upper-right fig. 6.5) and no tunneling of the topological charge to values larger than  $|Q| > 2$  could be found. Due to that two additional HMC-runs are started from configurations with a finite topological charge generated by the PSMS algorithm with  $n_0 = 75$  in order to observe tunneling back to zero charge. This does indeed happen (compare to the history of the upper-left fig. 6.5).

By increasing the number of pure gauge steps to  $n_0 = 300$  (see lower-left fig. 6.5) the Monte Carlo time of the PSMS algorithm to stay at a finite topological charge decreases and the topological susceptibility is given by  $Q^2 = 0.18(6)$  instead of  $Q^2 = 0.37(15)$  for  $n_0 = 75$  (compare tab. 6.3). The expectation from chiral perturbation theory in leading order is given by  $Q^2 \approx 0.19$ . However the large variation shows that a proper sampling of the topological charge is difficult for a lattice spacing corresponding to  $\beta = 5.8$  and the error of these measurements could in principle be underestimated. In the case of the open boundary condition the topological charge is not quantized and it is measured on the  $16^4$  core of the  $40 \times 16^3$  lattice (see lower-right fig. 6.5). The ensemble average of the topological charge agrees with zero for the four algorithms, only the replica average of the PSMS algorithm with  $n_0 = 300$  update steps deviates by one  $\sigma$  from zero.

The measurement of the integrated autocorrelation time is determined by using *UWerr* [78] and shown in tab. 6.3. The scaling with the lattice spacing  $a$  of the autocorrelation times in the case of the PSMS algorithm is shown in figure 6.6. and plotted in units of a complete update of the lattice. In the case of the PSMS algorithm by constant pure gauge updates  $n_0 = 75$  the scaling is given by  $\tau_{int,Q_3}(a) \sim \exp\{-11(4)\} \cdot a^{-4.6(13)}$  (blue solid line). The other fit was performed by only using the ensembles A3 and B4 (blue dotted line). The behavior changes

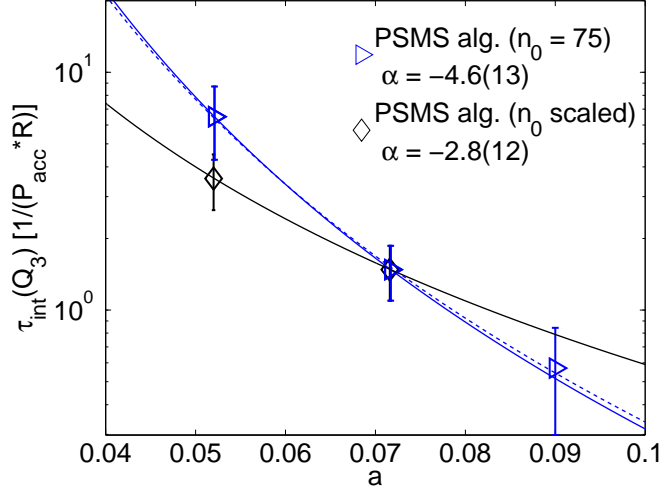


Figure 6.6.: The figure shows the scaling of the autocorrelation times  $\tau_{int}$  of the topological charge with the lattice spacing  $a$ ,  $\tau_{int} \propto a^\alpha$ . The properties of the ensembles with the three different parameter sets are listed in tab. 6.2 and are generated with a lattice volume of  $16^4$ . The scaling of the PSMS algorithm is analyzed by using a constant pure gauge update iteration with  $n_0 = 75$  (blue, triangle) for the Z4, A3 and Z4 ensembles. Another run of a PSMS algorithm for the finer lattice is done by increasing the numbers of pure gauge update by a factor 4 (black, diamond).

if  $n_0$  is scaled with the lattice spacing. The scaling reduces to  $a^{-2.8(11)}$  (black solid line) by using the data of the ensembles with  $n_0 = 300$  pure gauge update at  $\beta = 5.8$  and  $n_0 = 75$  at  $\beta = 5.6$ .

There are implications that the DD-HMC runs at  $\beta = 5.8$  have sampling problems. This can be observed by a replica analysis of the runs (see fig. 6.5 and [16]). The goodness of the replica distribution gives a value of 0.05 for the DD-HMC replica which is unlikely (for further details see [16] and [78]). For the PSMS algorithm with  $n_0 = 75$  ( $n_0 = 300$ ) a value of 0.7(0.5) is found. The bad quality of the DD-HMC replica distribution is due to the fact that the first run does not tunnel to other topological charges than 0. Due to that the autocorrelation time is underestimated and a scaling analysis would give a weaker scaling in the lattice spacing than expected. To conclude there are implications that by scaling the iterations of the pure gauge update proportional to the expected lattice spacing behavior of the autocorrelation times with  $a^{-5}$  the fermion weighting in the PSMS algorithm can be decoupled from the  $a^{-5}$  scaling.

#### 6.4.4. Conclusion

By using the cost formula eq. (6.38) the results of the previous subsections are summarized to illustrate the pros and cons of the PSMS algorithm by using non-smearred fermion actions. If  $n_{it} = 2$  the master theorem gives a cost function which scales with  $c_{gl.step} \propto V^{5/4} \sqrt{a} = \frac{V_{phys}^{5/4}}{a^5} \sqrt{a}$ . This term is multiplied by  $\sqrt{a}$  because it scales with the number of interpolation steps  $N$  (see eq. (6.40)).

The global acceptance rate eq. (6.3) is given by the error function depending on the fluctuations of the global difference. For small fluctuations the function can be expanded by  $\text{erfc}(x) \approx 1 - 2x/\sqrt{\pi}$  and the inverse of the global acceptance rate is roughly given by  $P_{acc}^{-1}(U, U') \sim 1 + \sqrt{\frac{V_{phys} C'}{2\pi a^{2.5}}}$  if the stochastic fluctuations can be neglected. For the scaling in the lattice spacing of the autocorrelation time follows  $\sim a^{-3}$  if the iteration number of pure gauge update is increased. By inserting these scaling behaviors into eq. (6.38) a cost formula depending on the lattice spacing  $a$  and the physical volume  $V_{phys}$  is given by

$$\text{cost}(U \rightarrow U^{new}) \propto \sqrt{a} \frac{V_{phys}^{5/4}}{a^5} \cdot \left( 1 + \sqrt{\frac{V_{phys} C'}{2\pi a^{2.5}}} \right) \cdot \frac{1}{a^3} \approx V_{phys}^{5/4} a^{-7.5}. \quad (6.46)$$

However this behavior turns into  $c(U \rightarrow U^{new}) \propto V_{phys}^{3/4} a^{-3.25} \exp\{a^{-2.5} V_{phys} C'\}$  if the fluctuations of the acceptance steps are too large. Note that for the HMC with anti-periodic boundaries the behavior eq. (2.67) in the lattice spacing  $a$  is expected with  $\text{cost}(U \rightarrow U^{new}) \propto V_{phys}^{5/4} a^{-10}$ .

Moreover it is possible to compare the cost of the runs of the different algorithms by using the measured autocorrelation times in units of the total number of inversions (see tab. 6.3). To update the whole lattice in the case of the DD-HMC algorithm the numbers of inversion per step are multiplied by the autocorrelation time which gives  $N_{tot} = \tau_{int} \cdot N_{inv} = 47 \cdot 42 = 1974$  ( $N_{inv} = 21 \cdot 42 = 882$ ) for the B4 (A3) lattice. Note that the autocorrelation time determination of the B4 ensemble could be forged due to the bad sampling of the topological sectors. If for the autocorrelation time of the DD-HMC algorithm is an  $a^{-5}$  scaling assumed by using the autocorrelation time of the A3 ensemble it follows that the DD-HMC algorithm need  $N_{tot} \sim 9500$  at  $\beta = 5.8$ .

In the case of the PSMS algorithm the number of inversions to sample a new configuration is given by  $N_{tot} = 7968$  ( $N_{tot} = 1920$ ) by using the pure gauge update with iteration numbers  $n_0 = 300$  ( $n_0 = 75$ ) for the B4 (A3) ensemble. For these runs  $N = 96$  mass interpolation steps are used and the lattice is updated after  $\sim 23$  global acceptance steps. This number can be optimized, e.g. by using  $N = 24$  interpolation steps the acceptance rate is given by 42% and the lattice is

$i$	$n_i$	actions			$P_{\text{acc}}$
		$S^{(0)} = S_w$	$S^{(1)} = S_w^{\text{HYP}}$	$S^{(2)} = S_b$	
0	250	$\beta_0^{(0)} = 5.5874$	-	-	-
1	8	$\beta_1^{(0)} = -0.1122$	$\beta_1^{(1)} = 0.128$	-	40%
2	3	$\beta_2^{(0)} = 0.0011$	$\beta_2^{(1)} = 0.036$	$\beta_2^{(2)} = 0.975$	35%
3	4	$\beta_3^{(0)} = 0.0198$	$\beta_3^{(1)} = -0.143$	$\beta_3^{(2)} = 0.076$	79%
4	1	$\beta_4^{(0)} = 0.0039$	$\beta_4^{(1)} = -0.021$	$\beta_4^{(2)} = -0.051$	27%

Table 6.4.: The table shows optimal parameters for the 5-step PSMS algorithm (representative set) for partially smeared HYP Wilson fermions at  $\beta = 5.5$  and  $\kappa = 0.13$ . The parameters for  $S^{(3)} = \hat{S}_b$  are neglected because stochastic estimation is used to evaluate the exact number. Due to that every parameter except  $\beta_3^{(3)} = 1$  is zero.

updated after 45 steps. By rescaling the number of inversions by  $45 \cdot 24 / 23 \cdot 96 \sim 0.5$  it follows for  $N_{\text{tot}} \sim 4000$  ( $N_{\text{tot}} = 1000$ ). To conclude: the PSMS algorithm is competitive to the DD-HMC at a gauge coupling of  $\beta = 5.8$  and a lattice size of  $16^4$ .

In case of the open boundary run the lattice volume is increased by a factor 2.5. By using 2 additional force terms the number of inversions is given by  $N_{\text{tot}} = 5185$  for an update of the lattice which is roughly  $\sim 1700$  for the smallest mass. In general a better scaling of the autocorrelation times is expected for open boundary by  $\tau_{\text{int}} \approx a^{-2}$  (see for a review [134]) but due to the enlarged time extent it remains expensive. To be competitive to modern HMC versions the PSMS algorithm needs further improvements, however the results show that the PSMS algorithm becomes better for smaller lattice spacings.

## 6.5. Partially smeared HYP-runs

In this section it will be shown that the PSMS algorithm can sample configurations by using a partially smeared fermion action. The scale of the generated ensemble will be set by using the mass reweighting technique.

The PSMS algorithm does not need to compute a force term which is needed during the computation of the trajectory of the HMC algorithm. Due to that it is straightforward to simulate with the PSMS algorithm smeared link actions if they enter only the fermion correction step. Thus the PSMS algorithm can profit from several advantages of the smeared links. The smearing of the links smears out the UV-fluctuations, which do not contribute to the continuum physics, and

## 6. Partial Stochastic Multi Step Algorithm

$i$	$n_i$	actions			$P_{\text{acc}}$
		$S^{(0)} = S_w$	$S^{(1)} = S_w^{\text{HYP}}$	$S^{(2)} = S_b$	
0	250	$\beta_0^{(0)} = 5.6690$	-	-	-
1	8	$\beta_1^{(0)} = -0.0823$	$\beta_1^{(1)} = 0.0638$	-	54%
2	3	$\beta_2^{(0)} = -0.0062$	$\beta_2^{(1)} = 0.0778$	$\beta_2^{(2)} = 0.993$	31%
3	2	$\beta_3^{(0)} = 0.0172$	$\beta_3^{(1)} = -0.1256$	$\beta_3^{(2)} = 0.027$	82%
4	1	$\beta_4^{(0)} = 0.0022$	$\beta_4^{(1)} = -0.0160$	$\beta_4^{(2)} = -0.020$	54%

Table 6.5.: The table shows optimal parameters for the 5-step PSMS algorithm (representative set) for partially smeared HYP Wilson fermions at  $\beta = 5.6$  and  $\kappa = 0.128$ .

thus reduces the statistical fluctuations (see e.g. [135] [18]). The action setup will be a two-flavor mass-degenerate  $\mathcal{O}(a)$ -improved partially smeared Wilson Dirac fermions with a Wilson plaquette action. Only the links in the fermion action will be smeared so that the pure gauge update remains the same. In order to use an efficient hierarchical filter system with DD the action parts and so the blocks have to decouple at lower levels. However smearing uses neighbor links to smooths the gauge links. Due to that smeared links close to the block boundary contain information of links in the neighboring blocks. To update a large enough amount of gaugelinks active links with  $d = 1$  are used, e.g. this corresponds to  $6^4$  active links in a  $8^4$  block (see sec.4.1 and fig. 4.2). In this setup it is possible to smear the active links which coupled the next neighbor points in the Wilson Dirac operator by one level of hyper-cubic (HYP) smearing [21]. The links for the clover term have to remain unsmeared. The target probability distribution of the partially smeared fermion action is given by

$$V(U) = \exp\{-\beta S_g(U)\} \cdot \det\left(1 + \kappa\left(K_N(U^{\text{HYP}}) + c_{\text{SW}}K_{\text{csw}}(U)\right)\right)^2 \quad (6.47)$$

with  $U^{\text{HYP}}$  the 1-level HYP-smeared links,  $K_N$  the next neighbor coupling term and  $K_{\text{csw}}$  the clover term of the Wilson Dirac operator. The parameters for the HYP smearing are chosen as in [21].

A 5-step PSMS algorithm with a 4 level-hierarchical filter system is used to generate the HYP-smeared ensembles (see also tab. 6.4 and tab. 6.5). The five different action parts are given by the unsmeared Wilson plaquette gauge action ( $i=0$ ), by a 1-level HYP-smeared plaquette action ( $i=1$ ) and by a global Schur complement ( $i=4$ ),  $8^4$  Schur complements with Dirichlet boundaries ( $i=3$ ) and  $4^4$  block operators by using recursive DD ( $i=2$ ).

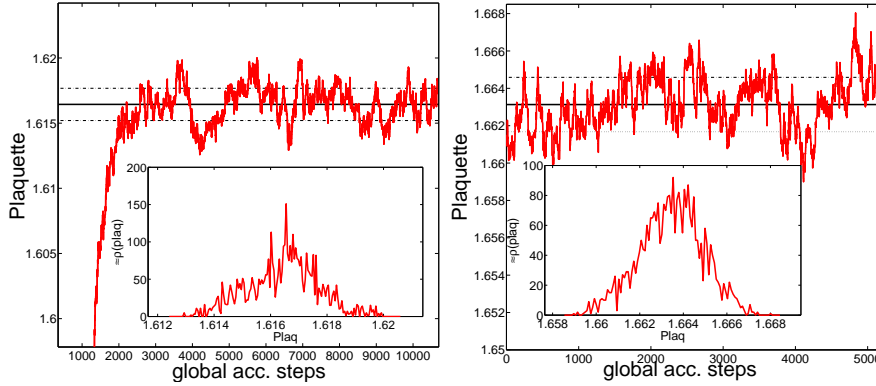


Figure 6.7.: The plaquette values are plotted versus the global acceptance steps. The left figure shows the plaquette value of the  $\beta = 5.5$  ensemble while the right figure shows the data of the  $\beta = 5.6$  ensemble. In the left figure the thermalization of the plaquette is shown while the measuring of the observables are started after 6000 global acceptance steps for the  $\beta = 5.5$  ensemble, after 2000 global acceptance steps for the  $\beta = 5.6$  ensemble respectively. The small figure shows a histogram of the plaquette.

The first step ( $i=0$ ) consists of a pure gauge update of the active links in the  $6^4$  sub-cube of the  $8^4$  blocks. At the first filter level ( $i=1$ ) the 1-level HYP-smeared plaquette action enters. The 1-level HYP-smeared plaquette action has a large correlation with the smeared fermion action, needs only a relatively small numerical effort to be computed and pushes the acceptance rates of the second and third filter level to a reasonable level. At the second level ( $i=2$ ) the determinants of the  $4^4$ -block operators enter the accept-reject step while at the last filter step ( $i=3$ ) the determinant of the  $8^4$  Schur complement enters. These steps are iterated in order to have a reasonably large amount of proposed links for the global acceptance step ( $i=4$ ).

### 6.5.1. Runs

Two ensembles are generated with two different pure gauge couplings  $\beta = 5.5$  and  $\beta = 5.6$ . For both ensembles a clover parameter of  $c_{sw} = 1.0$  is used and a lattice size of  $32 \times 16^3$  with anti-periodic boundary condition is chosen. The quark mass is guessed by setting the bare mass parameter to  $\kappa = 0.13$  for the coarser lattice, and  $\kappa = 0.128$  for the finer one respectively. The parameters used for the different filter steps are shown in table 6.4 for the  $\beta = 5.5$  run and in table 6.5 for the  $\beta = 5.6$  run.

## 6. Partial Stochastic Multi Step Algorithm

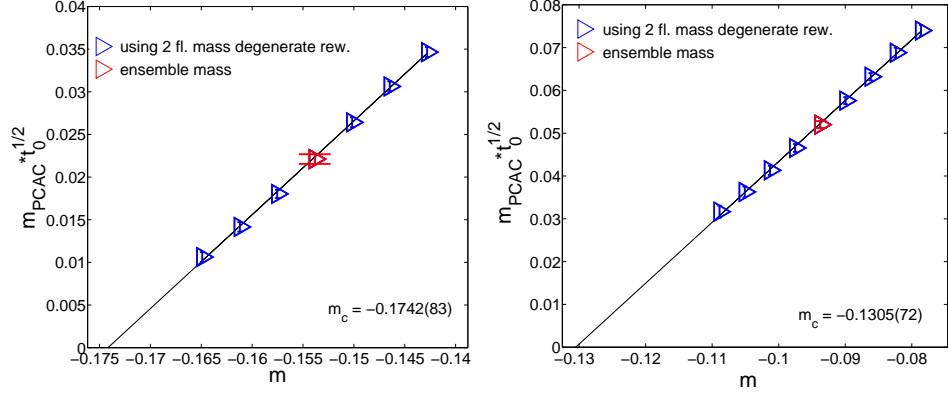


Figure 6.8.: The quantity  $\sqrt{t_0} m_{PCAC}$  is plotted against the bare mass value of the Wilson Dirac operator and extrapolated to the critical bare mass value. The left figure shows the values of the  $\beta = 5.5$  ensemble and the right one the values of the  $\beta = 5.6$  ensemble.

The corresponding plaquettes of both runs are shown in figure 6.7 with an auto-correlation time of  $\tau_{int} = 81(31)$  in units of global acceptance steps for the coarser lattice and  $\tau_{int} = 148(65)$  for the finer lattice ( $\beta = 5.6$ ) respectively. The global acceptance rate is given by 27% respectively 54%, and by updating at every acceptance step 7.8% of the links a “new” configuration is generated after 50 respectively 24 steps. The observables are measured for both ensembles after each group of 20 global acceptance steps.

### 6.5.2. Results

Using two flavor mass-degenerate reweighting it is possible to deduce the critical mass value of both ensembles (see fig. 6.8 and subsec. 5.5.1). The  $m_{PCAC}$  mass is multiplied by  $\sqrt{t_0}$  in order to minimize  $\mathcal{O}(a)$ -effects.

By using the Wilson flow the observable  $t_0$  is calculated (see subsec. 5.5.2). The scale is determined by using the continuum result of  $t_0 = 2.369(36) \cdot 10^{-2}$  [fm<sup>2</sup>] in the chiral limit for the  $N_f = 2$  case [118]. The mass dependence of  $t_0$  is deduced with two flavor mass-degenerate reweighting and  $t_0/a^2$  is extrapolated to the chiral limit (see fig. 6.9). The lattice spacing is given by  $a = 0.112(1)$  fm for the  $\beta = 5.5$  ensemble and  $a = 0.090(1)$  fm for the  $\beta = 5.6$  ensemble. The mass range of the pseudoscalar mass for the extrapolation towards the chiral limit is between 300 MeV and 520 MeV for the  $\beta = 5.5$  ensemble and between 460 MeV and 740 MeV for  $\beta = 5.6$  while the pseudoscalar ensemble mass of the  $\beta = 5.5$  ensemble corresponds to  $M_{PS} = 417(6)$  MeV and  $M_{PS} = 596(15)$  for the  $\beta = 5.6$  ensemble



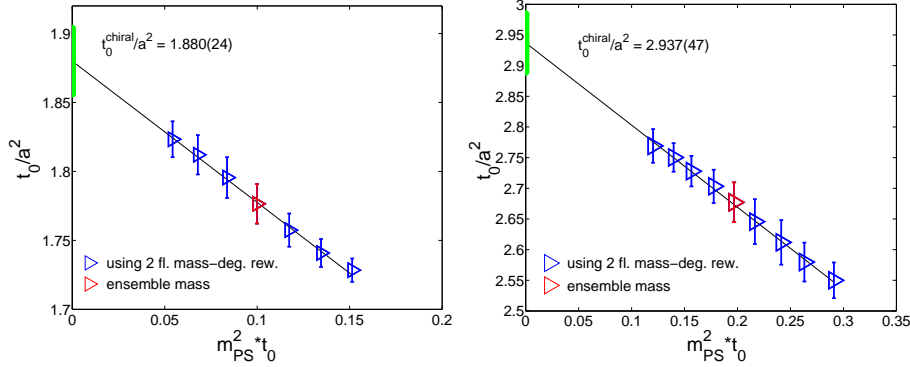


Figure 6.9.: The observable  $t_0/a^2$  is plotted versus the quantity  $t_0 \cdot M_{PS}^2$  in order to perform the chiral limit for  $t_0/a^2$ . The left figure shows the values of the  $\beta = 5.5$  ensemble and the right one the values of the  $\beta = 5.6$  ensemble.

respectively.

The autocorrelation times of the effective masses are below  $\tau_{int} < 4$ , 2 and below  $\tau_{int} < 8$ , 6 for the Wilson flow observable  $t_0$  in units of the measurements (every 20th global acceptance step). In summary 30 decorrelated configurations are generated for the  $\beta = 5.5$  and 25 for the  $\beta = 5.6$  ensemble respectively.

To conclude the PSMS algorithm is able to simulate smeared-fermion actions up to lattices of sizes of  $(2.1 \text{ fm})^4$  and further improvements in the pure gauge update are possible to increase the low-level acceptance (see next sec.6.6.2). However the generation of ensembles with a smeared fermion action suffers from relatively large autocorrelation times. But by using the mass reweighting techniques the scale is set and the critical mass is estimated in the case of the two generated ensembles.

## 6.6. Prospects

There are indications that the PSMS algorithm can decouple slow autocorrelation modes from the correction step with the fermion weight. However the PSMS algorithm is only efficient if a proper hierarchical filter system with parametrization of correlations is used. This ties the proposal to the fermion weight. This filter system has to be further optimized for larger lattices or different lattice actions. For example to update more active links or when using smeared fermion action it is necessary to improve the UV-filter system, for larger volumes it is necessary to improve the IR-filter system. In this section some ideas for improvements will be pointed out.

$i$	without 6-links		with 6-links	
	$n_i$	$P_{\text{acc}}$	$n_i$	$P_{\text{acc}}$
0	250	-	100	-
1	8	40%	4	50%
2	3	35%	3	54%
3	4	79%	3	73%
4	1	27%	1	26%

Table 6.6.: The table compares the acceptance rates of the 5-step PSMS algorithm with a partially smeared HYP action at  $\beta = 5.5$  and  $\kappa = 0.13$  by using a gauge action with/without six-link loops for the proposal.

### 6.6.1. UV - Improvements

The dependence of the UV-fluctuations on the fermion determinant can be described in terms of the hopping parameter expansion of the Wilson Dirac operator (see sec. 4.2). The largest contribution to the fluctuations has the plaquette term, which can be used by introducing a  $\beta$ -shift which increases the acceptance of the low level filter steps to an adequate level (e.g. see tab. 1-2 of [16]). The next higher contributions are the six link loop terms.

In addition to the plaquette term all three types of the six-terms were implemented (e.g. see [57] [58]) based on the package DD-HMC [96] for this work.

The  $\beta = 5.5$  ensemble of the sec. 6.5 with a partially smeared Wilson fermion action is simulated by a pure gauge update by using the plaquette action together with the 6-link action. The parameters of the 6-link action are summed up to zero by including all acceptance levels. The effect is shown in table 6.6 by using all three kinds of six-loops, which are 12 rectangle terms, 48 chair terms and 16 twisted chair terms. The computational operations increase by roughly a factor 14 compared to the plaquette action. Furthermore the active links are limited to the core of the sub-domains, e.g. by using the rectangle term and by using  $8^4$  blocks  $6^4$ -active links have to be used to decouple the block-determinants from each other.

The six link loop pure gauge action is efficient to reduce UV-fluctuations in case of smeared fermion action (see tab. 6.6) and it is interesting as it can be used for the simulation with an improved gauge action, e.g. the Lüscher-Weisz [58] or the Iwasaki pure gauge action [57].

### 6.6.2. IR - Improvements

One of the challenges of the PSMS algorithm is to push the global acceptance rate to the linear dependence of the error-function  $\text{erfc}(\sqrt{\sigma^2/8})$ . To reach larger volumes it is necessary to introduce an efficient IR-filter, which has to capture effectively IR-fluctuations with simultaneously moderate cost. In the literature several techniques exist which could in principle be efficient to capture the IR fluctuations. In general such filter steps can be introduced before the global acceptance step. If the step rejects the new configuration the global acceptance can be neglected. An example is mass preconditioning as in the HMC with the Hasenbusch approach [86]. Here, the global acceptance step can be splitting up by factorizing

$$\det D(U, m_1) = \det M(U, m_1, m_2) \cdot \det D(U, m_2) \quad (6.48)$$

with the ratio matrix  $M = D^{-1}(U, m_2)D(U, m_1)$ . In the case of the PSMS algorithm the weight of the ratio matrices  $M(U, m_1, m_2)$  and  $M(U', m_1, m_2)$  would enter the first step with  $U'$  the proposed configuration. The gauge interpolation are then performed at the larger mass  $m_2$  where the numerical cost of the solver are reduced compare to the light mass  $m_1$ . In general this approach would be efficient if the first step captures efficiently the IR-fluctuations. Other filter steps could be block link actions or coarse grids, which are used to optimize solvers like [92] [136].

### 6.6.3. Conclusion

The PSMS algorithm is competitive to modern HMC algorithms on moderate lattices up to lattice volumes of  $32 \times 16^3$  at a lattice spacing of  $a = 0.052$  fm. The main results of the analysis are

- Autocorrelation: The slow modes of the autocorrelation time can be decoupled from the fermion weighting by increasing the frequency of the pure gauge update steps (see fig. 6.6).
- Smearred action: The PSMS algorithm is able to generate dynamical ensembles by using a smeared fermion action.
- Alternative for the HMC algorithm: The PSMS algorithm belongs to another class of LQCD algorithms than the HMC algorithm. It avoids force computation which is interesting in cases of smeared fermion actions or for chiral fermions.



## 7. Mass–Split Domain Decomposition HMC Algorithm

Monte Carlo simulations of LQCD have to face several difficult aspects when approaching physical quark masses. A first aspect is that the small eigenvalues of the lattice Dirac operator tend to zero which increases the costs of the solver, increases the fluctuations of the force term in the HMC and thus leads to instabilities of the algorithms of the simulations. A second aspect is that with the increasing precision of LQCD simulations, effects of the isospin breaking by different up- and down-quark masses have to be included (also electromagnetic effects should be taken into account). However lattice methods exist to solve these aspects separately, e.g. for the former case by introducing a finite twisted mass term [32] combined with twisted mass reweighting [109] and for the latter case by using mass reweighting techniques (see chapter 5.2). In this chapter a method is presented to address both at the same time by using DD (see sec.4.1 or [31]). DD separates UV- and IR-fluctuating modes by decomposing the lattice into sub-domains (see sec. 4.1). This factorizes the determinant of the Wilson Dirac operator into  $\det D = \det \hat{D} \cdot \prod_k \det D_k$ , with  $D_k$  the block operators which correspond to the sub-domain  $k$ . Using DD in the HMC the force-term of the Schur complement  $\hat{D}$  is the one that destabilizes the molecular dynamics due to large fluctuations, originally introduced by the small eigenvalues of the Dirac operator. The idea is to introduce a cut-off parameter in the Schur complement in order to shift the small eigenvalues to larger values. An effective cut-off parameter can be a larger mass value (see section 7.1). Using this weight factor to generate an ensemble the weight has to be corrected towards the desired one, i.e. by using one flavor mass reweighting (see section 7.2). The cost of this combined method, Mass-split DD-HMC (MDD-HMC), benefits from the larger mass but suffers from the fluctuations introduced by reweighting. However the fluctuations of the Schur complement have a weaker volume dependence than the full Dirac operator [112] and by using anti-correlations with the determinants of the block operators the expectation is that fluctuations can be significantly reduced.

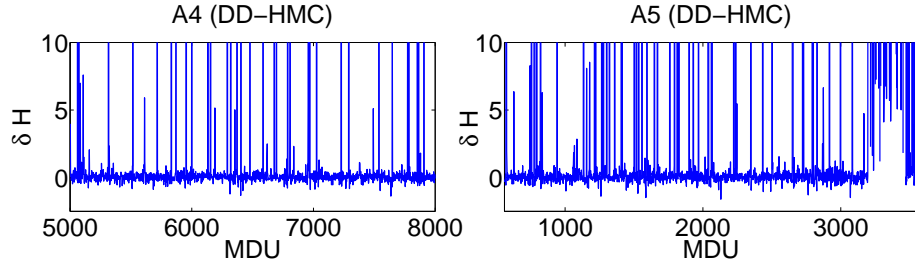


Figure 7.1.: The figure shows a comparison of the energy violation  $\delta H$  plotted against the molecular dynamic units (MDU) for the DD-HMC algorithm with two different quark masses. The left plot corresponds to the run A4 while the right plot corresponds to the run A5.

## 7.1. Properties of the Algorithm

The Boltzmann weight of the MDD-HMC algorithm is given by

$$P_{1,2}(U) = \exp\{-\beta S_g(U)\} \cdot \det \hat{D}^2(m_1, U) \cdot \prod_k \det D_k^2(m_2, U). \quad (7.1)$$

by choosing for the Schur complement  $m_1$  a mass different from the block operators with  $m_2$ . Note by choosing  $m_1 > m_2$  the numerical cost for each trajectory decreases compared to a trajectory at mass  $m_1 = m_2$  for constant  $m_2$ .

The MDD-HMC algorithm can be understood as a modification of the DD-HMC algorithm (see subsec. 4.1.2 and 2.5.1). A crucial point is that step one of the DD-HMC has to be modified. The weight eq. (7.1) is not invariant under a shift of the lattice. A Metropolis accept-reject can be introduced to correct the Boltzmann weight after a shift (see subsec. 7.1.3).

### 7.1.1. Motivation

The smallest eigenvalue of the Dirac operator  $D(m_1)$  is shifted by  $m_1 - m_2$  compared to the Dirac operator at  $m_2$  if a mass shift  $m_2 \rightarrow m_1$  is performed. In general a similar effect is expected for the smallest eigenvalue of the Schur complement. This increase of the smallest eigenvalue stabilizes the energy violation of the discretized trajectory and suppresses large condition numbers of the operator.

The stabilization effect is shown in fig. 7.1 for the DD-HMC runs A4 and A5 of the CLS consortium (see e.g. [98] and tab. 7.1). The energy violation  $\delta H$  for the A5 ( $m_1 = m_2 = m(A5)$ ) ensemble increases compared to the A4 ( $m_1 = m_2 = m(A4)$ )

Table 7.1.: The table shows the parameters of the MDD- HMC runs by using a block size of  $8^4$  and the Wilson plaquette action and the  $\mathcal{O}(a)$ -improved Wilson Dirac operator (for further information of the properties of the A- and E-lattices see [98]).

	A-lattices	E-lattices
$a$	0.076 fm	0.066 fm
$c_{SW}$	2.017147	1.90952
$m_{PS}(m_1)$	380 MeV (A4)	440 MeV (E5)
$m_{PS}(m_2)$	330 MeV (A5)	310 MeV (E6)
$V$ (MDD-HMC)	$32 \times 16^3, 16^4$	$64 \times 32^3, 32 \times 16^3, 16^4$
$V$ (DD-HMC)	$64 \times 32^3$	$64 \times 32^3$

ensemble. Furthermore the algorithm gets stuck at 3200 MDU due to large energy violation during the HMC trajectory in A5 run. In the case of the MDD-HMC algorithm a similar effect as for the A4 run is expected if the mass of the Schur complement is set to the mass parameter of the A4 ensemble and the mass of the blocks is set to the A5 mass.

### 7.1.2. MDD-HMC Simulations

Several runs are performed to analyze and to compare the properties of the MDD-HMC algorithm (see tab. 7.1). The runs of the MDD-HMC algorithm are done for two different lattice spacings. For the E lattice with  $a = 0.066$  fm lattice volumes up to  $64 \times 32^3$  are simulated while for the A lattices with  $a = 0.075$  fm the largest is given by  $32 \times 16^3$ . For all runs the block length is set to  $l = 8$ . Properties of the MDD-HMC are compared to the CLS ensembles A4, A5, E5 and E6 (see e.g. [98]). The MDD-HMC ensembles are labeled by A4spA5 for the large A-lattice and E5spE6 for the large E-lattice.

The energy violation in the case of the E5spE6 run behave as for the E5 run. By using a leap frog integration scheme the energy violation behaves proportional to  $\delta H \propto \epsilon^2 \tau$  with trajectory length  $\tau$  and the step size  $\epsilon$ . In the case of the E5 run by using  $\tau = 4$  and  $\epsilon = 0.0227$  with a statistic of 4045 trajectories 1.9% of  $\delta H$  are larger then 10. This is comparable to the E5spE6 run with  $\tau = 2$  and  $\epsilon = 0.0233$  where 1.2% of the  $\delta H$  are larger then 10. Note this is measured on a smaller ensemble size with 256 trajectories. Moreover the DD-HMC is not able to simulate an E6 ensemble because the algorithm gets stuck due to large  $\delta H$ . This shows that in principle smaller quark masses can be reached by the MDD-HMC algorithm.

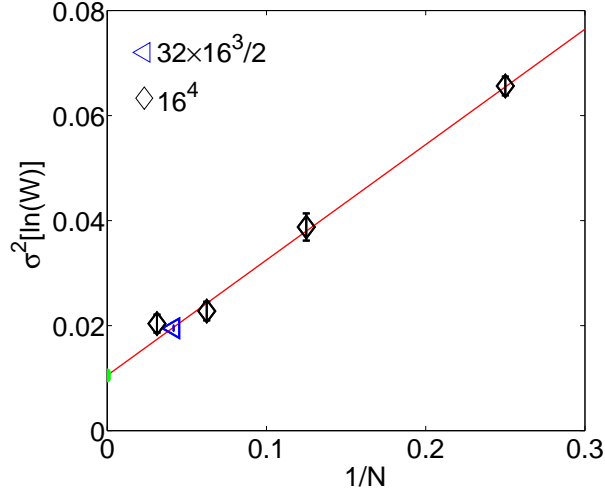


Figure 7.2.: The variance  $\sigma^2(\ln W)$  of the reweighting factor due to the shift (see eq. (7.3)) is plotted against the inverse numbers of mass interpolation steps  $N$ . The variance of the E5spE6 lattice with lattice size  $16^4$  (black, triangle) and  $32 \times 16^3$  (blue, triangle) can be fitted linearly with  $\chi^2/dof = 3.9/3$  (degrees of freedom). The latter one is divided by 2 because the number of blocks increases linearly with the volume.

### 7.1.3. Shift of the Blocks

Only the active links inside the blocks with  $d = 0$  are updated (see subsec. 4.1.2). To update all links a shift of the blocks has to be performed at the beginning of a trajectory. If  $m_1 = m_2$  the shift does not change the Boltzmann weight eq. (7.1). If the shift is random as in the case of the DD-HMC algorithm detailed balance is fulfilled (see app. C of [31] for a detailed discussion). Moreover the acceptance step of the shift and the HMC step are a combination of two update algorithms. Each update algorithm fulfills detailed balance and due to that also the combination. In the case of the MDD-HMC algorithm, where  $m_1 \neq m_2$ , the shift changes the Boltzmann weight eq. (7.1). This can be corrected by using a Metropolis accept-reject step before performing the HMC trajectory. The transition probability  $T(U \rightarrow U')$  for the shift is given by

$$T(U \rightarrow U') = \min \left\{ 1, \frac{P_{1,2}(U')}{P_{1,2}(U)} \right\}. \quad (7.2)$$



The shift of the blocks is implemented by changing the gauge links  $U_\mu(x) \rightarrow U'_\mu(x) = U_\mu(x+s)$  with a shift vector  $s$ . The ratio of eq. (7.2) can be rewritten in terms of the block determinants as

$$W = \frac{P_{1,2}(U')}{P_{1,2}(U)} = \prod_k \frac{\det D_k^2(U', m_2) \det D_k^2(U, m_1)}{\det D_k^2(U', m_1) \det D_k^2(U, m_2)} \quad (7.3)$$

by using the identities  $\det D(m, U') = \det D(m, U)$  and  $S_g(U) = S_g(U')$ . In general if the block length is given by  $l \leq 6$  the determinants can be exactly calculated. For larger block sizes recursive DD can be used to factorize the block determinants further. The Dirichlet Schur complements can be treated stochastically while the smaller blocks can be evaluated exactly. The accept-reject step is accomplished by replacing eq. (7.2) by a stochastic estimator (like it is done in the PSMS algorithm see chap. 6).

The stochastic estimation is done by using similarly to the two flavor mass-degenerate reweighting case a linear interpolation in the mass with  $D_k^2(U, m_1) \rightarrow D_k^2(U, m_2)$  and  $D_k^2(U', m_2) \rightarrow D_k^2(U', m_1)$ . To ensure detailed balance by using stochastic estimation only one pseudofermion field has to be drawn during the mass interpolation for each ratio (see app. E).

The crucial quantity of the accept-reject step is the acceptance rate. The acceptance rate is given by eq. (6.3)

$$\langle P_{acc} \rangle_{U, U'} = \text{erfc} \left\{ \sqrt{\frac{\sigma^2}{8}} \right\} \quad (7.4)$$

with the variance of the logarithm of the weight eq. (7.3). Similar to the analysis of the PSMS algorithm in subsec. 6.4.2 the effects of the stochastic and the ensemble fluctuations can be separated by plotting  $\ln(\sigma^2 W) = C + B/N$  against the inverse number of mass interpolation steps  $N$  with the constant  $C$  and  $B$ . This is done for the E5spE6 lattice with a lattice volume of  $16^4$  with  $8^4$  blocks (see fig. 7.2).

The exact acceptance rate is derived by performing a linear fit in  $1/N$ . The extrapolation gives  $C = 1.05(7) \cdot 10^{-2}$  for the ensemble fluctuations of the  $16^4$  lattice which corresponds to an acceptance rate of  $P_{acc} = 0.988\%$ . In general the evaluation of the weight factor  $W$  needs  $2N$  block inversions for each block.

Although the variance of the ratio eq. (7.3) scales linear with the volume  $V$  it is tamed by the mass shift  $\Delta m^2$ . In principle the acceptance is large for lattices up to  $128 \times 64^3$  with  $P_{acc} = 20\%$  for the E5spE6 lattice if the block size is  $8^4$ . The numerical cost of the accept-reject step is moderate because the ratio eq. (7.3) can be calculated in parallel without any communication during the computation.

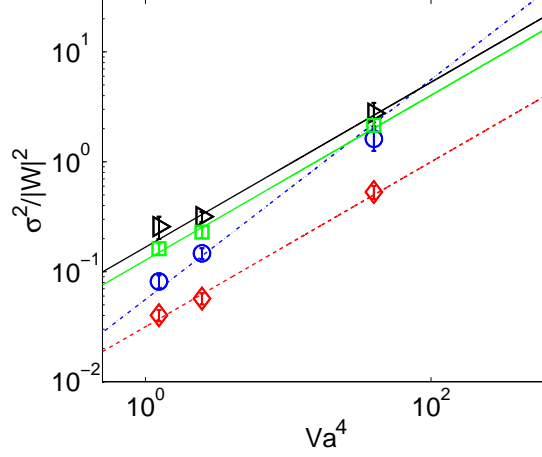


Figure 7.3.: The figure shows the volume scaling of the reweighting factors for the four different cases with a mass shift  $\Delta\bar{m} \sim 16.2$  MeV and a lattice spacing  $a = 0.066$  fm . Note that the four different cases are listed in the text.

## 7.2. Properties of the Reweighting

In order to obtain a proper theory of  $n_f = 1 + 1$ -quarks the sampled ensemble has to be weighted by

$$P_{u,d} = \exp\{-\beta S_g\} \cdot \det D(m_u) \cdot \det D(m_d) \quad (7.5)$$

with  $m_u$  the mass parameter which corresponds to the up-quark mass and  $m_d$  to the down-quark mass. Sampled ensembles by eq. (7.1) have to be corrected to eq. (7.5). This is possible by using mass reweighting with the reweighting factor

$$W = \frac{\det \hat{D}(m_u) \cdot \prod_k \det D_k(m_u) \det \hat{D}(m_d) \cdot \prod_k \det D_k(m_d)}{\det \hat{D}^2(m_1) \cdot \prod_k \det D_k^2(m_2)} \quad (7.6)$$

such that  $P_{u,d} = W \cdot P_{1,2}$ .

To calculate the reweighting factor the one flavor reweighting technique with mass-interpolation is used (see sec. 5.2). Additional reweighting introduces ensemble fluctuations which increase the statistical error of the observables and scale with the mass shift  $\Delta m^2 = (m_d - m_u)^2$  (compare sec. 5.4).

If the blocks are reweighted in the reverse mass direction as the Schur complement a large anti-correlation is expected. This anti-correlation given by the covariance of the form  $\text{cov}[\det \hat{D}(m_2) / \det \hat{D}(m_1), \prod_k \det D_k(m_1) / \det D_k(m_2)]$  is of the size of the fluctuations of the Schur complement  $\text{var}[\det \hat{D}(m_2) / \det \hat{D}(m_1)]$  for blocks with block length  $l = 8$ . Note that the ensemble fluctuations are defined by  $\sigma^2 = \langle \ln^2 W \rangle - \langle \ln W \rangle^2$ .

The specific volume behavior of the fluctuations is analyzed for a constant block size with  $l = 8$  at four representative points of the corrected Boltzmann weight. These points correspond to Boltzmann weights with 1 + 1 fermions and 2 mass-degenerate fermions. The volume behavior of the fluctuations of the different reweighting factors towards the points are deduced on the  $16^4$ ,  $32 \times 16^3$  and  $64 \times 32^3$  lattice with a lattice spacing  $a = 0.066$  fm (see fig. 7.3). The properties of these points are given by

- 1 + 1 point with  $m_u = m_2$  and  $m_d = m_1$ : the volume dependence is given by  $\approx V^\alpha$  with  $\alpha = 0.76(4)$  and the points are labeled by (red, diamond) and connected by the curve (red, dashed).
- 2 flavor mass-degenerate point with  $m = 0.5(m_1 + m_2)$ : the volume dependence is given like in the 1 + 1-case by  $\alpha = 0.75(5)$ . The points are labeled by (green, square) and connected by a green solid curve.
- 2 flavor mass-degenerate point with  $m = m_2$ : the volume dependence is given by the 2 flavor reweighting factor of the Schur complement with  $\alpha = 0.73(9)$ . The points are labeled by (black, triangle) and connected by a black solid curve.
- 2 flavor mass-degenerate point with  $m = m_1$ : the volume dependence is given by the 2 flavor reweighting factor of the blocks with  $\alpha = 0.86(8)$ . The points are labeled by (blue, circle) and connected by a blue dash-dotted curve.

The scaling behavior is shown in figure 7.3. For the plotted curves the parameter  $\alpha$  is set to  $\alpha = 0.75$  for the first three different cases and  $\alpha = 1.0$  for the last case. Note this is due to the fact that the number of the blocks scales linear with the volume. However this behavior is not found. A possible explanation could be that the statistic with 512 MDU's is not large enough for the largest volume.

### 7.3. Costs

The MDD-HMC algorithm can handle several difficult aspects which become important for physical quark masses. In this section the cost of the MDD-HMC algorithm will be compared for different cases to standard methods. In general the

cost of the MDD-HMC algorithm is dominated by the molecular dynamics and the effective number of configurations which are reduced by the covariance of the reweighting factor with a specific observable. In general the effectiveness of the algorithm is increased because the trajectory for the IR-part is done for larger masses. The reweighting decreases the effectiveness. How this acts on the competitiveness of the MDD-HMC algorithm will be discussed in this section.

**Comparison to DD-HMC:** The two flavor mass-degenerate case with  $m_{ud} = m_2$  can be compared to the DD-HMC. For this comparison the CLS ensembles are used to estimate the cost of the trajectory during the ensemble generation. The cost of the DD-HMC is given in units of inversions of the Dirac operator by a rough estimate with  $cost(m) = 2N_{tr/cnfg}N_{iter}(m)N_0(m)$  where  $N_{tr/cnfg}$  the number of trajectories per configuration,  $N_{iter}(m)$  the number of iteration of the solver to invert the Dirac operator and  $N_0(m)$  the number of discretization steps per molecular dynamics trajectory. The cost for the reweighting is roughly given by  $cost_{mrew} = N_{rew}N_{iter}(m_{12})$  with  $N_{rew} \sim 60$  the numbers of inversions per reweighting factor and the average mass  $2m_{12} = m_1 + m_2$ .

The reweighting increases the statistical error of an observable which depend on the covariance of the observable with the reweighting factor. In general the increase is moderate for the E5spE6 ensemble at the two flavor point with the E6 mass, e.g. in the case of gluonic observables the error increases only slightly by at least a factor  $\sim 1.22$  which correspond to a reduction of the effective number of the ensemble by  $\sim 0.66$ . This analysis is more complicated for fermion observable due to the fact that the observable depends directly on the quark mass. The error increases in the case of the  $f_{PP}$  correlator by a factor  $\sim \sqrt{3}$  at the E6 point with the 2 flavor mass-degenerate reweighting factor compared to the quenched E5 point without reweighting factor. In general this shows that the error in observables increases not dramatically also for a mass split of  $\sim 16$  MeV on the E5spE6 ensemble.

The comparison between the MDD-HMC and DD-HMC is shown in table 7.2. The numbers show that also for larger lattice sizes the numerical effort of the MDD-HMC is competitive to the DD-HMC algorithm. Moreover the MDD-HMC algorithm can simulate smaller quark masses than the DD-HMC due to the higher mass term in the Schur complement. For example the DD-HMC algorithm is unstable at a quark mass which corresponds to the A5 ensemble (compare fig. 7.1).

**Comparison to 1+1 sampling:** It is possible to sample directly a 1+1 ensemble (e.g. [51]). For the direct approach the rational HMC (RHMC) algorithm can be used [137] [138]. In order to sample a 1+1 ensemble an additional force-term has to be introduced. This increases the cost by at least a factor two compared to the DD-HMC. The variance of the reweighting factor for the 1+1 case with  $m_d = m_1$  and  $m_u = m_2$  of the MDD-HMC is less than in the two flavor mass-degenerate case with  $m = m_2$  (see fig. 7.3) which improves the numbers of table 7.2. Moreover the

Table 7.2.: The table shows a comparison of the cost of the DD-HMC and the MDD-HMC algorithm for the two flavor mass-degenerate case at the smallest mass  $m_2$ . However this is only a rough estimate, i.e. the DD-HMC algorithm is not able to simulate the ensemble A5 because of instabilities in  $\delta H$ . The effective number of configurations decreases due to the fluctuations of the reweighting factor. Here, the relative increase of the square of the error  $\delta_{OW}^2$  normalized by square of the error  $\delta_O^2$  without the reweighting factor is used to approximate the reduction of the effective number of configurations.

	DD-HMC	MDD-HMC	“+”mass-reweighting (upper-bound)
X	1	$\frac{\text{cost}(m_1)}{\text{cost}(m_2)} + \frac{\text{cost}_{mrew}}{\text{cost}(m_2)}$	$\frac{\delta_{OW}^2}{\delta_O^2} \frac{\text{cost}(MDD)}{\text{cost}(DD)}$
A5	1	0.76 + 0.06	–
E6	1	0.41 + 0.10	$3 \cdot 0.51 \sim 1.5$

mass split of the isospin broken point  $\Delta\overline{m} \sim 2.5$  MeV is much smaller than for the analyzed E5spE6 ensemble. Here the shift is given by  $\Delta\overline{m} \cong 16$  MeV (see tab. 5.2) and compared to the physical shift the fluctuations would decrease by roughly a factor 40. The conclusion is that the MDD-HMC algorithm is competitive with the RHMC or even more efficient.

## 7.4. Conclusion

A splitting-of of the mass parameter by using DD stabilizes the simulation by using the mass parameter of the Schur complement as a cut-off parameter. By using one flavor mass reweighting it is possible to get a 1+1 ensemble with a moderate increase of the statistical error. The statistical error introduced by the fluctuations of the reweighting factor can be tamed by the anti-correlation of the block operators with the Schur complement determinants. Moreover the fluctuations of the Schur complement has a mild volume scaling with roughly  $V^{3/4}$ . In general a study with improved statistics is necessary before further improvement steps are taken like the usage of recursive DD [16] by setting the Dirichlet Schur complement to the average quark mass  $m_3 = (m_1 + m_2)/2$  or the usage of mass-preconditioning [86] for the Schur complement which reduces large spikes in  $\delta H$ . To conclude there are indications that the MDD-HMC algorithm can be competitive to generate 1+1 ensembles towards physical quark masses.



## 8. Conclusion

The basis of the introduced methods is the stochastic estimation of determinant ratios of the fermion weight. Thereby stochastic and ensemble fluctuations are introduced which have to be understood and controlled. The results of chap. 3 are:

**Introduction of an integral representation for complex determinants:** An integral representation for a determinant of a square complex matrix  $A$  is introduced eq. (3.2) which exists if the condition  $\lambda(A + A^\dagger) > 0$  is fulfilled.

**Fluctuations of stochastic estimation:** The origin of the fluctuations of a stochastic estimation of ratio matrices can be understood by a perturbative approach. For that the ensemble and stochastic fluctuations are given by traces of the square of the first order term of the perturbation, which is a good approximation if the eigenvalues of the matrix are close to one (see app. B).

**Interpolation technique to control stochastic fluctuations:** Determinant ratios can be further factorized by introducing an interpolation in the difference of the operators. In principle such an interpolation scheme can reduce the stochastic fluctuations by  $\frac{1}{N}$  with  $N$  the number of interpolation steps.

These techniques are used for the three main methods.

### Mass Reweighting

Mass reweighting can be used to shift the sea quark masses of a generated ensemble, i.e. by introducing the one flavor and two flavor mass reweighting factor. The main results are:

**Techniques to control the stochastic fluctuations:** The stochastic fluctuations can be controlled by using DD and mass interpolation. The improvements depend on the reweighting method. For one flavor reweighting the even-odd Schur complement and mass interpolation are necessary. For two flavor reweighting, in the isospin reweighting case or the strange quark reweighting case, only mass interpolation improves the estimation (see for details subsec. 5.3.4). Note for a zero crossing eigenvalue of the Dirac operator during the mass interpolation a twisted mass detour ( $\mu$ -detour) can be introduced.

**Techniques to control the ensemble fluctuations:** The ensemble fluctuations can be understood by using DD and analyzing the different behavior of the fluctuations of the different parts, the block parts which capture the UV-fluctuations and the Schur complement part which captures the IR-fluctuations. Furthermore correlations with different action can be used to tame the ensemble fluctuations, e.g. the correlations with the plaquette by a shift in the gauge coupling  $\beta$  or the correlations with other mass reweighting factors, in the case of strange quark mass correction by simultaneously shifting the light quark masses.

**Scaling behavior of mass reweighting factors:** In this work for the stochastic fluctuations it is found that

$$\left\langle \frac{\sigma_{st,p}^2}{W^2} \right\rangle = \frac{k_{st}^{(pf)}}{NN_\eta} \frac{V \Delta \overline{m}^{2p}}{r_0^{4-2p+q} \overline{m}^q}. \quad (8.1)$$

For the one flavor case  $p = 1$  only a weak quark mass dependence is found by using DD. The quark mass dependence is roughly given by  $q \sim 0$  by using the full operator. For the isospin reweighting case  $p = 2$  it follows from the analysis  $q \sim 2.6(1)$ . For the ensemble fluctuations it is found

$$\sigma_{en,pf}^2 = k_{en}^{(pf)} \frac{V^r \Delta \overline{m}^{2p}}{r_0^{4r-2p+q'} \overline{m}^{q'}}, \quad (8.2)$$

where for the one flavor case ( $p = 1$ )  $r = 1$  and  $q' \sim 0$  and for the isospin reweighting case ( $p = 2$ )  $r \approx 0.25 \dots 0.75$  and  $q' \approx 4 \dots 3$ .

**Cost of mass reweighting:** The cost to evaluate the reweighting factor is given by fixing the noise to signal ratio (stochastic over ensemble fluctuations). In the case of one flavor reweighting this ratio is given by

$$\frac{\sigma_{st,rel}^2}{\sigma_{en}^2} NN_\eta = \frac{k_{st}}{k_{en}} \sim 2.5 \dots 7.5 \quad (8.3)$$

with the relative stochastic fluctuations  $\sigma_{st,rel}^2 = \langle \sigma_{st}^2 / W^2 \rangle$ . In the case of isospin reweighting the noise to signal ratio is given by

$$\frac{\sigma_{st,rel}^2}{\sigma_{en}^2} NN_\eta \sim \frac{9V^{1-r}}{(48 \times 28^3)^{1-r}} \frac{a^{4(1-r)}}{[0.066 \text{ fm}]^{4(1-r)}} \frac{[32 \text{ MeV}]^{q'-3}}{\overline{m}^{q'-3}} \quad (8.4)$$

with  $r \approx 1/4 \dots 3/4$  and  $q' \approx 4 \dots 3$

**Error:** The statistical error of observables increases by using mass reweight-



---

ing. This increase depends mainly on the covariance of the observable with the reweighting factor and can be approximated by (see also app. D)

$$\delta_O^2 \sim \frac{1}{N^2 \langle W \rangle^2} \sum_{i,j} [(O_i - \langle O \rangle) W_i (O_j - \langle O \rangle) W_j]. \quad (8.5)$$

Note reweighting introduces bias which can become important for larger mass shifts or large ensemble fluctuations.

Applications of mass reweighting are interesting to determine mass dependencies of observables. In general the bare parameters have to be tuned properly so that the continuum physics can be extracted. For that dimensionless ratios are introduced. In detail these ratios are  $R_1$  to tune the strange quark mass  $\kappa_s$ , here a quenched strange quark,  $R_2$  to tune the mass splitting  $\Delta m_{ud}$  in the down- and up-quark and  $R_3$  to tune the light average quark mass  $m_{ud}$ . Mass reweighting can be used to tune the three ratios. To tune  $R_1$  and  $R_2$  the ensemble fluctuations are tamed by holding the quark mass sum constant eq. (5.61)

$$const = \frac{m_u + m_d}{2\gamma} + m_s \quad (8.6)$$

with a properly tuned  $\gamma$ . The results are:

**Isospin Reweighting:** The isospin splitting in the light quark masses  $\Delta m_{ud}$  can be tuned by using isospin reweighting. The numerical effort for isospin reweighting scales roughly with  $\mathcal{O}(V^{3/2})$  and for the F7 ensemble  $\sim 96$  inversions are adequate to suppress the stochastic fluctuations. Moreover the additionally introduced ensemble fluctuations are small and become only visible for very small quark masses, e.g. the sea quark effects in the pion mass are around  $\sim 0.5$  MeV at the physical mass at finite lattice spacing  $a = 0.066$  fm. Furthermore by using  $R_2$  and  $R_3$  it is possible to extract the light quark masses where the mass splitting is given by  $\Delta \bar{m}_{ud} = 2.49(10)$  MeV and the average quark mass given by  $\bar{m}_{ud} = 3.19(11)$  MeV for a finite lattice spacing at  $a = 0.066$  fm.

**Two flavor mass-degenerate reweighting:** Two flavor mass-degenerate reweighting can be used to perform the extrapolation towards the physical and chiral point by extrapolating in  $R_3$  if the isospin splitting is not tuned. The numerical effort is given by  $\sim 48$  inversions for a reasonable noise over signal ratio and depends on the solver cost  $\mathcal{O}(V)$ . However the ensemble fluctuations of two flavor mass-degenerate reweighting are large and limit the reweighting range for larger volumes. Nevertheless two flavor mass-degenerate reweighting can be used to improve the extrapolation and thus to increase the precision of lattice results (see sec. 5.5.2 and sec. 5.5.1). Moreover

## 8. Conclusion

---

it is possible to determine the critical mass and to set the lattice spacing  $a$  by using only one ensemble (see e.g. sec. 6.5).

In general mass reweighting has many interesting features which can be used to extract high precision results from the lattice.

### PSMS algorithm

The PSMS algorithm is a Monte Carlo algorithm to generate dynamical fermion ensembles for different kinds of fermion action. The idea is to split up the weighting into a pure gauge proposal and into Metropolis accept–reject steps where the fermion weight enters. The fermion weight can be evaluated stochastically. Several techniques have to be developed that such an algorithm has a proper acceptance rate in the different accept–reject steps.

**Controlling the stochastic fluctuations:** By using DD it is possible to split up the determinant exactly into local parts, the block determinants, and a global part the determinant of the Schur complement. For block sizes  $l \leq 6$  the determinant can be calculated exactly. The determinant of ratios of Schur complements can be evaluated stochastically. Thereby the stochastic fluctuations can be controlled by using gauge interpolation combined with relative gauge fixing.

**Controlling the ensemble fluctuations:** The ensemble fluctuations can be controlled by factorizing the Boltzmann weight, e.g. by using recursive DD, and thus by introducing hierarchical accept–reject steps. The effectiveness of these hierarchies can be tuned by introducing a parametrization of correlations between different parts of the action which enter the specific filter step.

The numerical results by using these techniques are given by:

**Scaling of the acceptance rate:** The fluctuations are directly connected to the acceptance rate and scale with the lattice volume. An analysis in the lattice spacing shows that the stochastic fluctuations scale roughly with  $a^{-2}$  and the ensemble fluctuations with  $a^{-2.5}$ . This means that the number of interpolation steps, if the ratio of ensemble to stochastic fluctuations is fixed, is reduced by decreasing lattice spacing and is given by (see eq. (6.45))

$$N(a) = \frac{1}{const} \frac{C'}{B'} a^{d-c} \quad (8.7)$$

with constants  $C'/B' = 244(241)$  and  $d - c \sim 0.5$ . However by fixed physical volume the acceptance rate decreases for decreasing lattice spacing.

---

**Autocorrelation time of the topological charge:** For the analysis of the autocorrelation times several ensembles of different lattice spacing and different setups are generated with the PSMS-, the DD-HMC and the openQCD-HMC algorithm. The analysis shows that by scaling the iteration numbers of the pure gauge proposal with the lattice spacing in the PSMS algorithm the autocorrelation times can be tamed. In this case the scaling in the lattice spacing is roughly proportional to  $a^{-2.8}$  (see subsec. 6.4.3).

**Cost comparison:** The cost of the PSMS algorithm to generate a new decoupled configuration scales for moderate lattice sizes with (eq. (6.46))

$$\text{cost}(U \rightarrow U^{new}) \propto V_{phys}^{5/4} a^{-7.5}. \quad (8.8)$$

For larger volumes further improvements have to be introduced in the filter structure that the acceptance rate does not decrease with  $\propto \exp\{-V\}$ . A direct cost comparison by using the autocorrelation time of the topological charge shows that the PSMS algorithm is competitive for small lattice spacing  $a < 0.07$  fm with the DD-HMC for moderate lattice sizes of  $V \sim (1.2 \text{ fm})^4$ .

Furthermore the PSMS algorithm can sample smeared fermion action, e.g. a partially HYP-smeared Wilson fermion action is simulated. It is shown that by using mass reweighting the scale and the critical mass parameter can be determined by using only one ensemble.

### MDD algorithm

The introduced MDD-HMC algorithm is a novel algorithm which combines the DD-HMC algorithm with the technique mass reweighting by using advantages to suppress disadvantages of both methods. In general the features are given by

**Algorithm:** The idea is to split up the mass parameter of the Schur complement and of the blocks operators. By setting a higher mass to the Schur complement an effective cut-off parameter is introduced and the simulation can be stabilized that it is possible to simulate smaller quark masses. However a Metropolis accept-reject step has to be introduced in order to update every link of the lattice if the update is restricted to the active links. The computation for this accept-reject step can be performed locally and the acceptance is also reasonable for large lattices up to  $128 \times 64^3$  at  $a = 0.066$  fm with  $P_{acc} = 20\%$  at a mass shift of  $\Delta\bar{m} \cong 16 \text{ MeV}$ .

**Mass reweighting:** By using mass reweighting the ensemble weight can be corrected to 1+1 ensembles or two flavor mass-degenerate ensembles.

## 8. Conclusion

---

Thereby the introduced fluctuations are tamed by anti-correlations between the terms of the blocks and the Schur complement which enter the reweighting factor. In general the introduced ensemble fluctuations have a mild volume scaling with  $V^{3/4}$  if an isospin splitting is introduced or/and if the reweighting factor of the Schur complement enters the game.

There are indications that the MDD-HMC algorithm is competitive to modern algorithms. However more statistics is needed to confirm this. To conclude the MDD-HMC algorithm is able to generate 1+1 ensembles.

### Remarks

Most numerical calculations of this thesis are done by implementing routines in the DD-HMC package [96]. Moreover methods like recursive DD or a 6-link pure gauge action are additionally implemented in the framework of the DD-HMC code. All numerical simulations are performed by using the local cluster Stromboli/Vulcano at the university of Wuppertal. For the analysis of mass reweighting gauge ensembles of the CLS consortium are used.

# Appendix

## A. Proof of the Integral Representation

In this appendix the validity of the integral eq. (3.2) will be shown by using the Gauß elimination method of a matrix (e.g. see [139]). However a more simple proof is already presented in app. A of [10] and in [140] for the two dimensional case. In general the integral representation is given by eq. (3.2)

$$\frac{1}{\det A} = \int \exp\{-\eta^\dagger A \eta\} D[\eta] \quad \text{if } \operatorname{Re}(\eta^\dagger A \eta) > 0 \quad \forall \eta \in \mathbb{C}^n \setminus 0 \quad (\text{A.1})$$

with a complex pseudofermion field  $\eta \in \mathbb{C}^n$ , a complex matrix  $A \in \mathbb{C}^{n \times n}$  and a normalized integral measure by  $D[\eta] = \prod_{j=1}^n dx_j dy_j / \pi$  with  $\eta_j = x_j + iy_j$ . Note that the condition for the validity of the integral eq. (A.1) is equivalent to  $\lambda\{A + A^\dagger\} > 0$ . However the proof will start by showing the validity of a rather similar integral

$$\frac{1}{\det A} = \int \exp\{-x^T A^T A x\} D[x] \quad \text{if } \operatorname{Re}(x^T A^T A x) > 0 \quad \forall x \in \mathbb{R}^n \setminus 0 \quad (\text{A.2})$$

with a real pseudofermion field  $x \in \mathbb{R}^n$ , a symmetric matrix  $A^T A \in \mathbb{C}^{n \times n}$  and a normalized integral measure  $D[x] = \int_{i=1}^n \frac{dx}{\sqrt{\pi}}$ .

### A.1. Integral

In this part the following integral relation will be proven

$$\int_{-\infty}^{+\infty} \left( \int_{-\infty}^{+\infty} e^{-[a(x+\frac{c^2}{a}y)^2+(b-\frac{c^2}{a})y^2]} \frac{dx}{\sqrt{\pi}} \right) \frac{dy}{\sqrt{\pi}} = \frac{1}{\sqrt{a}} \int_{-\infty}^{+\infty} e^{-(b-\frac{c^2}{a})y^2} \frac{dy}{\sqrt{\pi}} \quad (\text{A.3})$$

with constant  $a, b, c \in \mathbb{C}$  with  $\operatorname{Re}(a) > 0$ ,  $\operatorname{Re}(b) > 0$  and  $\operatorname{Re}(b - c^2/a) > 0$ . The proof is simplified into two steps which will be proven separately. In step A the equation

$$\int_{-\infty}^{+\infty} \left( \int_{-\infty}^{+\infty} e^{-[a(x+\frac{c^2}{a}y)^2+(b-\frac{c^2}{a})y^2]} \frac{dx}{\sqrt{\pi}} \right) \frac{dy}{\sqrt{\pi}} \stackrel{(A)}{=} \int_{-\infty}^{+\infty} \left( \int_{-\infty}^{+\infty} e^{-[ax^2+(b-\frac{c^2}{a})y^2]} \frac{dx}{\sqrt{\pi}} \right) \frac{dy}{\sqrt{\pi}} \quad (\text{A.4})$$

will be shown, followed by step B

$$\int_{-\infty}^{+\infty} \left( \int_{-\infty}^{+\infty} e^{-[ax^2+(b-\frac{c^2}{a})y^2]} \frac{dx}{\sqrt{\pi}} \right) \frac{dy}{\sqrt{\pi}} \stackrel{(B)}{=} \frac{1}{\sqrt{a}} \int_{-\infty}^{+\infty} e^{-(b-\frac{c^2}{a})y^2} \frac{dy}{\sqrt{\pi}}. \quad (\text{A.5})$$

Furthermore the prove will only show the steps with an imaginary transformation. The generalization to arbitrary complex numbers is then straightforward. Note for the definition of the integral eq. (A.3) it is necessary that the real term of the exponent is strictly positive. By defining a matrix  $A \in \mathbb{C}^{2 \times 2}$  with

$$A = \begin{bmatrix} a & \frac{\zeta}{2} \\ \frac{\zeta}{2} & b \end{bmatrix}. \quad (\text{A.6})$$

it follows that

$$\operatorname{Re}(v^T A v) > 0 \quad \text{for all } v \in \mathbb{R}^2 \setminus 0. \quad (\text{A.7})$$

**(A):** The step (A) is proven by simplifying the integral eq. (A.4). By setting  $c = i\zeta y$ , demanding  $\zeta \in \mathbb{R}$  and setting  $a = 1$  it follows

$$\int_{-\infty}^{+\infty} \int_{-\infty}^{+\infty} e^{-(x^2 + 2i\zeta xy + by^2)} \frac{dx dy}{\pi} = \int_{-\infty}^{+\infty} \int_{-\infty}^{+\infty} e^{-((x+i\zeta y)^2 + (b+\zeta^2)y^2)} \frac{dx dy}{\pi}. \quad (\text{A.8})$$

If and only if the condition  $\operatorname{Re}(b) > 0$  is fulfilled it follows

$$\int_{-\infty}^{+\infty} \int_{-\infty}^{+\infty} e^{-((x+i\zeta y)^2 + (b+\zeta^2)y^2)} \frac{dx dy}{\pi} = \int_{-\infty}^{+\infty} e^{-(b+\zeta^2)y^2} \frac{dy}{\sqrt{\pi}}. \quad (\text{A.9})$$

The proof can be done by using Cauchy's Integral Theorem (see e.g. [141])

$$\int_{\gamma_R} f(z) dz = 0 \quad (\text{A.10})$$

by integrating over a compact contour  $\gamma_R$ . A finite rectangular contour with corners  $R$ ,  $R + i\zeta y$ ,  $-R + i\zeta y$  and  $-R$  is defined. The path integral over  $-R$  to  $R$  in the limit  $R \rightarrow \infty$  is given by

$$\int_{-\infty}^{+\infty} e^{-x^2} \frac{dx}{\sqrt{\pi}} = 1. \quad (\text{A.11})$$

The path integral over one side which enters the complex plain is given by

$$\begin{aligned} I(R) &= \int_{-\infty}^{+\infty} \int_0^{y\zeta} i f(R + iu) e^{-(b+\zeta^2)y^2} \frac{du dy}{\pi} \\ &= \int_{-\infty}^{+\infty} \int_0^{y\zeta} i e^{-R^2 - 2iRu + u^2 - (b+\zeta^2)y^2} \frac{du dy}{\pi} \end{aligned} \quad (\text{A.12})$$

with  $f(v) = e^{-v^2}$ . Now an upper bound to the integral is given by

$$|I(R)| < \left| \int_{-\infty}^{+\infty} C e^{-R^2 - by^2} \frac{dy}{\sqrt{\pi}} \right| \quad (\text{A.13})$$

with a constant  $C$  and with (B) of integral eq. (A.3) the integral  $I(R)$  converges to 0 for  $R \rightarrow \infty$ .

**(B):** The step (B) eq. (A.3) is proven

$$\int_{-\infty}^{+\infty} e^{-ax^2} \frac{dx}{\sqrt{\pi}} = \frac{1}{\sqrt{a}} \quad (\text{A.14})$$

by neglecting the integration over  $y$  and setting  $||a|| = 1$ . By applying a parameter transformation  $\sqrt{a}x \rightarrow x'$  and writing  $a = e^{i2\theta}$  with  $\theta \in \mathbb{R}$  the integral is given by

$$\int_{-\infty}^{+\infty} e^{-ax^2} \frac{dx}{\sqrt{\pi}} = \int_{-e^{-i\theta}\infty}^{e^{-i\theta}\infty} e^{-x^2} \frac{dx}{\sqrt{\pi}e^{i\theta}}. \quad (\text{A.15})$$

Again Cauchy's theorem can be used by defining a contour with corners  $-R$ ,  $R$ ,  $e^{-i\theta}R$  and  $-e^{-i\theta}R$ . The integral from  $-R$  to  $R$  by taking the limit  $R \rightarrow \infty$  is given by

$$\lim_{R \rightarrow \infty} \int_{-R}^{+R} e^{-x^2} \frac{dx}{\sqrt{\pi}} = 1. \quad (\text{A.16})$$

For the integral of the twisting into the complex plain follows

$$\begin{aligned} I(R) &= \int_0^\theta -ie^{-R^2 e^{iu} - iu} \frac{du}{\sqrt{\pi}} \\ &= \int_0^\theta -ie^{-R^2 \cos u} (\cos[R^2 \sin(u) + u] - i \sin[R^2 \sin(u) + u]) \frac{du}{\sqrt{\pi}}. \end{aligned} \quad (\text{A.17})$$

An upper bound for the integral follows with

$$|I(R)| = C e^{-R^2 \cos \theta} \quad (\text{A.18})$$

which converges to 0 for  $\theta \in (-\pi/2, \pi/2)$  by performing the limit  $R \rightarrow \infty$ . This is fulfilled if  $\text{Re}(a) > 0$ .

By using step (A) and step (B) and generalizing the constant to complex numbers the integral equation eq. (A.3) is proven.



## A.2. Proof: Gauß Elimination without Gauß Elimination

The proof is done by transforming the integral by completing the square. The essence of the proof reduces to a Gaußelimination of the matrix  $A$  or  $A^T A$ .

The properties of the previous section are used to transform the expression

$$x^T B x = \sum_{i=1}^n b_{ii} x_i^2 + 2 \sum_{1=i<j}^{n-1,n} b_{ij} x_i x_j \quad (\text{A.19})$$

with  $B = A^T A$  and  $A \in \mathbb{C}^{n \times n}$ .

In the following part the notation will be simplified. For that the integral will be hidden and the derived rules for the integral transformation will be used. Due to that the symbol  $=$  will be substituted by the symbol  $\Rightarrow$  if the equation is connected by a variable transformation.

Now, let us take a closer look at the terms of eq. (A.19) which only depend on  $x_1$

$$\begin{aligned} b_{11} x_1^2 + 2 \sum_{1<j}^n x_1 x_j b_{1j} &= b_{11} \left( x_1 + x_2 \frac{b_{12}}{b_{11}} \right)^2 - x_2^2 \frac{b_{12}^2}{b_{11}} + 2 \sum_{j=2}^n x_1 x_j b_{1j} \\ &\quad x_1 \rightarrow x_1 - x_2 \frac{b_{12}}{b_{11}} \\ \Rightarrow b_{11} \left( x_1 + x_3 \frac{b_{13}}{b_{11}} \right)^2 &- \sum_{j=2}^3 x_j^2 \frac{b_{1j}^2}{b_{11}} + 2 \sum_{j=3}^n x_1 x_j b_{1j} \\ &\quad - 2 \sum_{k=3}^n x_2 x_k \frac{b_{12} b_{1k}}{b_{11}} \\ &\quad \vdots \\ \Rightarrow b_{11} x_1^2 - \sum_{j=2}^n x_j^2 \frac{b_{1j}^2}{b_{11}} &- 2 \sum_{2=j<k}^{n-1,n} x_j x_k \frac{b_{1j} b_{1k}}{b_{11}} \end{aligned} \quad (\text{A.20})$$

Now eq. (A.19) can be rewritten by

$$\begin{aligned}
 x^T B x &\Rightarrow b_{11} x_1^2 + \sum_{i=2}^n \left( b_{ii} - \frac{b_{1i}^2}{b_{11}} \right) x_i^2 + 2 \sum_{1=i<j}^{n-1,n} x_i x_j \left( b_{ij} - \frac{b_{1i} b_{1j}}{b_{11}} \right) \\
 &\Rightarrow b_{11} x_1^2 + \sum_{i=2}^n b_{ii}^{(2)} x_i^2 + 2 \sum_{1=i<j}^{n-1,n} b_{ij}^{(2)} x_i x_j \\
 &\Rightarrow \sum_{i=1}^n b_{ii}^{(i)} x_i^2
 \end{aligned} \tag{A.21}$$

with the coefficient

$$b_{kl}^{(n)} = b_{kl} - \sum_{m<n} \frac{b_{km}^{(m)} b_{ml}^{(m)}}{b_{mm}^{(m)}} \tag{A.22}$$

with  $b_{11}^{(1)} = b_{11}$ . The coefficients  $b_{kk}^{(n)}$  are equal to the diagonal coefficient of the triangle matrix  $U$  with  $B = LU$  generated by a Gauß elimination. Transforming  $x_i \rightarrow \frac{1}{\sqrt{b_{ii}^{(i)}}} x_i$  it follows

$$\sqrt{\prod b_{ii}^{(i)}} = \sqrt{\det B} = \det A \tag{A.23}$$

the proof of the eq. (A.2).

The proof for the unsymmetrical case with the complex valued field  $\eta = x + i \cdot y$  is similar to the symmetric case for  $n > 2$ . For this reason the proof is simplified by using a complex  $2 \times 2$ -matrix  $A$ . It follows

$$\eta^\dagger A \eta = a_{11} \left( (x_1 + c_1)^2 + (y_1 + e_1)^2 \right) - a_{11} (c_1^2 + e_1^2) + (x_2^2 + y_2^2) a_{22}$$

with

$$c_1 = \frac{1}{2a_{11}} (a_{12}(x_2 + i \cdot y_2) + a_{21}(x_2 - i \cdot y_2)) \tag{A.24}$$

and

$$e_1 = \frac{1}{2a_{11}} (a_{12}(y_2 - i \cdot x_2) + a_{21}(y_2 + i \cdot x_2)). \tag{A.25}$$

The evaluation of  $c_1^2$  gives

$$\begin{aligned}
 4a_{11}^2 c_1^2 &= (a_{12}^2 + 2a_{12}a_{21} + a_{21}^2) x_2^2 + (-a_{12}^2 + 2a_{12}a_{21} - a_{21}^2) y_2^2 \\
 &\quad + 2i \cdot x_2 y_2 (a_{12}^2 - a_{21}^2)
 \end{aligned} \tag{A.26}$$

and similar for  $e_1^2$  by interchanging  $a_{12} \leftrightarrow a_{21}$  and  $y_2 \leftrightarrow x_2$

$$4a_{11}^2 e_1^2 = (a_{21}^2 + 2a_{21}a_{12} + a_{12}^2)y_2^2 + (-a_{21}^2 + 2a_{21}a_{12} - a_{12}^2)x_2^2 + 2i \cdot y_2 x_2 (a_{21}^2 - a_{12}^2). \quad (\text{A.27})$$

Now it follows

$$a_{11}^2 (c_1^2 + e_1^2) = a_{12}a_{21}x_2^2 + a_{12}a_{21}y_2^2. \quad (\text{A.28})$$

By comparing this result with the symmetric case, the term  $\frac{a_{12}a_{21}}{a_{11}}$  has to be subtracted from  $a_{22}$ . This is the Gaußelimination for the unsymmetrical case. The coefficients of the Gaußelimination for the unsymmetrical case are given by

$$a_{kl}^{(n)} = a_{kl} - \sum_{m < n} \frac{a_{km}^{(m)} a_{ml}^{(m)}}{a_{mm}^{(m)}}. \quad (\text{A.29})$$

It follows the proof of eq. (A.1)

$$\sqrt{\prod a_{ii}^{(i)}} \sqrt{\prod a_{ii}^{(i)}} = \sqrt{\det A} \sqrt{\det A} = \det A. \quad (\text{A.30})$$

In general the coefficients  $a_{ii}^{(i)}$  have to fulfill the condition  $\text{Re}(a_{ii}^{(i)}) > 0$ . The condition is fulfilled if  $\text{Re}(\eta^\dagger A \eta) > 0 \quad \forall \eta \in \mathbb{C}^n \setminus 0$  is satisfied. By using the Gaußelimination the matrix  $A$  can be decomposed into  $A = L \cdot U$  with  $L$  a lower triangular matrix with unit diagonal elements and  $U$  an upper triangular with the coefficients  $a_{ii}^{(i)}$  as diagonal elements. Note that  $L$  is invertible. Now, it follows

$$\text{Re}(\eta^\dagger A \eta) > 0 \Leftrightarrow \text{Re}(\chi^\dagger U L^{\dagger -1} \chi) > 0 \quad \text{with} \quad \chi = L^\dagger \eta. \quad (\text{A.31})$$

Note that the matrix  $R = U L^{\dagger -1}$  is an upper triangular matrix with corresponding diagonal elements  $a_{ii}^{(i)}$ . Now, it is straightforward that eq. (A.31) only holds if the diagonal elements of  $R$  fulfill  $\text{Re}(a_{ii}^{(i)}) > 0$ .

## B. Fluctuations

In this appendix some facts about the variance of the stochastic estimation will be discussed. These will be a description of variances of a complex estimate and a definition of the used variance in this thesis and of [10]. At the end of this appendix a comparison of the root method to the interpolation method for the hermitian case will be presented.

### B.1. Fluctuations of a complex Estimate

In general the variance of a real quantity is defined as the square deviation from the mean value and is given by

$$\sigma^2(X) = \langle (X - \langle X \rangle)^2 \rangle = \langle X^2 \rangle - \langle X \rangle^2 \quad (\text{B.1})$$

with  $\langle X \rangle = \lim_{N \rightarrow \infty} 1/N \sum_{i=1}^N X_i$  the so called ensemble average of the quantity  $X$  by dropping the index  $i$ . The variance  $\sigma^2(X)$  is semi positive definite  $\sigma^2(X) \geq 0$  and is real. Strictly speaking the variance is the measure of the fluctuations of a one dimensional function. For a complex number  $X \in \mathbb{C}$  this function can be for example the real part  $\text{Re}(X) = 0.5(X + X^\dagger)$ , the imaginary part  $\text{Im}(X) = 0.5i(X^\dagger - X)$  or the absolute value  $R(X) = \sqrt{XX^\dagger}$ . In detail these variances are given for the real part by

$$\sigma_{Re}^2 = \frac{1}{2} \sigma_{(1)}^2 + \frac{1}{4} (\sigma_{(2)}^2 + \sigma_{(3)}^2), \quad (\text{B.2})$$

for the imaginary part by

$$\sigma_{Im}^2 = \frac{1}{2} \sigma_{(1)}^2 - \frac{1}{4} (\sigma_{(2)}^2 + \sigma_{(3)}^2) \quad (\text{B.3})$$

and for the absolute value by

$$\sigma_{ABS}^2 = \sigma_{(4)}^2. \quad (\text{B.4})$$

The different terms are given by

$$\begin{aligned} \sigma_{(1)}^2 &= \langle XX^\dagger \rangle - \langle X \rangle \langle X^\dagger \rangle \\ \sigma_{(2)}^2 &= \langle X^2 \rangle - \langle X \rangle^2 \\ \sigma_{(3)}^2 &= \langle X^{\dagger 2} \rangle - \langle X^\dagger \rangle^2 \\ \sigma_{(4)}^2 &= \langle XX^\dagger \rangle - \langle \sqrt{XX^\dagger} \rangle^2. \end{aligned} \quad (\text{B.5})$$

Throughout this thesis a variance term is used which is defined by

$$\sigma^2 = \sigma_{Re}^2 + \sigma_{Im}^2 = \sigma_{(1)}^2 = \text{cov}(X, X^\dagger) \quad (\text{B.6})$$

with  $\text{cov}(Y, Z)$  the covariance of two quantities  $Y, Z$ .

## B.2. Fluctuations by using Stochastic Estimation

The average by using a stochastic estimation of a fermion determinant by using the integral representation eq. (3.2) (or eq. (A.1)) is given by the ensemble average and the average over the pseudofermion  $\eta$ . For example the variance for the real term is given by

$$\sigma_{Re}^2 = \left\langle \left[ \text{Re exp}\{-\eta^\dagger(A-1)\eta\} \right]_{\eta,U}^2 \right\rangle - \left\langle \text{Re exp}\{-\eta^\dagger(A-1)\eta\} \right\rangle_{\eta,U}^2 \quad (\text{B.7})$$

while the matrix  $A$  depends on the gauge field. Performing the integral over  $\eta$  it follows

$$\sigma_{(1)}^2 = \left\langle \frac{1}{\det(A+A^\dagger-1)} \right\rangle_U - \left\langle \frac{1}{\det(A)} \right\rangle_U \left\langle \frac{1}{\det(A^\dagger)} \right\rangle_U \quad (\text{B.8})$$

$$\sigma_{(2)}^2 = \left\langle \frac{1}{\det(2A-1)} \right\rangle_U - \left\langle \frac{1}{\det(A)} \right\rangle_U^2 \quad (\text{B.9})$$

$$\sigma_{(3)}^2 = \left\langle \frac{1}{\det(2A^\dagger-1)} \right\rangle_U - \left\langle \frac{1}{\det(A^\dagger)} \right\rangle_U^2 \quad (\text{B.10})$$

and

$$\sigma_{(4)}^2 = \left\langle \frac{1}{\det(A+A^\dagger-1)} \right\rangle_U - \left\langle \frac{1}{\det(\frac{1}{2}(A+A^\dagger))} \right\rangle_U^2 \quad (\text{B.11})$$

By writing the matrix  $A = 1 + \epsilon H + \epsilon^2 G + \mathcal{O}(\epsilon^3)$  and using the expansion shown in section B.3 it follows

$$\sigma_{(1)}^2 = \epsilon^2 \left[ \left\langle \text{Tr}(HH^\dagger) \right\rangle_U + \text{cov} \left( \text{Tr}(H), \text{Tr}(H^\dagger) \right) \right] + \mathcal{O}(\epsilon^3) \quad (\text{B.12})$$

$$\sigma_{(2)}^2 = \epsilon^2 \left[ \left\langle \text{Tr}(H^2) \right\rangle_U + \text{var} \left( \text{Tr}(H) \right) \right] + \mathcal{O}(\epsilon^3) \quad (\text{B.13})$$

$$\sigma_{(3)}^2 = \epsilon^2 \left[ \left\langle \text{Tr}(H^{\dagger 2}) \right\rangle_U + \text{var} \left( \text{Tr}(H^\dagger) \right) \right] + \mathcal{O}(\epsilon^3) \quad (\text{B.14})$$

and

$$\sigma_{(4)}^2 = \epsilon^2 \left[ \left\langle \text{Tr}(HH^\dagger) \right\rangle_U + \text{cov} \left( \text{Tr}(H), \text{Tr}(H^\dagger) \right) \right] + \mathcal{O}(\epsilon^3) \quad (\text{B.15})$$

with  $\text{var}(X) = \langle X^2 \rangle_U - \langle X \rangle_U^2$  the ensemble variance of the quantity  $X$ . Note that the terms  $\sigma_{(1)}^2$  and  $\sigma_{(4)}^2$  are the same up to the second order in  $\epsilon$ .

The ensemble average is performed by a summation over the gauge configurations and the pseudofermion fields. By separating these averages also the stochastic and the ensemble fluctuations are separated. Here this will be discussed for the term  $\sigma_{(1)}^2$ . The stochastic fluctuations on one configuration is obtained by only averaging over the pseudofermion fields and are given by

$$\sigma_{st}^2(N_\eta = 1) = \epsilon^2 \text{Tr}(HH^\dagger) + \mathcal{O}(\epsilon^3) \quad (\text{B.16})$$

for  $N_\eta = 1$ . For the stochastic error on one configuration follows  $\delta = \sqrt{\sigma^2(1)_{st}/N_\eta}$  (see sec. 3.3 for a deviation of the fluctuations with finite  $N_\eta$ ). The ensemble fluctuations are obtained by only averaging over the gauge configurations by using the exact determinant ratios and they are given by

$$\sigma_{ens}^2 = \epsilon^2 \text{cov} \left( \text{Tr}(H), \text{Tr}(H^\dagger) \right) + \mathcal{O}(\epsilon^3). \quad (\text{B.17})$$

The approximated fluctuations are given by traces of the matrix  $H$  which are known for some applications, e.g. in the case of the stochastic fluctuations of the mass reweighting in chiral perturbation theory (see e.g. [140], [116]). However the  $\epsilon^2$ -order terms only dominate the fluctuations if  $\epsilon$  is a proper expansion parameter. In general this can be achieved by using interpolation techniques.

### B.3. Expansion

If a matrix can be written as a matrix polynomial in terms of an expansion parameter  $\epsilon$  the inverse determinant function is given by

$$f(\epsilon) = \left\langle \frac{1}{\det[1 + \epsilon X + \epsilon^2 Y + \mathcal{O}(\epsilon^3)]} \right\rangle. \quad (\text{B.18})$$

By using  $\det A = \exp\{\text{Tr} \ln A\}$  and expanding  $\ln(1 + \epsilon X + \epsilon^2 Y + \mathcal{O}(\epsilon^3)) = \epsilon X + \epsilon^2(Y + X^2/2) + \mathcal{O}(\epsilon^3)$  it follows

$$f(\epsilon) = \left\langle \exp \left\{ \text{Tr} \left( -\epsilon X - \frac{\epsilon^2}{2} (2Y - X^2) + \mathcal{O}(\epsilon^3) \right) \right\} \right\rangle \quad (\text{B.19})$$

Expanding the exponential function it follows

$$\begin{aligned}
 f(\epsilon) &= 1 - \epsilon \langle \text{Tr}(X) \rangle \\
 &\quad + \frac{\epsilon^2}{2} \left( -2 \langle \text{Tr}(Y) \rangle + \langle \text{Tr}(X^2) \rangle + \langle (\text{Tr}(X))^2 \rangle \right) + \mathcal{O}(\epsilon^3).
 \end{aligned}
 \tag{B.20}$$

Eq. (B.20) is used in the expansion of eq. (B.8)–eq. (B.11) leading to eq. (B.12)–eq. (B.12).

#### B.4. Comparing with $n$ th Root

The  $n$ th root method [142] [87] is comparable to the linear interpolation method. The hermitian case which corresponds to two flavor mass-degenerate reweighting with the ratio matrix  $M^\dagger M = D^\dagger(m)D^{\dagger-1}(m')D^{-1}(m')D(m)$  is analyzed. In this work the hermitian case is used in two flavor mass-degenerate reweighting and the PSMS algorithm. The  $n$ th root method shifts the eigenvalues towards one by taking the  $n$ th root

$$\begin{aligned}
 \lambda &= 1 + \epsilon \lambda^{(1)} + \mathcal{O}(\epsilon^2) \quad \longrightarrow \quad (1 + \epsilon \lambda^{(1)} + \mathcal{O}(\epsilon^2))^{\frac{1}{n}} \\
 &= 1 + \frac{\epsilon}{n} \lambda^{(1)} + \mathcal{O} \left( \epsilon^2 \left( -\frac{1}{n} + \frac{1}{n^2} \right) \right)
 \end{aligned}
 \tag{B.21}$$

with  $M^\dagger M = 1 + \epsilon(H^\dagger + H) + \mathcal{O}(\epsilon^2)$ . To calculate the  $n$ th root of a matrix a matrix function has to be used. This increases the cost and by using Chebyshev polynomials the spectrum has to be real and in the range  $[\delta, C]$  with  $C > \delta > 0$  (see e.g. [143–146]). The stochastic fluctuations are given by

$$\begin{aligned}
 \sigma_{st}^2(n, N_\eta) &= \prod_{i=1}^n \frac{1}{N_\eta} \left( \frac{1}{\det[2(M^\dagger M)^{1/n} - 1]} + \frac{N_\eta - 1}{\det(M^\dagger M)^{2/n}} \right) \\
 &\quad - \frac{1}{\det(M^\dagger M)^2}.
 \end{aligned}
 \tag{B.22}$$

with  $n$  roots and  $N_\eta$  estimation for each ratio. The term can be rewritten by

$$\sigma_{st}^2(n, N_\eta) = \frac{1}{\det(M^\dagger M)^2} \left( \prod_{i=1}^n \frac{1}{N_\eta} \left( \frac{\det(M^\dagger M)^{2/n}}{\det[2(M^\dagger M)^{1/n} - 1]} + N_\eta - 1 \right) - 1 \right)
 \tag{B.23}$$

and by using the eigenvalues expansion eq. (B.21) it follows

$$\begin{aligned} \sigma_{st}^2(n, N_\eta) &= \frac{1}{\det(M^\dagger M)^2} \left( \prod_{i=1}^n \frac{1}{N_\eta} \left( \prod_{j=1}^{\dim(M)} \left( 1 + \frac{1}{n^2} \epsilon^2 \lambda_j^{(1)^2} \right) + N_\eta - 1 \right) - 1 \right) \\ &+ \mathcal{O}(\epsilon^3). \end{aligned} \quad (\text{B.24})$$

By neglecting all higher terms with  $\epsilon^3/n^2$  it follows

$$\sigma_{st}^2(n, N_\eta) = \frac{1}{nN_\eta} \frac{\sum_{j=1}^{\dim(M)} \epsilon^2 \lambda_j^{(1)^2}}{\det(M^\dagger M)^2} + \mathcal{O}\left(\frac{\epsilon^3}{n^2 N_\eta}\right). \quad (\text{B.25})$$

Note that if the next order term contributes significantly to the fluctuations increasing  $n$  is more efficient than to increase  $N_\eta$ .

The behavior of the  $n$ th root method is comparable to the behavior of the interpolation techniques which are introduced to control the stochastic fluctuations (see e.g. sec. 3.4, subsec. 5.3.1 and subsec. 6.2.1). The difference is that during the interpolation the matrices of the corresponding ratios change and thus the eigenvalues. In general the eigenvalues behave quite similar if interpolation techniques are used. The  $i$ th ratio matrix is given by

$$M_i^\dagger M_i = 1 + \frac{1}{N} (\epsilon^\dagger H_i^\dagger + H_i \epsilon) + \mathcal{O}\left(\frac{1}{N^2}\right). \quad (\text{B.26})$$

Now, it is possible by using  $1/N$  as an expansion parameter to derive a similar behavior to eq. (B.21) for the eigenvalues by

$$\lambda_j^{(i)} = 1 + \frac{\lambda_j^{(1,i)}}{N} + \mathcal{O}\left(\frac{1}{N^2}\right) \quad (\text{B.27})$$

with the definition  $(\epsilon^\dagger H_i^\dagger + H_i \epsilon) \psi_j^{(0)} = \lambda_j^{(1,i)} \psi_j^{(0)}$ . By using interpolation techniques it is not obvious how the eigenvalues behave during the interpolation, e.g. in the case of gauge field interpolation relative gauge fixing has to be used so that the spectra of the ratio matrices are similar to each other. Note only if the matrices are non singular during the interpolation, increasing  $N$  improves the stochastic estimation. To conclude interpolation techniques can be understood as approximations to the  $n$ th root methods.



## C. Recursive Domain Decomposition

In this appendix a description will be given how to implement recursive DD in the DD-HMC package [96].

In many applications it is necessary to decompose the blocks further for blocks with a block length of  $l > 6$ , e.g. to calculate the determinant more efficiently. In a recursive DD scheme the remaining blocks are again decomposed into smaller blocks and into Schur complements which couple the boundaries of the new small blocks but not between each other. The new Schur complement has Dirichlet boundaries due to the fact that it remains from the decomposition of the larger block. The mathematical equation for the Dirichlet Schur complement is similar to the Schur complement with periodic boundaries and is given by

$$\hat{S} = 1 - P_{wb} \cdot D_{bb}^{-1} D_{bw} D_{ww}^{-1} D_{wb} P_{wb} \quad (\text{C.1})$$

and the inverse

$$\hat{S}^{-1} = 1 - P_{wb} \cdot (\hat{D}^{-1})_{bw} D_{wb} P_{wb} \quad (\text{C.2})$$

with the larger block  $\hat{D}$  with block length  $l$ , the smaller blocks  $D_{ww}, D_{bb}$  with block-length  $l' \leq l$  and the boundary operators  $D_{wb}$  and  $D_{bw}$ . The boundary operators project to zero at the boundaries of  $\hat{D}$ . This modifies also the projector  $P_{wb}$ .

In the following technical part it will be shown how to implement recursive DD in the DD-HMC package. The following objects have to be implemented or improved:

1. Definition of two different block architectures based on *HMC-Blocks*.
2. Definition of a new Projector  $P$ : the projector  $1 - P$  has to project also to the boundaries of the larger blocks.
3. The block interaction terms  $D_{bw}$  and  $D_{wb}$  do not map from a larger block to another larger block.

To realize point 1. two block structures are defined by using the *HMC-Blocks*. In details these are *PSD\_LBLKS* for the larger blocks and *PSD\_SBLKS* for the smaller blocks. Additionally corresponding block field structures are defined, *psdflds\_blk* for the larger and *psdflds\_sblk* for the smaller blocks respectively. The requirement of the DD-HMC package for the larger block size is, that at least two blocks have to fit into the local lattice. To implement point 2. and point 3. some indices of the smaller blocks have to be modified. This can be done in the case of the projector (2.) by modifying the index *ifc* of the structure field *psdflds\_sblk*. If a boundary point matches with one of the larger blocks, the index *ifc* is set to the value 9. Now for *ifc* = 9 the point corresponds to a boundary point and is projected to

zero. In the case of the block interaction terms (3.) the index  $ifc$  in the structure  $psdflds\_sblk$  can be modified. If a boundary point matches with one of the larger blocks, the index is set to the value 8. Now the corresponding gauge links are set to zero if the gauge field is copied to the smaller blocks. This is sufficient to define recursive Domain Decomposition in the DD-HMC package.

## D. Error

In this appendix the origins of the error of observables which are evaluated on finite ensembles generated by Monte Carlo integration are discussed. The first part describes the general framework based on [78]. The last part is based on an internal note [147] and illustrates the error of a primary observable by using mass reweighting

### D.1. Error and Bias

Monte Carlo simulations are based on a Markov chain, the proposed new configuration is based on the previous one. The new configuration is correlated with the old one. This increases the absolute error and decreases the ensemble size. Moreover the ensemble size is finite and observable  $\bar{F}$  given by

$$\bar{F} = f(A_\alpha) \quad (\text{D.1})$$

with a function  $f$  which depends on the primary observables  $a_\alpha$ . The primary observable is given by the summation over every configuration in the ensemble

$$A_\alpha = \frac{1}{N} \sum_{i=1}^{N_{\text{cnfg}}} a_\alpha^i \quad (\text{D.2})$$

with  $a_\alpha^i$  depends on  $U_i$  the  $i$ th configuration of the ensemble. The error is defined by

$$\delta_\alpha^i = a_\alpha^i - A_\alpha \quad (\text{D.3})$$

with the ensemble average  $A_\alpha$ . For enough statistic follows  $\langle \delta_\alpha \rangle = 0$ . The covariance matrix is defined by

$$\langle \delta_\alpha \delta_\beta \rangle = \frac{1}{N} C_{\alpha,\beta} + \mathcal{O}\left(\frac{1}{N^2}\right) \quad (\text{D.4})$$

with

$$C_{\alpha,\beta} = \sum_{t=-\infty}^{\infty} \Gamma_{\alpha,\beta}(t) \quad (\text{D.5})$$

the autocorrelation function is given by

$$\Gamma_{\alpha,\beta}(i-j) = \langle \delta_\alpha^i \delta_\beta^j \rangle - \langle \delta_\alpha^i \rangle \langle \delta_\beta^j \rangle \quad (\text{D.6})$$

with  $i - j$  the distance between the measurements of  $a_\alpha$  and  $a_\beta$  in the time of the Markov chain. Note from now on the index  $i$  of  $a^i$  is dropped. Now, the estimator  $\bar{F}$  can be expanded by a Taylor expansion of the function  $f$  in the fluctuations. It follows

$$\bar{F} = F + \sum_{\alpha} f_{\alpha} \delta_{\alpha} + \frac{1}{2} \sum_{\alpha, \beta} f_{\alpha\beta} \delta_{\alpha} \delta_{\beta} + \dots \quad (\text{D.7})$$

with the exact value  $F$  and the derivatives

$$f_{\alpha} = \frac{\partial f}{\partial A_{\alpha}} \quad \text{and} \quad f_{\alpha\beta} = \frac{\partial^2 f}{\partial A_{\alpha} \partial A_{\beta}}. \quad (\text{D.8})$$

If the second derivatives of  $\bar{F}$  do not vanish the estimator is biased and the total shift is given by

$$\langle \bar{F} - F \rangle = \frac{1}{2N} \sum_{\alpha, \beta} f_{\alpha\beta} C_{\alpha, \beta} + \dots \quad (\text{D.9})$$

For the error  $\delta_F$  follows

$$\delta_F^2 = \langle (\bar{F} - F)^2 \rangle = \frac{1}{N} \sum_{\alpha, \beta} f_{\alpha} f_{\beta} C_{\alpha, \beta} + \dots \quad (\text{D.10})$$

In general this expression is rewritten by

$$\delta_F^2 = \frac{2\tau_{int, F}}{N} \sigma_F^2 \quad (\text{D.11})$$

with the correlation function  $\sigma_F^2 = \sum_{\alpha, \beta} f_{\alpha} f_{\beta} \Gamma_{\alpha, \beta}(0)$  for time  $t = 0$  and the integrated autocorrelation time

$$\tau_{int, F} = \frac{1}{2\sigma_F^2(0)} \sum_{t=-\infty}^{\infty} \sum_{\alpha, \beta} f_{\alpha} f_{\beta} \Gamma_{\alpha, \beta}(t). \quad (\text{D.12})$$

For no correlation between the different ensembles the autocorrelation time is given by  $2\tau_{int} = 1$ . In general  $\Gamma_{\alpha, \beta}(t)$  is a complicated function and  $\tau_{int}$  is generally difficult to extract if the ensemble size is not large enough. For the case that it decays exponentially like  $\exp\{-t/\tau\}$  it follows  $\tau_{int} = \tau + \mathcal{O}(1/\tau)$  and the effective ensemble size decreases with  $N/(2\tau)$ . Note the evaluation of the error and the suppression of the bias can only be done based on the finite data sample and for a sufficient evaluation the sample size has to be large enough. Throughout this thesis the public program *UWerr.m* [148] [78] is used to propagate the statistical error and to estimate  $\tau_{int}$ . Moreover in LQCD for decreasing lattice spacing the autocorrelation times of slow modes increases and  $\tau_{int}$  can be underestimated. A

more conservative strategy is to take these expected slow autocorrelation times into account by introducing a  $\tau_{exp}$  (see [27], [98]). In this work  $\tau_{exp}$  is only used for a comparison of results.

## D.2. Error and Bias in the Case of Reweighting

In this part of the appendix the error and the bias which is introduced by reweighting is discussed. The primary observable  $\mathcal{O}$  at the parameter set  $b$  on an ensemble generated at the parameter set  $a$  is given by

$$\langle \mathcal{O} \rangle_W = \frac{\langle \mathcal{O}W \rangle}{\langle W \rangle} \quad (\text{D.13})$$

with  $W$  the reweighting factor which corrects the weight from set  $a$  to set  $b$ . Equation eq. (D.13) can be rewritten to

$$\langle \mathcal{O} \rangle_W = A_0 + \frac{A_{02}}{A_2} \quad (\text{D.14})$$

by using  $A_0 = \langle \mathcal{O} \rangle$ ,  $A_2 = \langle W \rangle$  and the covariance  $A_{02} = \text{cov}(\mathcal{O}, W)$  as a new primary observable and dropping the index  $i$  for the explicit dependence on the configuration  $i$ .

Now an estimator can be assumed for the observable  $F$  given by

$$\bar{F} = f(a_0, a_2, a_{02}). \quad (\text{D.15})$$

and  $a_{02} = \delta_0 \delta_2$ . Using eq. (D.14) the derivatives are given by

$$f_0 = 1, \quad f_2 = \frac{-A_{02}}{A_2^2}, \quad f_{02} = \frac{1}{A_2}, \quad (\text{D.16})$$

$$f_{0,\beta} = f_{02,02} = 0, \quad f_{02,2} = \frac{-1}{A_2^2} \quad \text{and} \quad f_{2,2} = \frac{2A_{02}}{A_2^3}. \quad (\text{D.17})$$

The second derivatives do not vanish and the estimator is biased

$$\langle \bar{F} - F \rangle \simeq -\frac{1}{A^2} C_{02,2} + \frac{A_{02}}{A_2^3} C_{2,2} \quad (\text{D.18})$$

The error  $\delta_F$  is given by

$$\delta_F^2 \simeq \frac{1}{N} \left( C_{0,0} + \frac{2}{A_2} C_{0,02} - \frac{2A_{02}}{A_2^2} C_{0,2} + \frac{1}{A_2^2} C_{02,02} - \frac{2A_{02}}{A_2^3} C_{02,2} + \frac{A_{02}^2}{A_2^4} C_{2,2} \right). \quad (\text{D.19})$$

### D.3. Expansion

Most of the terms of the error eq. (D.19) depend on the covariance of the observable with the reweighting factor. The idea is to expand the reweighting factor in  $\epsilon$  with

$$a_2 = 1 + \epsilon a_3 + \epsilon^2 a_4 + \mathcal{O}(\epsilon^3) \quad (\text{D.20})$$

and

$$A_2 = 1 + \epsilon A_3 + \epsilon^2 A_4 + \mathcal{O}(\epsilon^3). \quad (\text{D.21})$$

For the primary observable  $A_{02}$  follows

$$A_{02} = \epsilon \text{cov}(O, A_3) + \epsilon^2 \text{cov}(O, A_4) + \mathcal{O}(\epsilon^3) = \epsilon A_{03} + \epsilon^2 A_{04} + \mathcal{O}(\epsilon^3) \quad (\text{D.22})$$

and  $a_{02} = \epsilon a_{03} + \epsilon^2 a_{04} + \mathcal{O}(\epsilon^3)$ . Now, the terms of eq. (D.18) and eq. (D.19) can be rewritten by

$$C_{0,02} = \epsilon C_{0,03} + \epsilon^2 C_{0,04} + \mathcal{O}(\epsilon^3), \quad (\text{D.23})$$

$$C_{0,2} = \epsilon C_{0,3} + \epsilon^2 C_{0,4} + \mathcal{O}(\epsilon^3), \quad (\text{D.24})$$

$$C_{02,02} = \epsilon^2 C_{03,03} + \mathcal{O}(\epsilon^3), \quad (\text{D.25})$$

$$C_{02,2} = \epsilon^2 C_{03,3} + \mathcal{O}(\epsilon^3) \quad \text{and} \quad (\text{D.26})$$

$$C_{2,2} = \epsilon^2 C_{3,3} + \mathcal{O}(\epsilon^3). \quad (\text{D.27})$$

The bias is given by

$$\langle \bar{F} - F \rangle \simeq -\epsilon^2 C_{03,3} + \mathcal{O}(\epsilon^3) \quad (\text{D.28})$$

and similar the error

$$\delta_F^2 \simeq \frac{1}{N} \left( C_{0,0} + 2\epsilon C_{0,03} + \epsilon^2 [C_{03,03} + 2C_{0,04} - 2A_3 C_{0,03} - 2A_{03} C_{0,3}] + \mathcal{O}(\epsilon^3) \right). \quad (\text{D.29})$$

For the numerical analysis of the error the expansion in  $\epsilon$  is not feasible. However the analysis shows that the order up to  $\epsilon^2$  dominates the error and the bias. The

bias eq. (D.18) can be approximated by

$$\langle \bar{F} - F \rangle \sim -\frac{1}{A^2} C_{02,2} \quad (D.30)$$

and similar for the error

$$\delta_F^2 \sim \frac{1}{N} \left( C_{0,0} + \frac{2}{A_2} C_{0,02} + \frac{1}{A_2^2} C_{02,02} - \frac{2A_{02}}{A_2^2} C_{0,2} \right) \quad (D.31)$$

Note this includes also autocorrelation terms between these observables. In the case of mass reweighting the numerical analysis of the error terms shows that the term  $-2A_{02}C_{0,2}/A_2^2$  is small compared to the other terms for gluonic and fermionic observables. Note a possible reason is that the correlation of  $A_0$  with  $A_{02}$  is larger due to the fact that  $A_{02}$  depends on  $a_0$ . By neglecting the term  $-2A_{02}C_{0,2}/A_2^2$  the error can be cast into the form

$$\delta_F^2 \sim \frac{1}{N^2 A_2^2} \sum_{i,j} \left[ (a_0^i - A_0) a_2^i (a_0^j - A_0) a_2^j \right]. \quad (D.32)$$

Note that the error is proportional to  $\sqrt{1/N}$ . Moreover eq. (D.32) is exact if and only if the denominator of eq. (D.13) and so  $A_2$  do not fluctuate. The analysis shows that the term eq. (D.32) can describe the error also for larger mass shifts, in the case of the D5 ensemble up to  $\Delta m_q \sim 12$  MeV, very well for primary fermionic observables, like the correlation functions  $f_{AP}$  or  $f_{PP}$ . Note in this case the autocorrelation is important. In the case of gluonic observables, like  $t_0$  or the plaquette term, the approximated error term eq. (D.32) overestimate the error for larger mass steps. However the autocorrelation is less important.

## E. Detailed Balance

In this appendix the condition detailed balance eq. (2.50)

$$P_a(U)T(U \rightarrow U') = P_a(U')T(U' \rightarrow U) \quad \forall U, U'. \quad (\text{E.1})$$

with respect to the PSMS algorithm is discussed and shown. If the transition probability of a Markov chain fulfills detailed balance according to the global weight it follows that the algorithm converges towards the equilibrium distribution for large enough Monte Carlo time (see sec. 2.5).

Note in this appendix only the two-level PSMS algorithm is illustrated but it is straightforward to generalize the following arguments to the general case. This appendix follows closely the argumentation of the app. A of [16] as well as the app. A of [89].

### E.1. Accept-reject Steps with exact Weight

The two-level PSMS algorithm consists of a pure gauge proposal of a new configuration followed by an accept-reject step with the fermion weight. The transition probability of the pure gauge proposal is given by  $T_0(U \rightarrow U')$  and it satisfies detailed balance with respect to the pure gauge weight

$$P_0(U) = \frac{\exp\{-S_g(U)\}}{Z_0}, \quad (\text{E.2})$$

where  $Z_0$  is the partition function for the gauge action  $S_g$ . The global weight is corrected by a Metropolis accept-reject step with the probability

$$P_{\text{acc}}(U, U') = \min \left\{ 1, \frac{P_0(U)P(U')}{P(U)P_0(U')} \right\}. \quad (\text{E.3})$$

The transition probability for this algorithm is given by

$$T(U \rightarrow U') = T_0(U \rightarrow U')P_{\text{acc}}(U, U') + \delta(U - U') \left( 1 - \int T_0(U \rightarrow U'')P_{\text{acc}}(U, U'') \mathcal{D}[U''] \right). \quad (\text{E.4})$$

The transition probability satisfies detailed balance for the probability  $P$  if the pure gauge probability  $T_0$  satisfies detailed balance with respect to  $P_0$ .



### Pure Gauge Update

The pure gauge update is a sequence of link updates. By using hierarchical acceptance steps the updates have to be symmetrized or randomized in order to satisfy detailed balance [30]. Here the symmetrized iteration is used. This means a symmetrized ordering of the chosen  $SU(2)$ -subgroups in the heat bath and overrelaxation steps and symmetrized combination of heat bath [126] and overrelaxation steps [127] [128] are chosen. The symmetrized iteration is given by forward steps by updating all active links by using a constant ordering of the  $SU(2)$ -subgroups. This is directly followed by reflected backward steps which use the reverse ordering of the  $SU(2)$ -subgroups. Also the combination of the heat bath and overrelaxation steps are symmetrized by choosing first  $l/2$  overrelaxation steps, second one heat bath step which is again followed by  $l/2$  overrelaxation steps with  $l$  the block length of the sub-domains. To summarize, all iterations in the pure gauge update are symmetrized which fulfills the condition detailed balance.

### E.2. Accept–reject Steps with partial stochastic Weight

By introducing stochastic estimation the system is enlarged by auxiliary stochastic variables. The so called pseudofermion field appears only in the stochastic accept–reject step. By introducing the pseudofermion field  $\eta$  the enlarged equilibrium probability distribution is given by

$$\hat{P}(\eta, U) = \frac{e^{-|D(U)^{-1}\eta|^2} \exp(-S_g(U))}{Z} \quad (\text{E.5})$$

with the scalar product

$$|\eta|^2 = (\eta, \eta) = \sum_{x,\alpha} \eta_{x,\alpha}^* \eta_{x,\alpha} \quad (\text{E.6})$$

of the complex valued field  $\eta$  while the index  $\alpha$  contains the spin and color degrees of freedom. The “exact” equilibrium probability distribution is obtained by

$$P(U) = \int \hat{P}(\eta, U) D[\eta] \quad (\text{E.7})$$

with the measure

$$D[\eta] = \prod_{x,\alpha} \frac{d\text{Re}(\eta_{x,\alpha}) d\text{Im}(\eta_{x,\alpha})}{\pi}. \quad (\text{E.8})$$

The pseudofermion field  $\eta$  is generated due to the conditional probability given by

$$\hat{P}(\eta|U) = \frac{\hat{P}(\eta, U)}{P(U)} = \frac{e^{-|D(U)^{-1}\eta|^2}}{|\det D(U)|^2}. \quad (\text{E.9})$$

The enlarged system consists of two Markov steps. The first step is a global heat bath step which updates the pseudofermion field  $\eta$  according to  $\hat{P}(\eta|U)$  by

$$\eta = D(U)\xi. \quad (\text{E.10})$$

The field  $\xi$  is a complex-valued random field distributed with the Gaussian probability  $p(\xi) = \pi^{-12V} \exp(-|\xi|^2)$ . The second step is the stochastic accept-reject step for the proposed gauge field with updated pseudofermion field. Now the partial stochastic two-step algorithm consists of a proposal of a new gauge configuration done with the pure gauge transition probability  $T_0$  followed by the stochastic accept-reject step with the probability

$$\min \left\{ 1, \frac{P_0(U)\hat{P}(\eta, U')}{\hat{P}(\eta, U)P_0(U')} \right\} = \min \left\{ 1, \frac{e^{-|D(U')\eta|^2}}{e^{-|D(U)\eta|^2}} \right\}. \quad (\text{E.11})$$

Because the heat bath- and the Metropolis accept-reject step fulfill detailed balance according to the distribution  $\hat{P}(\eta, U)$  of eq. (E.5) the composition of both steps fulfills also detailed balance (see [149], [30]).

With this approach the pseudofermion field is used as an additional variable for the updating process, as it is done in the HMC (see discussion in subsec. 3.1). However another point of view can be assumed by considering that only the second step is a correction of the weight by neglecting the first step. Then the acceptance probability is given by

$$\begin{aligned} P_{\text{acc}}(U, U') &= \int \hat{P}(\eta|U) \min \left\{ 1, \frac{P_0(U)\hat{P}(\eta, U')}{\hat{P}(\eta, U)P_0(U')} \right\} \mathcal{D}[\eta] \\ &= \int e^{-|\xi|^2} \min \left\{ 1, e^{-|M\xi|^2+|\xi|^2} \right\} \mathcal{D}[\xi] \end{aligned} \quad (\text{E.12})$$

with the ratio matrix  $M$ . For the associated transition probability follows detailed balance according to the equilibrium probability because of the property [17]

$$\frac{P_{\text{acc}}(U, U')}{P_{\text{acc}}(U', U)} = |\det(M)|^{-2}. \quad (\text{E.13})$$

Note eq. (E.13) is only satisfied if only one pseudofermion field  $\eta$  is drawn per accept reject step.

### E.3. Accept–reject Steps with Gauge field Interpolation

Gauge field interpolation split up the ratio in several parts sec. 6.2.1. The idea is that the product of the estimate of each ratio can be used as the weight in the Metropolis accept–reject step. From the analysis in subsec. 6.2.4 follows that the stochastic fluctuations can be suppressed for a large enough amount of interpolation steps  $N$ . For an unbiased estimate for each ratio operator a new pseudofermion field  $\eta_i$  has to be introduced with  $i = 0, 1, \dots, N - 1$ . The equilibrium probability distribution is then given by

$$\hat{P}(\{\eta_j\}, U, U') = \frac{e^{-|D(U^g)^{-1}\eta_0|^2} e^{-S_g(U)}}{Z} \prod_{i=1}^{N-1} \frac{e^{-|D(U_i)^{-1}\eta_i|^2}}{|\det(D(U_i))|^2} \quad (\text{E.14})$$

which depends also on the proposed configuration  $U'$  due to the gauge field interpolation. By integrating over the pseudofermion fields the target probability distribution is recovered

$$P(U) = \int \prod_{i=0}^{N-1} \hat{P}(\{\eta_j\}, U, U') D[\eta_i]. \quad (\text{E.15})$$

The conditional probability is given by

$$\hat{P}(\{\eta_j\}|U, U') = \frac{\hat{P}(\{\eta_j\}, U, U')}{P(U)} = \prod_{i=0}^{N-1} \frac{e^{-|D(U_i)^{-1}\eta_i|^2}}{|\det(D(U_i))|^2}. \quad (\text{E.16})$$

In order to show detailed balance the reverse transition  $U' \rightarrow U$  is considered. In general for the reverse transition is assumed that the trajectory of the intermediate configuration is the same as the reverse forward direction. Now the pseudofermion field is associated with the transition  $U_{i+1} \rightarrow U_i$ . The probability distribution for the reverse transition is given by

$$\hat{P}(\{\eta_j\}, U', U) = \frac{e^{-|D(U'^g)^{-1}\eta_{N-1}|^2} e^{-S_g(U')}}{Z} \prod_{i=0}^{N-2} \frac{e^{-|D(U_{i+1})^{-1}\eta_i|^2}}{|\det(D(U_{i+1}))|^2} \quad (\text{E.17})$$

and for the conditional probability follows

$$\hat{P}(\{\eta_j\}|U', U) = \frac{\hat{P}(\{\eta_j\}, U', U)}{P(U')} = \prod_{i=0}^{N-1} \frac{e^{-|D(U_{i+1})^{-1}\eta_i|^2}}{|\det(D(U_{i+1}))|^2}. \quad (\text{E.18})$$

The acceptance probability for the proposal  $U \rightarrow U'$  is given by

$$\begin{aligned}
 P_{\text{acc}}(U, U') &= \int \prod_{i=0}^{N-1} \hat{P}(\{\eta_j\} | U, U') \min \left\{ 1, \frac{P_0(U) \hat{P}(\{\eta_j\}, U', U)}{\hat{P}(\{\eta_j\}, U, U') P_0(U')} \right\} D[\eta_i] \\
 &= \int \prod_{i=0}^{N-1} e^{-|\xi_i|^2} \min \left\{ 1, e^{\sum_{j=0}^{N-1} -|M_j \xi_j|^2 + |\xi_j|^2} \right\} D[\xi_i], \quad (\text{E.19})
 \end{aligned}$$

with the ratio matrix  $M_i = D(U_{i+1})^{-1} D(U_i)$ . It follows that  $P_{\text{acc}}(U, U')$  fulfills detailed balance because the condition

$$\frac{P_{\text{acc}}(U, U')}{P_{\text{acc}}(U', U)} = |\det(M)|^{-2}, \quad M = D(U')^{-1} D(U). \quad (\text{E.20})$$

is satisfied. Also here eq. (E.20) is only satisfied if only one pseudofermion field for each ratio is drawn.

#### E.4. Remarks

In this appendix is shown that detailed balance is fulfilled for the two-step algorithm. It is straightforward to show that it is also satisfied for an arbitrary number of steps. In this case detailed balance is always satisfied if the order and the iteration of the accept-reject steps respectively the pure-gauge updating steps do not depend on the gauge field and are constant during the Markov process.

Table F.1.: The table shows the data of the measurements of the plain Wilson ensembles Z0, Z1 and Z2. The observables are the pseudoscalar mass, the PCAC mass and the Wilson flow observables  $t_0$  and  $w_0^2$  in lattice units  $a$

Ensembles	$\kappa$	$aM_{PS}$	$am_{PCAC}$	$t_0/a^2$	$w_0^2/a^2$
Z0	0.15850	0.4962(19)	0.06581(22)	1.773(14)	1.858(31)
Z1	0.15950	0.3770(18)	0.04038(25)	2.090(33)	2.254(48)
Z2	0.16050	0.2644(29)	0.01598(28)	2.495(67)	2.730(83)

## F. Plain Wilson Ensembles at $\beta = 5.5$

In this appendix the parameter tuning for a two flavor mass-degenerate plain Wilson ensemble with a Wilson gauge action with a gauge parameter of  $\beta = 5.5$  will be described. The idea is to sample a third ensemble for the analysis of the PSMS algorithm in addition to the finer plain Wilson ensembles A3 with  $\beta = 5.6$  and B4 with  $\beta = 5.8$  [8,132] (see also tab. 6.2). The critical mass parameter and the lattice spacing will be determined by an extrapolation towards the chiral limit.

These are done by generating three ensembles of lattice size  $32 \times 16^3$  with different mass parameters (see tab. F.1). To determine the pseudoscalar mass and the  $m_{PCAC}$  mass the two point functions  $f_{PP}$  and  $f_{AP}$  are evaluated and the derived masses are shown in tab. F.1. Note the improvement parameter  $c_A = 0$  is set to zero. Furthermore the Wilson flow is used to determine  $t_0/a^2$ . Note the value of a similar Wilson flow observable  $w_0^2/a^2$  is also shown [150].

The critical mass parameter is determined by multiplying the PCAC mass with  $\sqrt{t_0}/a$ . The critical hopping mass parameter is given by  $\kappa_{crit} = 0.16134(35)$ . The lattice spacing is determined by extrapolating  $t_0$  towards the chiral limit with  $t_0^{chiral}/a^2 = 2.949(13)$ . By using the chiral value for  $t_0$  of [118] the lattice spacing is given by  $a = 0.0901(7)$ . Note if Z0 is neglected from the extrapolation the lattice spacing is given by  $a = 0.0883(8)$ . This shows that the determination has a large systematic error  $\delta_{sys}a \sim 0.12$  which has to be improved for a more precise analysis.

The analysis in the PSMS algorithm is done by sampling the Z4 ensemble by using a hopping mass parameter of  $\kappa = 0.160927$ . The pion mass of Z4 is given by  $M_\pi = 360$  MeV by extrapolating the square of the pion masses of Z0, Z1 and Z2 towards  $\kappa = 0.160927$ . Note this changes to  $M_\pi = 430$  MeV if only Z1 and Z2 are used for the extrapolation. To conclude the fixing of the hopping parameter for the Z4 ensemble is a rough estimate and has a large systematic error with  $\delta_{sys}M_\pi \sim 70$  MeV. Note additional finite volume effects in the pseudoscalar mass are not subtracted.

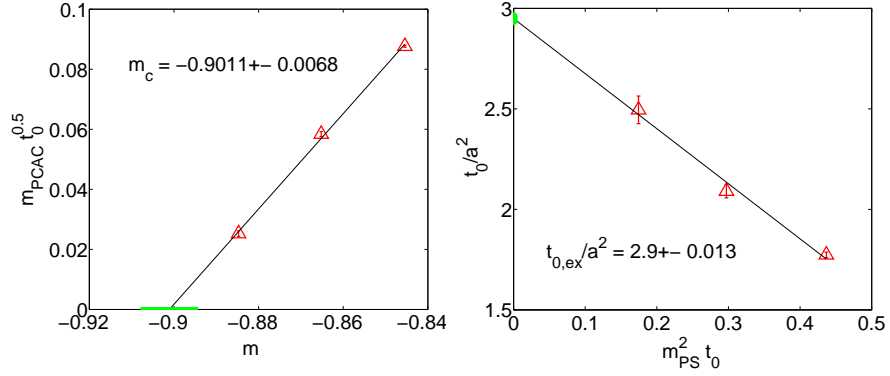


Figure F.1.: The figure shows the chiral extrapolation of the observables  $m_{PCAC}$  and  $t_0$  of the Z ensembles.

Table F.2.: The table shows the parameter-set of the 5-step PSMS algorithm which is used to simulate the Z4 ensemble.

$i$	$n_i$	actions			$P_{acc}$
		$S^{(0)} = S_w$	$S^{(1)} = S_w^{HYP}$	$S^{(2)} = S_b$	
0	75	$\beta_0^{(0)} = 5.7134$	-	-	-
1	4	$\beta_1^{(0)} = -0.0952$	$\beta_1^{(1)} = 0.238$	-	48%
2	4	$\beta_2^{(0)} = -0.0800$	$\beta_2^{(1)} = 0.009$	$\beta_2^{(2)} = 0.983$	68%
3	4	$\beta_3^{(0)} = -0.0382$	$\beta_3^{(1)} = -0.247$	$\beta_3^{(2)} = 0.017$	28%
4	1	$\beta_4^{(0)} = 0.0000$	$\beta_4^{(1)} = 0.000$	$\beta_4^{(2)} = -0.000$	29%

The parameter of the PSMS algorithm which is used to simulate the Z4 ensemble is listed in tab. F.2. In general a 5-step algorithm is chosen with  $6^4$  links inside  $8^4$  blocks. For the gauge field interpolation of the global acceptance step it is found that the trajectory is stable for  $N \geq 96$  interpolation steps. For larger step sizes with  $N = 48$  it happens once that the estimate is given by  $\sim 10^{-15}$ . This could be a sign of a poorly conditioned ratio matrix. However large discretization errors appear also in the DD-HMC in  $\delta H$  by simulating the Z4 ensemble. To conclude the PSMS algorithm is able to sample the Z4 ensemble.

# Bibliography

- [1] K.G. Wilson, Phys. Rev. D10 (1974) 2445.
- [2] H. Fritzsch, M. Gell-Mann and H. Leutwyler, Phys.Lett. B47 (1973) 365.
- [3] K.G. Wilson, New Phenomena In Subnuclear Physics. Part A. Proceedings of the First Half of the 1975 International School of Subnuclear Physics, Erice, Sicily, July 11 - August 1, 1975, ed. A. Zichichi, Plenum Press, New York, 1977, p. 69, CLNS-321.
- [4] D. Weingarten and D. Petcher, Phys.Lett. B99 (1981) 333.
- [5] F. Fucito, E. Marinari, G. Parisi and C. Rebbi, Nucl.Phys. B180 (1981) 369.
- [6] A. Hasenfratz and A. Alexandru, Nucl.Phys.Proc.Suppl. 119 (2003) 994, hep-lat/0209071.
- [7] H.A. Schwarz, Springer Verlag, Berlin vol. 2 (1890).
- [8] L. Del Debbio, L. Giusti, M. Lüscher, R. Petronzio and N. Tantalo, JHEP 0702 (2007) 082, hep-lat/0701009.
- [9] M. Lüscher, JHEP 1008 (2010) 071, 1006.4518.
- [10] J. Finkenrath, F. Knechtli and B. Leder, Nucl.Phys. B877 (2013) 441, 1306.3962, Corrigendum Nuclear Physics, Section B (2014), pp. 574-575.
- [11] A. Ferrenberg and R. Swendsen, Phys.Rev.Lett. 61 (1988) 2635.
- [12] A. Hasenfratz, R. Hoffmann and S. Schaefer, Phys.Rev. D78 (2008) 014515, 0805.2369.
- [13] PACS-CS Collaboration, S. Aoki et al., Phys.Rev. D81 (2010) 074503, 0911.2561.
- [14] RBC Collaboration, UKQCD Collaboration, Y. Aoki et al., Phys.Rev. D83 (2011) 074508, 1011.0892.
- [15] S. Aoki et al., Phys.Rev. D86 (2012) 034507, 1205.2961.

## Bibliography

---

- [16] J. Finkenrath, F. Knechtli and B. Leder, *Comput.Phys.Commun.* 184 (2013) 1522, 1204.1306.
- [17] ALPHA Collaboration, F. Knechtli and U. Wolff, *Nucl.Phys. B*663 (2003) 3, hep-lat/0303001.
- [18] A. Hasenfratz and F. Knechtli, *Comput.Phys.Commun.* 148 (2002) 81, hep-lat/0203010.
- [19] A. Hasenfratz, *Nucl.Phys.Proc.Suppl.* 119 (2003) 131, hep-lat/0211007.
- [20] A. Hasenfratz, P. Hasenfratz and F. Niedermayer, *Phys.Rev. D*72 (2005) 114508, hep-lat/0506024.
- [21] A. Hasenfratz and F. Knechtli, *Phys.Rev. D*64 (2001) 034504, hep-lat/0103029.
- [22] C. Morningstar and M.J. Peardon, *Phys.Rev. D*69 (2004) 054501, hep-lat/0311018.
- [23] A. Hasenfratz, R. Hoffmann and S. Schaefer, *JHEP* 0705 (2007) 029, hep-lat/0702028.
- [24] S. Capitani, S. Dürr and C. Hoelbling, *JHEP* 0611 (2006) 028, hep-lat/0607006.
- [25] S. Dürr et al., *JHEP* 1108 (2011) 148, 1011.2711.
- [26] W. Kamleh, D.B. Leinweber and A.G. Williams, *Phys.Rev. D*70 (2004) 014502, hep-lat/0403019.
- [27] ALPHA Collaboration, S. Schaefer, R. Sommer and F. Virota, *Nucl.Phys. B*845 (2011) 93, 1009.5228.
- [28] M. Lüscher and S. Schaefer, *JHEP* 1107 (2011) 036, 1105.4749.
- [29] N. Metropolis, A.W. Rosenbluth, M.N. Rosenbluth, A.H. Teller and E. Teller, *J. Chem. Phys.* 21 (1953) 1087.
- [30] M. Hasenbusch, *Phys.Rev. D*59 (1999) 054505, hep-lat/9807031.
- [31] M. Lüscher, *Comput.Phys.Commun.* 165 (2005) 199, hep-lat/0409106.
- [32] M. Lüscher and S. Schaefer, *Comput.Phys.Commun.* 184 (2013) 519, 1206.2809.
- [33] T.A. DeGrand, A. Hasenfratz and T.G. Kovacs, *Nucl.Phys. B*547 (1999) 259, hep-lat/9810061.



- [34] M. Gell-Mann, *Phys.Lett.* 8 (1964) 214.
- [35] G. Zweig, CERN Report 8419/TH.412 (1964) unpublished.
- [36] Particle Data Group, J. Beringer et al., *Phys. Rev. D* 86 (2012) 010001.
- [37] M.E. Peskin and D.V. Schroeder, *An Introduction to quantum field theory* (Addison-Wesley, Reading, USA, 1995).
- [38] H.D. Politzer, *Phys. Rept.* 14 (1974) 129.
- [39] D.J. Gross and F. Wilczek, *Phys. Rev. Lett.* 30 (1973) 1343.
- [40] M. Creutz, (1984).
- [41] S. Dürr et al., *Science* 322 (2008) 1224, 0906.3599.
- [42] E. Noether, *Nachr. D. König. Gesellsch. D. Wiss. Zu Göttingen Math-phys. Klasse* 1918 (1918) 235.
- [43] J. Bell and R. Jackiw, *Nuovo Cim.* A60 (1969) 47.
- [44] S.L. Adler, *Phys.Rev.* 177 (1969) 2426.
- [45] M. Lüscher, *Phys.Lett.* B428 (1998) 342, hep-lat/9802011.
- [46] C. Gattringer and C.B. Lang, *Lect.Notes Phys.* 788 (2010) 1.
- [47] Y. Nambu and G. Jona-Lasinio, *Phys. Rev.* 122 (1961) 345.
- [48] J. Goldstone, *Nuovo Cim.* 19 (1961) 154.
- [49] J. Goldstone, A. Salam and S. Weinberg, *Phys. Rev.* 127 (1962) 965.
- [50] S. Aoki et al., (2013), 1310.8555.
- [51] S. Borsanyi et al., (2014), 1406.4088.
- [52] R.P. Feynman, *Rev. Mod. Phys.* 20 (1948) 367.
- [53] R.P. Feynman and A.R. Hibbs, *Quantum Mechanics and Path Integrals* (McGraw-Hill Book Company).
- [54] I. Montvay and G. Munster, *Quantum fields on a lattice* (Cambridge Univ. Pr. (Cambridge monographs on mathematical physics), Cambridge, UK, 1994).
- [55] P.T. Matthews and A. Salam, *Nuovo Cim.* 12 (1954) 563.

- [56] C.N. Yang and R.L. Mills, *Phys. Rev.* 96 (1954) 191.
- [57] Y. Iwasaki, (2011), 1111.7054.
- [58] M. Lüscher and P. Weisz, *Commun.Math.Phys.* 97 (1985) 59.
- [59] T. DeGrand and C. DeTar, *LATTICE METHODS FOR QUANTUM CHROMODYNAMICS* (World Scientific Publishing Co. Pte Ltd., Singapore, 2006).
- [60] H.B. Nielsen and M. Ninomiya, *Nucl. Phys.* B185 (1981) 20.
- [61] H. Panagopoulos and Y. Proestos, *Phys.Rev.* D65 (2002) 014511, hep-lat/0108021.
- [62] M. Bochicchio, L. Maiani, G. Martinelli, G.C. Rossi and M. Testa, *Nucl.Phys.* B262 (1985) 331.
- [63] B. Sheikholeslami and R. Wohlert, *Nucl. Phys.* B259 (1985) 572.
- [64] ALPHA collaboration, K. Jansen and R. Sommer, *Nucl.Phys.* B530 (1998) 185, hep-lat/9803017.
- [65] H. Neuberger, *Phys.Lett.* B417 (1998) 141, hep-lat/9707022.
- [66] P.H. Ginsparg and K.G. Wilson, *Phys.Rev.* D25 (1982) 2649.
- [67] S. Schaefer, *PoS LAT2006* (2006) 020, hep-lat/0609063.
- [68] S.R. Sharpe, *Phys.Rev.* D46 (1992) 3146, hep-lat/9205020.
- [69] B. Orth, T. Lippert and K. Schilling, *Phys.Rev.* D72 (2005) 014503, hep-lat/0503016.
- [70] W. Feller, *An Introduction to Probability Theory and Its Applications, Volume 1* (John Wiley & Son, Inc. New York, 1950).
- [71] J. Hammersley and D. Handscomb, *Monte Carlo Methods* (Fletcher & Son Ltd, Norwich, 1964).
- [72] K.L. Chung, *Markov Chains, With Stationary Transition Probabilities* (Springer-Verlag).
- [73] G. Bhanot, *Rept. Prog. Phys.* 51 (1988) 429.
- [74] H. Rothe, *LATTICE GAUGE THEORIES, An Introduction* (World Scientific Publishing Co. Pte. Ltd., 1992).
- [75] J. Finkenrath, *Diploma thesis, Wuppertal University* (2010).

- [76] K. Fabricius and O. Haan, *Phys.Lett.* B143 (1984) 459.
- [77] A. Kennedy and B. Pendleton, *Phys.Lett.* B156 (1985) 393.
- [78] ALPHA collaboration, U. Wolff, *Comput.Phys.Commun.* 156 (2004) 143, hep-lat/0306017.
- [79] S. Duane, A.D. Kennedy, B.J. Pendleton and D. Roweth, *Phys. Lett.* B195 (1987) 216.
- [80] S.A. Gottlieb, W. Liu, D. Toussaint, R.L. Renken and R.L. Sugar, *Phys. Rev.* D35 (1987) 2531.
- [81] M. Lüscher, (2010) 331, 1002.4232.
- [82] D.J. Callaway and A. Rahman, *Phys.Rev.Lett.* 49 (1982) 613.
- [83] A. Kennedy, P. Silva and M. Clark, *Phys.Rev.* D87 (2013) 034511, 1210.6600.
- [84] M. Lüscher, *JHEP* 0707 (2007) 081, 0706.2298.
- [85] S. Schaefer, R. Sommer and F. Viotto, (2009), 0910.1465.
- [86] M. Hasenbusch, *Phys.Lett.* B519 (2001) 177, hep-lat/0107019.
- [87] A. Alexandru and A. Hasenfratz, *Phys.Rev.* D66 (2002) 094502, hep-lat/0207014.
- [88] B.F. Smith, P.E. Bjørstad and W.D. Gropp, *Domain Decomposition: Parallel Multilevel Methods for Elliptic Partial Differential Equations* (Cambridge University Press, New York, 1996).
- [89] M. Lüscher, *JHEP* 0305 (2003) 052, hep-lat/0304007.
- [90] M. Lüscher, *Comput.Phys.Commun.* 156 (2004) 209, hep-lat/0310048.
- [91] J. Sylvester, *Philosophical Magazine* 1 (1851) 295.
- [92] A. Frommer, K. Kahl, S. Krieg, B. Leder and M. Rottmann, (2013), 1303.1377.
- [93] T. Davis and I. Duff, *SIAM Journal on Matrix Analysis and Applications* 18 (1997) 140, <http://dx.doi.org/10.1137/S0895479894246905>.
- [94] T.A. Davis and I.S. Duff, *ACM Trans. Math. Softw.* 25 (1999) 1.
- [95] T.A. Davis, *ACM Trans. Math. Softw.* 30 (2004) 196.
- [96] M. Lüscher, <http://luscher.web.cern.ch/luscher/DD-HMC/index.html>.

## Bibliography

---

- [97] A.C. Irving and J.C. Sexton, *Phys.Rev. D*55 (1997) 5456, hep-lat/9608145.
- [98] P. Fritzsche et al., *Nucl.Phys. B*865 (2012) 397, 1205.5380.
- [99] M. Bruno, J. Finkenrath, F. Knechtli, B. Leder and R. Sommer, (2014), 1410.8374.
- [100] UKQCD Collaboration, C. Michael and J. Peisa, *Phys.Rev. D*58 (1998) 034506, hep-lat/9802015.
- [101] M. Lüscher, (1998) 229, hep-lat/9802029.
- [102] M. Della Morte, R. Hoffmann and R. Sommer, *JHEP* 0503 (2005) 029, hep-lat/0503003.
- [103] M. Lüscher, *PoS LATTICE2010* (2010) 015, 1009.5877.
- [104] M. Lüscher, *Commun.Math.Phys.* 293 (2010) 899, 0907.5491.
- [105] M. Atiyah and I. Singer, *Annals Math.* 87 (1986) 485.
- [106] M. Lüscher, S. Sint, R. Sommer and P. Weisz, *Nucl.Phys. B*478 (1996) 365, hep-lat/9605038.
- [107] S. Dürr, Z. Fodor, C. Hoelbling and T. Kurth, *JHEP* 0704 (2007) 055, hep-lat/0612021.
- [108] Z. Fodor and S. Katz, *Phys.Lett. B*534 (2002) 87, hep-lat/0104001.
- [109] M. Lüscher and F. Palombi, *PoS LATTICE2008* (2008) 049, 0810.0946.
- [110] M. Lüscher, <http://luscher.web.cern.ch/luscher/openQCD>.
- [111] B. Leder and J. Finkenrath, <https://github.com/bjoern-leder/mrw>.
- [112] J. Finkenrath, F. Knechtli and B. Leder, *PoS LATTICE2012* (2012) 190, 1211.1214.
- [113] S. Lottini, *PoS LATTICE2013* (2013) 315, 1311.3081.
- [114] R. Frezzotti, P.A. Grassi, S. Sint and P. Weisz, *Nucl.Phys.Proc.Suppl.* 83 (2000) 941, hep-lat/9909003.
- [115] W.A. Bardeen, A. Duncan, E. Eichten, G. Hockney and H. Thacker, *Phys.Rev. D*57 (1998) 1633, hep-lat/9705008.
- [116] L. Giusti and M. Lüscher, *JHEP* 0903 (2009) 013, 0812.3638.
- [117] R. Sommer, *Nucl.Phys. B*411 (1994) 839, hep-lat/9310022.

- [118] M. Bruno and R. Sommer, PoS (LATTICE2013) 321, 1311.5585.
- [119] S. Sint and P. Weisz, Nucl.Phys. B502 (1997) 251, hep-lat/9704001.
- [120] ALPHA Collaboration, M. Guagnelli et al., Nucl.Phys. B595 (2001) 44, hep-lat/0009021.
- [121] J. Gasser and H. Leutwyler, Nucl.Phys. B250 (1985) 465.
- [122] R. Dashen, Phys. Rev. 183 (1969) 1245.
- [123] M. Golterman, (2009) 423, 0912.4042.
- [124] T. Blum, T. Doi, M. Hayakawa, T. Izubuchi and N. Yamada, Phys.Rev. D76 (2007) 114508, 0708.0484.
- [125] B. Leder, J. Finkenrath and F. Knechtli, PoS LATTICE2011 (2011) 038, 1112.1243.
- [126] N. Cabibbo and E. Marinari, Phys.Lett. B119 (1982) 387.
- [127] S.L. Adler, Phys.Rev. D23 (1981) 2901.
- [128] R. Petronzio and E. Vicari, Phys.Lett. B245 (1990) 581.
- [129] G.G. Batrouni et al., Phys. Rev. D32 (1985) 2736.
- [130] C.T.H. Davies et al., Phys. Rev. D37 (1988) 1581.
- [131] T.H. Cormen, C.E. Leiserson and R.L. Rivest, Introduction to Algorithms, 3rd ed. (The MIT Press, 1992).
- [132] L. Del Debbio, L. Giusti, M. Lüscher, R. Petronzio and N. Tantalo, JHEP 0702 (2007) 056, hep-lat/0610059, TeX source, 17 pages, figures included.
- [133] L. Del Debbio, L. Giusti, M. Lüscher, R. Petronzio and N. Tantalo, JHEP 0602 (2006) 011, hep-lat/0512021.
- [134] S. Schaefer, PoS LATTICE2012 (2012) 001, 1211.5069.
- [135] A. Hasenfratz, R. Hoffmann and F. Knechtli, Nucl.Phys.Proc.Suppl. 106 (2002) 418, hep-lat/0110168.
- [136] A. Frommer, K. Kahl, S. Krieg, B. Leder and M. Rottmann, (2013), 1307.6101.
- [137] A. Kennedy, I. Horvath and S. Sint, Nucl.Phys.Proc.Suppl. 73 (1999) 834, hep-lat/9809092.
- [138] M. Clark and A. Kennedy, Phys.Rev.Lett. 98 (2007) 051601, hep-lat/0608015.

## *Bibliography*

---

- [139] G.H. Golub and C.F. Van Loan, *Matrix Computations* (3rd Ed.) (Johns Hopkins University Press, Baltimore, MD, USA, 1996).
- [140] B. Leder, J. Finkenrath and F. Knechtli, (2014), 1401.1079.
- [141] K. Fritzsche, *Grundkurs Funktionentheorie: Eine Einführung in die komplexe Analysis und ihre Anwendungen* (Spektrum Akademischer Verlag, 2008).
- [142] A. Hasenfratz and A. Alexandru, *Phys.Rev. D65* (2002) 114506, hep-lat/0203026.
- [143] I.B. Fox, L.; Parker, *Oxford University Press, London-New York-Toronto* (1968).
- [144] D. Young, *Iterative Solution of Large Linear Systems* (Dover Books on Mathematics Series (Dover Publications, 2003).
- [145] L. Berg, *ZAMM - Journal of Applied Mathematics and Mechanics / Zeitschrift für Angewandte Mathematik und Mechanik* 57 (1977) 731.
- [146] M. Lüscher, *Nucl.Phys. B418* (1994) 637, hep-lat/9311007.
- [147] B. Leder, *Internal notes* (2013).
- [148] U. Wolff, <http://www.physik.hu-berlin.de/com/ALPHAsoft>.
- [149] A. Kennedy, (2006), hep-lat/0607038.
- [150] S. Borsanyi et al., *JHEP* 1209 (2012) 010, 1203.4469.

## List of Figures

4.1. Domain Decomposition . . . . .	31
4.2. Active links . . . . .	35
4.3. Plateaus of pseudoscalar masses and PCAC masses . . . . .	38
5.1. Comparison of different mass interpolations . . . . .	54
5.2. Crossing zero of a real eigenvalue and history of D5 . . . . .	57
5.3. Scaling of stochastic fluctuations . . . . .	59
5.4. Scaling of ensemble fluctuations . . . . .	63
5.5. Deviation of the lattice spacing by using a $\beta$ -shift . . . . .	70
5.6. Chiral extrapolation by using mass reweighting . . . . .	71
5.7. Tuning of $\Delta m_{ud} = m_d - m_u$ by using $R_2$ . . . . .	76
5.8. Light quark masses . . . . .	78
5.9. Sea quark effects to the pion mass . . . . .	80
6.1. Plaquette during gauge field interpolation . . . . .	91
6.2. Volume scaling of fluctuations in the PSMS algorithm . . . . .	98
6.3. Exact acceptance of the PSMS algorithm . . . . .	101
6.4. Scaling of fluctuations with the lattice spacing . . . . .	102
6.5. Histories of different algorithms of $Q$ for $\beta = 5.8$ lattices . . . . .	105
6.6. Scaling of the autocorrelation time of $Q$ . . . . .	107
6.7. Partially smeared HYP: plaquette-histories . . . . .	111
6.8. Partially smeared HYP: critical mass extrapolation . . . . .	112
6.9. Partially smeared HYP: scale setting with $t_0$ . . . . .	113
7.1. Comparison of energy violation during the HMC trajectory . . . . .	118
7.2. Scaling of the shift accept-reject step . . . . .	120
7.3. Volume scaling of reweighting factor . . . . .	122
E.1. Chiral extrapolation of $m_{PCAC}$ and $t_0$ on Z ensembles . . . . .	158





# List of Tables

2.1. Quarks . . . . .	6
2.2. Hadrons . . . . .	9
5.1. CLS ensembles used for mass reweighting . . . . .	50
5.2. Mass reweighting of CLS ensembles . . . . .	51
5.3. Used statistics of the CLS ensembles . . . . .	66
5.4. Critical $\kappa$ and chiral $t_0/a^2$ . . . . .	72
5.5. Isospin tuning of $\kappa_u$ and $\kappa_d$ . . . . .	77
6.1. Structure of a possible PSMS $n$ -step algorithm . . . . .	96
6.2. Plain Wilson ensembles . . . . .	99
6.3. Topologies and autocorrelation times of plain Wilson runs . . . . .	104
6.4. Parameter-set 1 of the PSMS algorithm for partially smeared HYP . . . . .	109
6.5. Parameter-set 2 of the PSMS algorithm for partially smeared HYP . . . . .	110
6.6. Effect of improved pure gauge action . . . . .	114
7.1. Run parameter of the MDD-HMC . . . . .	119
7.2. Comparison of the numerical effort for the algorithms . . . . .	125
F.1. Observables of plain Wilson $\beta = 5.5$ ensembles . . . . .	157
F.2. Parameter-set of the PSMS algorithm for Z4 . . . . .	158



# Acronyms

**chap.** chapter

**sec.** section

**subsec.** subsection

**app.** appendix

**eq.** equation

**tab.** table

**fig.** figure

**e.g.** *exempli gratia*, for example

**i.e.** *id est*, that is

**QCD** Quantum ChromoDynamics

**QED** Quantum ElectroDynamics

**LQCD** Lattice Quantum ChromoDynamics

**HMC** Hybrid Monte Carlo

**DD** Domain Decomposition

**PSMS** Partial Stochastic Multi Step

**MDD** Mass split Domain Decomposition

**IR** InfraRed

**UV** UltraViolet

**HYP** Hypercubic



# Curriculum Vitae

Name: Jacob Friedrich Finkenrath  
(forename, middle name, surname)

Gender: male

Nationality: german

Address: Ewaldstr. 8,  
42107 Wuppertal,  
Germany

Email address: Jacob-Finkenrath@web.de

## Chronicle:

26.05.1985:

birth, Herdecke, Germany,  
Mother: Monika Käthe Finkenrath (nee Konrad)  
Father: Werner Dietmar Finkenrath

1990/91 - 2003/04:

Rudolf Steiner Schule Wuppertal,  
completed with "Abitur" (University Entrance Diploma)

10/2004 - 06/2005:

Civil-work at Johanniter Unfallhilfe e.V. Wuppertal

09/2005:

Rettungssanitäter (inactive)

10/2005 - 06/2010:

Bergische Universität Wuppertal, Diplom II in physics,  
completed with "Diplom Physiker" (Graduate Physicist)

09/2010 - now:

PhD. student at Bergische Universität Wuppertal,  
Theoretical particle physics in the local group of Prof. Dr. Knechtli



## Acknowledgements

Before closing this thesis I want to express my gratitude and honor to those who supported me and helped to make this work possible.

I am very grateful to Prof. Dr. Francesco Knechtli for his support. It was a great opportunity to work, to develop and to discuss physics and numerical methods in the last five years under his guidance.

These gratitudes go also to my office neighbor Dr. Björn Leder. His guidance over the last 5 years was essential and he introduced me to several topics in LQCD. In general the relaxed and productive atmosphere in the group supports the creation and the invention of the introduced numerical methods.

Furthermore I want to thank Dr. Graham Moir, Dr. Markus Mechtel and Peter Schottler for reading and correcting parts of my thesis.

Moreover I want to thank also the local group members especially Peter Funke, Kyoko Yoneyama and Peter Dziennik. In general I wish to thank the Bergische University of Wuppertal for the opportunity to do my PhD in Wuppertal and for the usage of the local cluster Stromboli/Vulcano, on which all computation of this thesis were done. Furthermore I want to thank the research projects SFB-Transregio 55, the European PhD program Strong Net for their support during my PhD and the CLS consortium for providing their gauge configurations. Moreover I want to mention the useful discussions with the numerical mathematician of the local group of Prof. Dr. Frommer. Furthermore I want to thank Mattia Bruno for providing the  $t_0/a^2$  data in the chiral limit.

Many thanks to my family, my mother Monika Finkenrath, my father Dietmar Finkenrath and my sisters Viola and Mareike Finkenrath for their support and encouragement. Furthermore I want to express my thanks to all my friends who supported me through the years of writing this thesis. Special thanks go to Yan Entes, Mirco Tischler, Tanja Duttenhofer, Kathrin Becker, Franziska Szeibert, Tomoko Kikuchi, Konrad Ploch, Sebastian Szillat, Daniel Zander, Gordon Keiper and many many others. Finally I want to thank my football mates from Stahlwille and from Lokomotive Barmen. It is good to know you!





# **Selbständigkeitserklärung**

Ich erkläre, dass ich die vorliegende Arbeit selbständig und nur unter Verwendung der angegebenen Literatur und Hilfsmittel angefertigt habe.

Wuppertal, den 13.03.2015

Jacob Friedrich Finkenrath